



<https://theses.gla.ac.uk/>

Theses Digitisation:

<https://www.gla.ac.uk/myglasgow/research/enlighten/theses/digitisation/>

This is a digitised version of the original print thesis.

Copyright and moral rights for this work are retained by the author

A copy can be downloaded for personal non-commercial research or study,
without prior permission or charge

This work cannot be reproduced or quoted extensively from without first
obtaining permission in writing from the author

The content must not be changed in any way or sold commercially in any
format or medium without the formal permission of the author

When referring to this work, full bibliographic details including the author,
title, awarding institution and date of the thesis must be given

Enlighten: Theses

<https://theses.gla.ac.uk/>
research-enlighten@glasgow.ac.uk



**UNIVERSITY
of
GLASGOW**

**Modulation of spontaneous Ca²⁺ release from
the sarcoplasmic reticulum by FKBP12.6 in
rabbit ventricular cardiomyocytes**

Christopher Michael Loughrey BVMS MRCVS

**Submitted July 2003 in fulfilment of the degree Doctor of Philosophy
to the Faculty of Veterinary Medicine, University of Glasgow, U.K.**

**Research carried out within the Faculty of Biomedical & Life Sciences,
University of Glasgow, U.K.**

**GLASGOW
UNIVERSITY
LIBRARY:**

13157 COPY 1

ProQuest Number: 10646761

All rights reserved

INFORMATION TO ALL USERS

The quality of this reproduction is dependent upon the quality of the copy submitted.

In the unlikely event that the author did not send a complete manuscript and there are missing pages, these will be noted. Also, if material had to be removed, a note will indicate the deletion.



ProQuest 10646761

Published by ProQuest LLC (2017). Copyright of the Dissertation is held by the Author.

All rights reserved.

This work is protected against unauthorized copying under Title 17, United States Code
Microform Edition © ProQuest LLC.

ProQuest LLC.
789 East Eisenhower Parkway
P.O. Box 1346
Ann Arbor, MI 48106 – 1346

DECLARATION

The material contained within this thesis is my own work, except where stated. This material has not been submitted for the fulfilment of any other degree.

Some of the results obtained have been published in paper and abstract form and are detailed below:

C. M. Loughrey, K. E. MacEachern, P. Neary, and G. L. Smith: The relationship between intracellular $[Ca^{2+}]$ and Ca^{2+} wave characteristics in permeabilised cardiomyocytes from the rabbit. *J Physiol (Lond)* 2002 543: 859-870.

C. M. Loughrey, K. E. MacEachern, J. Cooper and G. L. Smith: Measurement of the dissociation constant of Fluo-3 for Ca^{2+} in isolated rabbit cardiomyocytes using Ca^{2+} wave characteristics. *Cell Calcium* 2003 34: (1) 1-9.

H. Zhang, D. Noble, M. Cannell, C. Orchard, M. Lancaster, M. R. Boyett, A.V. Holden, M. Saleet Jafri, E.A. Sobie, W.J. Lederer, S.S. Demir, A. Michailova, F. DelPrincipe, M. Egger, E. Niggli, G.L. Smith, C.M. Loughrey, N. MacQuaide, J. Dempster, A.T. Trafford: Dynamics of cardiac intracellular Ca^{2+} handling – from experiments to virtual cells. *International Journal of Bifurcation and Chaos* (In press - September 2003).

C. M. Loughrey, K. E. MacEachern, P. Neary, and G. L. Smith: Relationship between extracellular $[Ca^{2+}]$ and intracellular Ca^{2+} wave characteristics in β - escin-permeabilised single cardiomyocytes (rabbit). Abstract - Physiological Society Bristol meeting, *J Physiol* 2001 PS C54.

C. M. Loughrey, K. E. MacEachern and G. L. Smith: Intracellular Ca^{2+} waves in heart

muscle: source of triggered arrhythmias. Abstract – Association of Veterinary Teachers and Research workers Annual conference, *Research in Veterinary Science* 2001; 70: supp A, (13).

C.M. Loughrey, A. Rankin, D.F. Reynolds, G. Hasenfuss, J. Prestle, G.L. Smith. Ca^{2+} spark and Ca^{2+} wave characteristics in permeabilised adult cardiomyocytes are altered by FKBP12.6 over-expression. Abstract – Physiological Society meeting Tubingen, *J Physiol* 2002.

C.M. Loughrey, A. Rankin, D.F. Reynolds, G. Hasenfuss, J. Prestle, G.L. Smith. FKBP12.6 over-expression alters the characteristics of SR Ca^{2+} release in permeabilised adult cardiac myocytes. Abstract – Biophysical Meeting, San Francisco, *Biophys J* 2002; Vol.82; No.1.

T. Seidler, D. Zibrova, D.Reynolds, C.M.Loughrey, A. Kania, N, Teucher, S.Wagner, J, Prestle, H. Kogler, G, Hasenfuss, G.L.Smith: FKBP12 overexpression in isolated rabbit cardiomyocytes enhances intracellular Ca^{2+} transients, SR Ca^{2+} content and contractility. Abstract – American Heart Association meeting 2002.

C.M. Loughrey, A. Rankin, D.F. Reynolds, G. Hasenfuss, J. Prestle, G.L. Smith, Over-expression of FK506-binding protein in cardiomyocytes alters Ca^{2+} spark characteristics and increases the synchronicity of Ca^{2+} release: Abstract - British Cardiac Society Annual Scientific Conference May, *Heart* 2003; 89: supp 1 (A52).

SUMMARY

Spontaneous sarcoplasmic reticulum (SR) Ca^{2+} -release and propagated intracellular Ca^{2+} waves are a consequence of cellular Ca^{2+} overload in cardiomyocytes. We examined the relationship between the average intracellular $[\text{Ca}^{2+}]$ and Ca^{2+} wave characteristics. Amplitude, time course and propagation velocity of Ca^{2+} waves were measured using line-scan confocal imaging of β -escin permeabilised cardiomyocytes perfused with $10\mu\text{M}$ Fluo-3 or Fluo-5F. Spontaneous Ca^{2+} waves were evident at cellular $[\text{Ca}^{2+}] >200\text{nM}$. Peak $[\text{Ca}^{2+}]$ during a wave was $2\text{--}2.2\mu\text{M}$; minimum $[\text{Ca}^{2+}]$ between waves was $120\text{--}160\text{nM}$; wave frequency was $\sim 0.1\text{Hz}$. Raising mean cellular $[\text{Ca}^{2+}]$ caused increases in all three parameters, particularly Ca^{2+} wave frequency. Increased rate of SR Ca^{2+} -release and Ca^{2+} -uptake were observed at higher cellular $[\text{Ca}^{2+}]$, indicating Ca^{2+} -sensitive regulation of these processes. At extracellular $[\text{Ca}^{2+}] >2\mu\text{M}$, the mean intracellular $[\text{Ca}^{2+}]$ inside the permeabilised cell did not increase above $1.5\mu\text{M}$. This extracellular-intracellular Ca^{2+} gradient could be maintained for periods of up to 5min before the cardiomyocyte developed a sustained and irreversible hypercontraction. Inclusion of mitochondrial inhibitors ($2\mu\text{M}$ CCCP and $2\mu\text{M}$ oligomycin) while perfusing with $>2\mu\text{M}$ Ca^{2+} abolished the extracellular-intracellular Ca^{2+} gradient through the generation of Ca^{2+} waves with a higher peak $[\text{Ca}^{2+}]$ compared to control conditions. Under these conditions, cardiomyocytes rapidly ($<2\text{min}$) developed a sustained and irreversible contraction. These results suggest that mitochondrial Ca^{2+} uptake acts to delay an increase in intracellular $[\text{Ca}^{2+}]$ by blunting the peak of the Ca^{2+} wave. The Ca^{2+} dissociation constant (K_d) of Fluo-3 was

determined using confocal fluorescence microscopy in two different situations: (i) within the cytosol of a permeabilised cardiomyocyte and (ii) in an intact cardiomyocyte after incubation with the acetoxymethyl ester form of Fluo-3 (AM). Measurements were made on isolated rabbit ventricular cardiomyocytes after permeabilisation by a brief treatment with β -escin ($0.1\text{mg}\cdot\text{ml}^{-1}$) and equilibration with $10\mu\text{M}$ Fluo-3. The K_d of Fluo-3 within the cytosol was not significantly different from that in free solution ($558\pm 15\text{nM}$, $n=6$). The characteristics of spontaneous Ca^{2+} waves in permeabilised cardiomyocytes as characterised above indicated that the minimum $[\text{Ca}^{2+}]$ reached between Ca^{2+} waves was relatively constant over a range of intracellular $[\text{Ca}^{2+}]$. After loading intact cardiomyocytes with Fluo-3 by incubation with the -AM, spontaneous Ca^{2+} waves were produced by incubation with strophanthidin ($10\mu\text{M}$). By assuming a common minimum $[\text{Ca}^{2+}]$ in permeabilised and intact cells, the intracellular K_d of Fluo-3 was estimated to be $898\text{nM}\pm 64$ ($n=6$). Application of this K_d to fluorescence records predicted Ca^{2+} waves in intact cells with similar amplitudes to those in permeabilised cells. Stimulation of cardiac myocytes at 0.5Hz in the absence of strophanthidin (room temperature) resulted in a Ca^{2+} transient with a maximum and minimum $[\text{Ca}^{2+}]$ of $1190\pm 200\text{nM}$ and $158\pm 30\text{nM}$, ($n=11$) respectively. Ultimately, the above data characterising the release of Ca^{2+} from the SR and the K_d of Fluo-3 allowed investigation of the role of FK506-binding protein (FKBP12.6) using adenoviral-mediated gene transfer to over-express FKBP12.6 (Ad-FKBP12.6) in adult rabbit ventricular cardiomyocytes. Infection with a β -galactosidase-expressing adenovirus (Ad-LacZ) was used as a control. Peak-systolic intracellular $[\text{Ca}^{2+}]$ (measured with Fura-2) was higher in the Ad-FKBP12.6 group

($845 \pm 75 \text{ nM}$, $n=25$) compared to Ad-LacZ ($625 \pm 56 \text{ nM}$, $n=25$, $P < 0.05$); end-diastolic intracellular $[\text{Ca}^{2+}]_i$ was unchanged (1 Hz field stimulation at 37°C). The amplitude of caffeine-induced Ca^{2+} -release was also greater ($1360 \pm 103 \text{ nM}$ vs. $980 \pm 63 \text{ nM}$ $p < 0.05$, $n=25$) indicating a higher SR Ca^{2+} content in the Ad-FKBP12.6 group. Line-scan confocal microscopy (Fluo-3 fluorescence) of intact cardiomyocytes stimulated at 0.5 Hz ($20\text{-}21^\circ\text{C}$) revealed a higher degree of synchronicity of SR Ca^{2+} release and fewer non-responsive Ca^{2+} release sites in the Ad-FKBP12.6 group compared to control. Ca^{2+} spark size and frequency was measured in β -escin permeabilised cardiomyocytes at a free $[\text{Ca}^{2+}]_i$ of 150 nM . All spark parameters were reduced in the Ad-FKBP12.6 group ($n=9$ cells) compared to Ad-LacZ ($n=18$ cells): Ca^{2+} spark peak, F/F_0 1.80 ± 0.03 vs. 1.96 ± 0.02 ; width, $3.15 \pm 0.07 \mu\text{m}$ vs. $3.33 \pm 0.07 \mu\text{m}$; duration, $26.09 \pm 1.5 \text{ ms}$ vs. $29.21 \pm 1.0 \text{ ms}$; and frequency, $0.04 \pm 0.007 \text{ events} \cdot \mu\text{m}^{-1} \cdot \text{s}^{-1}$ vs. $0.06 \pm 0.004 \text{ events} \cdot \mu\text{m}^{-1} \cdot \text{s}^{-1}$. Raising intracellular $[\text{Ca}^{2+}]_i$ to 400 nM in permeabilised cardiomyocytes, resulted in the appearance of coherent propagating Ca^{2+} waves in the Ad-FKBP12.6 group but only limited Ca^{2+} release events were recorded in the control group. In conclusion, this data suggests that FKBP12.6 over-expression enhances cardiac excitation-contraction coupling predominately by reducing diastolic Ca^{2+} leak from the SR, but also by increasing the synchrony of SR Ca^{2+} release. Finally Ca^{2+} sparks were examined in permeabilised rabbit ventricular cardiomyocytes (150 nM $[\text{Ca}^{2+}]_i$) over-expressing an FKBP12.6 mutant, which lacked the ability to bind to calcineurin. This was compared to control virus, (Ad-LacZ) and over-expression of FKBP12.6. No differences were found between over-expression of the mutant and FKBP12.6 suggesting that calcineurin

binding is not necessary for the observed decrease in spark size and frequency compared to control (Ad-LacZ).

AIMS

The general aim is to study the role of FKBP12.6 in regulating sarcoplasmic reticulum (SR) Ca^{2+} release in permeabilised cardiomyocytes.

(1) Initial work concerned the characteristics of spontaneous Ca^{2+} release from permeabilised cells. In particular, the aim was to discover the relationship between intracellular $[\text{Ca}^{2+}]$ and the ability of the SR to generate Ca^{2+} waves.

(2) The second aim was to compare the Ca^{2+} wave behaviour in permeabilised cardiomyocytes and Ca^{2+} wave behaviour within the intact cells and to use the wave characteristics in intact cells to calibrate the commonly used fluorescent Ca^{2+} indicator – Fluo-3/AM.

(3) The main aim of this thesis was to study the effects of adenoviral mediated over-expression of FKBP12.6 on Ca^{2+} sparks and Ca^{2+} waves within adult rabbit ventricular cardiomyocytes.

(4) The final aim was to study Ca^{2+} sparks within cardiomyocytes over-expressing a mutant form of FKBP12.6, which lacked the ability to bind to calcineurin.

Since this may be the only page that is comprehensible to them, this is perhaps the most important, and therefore...

I dedicate this thesis to my parents, without whom, I could not have achieved any of the things I have done.

ACKNOWLEDGEMENTS

Firstly, I would like to thank Dr. Karen MacEachern, who has provided me with endless support and kindness throughout my PhD. I have no doubt that my interest in cardiology is a reflection of her enthusiastic teaching of the subject to me as an undergraduate. I am indebted to Karen for this and for pointing me in the direction of this PhD.

Karen's direction led me to meet with Prof. Godfrey Smith. Godfrey has also provided me with continual support and kindness throughout my PhD. In the relatively short period of time we have known each other, I am honoured, that he has become both my mentor and friend, and I very much hope this will continue.

I would also like to thank my colleagues at work who have helped my PhD run smoothly. In particular, I would like to thank Debbie for sharing an office with me and providing me with much fun and friendship. I would also like to thank the 'N. Irish contingent - Stuart and Nial; the latter especially for continuing this thesis by producing 'The Model'. Many thanks to Sarah and Margaret-Anne who were with me when I first started this PhD. I also thank Elspeth, who kindly contributed a figure to this thesis and for her 'good natured fun'. I am also indebted to the technicians - Ann Ward and Aileen Rankin for their support, help and advice over the last few years.

The ability to work with adenoviruses would not have been possible had it not been for Tim Seidler, Jurgen Prestle, and Gerd Hasenfuss, (University

of Goettingen). This collaboration has been extremely beneficial and enjoyable and I hope it will continue.

The confocal microscope requires continual monitoring and fine-tuning in order to ensure that the tracking of $[Ca^{2+}]$ remains standardised each time the instrument is used. While this monitoring is carried out personally on a weekly basis it is often necessary to call on the expertise of either Mark Munroe of *BioRad* or David Wocosin of the Biophotonics centre, Strathclyde, U.K. Glasgow. Their expertise of the instrument is invaluable and I am indebted to them for providing essential help so willingly.

I thank Peter for reading sections of the thesis and for being a good friend to me.

Finally, I would like to thank Claire for her friendship, kindness, and for being there.

Financial support was gratefully received by the following:



CONTENTS

DECLARATION	2
SUMMARY	4
AIMS	8
ACKNOWLEDGEMENTS	10
CONTENTS	12
FIGURES	22
TABLES	24
ABBREVIATIONS	25
CHAPTER ONE	28
Excitation-contraction coupling & Ca²⁺ sparks and waves	28
1.1 INTRODUCTION.....	29
1.2 Ca ²⁺ entry into the ventricular cardiomyocyte	30
1.3 Ca ²⁺ induced Ca ²⁺ release (CICR) from the sarcoplasmic reticulum	33
1.4 The sarcoplasmic reticulum (SR).....	34
1.5 Identifying the source of the simulated Ca ²⁺ entry during CICR.....	36
1.6 Problems associated with the theory of CICR.....	38
1.7 Preventing positive feedback	38

1.8	A model of CICR that begins to fit the experiments	40
1.9	Evidence for local control of CICR	43
1.10	Ca ²⁺ sparks - a more complete picture of CICR	44
1.11	Why are Ca ²⁺ sparks helpful in understanding EC-coupling	46
1.12	Evidence that Ca ²⁺ sparks are triggered by LCCs.....	48
1.13	The use of Ca ²⁺ sparks to explain Ca ²⁺ transient characteristics	48
1.14	How many LCCs are required to trigger a cluster of RyRs?.....	50
1.15	How many RyRs contribute to a Ca ²⁺ spark?.....	52
1.16	How do Ca ²⁺ sparks contribute to the graded amplified nature of CICR	52
1.17	How is a Ca ²⁺ spark terminated?	54
1.18	Can Ca ²⁺ sparks and waves be measured in permeabilised ventricular cardiomyocytes, and if so, are they the same as those in intact cells?	59
1.19	What are the effects of intracellular [Ca ²⁺] and SR [Ca ²⁺] on Ca ²⁺ sparks?	60
1.20	Regulation of Ca ²⁺ sparks by [Ca ²⁺] within the SR lumen	60
1.21	RyR activity and SR Ca ²⁺ leak	62
1.22	Other sources of Ca ²⁺ entry	62
1.23	Cardiomyocyte relaxation.....	65
1.23.1	SR mediated Ca ²⁺ uptake	65
1.23.2	Na ⁺ /Ca ²⁺ exchange	66
1.23.3	Sarcolemmal mediated Ca ²⁺ extrusion.....	66
1.24	Mitochondria	66
1.24.1	Ca ²⁺ uptake into mitochondria.....	67
1.24.2	Inhibiting mitochondrial Ca ²⁺ uptake	67
1.24.3	Ca ²⁺ efflux from mitochondria.....	67
	CHAPTER TWO	69

General methods	69
2.1 Rabbit ventricular cardiomyocyte isolation.....	70
2.1.1 Isolation procedure.....	70
2.1.2 Cells required for permeabilisation experiments	71
2.1.3 Cells required for intact cell experiments	71
2.1.4 Primary ventricular cardiomyocyte culture	72
2.2 The use of recombinant adenovirus to transfect adult.....	73
cardiomyocytes	
2.2.1 Adenovirus	74
2.2.2 Generation of the Ad-FKBP 12.6 virus.....	75
2.2.3 Infection with adenovirus.....	76
2.3 Cell permeabilisation of cardiomyocytes	79
2.3.1 β -escin	79
2.3.2 Mechanism of action	80
2.3.3 Minimum effective concentration.....	80
2.3.4 Other uses for permeabilisation agents.....	82
2.3.5 Other permeabilising agents	83
2.4 Laser scanning confocal microscopy (LSCM).....	85
2.4.1 Tracking the dynamics of $[Ca^{2+}]$ within ventricular cardiomyocytes.....	85
2.4.2 How do we measure cell fluorescence?.....	86
2.4.3 How is the confocal principle achieved?	86
2.4.4 Image formation	87
2.4.5 What if events occur with frequencies greater than 1s?.....	88
2.4.6 Data recording and analysis.....	88
2.4.7 Perfusion of cardiomyocytes	91
2.4.8 Disadvantages of confocal microscopy	91
2.4.9 Analysis programs used.....	93
2.5 Automated Ca^{2+} spark detection method	94

2.5.1	Summarisation of Ca ²⁺ spark detection programme	94
2.5.2	Sensitivity and specificity	96
2.5.3	Ca ²⁺ spark detection from line-scan confocal images	97
2.5.4	What should the amplitude distribution for Ca ²⁺ sparks look like?... 98	
2.5.5	What should the width and duration distribution of Ca ²⁺ sparks look like?	99
2.5.6	Calculation of Ca ²⁺ spark width	100
2.5.7	Is the Ca ²⁺ spark a stereotyped event.....	101
CHAPTER THREE		103
The relationship between intracellular [Ca²⁺] and Ca²⁺ wave characteristics in permeabilised cardiomyocytes from the rabbit. ...		103
3.1	INTRODUCTION.....	104
3.1.1	The discovery of Ca ²⁺ waves	104
3.1.2	How do Ca ²⁺ waves propagate?	104
3.1.3	Mathematical modelling	105
3.1.4	Factors involved in Ca ²⁺ wave propagation.....	105
3.1.5	Inactivation of SR Ca ²⁺ release	107
3.1.6	Are there different forms of Ca ²⁺ waves?	108
3.1.7	The aim of this chapter.....	108
3.2	METHODS	109
3.2.1	Cell isolation and permeabilisation.....	109
3.2.2	Solutions	109
3.2.3	Data recording and analysis.....	109
3.2.4	Calibration of fluorescence indicators	110
3.2.5	Statistics.....	114
3.3	RESULTS	115
3.3.1	Measurement of Ca ²⁺ waves in permeabilised single myocytes ...	115

3.3.2	Ca ²⁺ wave characteristics measured at high cellular [Ca ²⁺]	118
3.3.3	Mitochondrial Ca ²⁺ -uptake affects Ca ²⁺ wave characteristics.....	121
3.3.4	Relationship between extracellular and intracellular [Ca ²⁺]	123
3.3.5	Time-course of the Ca ²⁺ wave is influenced by the mean cellular [Ca ²⁺]	125
3.4	DISCUSSION.....	128
3.4.1	Changes in Ca ²⁺ wave characteristics at a mean cellular [Ca ²⁺] <1.2μM.....	128
3.4.2	Ca ²⁺ wave time-course.....	131
3.4.3	Ca ²⁺ wave characteristics at high mean cellular [Ca ²⁺] levels (>2μM).	132
3.4.4	Mitochondrial inhibitors modify Ca ²⁺ wave characteristics in high [Ca ²⁺].....	133
3.4.5	SUMMARY.....	137
CHAPTER FOUR		138
Measurement of the dissociation constant of Fluo-3 for Ca²⁺ in isolated rabbit cardiomyocytes using Ca²⁺ wave characteristics.....		138
4.1	INTRODUCTION.....	139
4.2	METHODS	141
4.2.1	Cell isolation and permeabilisation.....	141
4.2.2	Solutions for the production of spontaneous Ca ²⁺ waves within permeabilised cells.....	141
4.2.3	Solutions for the production of spontaneous Ca ²⁺ waves within intact cells	142
4.2.4	Laser-scanning confocal Fluo-3 fluorescence measurements in free solution and permeabilised cardiomyocytes.....	142
4.2.5	Field stimulation of intact cardiomyocytes.....	144
4.3	RESULTS	145
4.3.1	The Ca ²⁺ sensitivity of Fluo-3 in free solution and in permeabilised	

cardiomyocytes	145
4.3.2 A Protocol to produce Ca ²⁺ waves in permeabilised cardiomyocytes	147
4.3.3 Ca ²⁺ wave characteristics in permeabilised cardiomyocytes.....	151
4.3.4 The use of Ca ²⁺ waves characteristics in permeabilised cells to calibrate the K _d of Fluo-3 in intact cardiomyocytes.....	152
4.3.5 Comparison of Ca ²⁺ wave characteristics in permeabilised and intact cardiomyocytes.	154
4.3.6 Stimulated Ca ²⁺ transient characteristics.	155
4.4 DISCUSSION.....	158
4.41 The K _d value for Fluo-3 in free solution	158
4.4.2 The K _d value for Fluo-3 in permeabilised cardiomyocytes.....	158
4.4.3 The K _d value for Fluo-3 in intact cardiomyocytes	159
4.4.4 The use of Ca ²⁺ wave characteristics to assess Fluo-3 K _d	160
4.4.5 Characteristics of Ca ²⁺ waves within intact cells	161
4.4.6 Characteristics of electrically stimulated Ca ²⁺ transients.....	161
CHAPTER FIVE.....	164
The role of FK506-binding protein in ventricular cardiomyocytes	164
5.1 INTRODUCTION.....	165
5.2 FK506 Binding Protein 12.0	166
5.2.1 Discovery of the association between FKBP12.0 and RyR1	166
5.2.2 The role of the association between FKBP12.0 and RyR1	167
5.2.3 Further studies on the role of FKBP on RyR	168
5.2.4 How does FKBP stabilise RyR?	170
5.2.5 Coupling of RyRs by FKBP	170
5.2.6 Is there a role for the PPlase activity of FKBP?	172
5.3 FK506 Binding Protein 12.6	173
5.3.1 The discovery of the association between FKBP12.6 and RyR2 ...	173

5.3.2	Are all potential RyR sites filled with FKBP?	174
5.3.3	Specificity of binding	175
5.3.4	Does FKBP12.6 affect RyR2?.....	175
5.3.5	The role of FKBP12.6 in ventricular cardiomyocytes.....	176
5.3.6	Does FKBP12.6 play a role in coupling of RyR2s?	178
5.4	On the scale of things	179
5.4.1	The progression from molecule to bedside	179
5.4.2	A step in the right direction.....	181
5.4.3	The role of FKBP12.6 on EC-coupling in intact cardiomyocytes	181
5.4.4	The effects of FK506 on ventricular cardiomyocytes.....	183
5.4.5	The effects of FK506 at rest in ventricular cardiomyocytes.....	185
5.5	The need for novel techniques	186
5.5.1	The use of permeabilised cells to study the role of FKBP12.6	187
5.6	The biomedical significance of FKBP12.6	189
5.6.1	Are these studies relevant to the whole heart?	189
5.6.2	Should the Ca ²⁺ transient be increased or decreased on removal of FKBP12.6?.....	191
5.6.3	Concerns.....	197
5.6.4	Future work is needed.....	198
5.6.5	The importance of FKBP12.6 stoichiometry within cardiomyocytes	198
5.7	The balance between phosphorylation and phosphatase activity ...	200
5.7.1	The testing of other heart failure models.....	201
5.7.2	Controversy in interpretation of results due to PKA phosphorylation of RyR2	203
5.8	The use of transgenic whole animal models	205
5.9	Novel modulators of RyR involving FKBP	210
5.10	Bastadins	210
5.11	Ivermectin and Midecamycin.....	213

5.12	Unresolved issues.....	216
5.12.1	What is the function of FKBP12.0 in cardiomyocytes?.....	216
5.12.2	What is the function of FKBP12.6 in EC coupling?	218
5.12.3	Is calcineurin activity required for modulation of RyR by FKBP? .	218
5.13	Over-expression of FK506-binding protein FKBP12.6 increases the synchronicity of SR Ca²⁺ release in adult rabbit cardiomyocytes.	219
5.13.1	METHODS	219
5.13.2	Single ventricular cardiomyocyte isolation from the rabbit heart ...	219
5.13.3	FK binding protein 12.6 over-expression within rabbit cardiomyocytes	219
5.13.4	Measurement of intracellular Ca ²⁺ within intact cardiomyocytes ...	219
5.13.5	Simultaneous field stimulation of intact cardiomyocytes with confocal imaging.....	220
5.13.6	Ca ²⁺ spark and wave measurements in permeabilised cardiomyocytes	220
5.13.7	Statistics.....	222
5.14	RESULTS	223
5.14.1	Measurement of Ca ²⁺ transients in intact ventricular cardiomyocytes using Fura-2	223
5.14.2	Line-scan imaging of Ca ²⁺ transients in cardiomyocytes.....	225
5.14.3	Quantitative assessment of the degree of synchrony of Ca ²⁺ release during stimulated Ca ²⁺ transients using confocal line-scan imaging.	226
5.14.4	Measurements in permeabilised cardiomyocytes.....	229
5.14.5	Ca ²⁺ sparks and caffeine-induced Ca ²⁺ release in permeabilised cardiomyocytes overexpressing FKBP12.6	233
5.14.6	Effects of higher [Ca ²⁺] on permeabilised cardiomyocytes overexpressing FKBP12.6.....	235
5.15	DISCUSSION.....	239
5.15.1	Effects of FKBP12.6 over-expression on synchronicity of E-C	

coupling.....	241
5.15.2 Effects of FKBP12.6 over-expression of Ca ²⁺ sparks in permeabilised cardiomyocytes.....	242
5.15.3 Effects of FKBP12.6 over-expression on spontaneous SR Ca ²⁺ release.	244
5.15.4 SUMMARY.....	245
CHAPTER SIX.....	247
Over-expression of an FKBP12.6 mutant lacking a calcineurin binding site in rabbit ventricular cardiomyocytes	247
6.1 INTRODUCTION.....	248
6.1.1 The many roles of calcineurin	248
6.1.2 The molecular structure of immunophilin ligands	248
6.1.3 Complexes formed between FKBP, its ligands and calcineurin.	249
6.1.4 Is calcineurin important in RyR2 activity?.....	250
6.1.5 The range of molecular species resulting from the use of drugs...	251
6.1.6 What if calcineurin does not just exist within the cytosol but forms part of the RyR2 macromolecular complex?	252
6.1.7 Is calcineurin ever <u>bound</u> to the RyR2 macromolecular complex?	253
6.1.8 So if calcineurin is indirectly bound to the RyR2 macromolecular complex does it play a role in RyR2 open probability?	253
6.1.9 Can conclusions be made on the functional role of calcineurin on RyR2 from the above study on the chronic application of cyclosporin?	254
6.1.10 Evidence for a role of calcineurin on RyR2 in skeletal muscle	255
6.1.11 The function of calcineurin on RyR2 within adult ventricular cardiomyocytes.....	256
6.1.12 Construction of the FKBP12.6 mutant virus	257
6.2 METHODS	259
6.2.1 Ca ²⁺ spark measurements in permeabilised cardiomyocytes.....	259

6.2.2	Statistics.....	259
6.3	RESULTS	260
6.4	DISCUSSION.....	262
6.4.1	Dynamic changes in $[Ca^{2+}]$	262
6.4.2	Evidence on the effect of calcineurin on RyR2.....	263
6.4.3	Specificity of agents use to investigate the action of calcineurin...	263
6.4.4	Further work.....	264
	CONCLUSIONS	265
	FINAL CONCLUSION	270
	APPENDIX.....	271
	Appendix 2.1	272
	Appendix 6.1	279
	Appendix 6.1.1 Base pair sequence	279
	Appendix 6.1.2 Amino acid sequence.....	279
	Appendix 6.1.3 Summary of construction of FKBP12.6 mutant	280
	REFERENCES	281

FIGURES

Figure 1.1	The dynamic movement of Ca^{2+}	30
Figure 1.2	Voltage dependence of the L - type Ca^{2+} current	32
Figure 1.3	Characteristics of CICR in skinned purkinje fibres	35
Figure 1.4	Location of LCCs and RyRs	36
Figure 1.5	'Common pool' model for CICR	41
Figure 1.6	Local control theory for CICR	42
Figure 1.7	'Cluster bomb' model	43
Figure 1.8	Ca^{2+} Sparks	44
Figure 1.9	Depolarisation duration effects on the Ca^{2+} transient	46
Figure 1.10	Asymmetrical voltage dependence of the Ca^{2+} transient	49
Figure 1.11	The analog and digital gain of CICR	53
Figure 1.12	The 'sticky cluster model'	57
Figure 1.13	The 'fuzzy space'	63
Figure 2.1	The capsid of a typical adenovirus	74
Figure 2.2	Construction of Ad-FKBP12.6	77
Figure 2.3	Minimum effective concentration of β -escin	81
Figure 2.4	Line-scan confocal imaging	89
Figure 2.5	Computer automated Ca^{2+} spark detection	96
Figure 2.6	Amplitude histograms of Ca^{2+} sparks	98
Figure 2.7	Adjustment of width parameters within the algorithm	101
Figure 2.8	Effects of varying width search distance on width distribution	102
Figure 3.1	Line-scan epi-fluorescence imaging of cardiomyocytes	113
Figure 3.2	Analysis of confocal line-scan images of Ca^{2+} waves	116
Figure 3.3	Records of Ca^{2+} waves at different values of extracellular $[\text{Ca}^{2+}]$	119
Figure 3.4	Effect of prolonged exposure to high extracellular $[\text{Ca}^{2+}]$ on Ca^{2+} waves in cardiomyocytes	120
Figure 3.5	Effect of mitochondrial inhibitors on Ca^{2+} waves at high extracellular $[\text{Ca}^{2+}]$	122
Figure 3.6	Effect of mitochondrial inhibitors on $[\text{Ca}^{2+}]$ and Ca^{2+} wave parameters	124

Figure 3.7	Relationship between various mean intracellular $[Ca^{2+}]$ and Ca^{2+} wave parameters and mean extracellular $[Ca^{2+}]$	126
Figure 3.8	Relationship between wave velocity and wave amplitude at different values of intracellular $[Ca^{2+}]$	130
Figure 4.1	Establishing the K_d value for Fluo-3 in free solution and within a permeabilised cardiomyocyte.....	146
Figure 4.2	Protocol to produce Ca^{2+} waves within permeabilised cardiomyocytes.....	148
Figure 4.3	Ca^{2+} wave characteristics taken from permeabilised cardiomyocytes over a range of $[Ca^{2+}]$	150
Figure 4.4	Protocol to produce Ca^{2+} waves within intact cardiomyocytes.....	153
Figure 4.5	Using the K_d for Fluo-3AM to compare Ca^{2+} waves within permeabilised and intact cardiomyocytes.....	154
Figure 4.6	Stimulated $[Ca^{2+}]$ transient characteristics using the K_d of Fluo-3AM in intact cardiomyocytes.....	156
Figure 4.7	Prevention of Ca^{2+} waves within stimulated cells.....	163
Figure 5.1	Ca^{2+} transients and caffeine-induced Ca^{2+} release.....	224
Figure 5.2	Imaging of Ca^{2+} transients.....	226
Figure 5.3	Measurement of Ca^{2+} transient synchrony.....	228
Figure 5.4	Mean and range of $Time_{50}$ values.....	230
Figure 5.5	Ca^{2+} sparks and caffeine induced Ca^{2+} release in permeabilised cardiomyocytes.....	231
Figure 5.6	Mean Ca^{2+} spark characteristics.....	234
Figure 5.7	Ca^{2+} wave characteristics.....	236
Figure 6.1	Molecular structure of exogenous immunophilin ligands.....	249
Figure 6.2	The effect of the FKBP-FK506 complex on calcineurin.....	250
Figure 6.3	Various methods to elucidate the function of FKBP12.6 on RyR2.....	257
Figure 6.4	Effects of the FKBP12.6 mutant on Ca^{2+} sparks.....	261

TABLES

Table 2.1	The function of various regions of the transcriptional map of a typical adenovirus	75
Table 3.1	Calculation to determine the total amount of Ca^{2+} (μM) produced during a Ca^{2+} wave.....	135
Table 6.1	The use of various drugs to produce different molecular species to investigate the role of calcineurin on RyR2.....	252

ABBREVIATIONS

Ad-LacZ	adenovirus transfected cardiomyocytes with β -galactosidase DNA sequence
Ad-FKBP12.6	adenovirus transfected cardiomyocytes with FKBP12.6 DNA sequence
AM	acetoxymethyl ester
ATP	adenosine 5' triphosphate
ATPase	adenosine triphosphatase
Ba ²⁺	barium ion
BaCl ₂	barium chloride
BAPTA	1,2-bis(2-aminophenoxy)ethane N,N,N',N'-tetraacetic acid
BSA	bovine serum albumin
Ca ²⁺	calcium ion
Ca ²⁺ -ATPase	calcium pump
[Ca ²⁺]	calcium ion concentration
[Ca ²⁺] _i	intracellular calcium ion concentration
[Ca ²⁺] _{ic}	intracellular calcium ion concentration
[Ca ²⁺] _{EC}	extracellular calcium ion concentration
cAMP	adenosine 3':5'-cyclicmonophosphate
cADPR	adenosine 3';5'-cyclicdiphosphate ribose
CCCP	Carbonyl cyanide <i>m</i> -chlorophenolhydrazone
Cd ²⁺	cadmium ion
CICR	calcium-induced calcium release
Cl ⁻	chloride ion
cm	centimetre, length
Cs ⁺	caesium ion
DHP	dihydropyridine
DHPR	dihydropyridine receptor
DMSO	dimethylsulphoxide
E-C	excitation-contraction
EDTA	ethylenediaminetetraacetic acid
EGTA	ethylene glycol bis(β -aminoethyl ether)-N,N,N',N'-tetraacetic acid
E _m	membrane potential
Fluo-3	fluorescent indicator (calcium sensitive)
Fluo-5F	fluorescent indicator (calcium sensitive)
F _{max}	fluorescence measured at saturatingly high calcium
F _{min}	fluorescence measured at very low calcium
Fura-2	fluorescent indicator (calcium sensitive)
g	gram, weight

Abbreviations

<i>g</i>	acceleration due to gravity
GFP	green fluorescent protein
HCl	hydrochloric acid
HEK	human embryonic kidney
HEPES	N-2-hydroxyethylpiperazine-N'-2-ethanesulphonic acid
Hz	Hertz, frequency
I_{Ca}	calcium current
Ins(1,4,5)P ₃	inositol (1,4,5)-triphosphate
K ⁺	potassium ion
K _d	dissociation constant
K _i	inhibitory equilibrium constant
KOH	potassium hydroxide
l	litre, volume
LASER	light amplification by stimulated emission of radiation
LSCM	laser-scanning confocal microscopy
M	molar, concentration
Mg ²⁺	magnesium ion
mg	milligram, weight
MgCl ₂	magnesium chloride
min	minute, time
ml	milliliter, volume
mm	millimeter, length
mM	millimolar, concentration
mol	mole, quantity
ms	millisecond
mV	millivolt, electrical voltage
n	sample size
Na ⁺	sodium ion
NADH	β-nicotinamide adenine dinucleotide phosphate (reduced)
NaH ₂ PO ₄	sodium dihydrogen orthophosphate
NaOH	sodium hydroxide
nm	nanometer, length
nM	nanomolar, concentration
p	probability
PLB	phospholamban
PMT	photomultiplier tube
PRO	proline
RyR	ryanodine receptor
s	second, time

Abbreviations

SEM	standard error of the mean
SER	serine
SERCA	sarco(endo)plasmic reticulum calcium ATPase
SR	sarcoplasmic reticulum
U	unit of activity
V	volt, electrical charge
μg	microgram, weight
μl	microlitre, volume
μM	micromolar, concentration
$^{\circ}\text{C}$	degrees celsius, temperature

CHAPTER ONE

Excitation-contraction coupling & Ca²⁺ sparks and waves

1.1 INTRODUCTION

Ventricular cardiomyocytes are an essential component of the functional syncytium that forms the mammalian heart. Their main role is to contract during systole and relax during diastole, in a regulated manner. Each cell is stimulated to perform this process by electrical depolarisation, which ultimately leads to activation of myofilaments and cellular shortening. During diastole the myofilament interaction is inhibited and the cell relaxes. A chemical messenger - Ca^{2+} , provides the link between this electrical excitation and subsequent mechanical activity. Although a number of different ions play an important role in this process, it is the dynamic movement of Ca^{2+} from the extracellular space into the cell and its intracellular translocation between various micro-domains and organelles that constitutes E-C coupling (Figure 1.1). In fact without extracellular Ca^{2+} the heart does not contract because Ca^{2+} is directly required for myofilament activation [1]. The complete absence of Ca^{2+} is an extreme situation, which is unlikely to occur *in vivo*. However, a simple disruption to the tightly regulated process of cellular Ca^{2+} homeostasis may lead to an inefficient contracting/relaxing myocardium. This is apparent within the clinical condition of heart failure.

This chapter aims to discuss some important aspects of EC-coupling and in doing so provide background information relevant to the thesis. The brevity of discussion on other aspects of the process is not a reflection of their relative importance in regulating Ca^{2+} homeostasis.

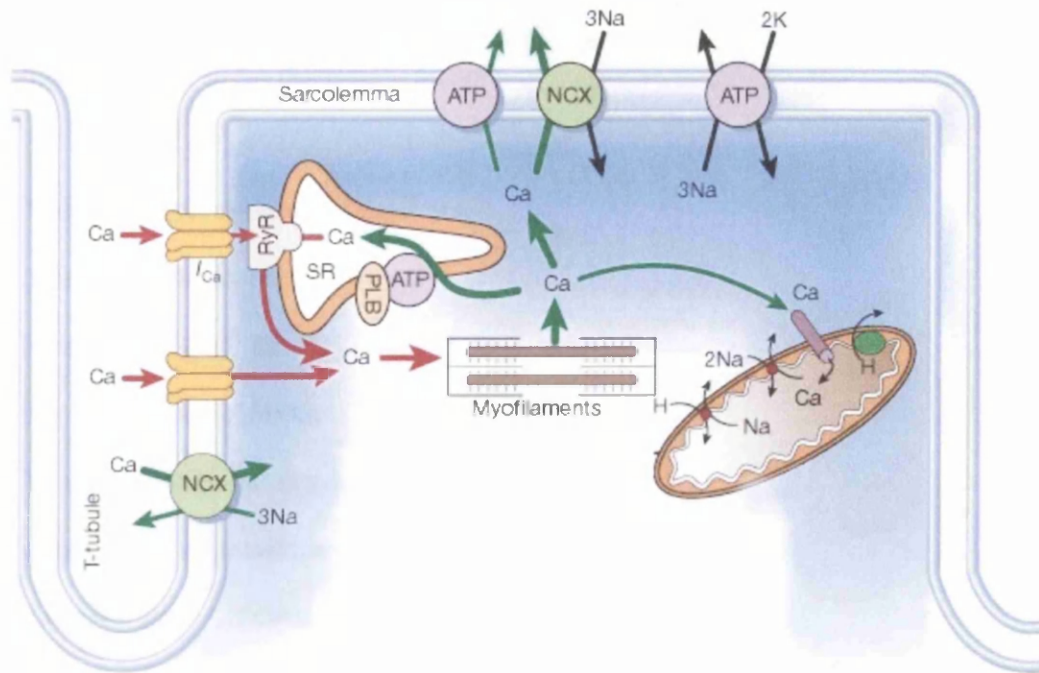


Figure 1.1 The dynamic movement of Ca^{2+}

Ca^{2+} enters the ventricular cardiomyocyte, is transported between various compartments and organelles, reversibly activates the myofilaments and is finally transported out of the cell. This process ensures that Ca^{2+} influx is equal to Ca^{2+} efflux under normal conditions. (NCX, $\text{Na}^+/\text{Ca}^{2+}$ exchange; ATP, ATPase; PLB, phospholamban; SR, sarcoplasmic reticulum). (Figure taken from Bers (2002) *Nature* 415, 198-205).

1.2 Ca^{2+} entry into the ventricular cardiomyocyte

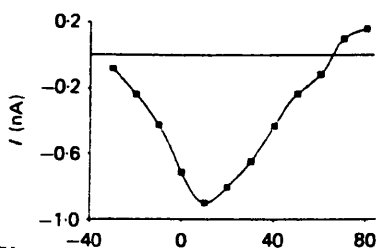
The driving force for Ca^{2+} entry into the cell is largely due to a concentration gradient across the cell membrane and the membrane potential relative to the Ca^{2+} equilibrium potential. However, Ca^{2+} does not 'flood' into the cardiomyocyte and the intracellular resting $[\text{Ca}^{2+}]$ remains low (150nM) while the extracellular $[\text{Ca}^{2+}]$ is high (1.5-2.0mM). In fact, if the resting $[\text{Ca}^{2+}]$ reached mM levels, irreversible activation of the myofilaments would occur together with enzymatic events which would lead to cell death. How then does intracellular $[\text{Ca}^{2+}]$ rise in a controlled manner in order for

myofilaments to be reversibly activated?

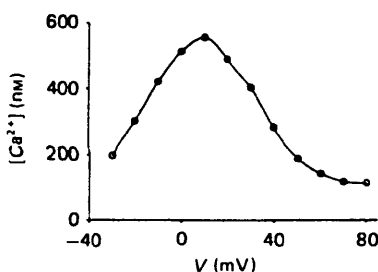
There are two sources of Ca^{2+} that could lead to a rise in myoplasmic $[\text{Ca}^{2+}]$ (the Ca^{2+} transient). Firstly the pool of extracellular Ca^{2+} , and secondly, intracellular Ca^{2+} stores. The extracellular pool has access to the interior of the cell via invaginations of the cell surface membrane (the sarcolemma). These extensions are known as transverse tubules (T-tubules). They account for approximately 3.6% of the cell volume and from 21 - 64% of the sarcolemma, the variation attributed to species differences [2-5]. Although their name implies a transverse arrangement, recent developments in two-photon microscopy have allowed visualisation of a more complex tubular network [5]. Entry of Ca^{2+} from this extracellular pool into the interior of the cell via the T-tubules is mainly by voltage dependent Ca^{2+} channels, namely L-type Ca^{2+} channels (LCCs) (T-type Ca^{2+} channels do exist in cardiomyocytes but their role in E-C coupling is not thought to be significant). That these channels are voltage dependent is of vital importance in terms of the timing and control of Ca^{2+} entry. Electrical excitation of the sarcolemma creates an action potential, which passes as a wave of depolarisation along the membrane down the T-tubules subsequently activating LCCs located here. LCCs are activated at negative membrane voltages (-40mV). The consequential current (I_{Ca}) is a product of the open probability of the channel and single channel conductance (i_{Ca}). Between -40mV and +10mV, I_{Ca} increases to a maximum. Over this voltage range the decrease in electrochemical driving force for Ca^{2+} entry is compensated for by the increase in channel open probability. However, even though the open probability continues to increase as the membrane

voltage rises to +60mV, the electrochemical drive for Ca^{2+} entry further decreases. I_{Ca} therefore decreases resulting in a bell shaped current voltage relationship [6] (Figure 1.2 Panel A(i)). The LCC shows relatively slow inactivation (60 - 200ms - hence Long (L-type) lasting current), which is voltage and Ca^{2+} dependent.

A(i)



(ii)



B

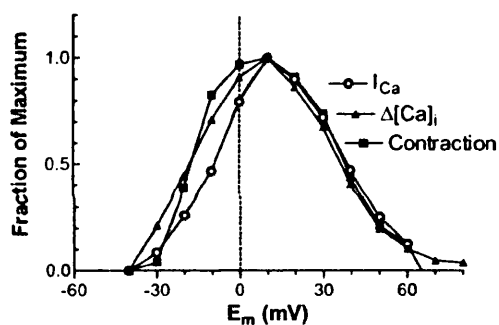


Figure 1.2 Voltage dependence of the L - type Ca^{2+} current

Panel A(i) shows an inverted bell shaped relationship between peak L-type Ca^{2+} current and membrane voltage (where V (volts) also refers to the E_m). Panel A(ii) shows the corresponding voltage dependence of the Ca^{2+} transient. Panel B shows the normalised relationship between L-type Ca^{2+} current, Ca^{2+} transient and contraction. (Panels adapted from (A) Beuckelmann *et al.* (1988) *J. Physiol.* 405 233-255), (B) Bers (2001) *Excitation-Contraction Coupling and Cardiac Contractile Force*, 2nd edition, Kluwer Academic, Dordrecht, Netherlands).

The influx of Ca^{2+} via LCC from the extracellular Ca^{2+} pool is insufficient to result in activation of the myofilaments in most mammalian species. This is due to an inadequate quantity of Ca^{2+} , the buffering of Ca^{2+} by intracellular

binding sites and diffusion [7]. In terms of the quantity of Ca^{2+} required for activation of the myofilaments it has been calculated that when using steady state Ca^{2+} loading conditions, approximately 60 - 70 $\mu\text{mol/L}$ cytosol is required to activate a normal ventricular twitch which is thought to be approximately 40% of maximal force at 25-30°C [8]. This would correspond to an increase to approximately 600nM free Ca^{2+} from a diastolic of 150nM assuming a cytosolic buffering of 100:1 (bound:free Ca^{2+}) [9]. The total Ca^{2+} influx due to LCC is dependant upon many factors. Species dependency is an important factor. The total amount of Ca^{2+} which enters the cell due to this channel in the rabbit is only approximately 12 $\mu\text{mol/L}$ cytosol which may even be reduced to 6 $\mu\text{mol/L}$ cytosol due to inactivation of the channel by Ca^{2+} [10]. Other reports suggest 21 $\mu\text{mol/L}$ cytosol for the rabbit and 14 $\mu\text{mol/L}$ cytosol for the rat using voltage clamped cells and action potential waveforms [11]. These values may be unexpectedly high due to the use of 10mM EGTA that would have suppressed Ca^{2+} inactivation. It can be seen therefore that in the rabbit, L-type Ca^{2+} influx can only account for approximately 23% of the total Ca^{2+} required to activate the myofilaments during a normal twitch [12]. Where does the remainder of the Ca^{2+} required to activate the myofilaments come from?

1.3 Ca^{2+} induced Ca^{2+} release (CICR) from the sarcoplasmic reticulum

In experiments involving the removal of the sarcolemma from Purkinje fibres using meticulous micro-dissection together with microprocessor-induced rapid changes of $[\text{Ca}^{2+}]$, Fabiato (1985) showed the second source of Ca^{2+} to be the sarcoplasmic reticulum (SR) [13-15]. Rapid exposure of Ca^{2+} (approx. 1ms) to the SR, triggers release of its stored Ca^{2+} and the

development of myofilament tension, a mechanism referred to as Ca^{2+} induced Ca^{2+} release (CICR). It is conceivable that the natural origin of this simulated Ca^{2+} trigger comes from the extracellular Ca^{2+} pool, the quantity of which is insufficient to cause a twitch in itself. This importantly implies that the process of CICR is able to amplify a small Ca^{2+} influx.

1.4 The sarcoplasmic reticulum (SR)

The SR is an intracellular organelle, which is intricately wrapped around the myofilaments [16]. Some of the SR lies adjacent to the T-tubules in expanded sacs known as junctional SR (terminal cisternae) and depending on their arrangement are termed dyadic or triadic junctions where triadic implies that two terminal cisternae lie either side of a T-tubule. There can also be junctions with the remaining sarcolemma (surface sarcolemma) or unattached SR expansions (corbular SR). That there is a higher proportion of the sarcolemma involved as a dyad in the rat (6.5-7.7% surface, 40-48% T-tubular) than rabbit (4.6 % surface, 20.6% T-tubular) [3;9] is of functional relevance. The rat twitch is more dependent on triggered SR Ca^{2+} release during CICR than on exposure to external Ca^{2+} , unlike the rabbit whose external Ca^{2+} contribution is greater than the rat.

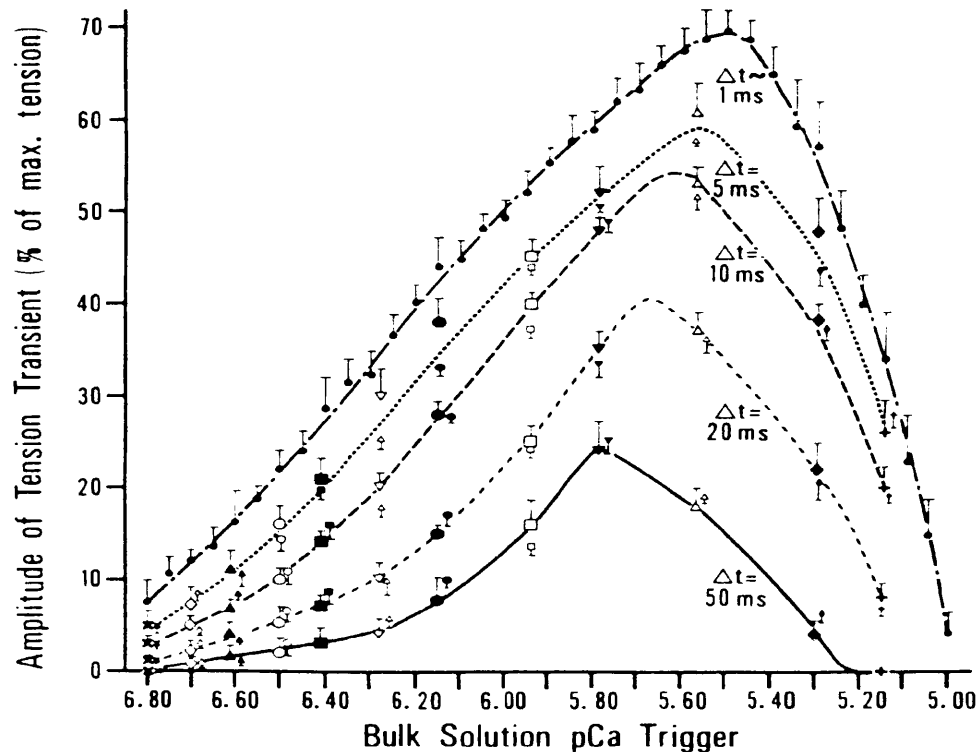


Figure 1.3 Characteristics of CICR in skinned purkinje fibres

As pCa trigger increases so does the amplitude of tension – (amplification). Above a supra-optimal $[\text{Ca}^{2+}]$, tension declines. Data is also shown for differing rates of application of trigger $[\text{Ca}^{2+}]$. Small filled black circles showing highest values are triggers induced by a very rapid micro-injection and subsequent aspiration of the solution, other rates are values are achieved by the mixing of high and low $[\text{Ca}^{2+}]$ solutions to vary rate of change of free $[\text{Ca}^{2+}]$ ($t=1-50\text{ms}$). Overall it can be seen that SR Ca^{2+} release is dependent on both the size of the trigger and its rate of $[\text{Ca}^{2+}]$ change – (graded response). (Figure taken from Fabiato, (1985) *J.Gen. Physiol.* 85 247-289).

As demonstrated by the pioneering work of Alex Fabiato, there are two main features of CICR in cardiomyocytes - amplification and the associated graded nature of the process. Application of increasing amounts of trigger Ca^{2+} , results in greater SR Ca^{2+} release, inducing a larger contracture (Figure 1.3). However if increasing supra-optimal amounts of Ca^{2+} are applied then tension begins to decrease. Additions of higher $[\text{Ca}^{2+}]$ ($10\mu\text{M}$)

to a skinned cell immediately after initiation of Ca^{2+} release results in almost complete inactivation of SR Ca^{2+} release. CICR also depends on how fast trigger Ca^{2+} is reached (time dependency). A faster trigger ($\sim 1\text{ms}$ compared to 50ms) leads to greater maximum tension development and an increase in the optimal amount of Ca^{2+} above which tension decreases (Figure 1.3). Therefore the Ca^{2+} inactivating effect occurs at lower $[\text{Ca}^{2+}]$ when the trigger $[\text{Ca}^{2+}]$ takes longer to be reached [14].

1.5 Identifying the source of the simulated Ca^{2+} entry during CICR

The trigger Ca^{2+} was simulated in the above experiments [14] by rapid solution changes. Is there a natural influx of Ca^{2+} that acts as a substitute for this simulation in the cardiomyocyte? There are many dyadic junctions in cardiomyocytes putting LCCs in the vicinity of the SR terminal cisternae. Located on these SR structures are the Ca^{2+} release channels/ryanodine receptors (RyRs). Many investigators have looked at the role of CICR in intact cardiomyocytes in particular the role Ca^{2+} entry via LCC plays in triggering CICR.

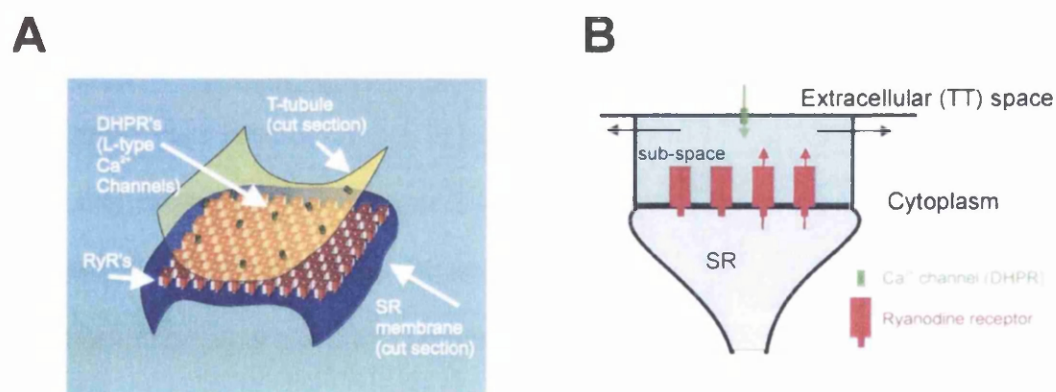


Figure 1.4 Location of LCCs and RyRs

Panel A shows a cut section of the T-tubule above which are located the LCC/Dihydropyridine receptors (DHPRs). These are in close apposition to the RyRs

located on the SR terminal cisternae. The close proximity of these two surfaces however forms a cleft/sub space as seen in panel B. The arrows in panel B denote routes of Ca^{2+} flux into and out of this cleft during CICR. (Figure taken from Sobie *et al.* (2002) *Biophys. J.* 83, 59-78).

The most compelling evidence that L-type Ca^{2+} influx is the trigger for SR Ca^{2+} release is demonstrated by the similarity between the relationship of (a) voltage dependence and L-type Ca^{2+} current, (b) SR Ca^{2+} release (Ca^{2+} transient), and (c) contraction [9;17-20] (Figure 1.2 Panel B). Proof that CICR occurs in intact cardiomyocytes is reinforced by the finding that the influx of Na^+ or Ba^{2+} current through the LCC does not elicit a Ca^{2+} transient even though there is still Ca^{2+} within the SR [21]. More technical approaches to demonstrate CICR in intact cardiomyocytes have involved the use of photolabile Ca^{2+} chelators. These have been performed in skinned cardiomyocytes [22], rat cardiomyocytes without voltage clamp [23] and with voltage clamp [24;25]. Cannell *et al* (1987) showed that LCC tail currents could elicit Ca^{2+} transients and cellular contraction [26]. This particular study also raised the possibility of an E_m dependence on CICR since Ca^{2+} transients were smaller when early repolarisation was induced. Several observations from various studies including: (1) the similarity between voltage dependence in L-type Ca^{2+} current and Ca^{2+} transient [17], (2) that caged Ca^{2+} can trigger SR Ca^{2+} release independent of membrane potential [25], (3) the methods using prevention of I_{Ca} at different potentials equivalently suppress Ca^{2+} transients [27] all suggest that E_m dependence is not important during CICR and it is sarcolemmal entry of Ca^{2+} that triggers SR Ca^{2+} release.

1.6 Problems associated with the theory of CICR

CICR implies in its title that a single trigger of Ca^{2+} can induce the release of SR Ca^{2+} . In theory, this initial release of SR Ca^{2+} could act as an independent trigger. This would stimulate further SR Ca^{2+} release and generate a positive feedback loop. This mechanism would be inherently unstable since there would be no negative feedback event to stop the cascading release of SR Ca^{2+} . However, under normal circumstances this does not happen. As described above, in intact cells, SR Ca^{2+} release is tightly controlled by L-type Ca^{2+} entry, i.e. they follow the same voltage dependent bell shaped relationship. Ca^{2+} entry via LCC stimulates a SR Ca^{2+} release that does not continually produce more and more Ca^{2+} . RyR mediated SR Ca^{2+} release is controlled by the LCC such that if the cardiomyocyte is repolarised to the holding potential or the Ca^{2+} reversal potential for LCC during the rising phase of the Ca^{2+} transient, SR Ca^{2+} release is suppressed [26]. How then does L-type Ca^{2+} current control CICR and prevent positive feedback?

1.7 Preventing positive feedback

Fabiato (1985) showed that the process of CICR was inactivated at high $[\text{Ca}^{2+}]$ and proposed a model whereby the process of CICR could be controlled [14]. The model was that the trigger Ca^{2+} activated binding sites on the SR Ca^{2+} release channel with a relatively low affinity but high on rate. These sites acted to stimulate Ca^{2+} release. However, the same trigger Ca^{2+} would also inactivate SR Ca^{2+} release by binding to a second type of site with higher affinity but slower association constant. Application of supra-optimal amounts of Ca^{2+} would therefore inhibit Ca^{2+} release by

overcoming the slower on rate to the inhibitory binding site. Unfortunately no intact cardiomyocyte work has provided evidence for Fabiato's inactivation model enabling prevention of a positive feedback response. In fact, the opposite has been observed. Nabauer *et al* (1990) used flash photolysis of caged Ca^{2+} during the rising phase of contraction in order to reproduce Fabiato's model of inactivation but showed an increase in contraction (it is possible that the release of Ca^{2+} by photolysis might not have been sufficient to result in inactivation however) [24].

Cannell *et al* (1987) also suggested that Fabiato's inactivation model is hard to reconcile with current experimental evidence [26]. If the cell is rapidly repolarised during the Ca^{2+} transient's rising phase the peak of the Ca^{2+} transient is depressed. Using Fabiato's model, one possible explanation is that during the very short time taken to deactivate LCCs by repolarisation, the influx of Ca^{2+} by LCC is increased due to the increased electrochemical drive. This could inactivate further SR Ca^{2+} release. However Cannell *et al* (1987) calculated that the repolarisation performed in this study from -24mV to -54mV could not increase the Ca^{2+} entry by more than 20% [26]. This entry of Ca^{2+} was not sufficient in time or quantity to account for the marked suppression of the Ca^{2+} transient. Furthermore Fabiato's inactivation theory was even harder to reconcile with experiments showing depolarisations inducing larger Ca^{2+} entry and thereby increasing the amplitude of the Ca^{2+} transient when by Fabiato's model, they should result in more suppression [26].

Cannell *et al* (1987) also suggested that perhaps the termination of Ca^{2+}

entry via the LCC during repolarisation decreases the binding of Ca^{2+} to the activator site and prevents autonomous SR Ca^{2+} release [26]. However, SR Ca^{2+} release is much larger than LCC entry, which suggests that the activation site will not deplete of Ca^{2+} [26].

One final important observation in intact cells that is hard to reconcile with the model of Fabiato is the asymmetrical nature of the bell shaped relationship between L-type Ca^{2+} current and Ca^{2+} transient peak (Figure 1.2 Panel B). If for instance an equivalent normalised I_{Ca} current is examined at both positive and negative E_m , a larger Ca^{2+} transient is observed at the negative cell membrane potential [9;17]. Fabiato's theory of CICR has no explanation of this phenomenon since the same trigger Ca^{2+} (I_{Ca}) should release the same amount of SR Ca^{2+} independent of how that trigger is achieved.

1.8 A model of CICR that begins to fit the experiments

Authors who had attempted to devise mathematical models of CICR also found it hard to reconcile the experimental evidence for CICR in intact cells and that of Fabiato's work in skinned cells. A theoretical paper by Stern (1992) however established a theory that enabled the intrinsic positive feedback effect of CICR to be overcome and the potential for SR Ca^{2+} release to be graded by the L-type Ca^{2+} influx [28].

Previously, the intact cardiomyocyte was conceived as a 'common pool' model. This implies that trigger Ca^{2+} reaches the SR via the same cytosolic Ca^{2+} pool into which the SR Ca^{2+} is released [29]. However by using this

type of model, CICR cannot achieve an amplification of trigger Ca^{2+} while still being able to prevent regenerative SR Ca^{2+} release. There is such a small window whereby both parameters are viable before instability arises. This is not thought to be a realistic way to regulate such a vital body system.

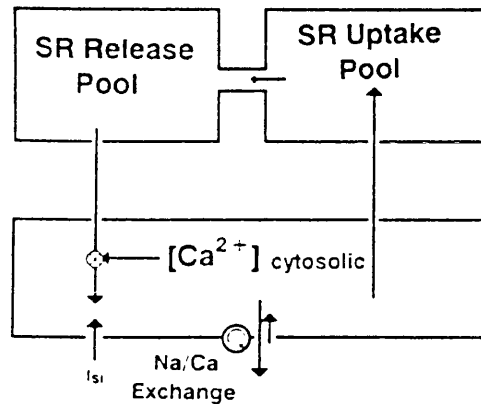


Figure 1.5 'Common pool' model for CICR

Ca^{2+} that leaves enters and leaves the cell does so via the same pool of cytosolic Ca^{2+} (I_{si} = Ca^{2+} entry via LCC). (Figure taken from Stern (1992) *Biophys. J.* 63 497-517).

Stern (1992) therefore looked at the ultra-structure of the cardiomyocyte [28]. Using the knowledge that in skeletal muscle the LCC lies in direct apposition to the Ca^{2+} release channel (RyR) [30], Stern devised a 'local control' as oppose to a 'common pool' model. The local control model relies on the ability of the LCC to have privileged access to the RyR. Due to the location of these components the sensitivity to Ca^{2+} can be lower. However, regeneration in these local control models does not occur because of the all-or-none nature of the single channel openings and the short diffusion times in the cleft between the channels. Firstly Stern devised a ' Ca^{2+} synapse' model, which involves a scenario whereby each SR release channel is immediately opposite and controlled by a

sarcolemmal LCC. The termination of Ca^{2+} release from the RyR can either be random, which if long enough allows the Ca^{2+} in the vicinity to diffuse away, or Ca^{2+} dependent in which the channel will still close at a finite rate and again the Ca^{2+} diffuses away from the cleft region between the LCC and RyR.

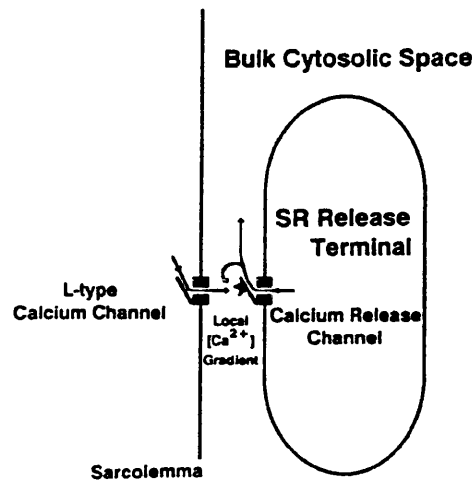


Figure 1.6 Local control theory for CICR

Ca^{2+} 'synapse model' would suggest that each RyR is controlled by Ca^{2+} released by one LCC. (Figure taken from Stern (1992) *Biophys. J.* 63 497-517).

Both of these mechanisms are considered equivalent and prevent positive feedback. This model has characteristics enabling the amplification of trigger Ca^{2+} and for amplified Ca^{2+} release to be graded by LCC. However the system requires an unreasonable conductance for a single SR Ca^{2+} release channel. A way around this problem is to have a number of SR Ca^{2+} release channels (a cluster) each channel having a smaller conductance but all channels in the cluster being governed by a single LCC. This is referred to as a 'cluster bomb' model. Within a cluster, Ca^{2+} release can be regenerative; however a single cluster cannot trigger release in an adjacent cluster because they are separated from one

another. This model therefore allows for amplification of trigger $[\text{Ca}^{2+}]$ (since one LCC activates a number of SR Ca^{2+} release channels) and provides a mechanism for SR Ca^{2+} release to be graded (since the trigger can recruit varying numbers of clusters).

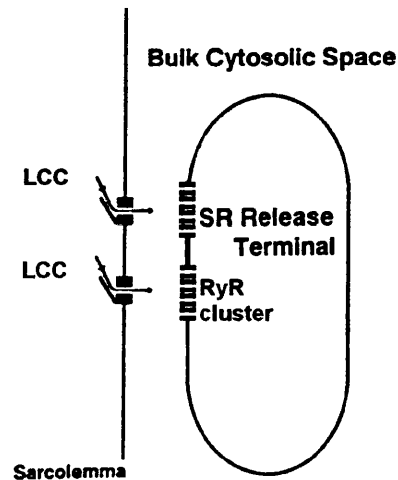


Figure 1.7 'Cluster bomb' model

The release of Ca^{2+} from a single LCC induces release of Ca^{2+} from a cluster of RyRs which is discretely spaced from the adjacent cluster of RyRs. (Figure taken from Stern (1992) *Biophys. J.* 63 497-517).

Although the clusters are spatially discrete and prevent positive feedback, positive feedback does exist within an individual cluster and its termination is essential. This will be discussed later.

1.9 Evidence for local control of CICR

Evolving technological advances in the ability to resolve temporal and spatial changes in intracellular $[\text{Ca}^{2+}]$ (especially line-scan confocal imaging (LSCM)) revealed evidence for local rises of $[\text{Ca}^{2+}]$ thought to originate from clusters of RyR as proposed by Stern (1992).

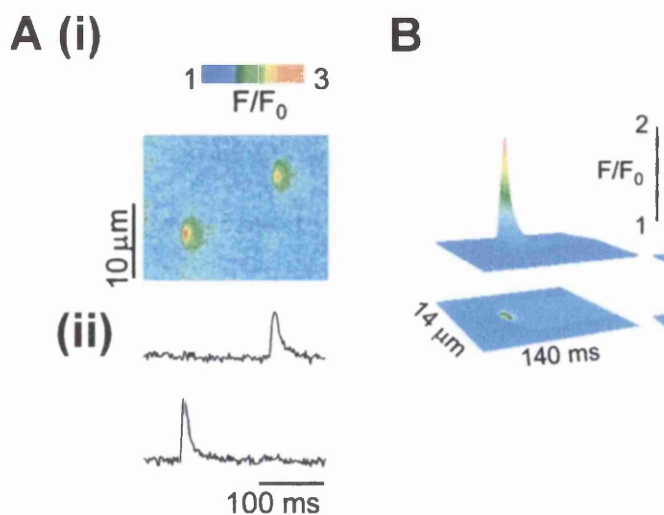


Figure 1.8 Ca^{2+} Sparks

Panel A(i) shows a line scanning confocal image of Ca^{2+} sparks with corresponding line profiles of these sparks in panel A(ii) top and bottom. Panel B shows a characteristic 3D plot and contour map of a Ca^{2+} spark. (Figure adapted from Terentyev *et al.* (2002) *Circ. Res.* 91, 414).

Cheng *et al* (1993) visualised these events for the first time in cardiomyocytes [31]. The events are termed Ca^{2+} sparks and provide some experimental evidence for Stern's mathematical modelling.

1.10 Ca^{2+} sparks - a more complete picture of CICR

Ca^{2+} sparks are local spontaneous increases in cytosolic $[\text{Ca}^{2+}]$, approximately 200nM, $2\ \mu\text{m}$ in diameter (confocal section), with a half-time decay of 25ms (compared to Ca^{2+} transients which can have a half-time decay of 164ms [31]. These events occur at a low rate at resting $[\text{Ca}^{2+}]$ (approx 150nM) with a frequency of 100 sparks/cell/s. Cheng *et al* (1993) showed that the Ca^{2+} flux of the Ca^{2+} spark is $2 \times 10^{-17}\ \text{mols}\cdot\text{s}^{-1}$, which is equivalent to approximately a current of 4pA. Due to this flux estimate the Ca^{2+} spark was thought to originate from a single RyR [32]. However at

present this is not thought to be the case, a point that will be discussed later. The Ca^{2+} spark originates from the SR and can be blocked by $1\mu\text{M}$ ryanodine. Lower concentrations of ryanodine ($100\text{-}300\text{nM}$ for $1\text{-}3\text{min}$) increase the frequency of Ca^{2+} sparks by approximately >2.2 fold although spark morphology remains unchanged. This is in line with the understanding that ryanodine increases the open probability of RyR at low concentrations and very high concentrations block the RyR. Intermediate concentrations can induce sub-conductance states that appear in a line-scan image as sparks with long durations $>1\text{s}$ but with a consistent amplitude, suggesting that the local SR is not depleted of Ca^{2+} during such long releases.

The discovery of local Ca^{2+} sparks without regenerative propagation provides physical evidence for the 'cluster bomb' theory [28]. It is still possible that all-or-none responses occur within a cluster of RyRs, however since clusters have a low sensitivity to trigger $[\text{Ca}^{2+}]$ and are more than likely spatially discrete, Ca^{2+} release by a cluster can still be localised. However, if external $[\text{Ca}^{2+}]$ is raised then the frequency of Ca^{2+} sparks increases. If a certain threshold is reached macro-sparks are produced. These are thought to be due to summation of a number of Ca^{2+} sparks and have accumulatively larger amplitudes (approx. 500nM). They usually occur at the beginning of Ca^{2+} waves, which are spontaneous releases of $[\text{Ca}^{2+}]$ that propagate from one end of the cell to the other. Since ryanodine increases the frequency of localised Ca^{2+} sparks but does not lead to propagating Ca^{2+} waves, an additional factor must be involved in producing Ca^{2+} waves other than a simple increase in spark frequency. This is now

thought to be the regulation of RyR by SR $[\text{Ca}^{2+}]$ content [33]. Ca^{2+} waves can be inhibited by high concentrations of ryanodine and therefore are also a result of SR Ca^{2+} release [31].

1.11 Why are Ca^{2+} sparks helpful in understanding EC-coupling

The production of Ca^{2+} sparks result from spontaneous SR Ca^{2+} release at resting $[\text{Ca}^{2+}]$ levels in the cardiomyocyte; however sparks can also be triggered by electrical depolarisation.

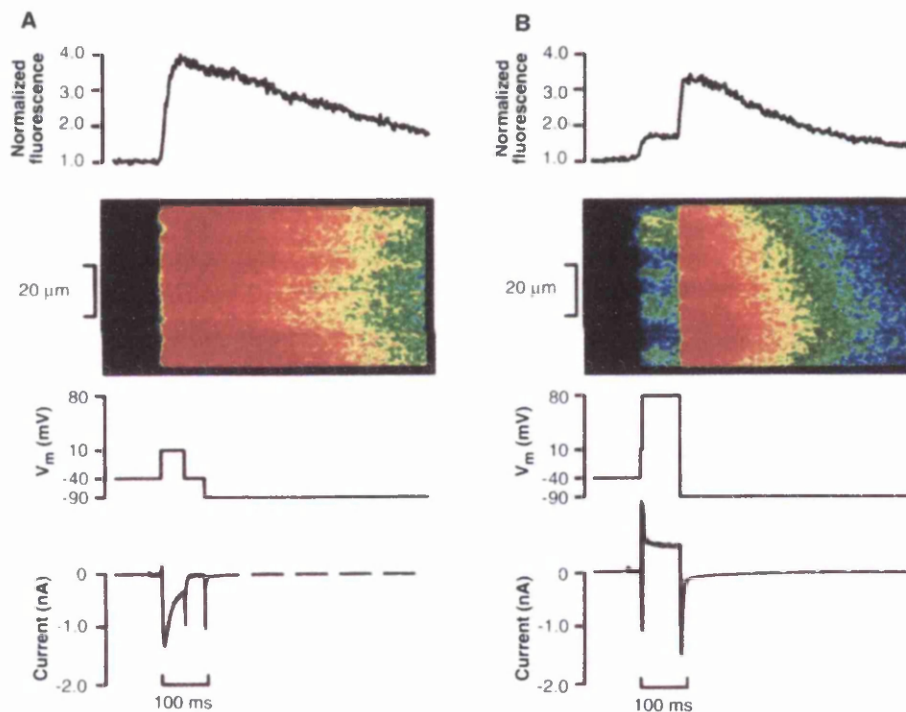


Figure 1.9 Depolarisation duration effects on the Ca^{2+} transient

Panel A from top to bottom shows, spatially averaged Ca^{2+} transients, corresponding confocal linescan image, membrane potential and membrane current. This cell is depolarised for 50ms leading to a uniform release of SR Ca^{2+} . Panel B follows the same format as Panel A. The LCC is activated for 3ms and then terminated abruptly by further depolarisation to +80mV for 80ms. Repolarising the cell to -90mV then produces the tail current. The abruptly terminated SR Ca^{2+} release is sparse whereas the tail current produces a more uniform release of SR Ca^{2+} . (Figure taken from Cannell (1995) *Science*)

268, 1045-1049).

Cannell *et al* (1995) developed this concept in a key study [34]: As discussed (section 1.5), the Ca^{2+} transient is a combination of the Ca^{2+} entry via LCCs (and possibly $\text{Na}^+/\text{Ca}^{2+}$ exchange) and SR Ca^{2+} release. It is the Ca^{2+} influx via the LCC, which regulates the transient in a strict manner. Ca^{2+} sparks are also a result of SR Ca^{2+} release and Cannell *et al* (1995) were able to identify the link between the Ca^{2+} transient, Ca^{2+} spark and the way they are both controlled by Ca^{2+} influx via LCCs. Cannell *et al* (1995) [34] repeated some experiments performed in 1987 [26] using the technique of voltage clamp but this time while imaging Ca^{2+} using confocal line-scan imaging. When cardiomyocytes are depolarised for 3ms from -40mV to +10mV the Ca^{2+} released from the SR can be abruptly terminated before the peak [Ca^{2+}] by further depolarising the cell to +80mV. Repolarising the cell back to -90mV produces a tail current. The tail current produces a synchronous release of SR Ca^{2+} albeit with a lower amplitude. (The tail current occurs since when the cell is depolarised to +80mV the Ca^{2+} channel opens but the driving force for Ca^{2+} entry is small, hence when repolarised to -90mV the driving force for Ca^{2+} increases such that the influx of Ca^{2+} through the open channels occurs before they can deactivate). However, if the initial abruptly terminated Ca^{2+} release is observed using confocal line-scan imaging it can be seen to occur at sparse points along the cell. These points change each time the protocol is performed (Figure 1.9 Panel B). The events resemble Ca^{2+} release at discreet sites. It was this observation that provided an indication that LCCs could trigger Ca^{2+} sparks.

1.12 Evidence that Ca^{2+} sparks are triggered by LCCs

Individual Ca^{2+} sparks can be triggered if short periods of depolarisation are performed from -40mV to -5mV for 0.75ms [34]. Further more, Ca^{2+} sparks are also triggered if the cell is depolarised from -50mV to -35mV albeit with a latency of $<2\text{ms}$. The Ca^{2+} sparks evoked have the same morphology as those occur during spontaneous Ca^{2+} sparks. The latency associated with the appearance of these events at more negative potentials but with similar morphology to Ca^{2+} sparks at more positive potentials (and spontaneous Ca^{2+} sparks), suggests that the latency is associated with a lower probability of LCC opening. This also suggests that the size of the Ca^{2+} spark is independent of Ca^{2+} entry via LCC and is a function of RyR. It follows from these observations that Ca^{2+} sparks are triggered via Ca^{2+} influx associated with LCC and that large influxes of Ca^{2+} can lead to the production of a large number of sparks which when temporally and spatially combined produce the Ca^{2+} transient. Further evidence that suggested that the Ca^{2+} transient is a result of the temporal-spatial summation of Ca^{2+} sparks can be seen when the LCC current is reduced via L-type channel antagonists [31;35] or low $[\text{Ca}^{2+}]$ [36] whereby Ca^{2+} sparks are easier to resolve.

1.13 The use of Ca^{2+} sparks to explain Ca^{2+} transient characteristics

With knowledge that the Ca^{2+} transient is the result of Ca^{2+} sparks, an explanation for the larger Ca^{2+} transients seen at more negative potentials and hence the asymmetry of the relationship between the L-type Ca^{2+} current and E_m discussed earlier can be provided. At more negative voltages the probability that a single LCC is open is lower than at more

positive potentials, however when a single LCC does open there is a larger flux of Ca^{2+} through it due to a higher electrochemical drive (Figure 1.10 panel A). The electrochemical driving force for Ca^{2+} entering the cell falls at more positive membrane potentials. Santana *et al* (1996) described the E_m dependence of a single channel i_{Ca} and showed that the spark probability normalised to i_{Ca} follows the same relationship as i_{Ca} (Figure 1.10 Panel B) [37]. Hence there is a greater influx of Ca^{2+} through an open channel at more negative potentials than at positive potentials, which in turn is more likely to trigger RyRs. This could not have been accounted for by Fabiato's work, which would have predicted the same release of SR Ca^{2+} independent of how the trigger was achieved.

To trigger a Ca^{2+} spark by Ca^{2+} entry via LCC requires at least $8\mu\text{M}$ $[\text{Ca}^{2+}]$ within a distance of $<20\text{nM}$. This can only be achieved by the close apposition of the LCC and RyR cluster [26].

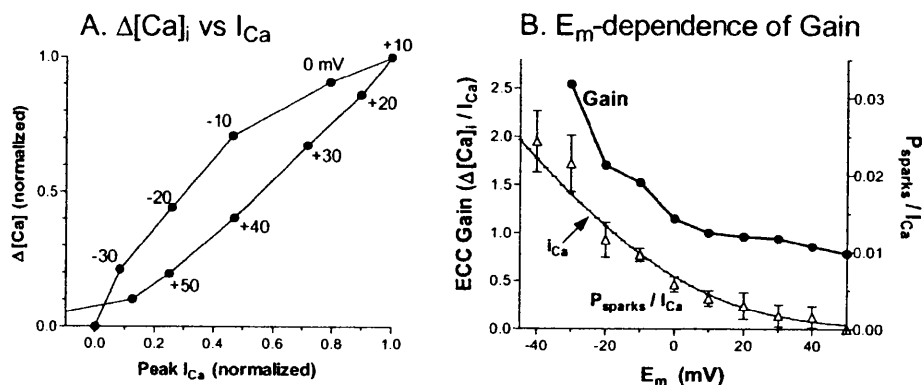


Figure 1.10 Asymmetrical voltage dependence of the Ca^{2+} transient

Panel A shows the relationship between normalised peak i_{Ca} and the amplitude of the normalised Ca^{2+} transient. It is noted that at the same i_{Ca} the Ca^{2+} transient is larger at more negative membrane potentials. Panel B takes the data from Panel A and calculates

the gain in relation to the membrane voltage. This follows the same relationship between membrane voltage and the probability of Ca^{2+} sparks occurring. Figures taken from Bers (2001) *Excitation-Contraction Coupling and Cardiac Contractile Force*, 2nd edition, Kluwer Academic, Dordrecht, Netherlands adapted from data by Beuckelmann *et al.* (1988) *J. Physiol.* 405 233-255 (Panel A) and Santana *et al.* (1996) *Circ. Res.* 78, 166-171 (Panel B).

This close proximity is critical since $[\text{Ca}^{2+}]$ in this small cleft will decrease rapidly when I_{Ca} influx terminates due to diffusion of Ca^{2+} out of the space formed between the two channels [9]. This is a further indication that only a single LCC can activate a cluster close to it within the cleft and not one further away. This principle leads to the localisation Ca^{2+} sparks.

1.14 How many LCCs are required to trigger a cluster of RyRs?

If the LCC is really the trigger for SR Ca^{2+} release then the rate of spark production should be related to the voltage dependence of the L-type Ca^{2+} current. If a cell is slowly depolarised from -70mV to -40mV i.e. over a range of voltages where the probability of channel opening is very low and opens by chance, Ca^{2+} sparks within the same cell also activate stochastically. Furthermore, between -70mV to -40mV, the Ca^{2+} spark rate increases exponentially to the same extent as the activation curve of LCC [34]. This observation provides evidence that a single LCC opening can trigger a Ca^{2+} spark [34]. Many subsequent papers have confirmed this [35;37;38]. It must be noted however that these experiments were carried out using protocols that reduced the probability of Ca^{2+} spark production. However, a recent study by Inoue *et al* (2003) uses a protocol that does not block LCC (i.e. by low external $[\text{Ca}^{2+}]$ or antagonists) a factor which increases the likelihood that a single LCC activates a single Ca^{2+} spark

[39]. The study firstly establishes the probability with which Ca^{2+} sparks are evoked by an action potential (AP) shaped voltage command using 2mM EGTA in the pipette solution. The probability that a Ca^{2+} spark appears with each AP is approximately unity (events being activated 2-6ms after the peak). Using unitary current recordings of LCC by voltage clamp, the authors also establishes that the probability of a single LCC opening at least once within 2-6ms after depolarisation is approximately 0.87, i.e. much lower than the spark probability. Therefore from this data Inoue *et al* (2003) suggests that at least 3-11 LCCs are required to produce a Ca^{2+} spark at the beginning of an action potential with a probability of approximately unity. Anatomical observations also suggest that this may be the case [40]. Wang *et al* (2001) acquired direct visualisation of a single LCC Ca^{2+} influx (Ca^{2+} sparklet) concurrent with Ca^{2+} spark measurements [41]. This meticulous work reinforces three principal ideas involving local control of CICR. Firstly, the visualised Ca^{2+} sparklet can be used as a representative measure of LCC unitary current (i_{Ca}) and under loose voltage clamp conditions the proportion of sparklets able to trigger a Ca^{2+} spark (LCC-RyR coupling fidelity) is 0.71, i.e. less than unity. Secondly, where a Ca^{2+} spark is successfully triggered the ability of the second sparklet to produce another Ca^{2+} spark is reduced, showing therefore use-dependent inactivation or adaptation of RyR (a point that will be discussed later). Thirdly, abolition of the sparklet during depolarisation by $2\mu\text{M}$ nifedipine or substitution of Ca^{2+} in the pipette with 20mM Ba^{2+} suggests that the sparklet is necessary for Ca^{2+} spark production and not merely changes in membrane voltage.

1.15 How many RyRs contribute to a Ca^{2+} spark?

Originally Cheng *et al* (1993) suggested that a Ca^{2+} spark was due to the flux associated with a single RyR (4pA x 10s) [31]. However, since it is now recognized that the Ca^{2+} flux through a single RyR is approximately 0.35-0.6pA [42] the Ca^{2+} spark must be a product of a number of RyRs. Wang *et al* (2001) using visualisation of the sparklet and Ca^{2+} spark showed that the rate of rise of the sparklet is seven times lower than Ca^{2+} sparks and from this the Ca^{2+} spark flux is calculated as approximately 2.1pA [41]. This is in agreement with other studies (2-10pA) [31;43;44]. Hence a sparklet [41] is thought to trigger 4-6 RyRs to generate a Ca^{2+} spark. Various studies produce results that resemble these numbers of RyR (6-20) [45;46]. Large numbers of RyRs (90-267) in a dyadic junction have been revealed using micrographs [47]. On average there are thought to be 100 RyRs [48]. In summary, functional studies suggest that various numbers of RyRs are in a functional cluster. These estimates are all less than ultrastructural micrographs measurements would suggest.

1.16 How do Ca^{2+} sparks contribute to the graded amplified nature of CICR

Entry of Ca^{2+} via LCCs only acts as a trigger for Ca^{2+} sparks. The spark size does not get larger if a greater amount of Ca^{2+} comes through LCC. How then is the trigger graded and amplified? The graded nature of CICR is a result of altering the probability of Ca^{2+} spark production. This explains the complex relationship between I_{Ca} , i_{Ca} , Ca^{2+} transient amplitude, and E_m discussed earlier. It must be remembered though that the Ca^{2+} spark is a function of the RyR and although whether it is elicited, depends on the

above parameters, once triggered, is independent of them. How then is trigger amplified? Cannell *et al* (1995) discussed how amplification comes from two mechanisms [34]. Firstly, the conductance of the RyR (2.2pA - see NB. below) [49] is greater than the LCC (0.3pA) [50]. Secondly, since RyRs are thought to be clustered and governed by a single or smaller number of LCCs, the conductance will be further increased [28;51]. This is referred to as analogue gain. (NB. Cannell *et al* (1995) had suggested that the flux associated with a single RyR was 2.2pA using a study by Rousseau *et al* 1989 [49]. While this value agrees with the flux associated with a Ca^{2+} spark (2.1pA) it does not agree with recent estimates of the unitary Ca^{2+} associated with the RyR (0.35-0.6pA) [42]). The final conclusions about analog gain are not changed however since the flux from the whole cluster producing the spark is still much larger than i_{Ca}). Thirdly, once triggered by LCC the cluster of RyRs will produce Ca^{2+} release that is regenerative but unable to reach the next cluster (as discussed above). The duration of this type of release is longer than the release associated with a LCC. This type of amplification has been referred to as digital 'pulse stretching' gain [34] (Figure 1.11).

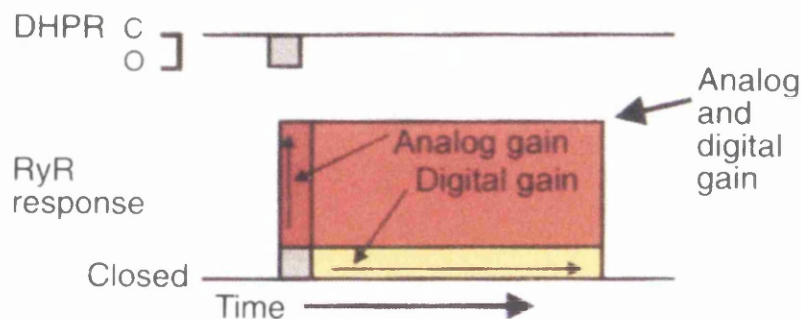


Figure 1.11 The analog and digital gain of CICR

A schematic to illustrate digital and analog gain. Both of these processes contribute to the

amplification factor applied to a small trigger $[\text{Ca}^{2+}]$ via the dihydropyridine receptor/LCC, which opens (O) and closes (C). The product of the analog and digital gain represents the overall gain of CICR. (Figure taken from Cannell *et al.* (1995) *Science* 268, 1045-1049).

1.17 How is a Ca^{2+} spark terminated?

So far the discussion has focused on how Ca^{2+} sparks are triggered. However, once triggered the RyR cluster releases Ca^{2+} independent of the entry of Ca^{2+} via LCC. In fact Cannell *et al* (1990) showed that the intracellular $[\text{Ca}^{2+}]$ during a transient continues to rise for approximately 10ms after I_{Ca} has terminated [34]. This suggests that once triggered the Ca^{2+} spark continues to rise due to the intrinsic function of the RyR cluster. The spatial separation of the clusters, which is thought to be present, prevents a global all-or-none response. However, within a cluster the response is very much a positive feedback event that requires a mechanism to terminate. This is essential if the $[\text{Ca}^{2+}]$ in the cleft is to diffuse away and thus be ready again for initiation on the next stimulation. How does termination therefore occur? There are various theories.

Before Ca^{2+} sparks were visualised, Stern (1992), had suggested several mechanisms for RyR cluster termination [28]. One such mechanism is **stochastic attrition**. This would suggest that at any particular moment after being triggered a proportion of RyRs within a cluster could close at the same time by chance. This would lower the threshold for further regenerative release and the remainder of the RyRs in the cluster would close. However while this mechanism certainly holds true for 3-6 RyR this becomes harder to accomplish if more RyR receptors are involved in the cluster, in fact if 10 RyR are involved then the cluster tends to 'latch open'

[28]. Since the number of RyRs in a cluster is controversial and may be as high as 100 [52] this mechanism is not likely to be the sole reason for Ca^{2+} spark termination.

Fabiato (1985) proposed a model whereby **Ca^{2+} -dependent inactivation** of RyR could prevent an all-or-none response (discussed above). This particular mechanism has not been observed in intact cardiomyocytes, in fact the opposite has been observed when simulated by caging compounds [24]. The mechanism has been observed in isolated SR vesicles, however the $[\text{Ca}^{2+}]$ required to inactivate the channel was in the mM range (approximately 10mM) whereas the $[\text{Ca}^{2+}]$ thought to be in the vicinity of the RyR cluster is 10-100 μM [53]. Physiological solutions also result in shifts of the $[\text{Ca}^{2+}]$ dependence of release far to the right of Fabiato's work [54][13;15;55]. Using confocal imaging and the use of Ca^{2+} spikes, Sham *et al* (1998) demonstrated that **use-dependent inactivation** of RyRs is the main mechanism for Ca^{2+} spark termination, while ruling out stochastic attrition or depletion of local SR Ca^{2+} [56]. LCC triggers are able to produce Ca^{2+} spikes but when repeated or prolonged are unable to reproduce those spikes. Furthermore, tail currents are also unable to reactivate the Ca^{2+} spikes. This is described as **absorbing inactivation** since the RyR cannot open again until it recovers. A problem with this experiment however was the use of high concentrations of EGTA (4mM) to produce Ca^{2+} spikes which may hide the real mechanisms occurring since, (1) additional buffering may decrease the ability of RyR to activate other RyRs within a cluster and therefore alter Ca^{2+} spark morphology, and/or (2) reduced activation of adjacent RyRs may indirectly reduce inactivation,

and/or (3) additional cell buffering may decrease Ca^{2+} uptake by SERCA leading to SR Ca^{2+} depletion [9]. It is therefore unknown how important this potential mechanism is in Ca^{2+} spark termination. Wang *et al* (2001) using visualisations of sparklets and Ca^{2+} sparks showed that the coupling fidelity between the two events is 0.71 on the first trigger but decreases to 0.30 if the stimulation occurs again at the same site [41]. This also suggests some kind of use-dependent inactivation however it is hard to separate this from local SR Ca^{2+} depletion that may also aid the termination of Ca^{2+} sparks.

It is also possible that RyR **adaptation** aids Ca^{2+} spark termination. Adaptation occurs when after activation of RyR the initial high open probability reduces gradually to a lower open probability but still maintains its ability to be reactivated by a sufficient trigger. However, this may occur too slowly and incompletely for Ca^{2+} spark termination [9;57;58].

It is possible that local **SR Ca^{2+} depletion** occurs in the vicinity of the Ca^{2+} spark and therefore reduces the possibility that the cluster is able to release further Ca^{2+} . However this is hard to reconcile with observations of prolonged Ca^{2+} sparks (>1s) during application of low concentrations of ryanodine. These Ca^{2+} sparks manage to maintain constant amplitude, which would be hard to achieve if the local SR [Ca^{2+}] were being depleted [31]. Furthermore during a Ca^{2+} transient, the SR is not thought to completely empty of Ca^{2+} [59;60]. It could be that movement of Ca^{2+} from different sites within the SR play an important part in maintaining a releasable amount of Ca^{2+} while preventing full SR depletion.

SERCA molecules within the vicinity of RyR clusters (co-localised) could act to terminate Ca^{2+} sparks by aiding faster diffusion of Ca^{2+} from the release sites and thereby increasing the probability that the cluster closes by stochastic attrition. However, no evidence exists for this theory at present.

It can be seen that each of the above mechanisms have evidence against the likelihood of it being the prime way in which Ca^{2+} sparks terminate, however one recent study devises a theory which fits the majority of experimental data [48]. Recent anatomical observations suggest that clusters of RyRs are arranged in arrays such that, the channels touch each other at their corners, with an accessory protein called FK-506 binding protein (FKBP) at or near the point of contact [61;62]. A model called the “**sticky cluster** model” (Figure 1.12) incorporates this concept. The “sticky” refers to the observed phenomenon of ‘coupling’ that exists between isolated RyRs due to the accessory protein FKBP, i.e. FKBP allows for simultaneous openings/closings of RyRs when grouped together [63].

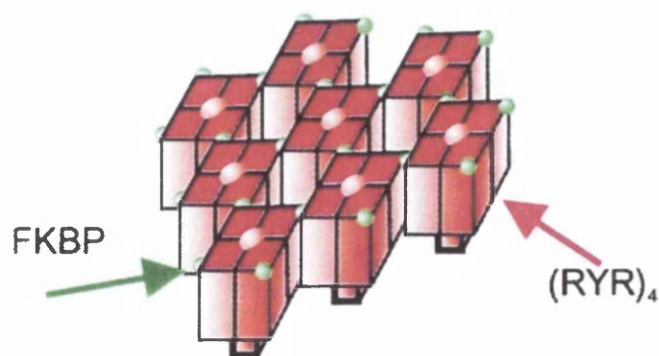


Figure 1.12 The ‘sticky cluster model’

A schematic illustrating the location of FKBP in relation to the RyRs within a cluster.

(Figure taken from Sobie *et al.*(2002) *Biophys. J.* 83, 59-78).

There are three major themes that underlie this model: (1) by defining coupling, using a cooperativity factor (1 being high, <1 - reduced coupling) a reduction in this parameter prolongs Ca^{2+} sparks, i.e. clusters of RyRs are unable to efficiently switch off and terminate the Ca^{2+} spark, (2) increases of sub space and SR luminal $[\text{Ca}^{2+}]$ lead to an increase in frequency of Ca^{2+} sparks, however, an increase in SR luminal $[\text{Ca}^{2+}]$ (while increasing Ca^{2+} spark frequency in a highly non-linear fashion) does not affect duration except at very low $[\text{Ca}^{2+}]$ where Ca^{2+} sparks terminate prematurely (3) the above observations are seen with a control number of 50 RyRs within a cluster, however the Ca^{2+} spark duration is relatively insensitive to RyR cluster size if between 10 - 100.

The process of inactivation or adaptation is not required within the model presented above, however, as suggested, this does not rule out the possibility that these mechanisms play a role in Ca^{2+} spark termination. Stochastic attrition is however intrinsic to the above model and together with luminal Ca^{2+} regulation of RyR and a cooperativity factor, a good stable model of Ca^{2+} spark termination has been established.

One major problem with this study is the inability to match the simulated Ca^{2+} spark width to that found in experiments. Model Ca^{2+} sparks were almost half the size of those found in experiments. This could be due to insufficient knowledge regarding parameters associated with Fluo-3 binding/buffering.

It seems therefore that accessory proteins associated with RyR can have an effect on CICR, FKBP in particular in terms of Ca²⁺ spark termination. Ca²⁺ spark termination is essential if a local regenerative response is not to proceed and lead to abnormally large amounts of diastolic SR Ca²⁺ leak. Both of these events could be detrimental to Ca²⁺ homeostasis and ultimately the contractile function of the ventricular cardiomyocyte. One of the main aims of this thesis is therefore to examine whether or not FKBP does affect the size and frequency of Ca²⁺ sparks in rabbit ventricular cardiomyocytes, using the two techniques of cell permeabilisation and FKBP over-expression. There are many factors, which could affect Ca²⁺ release from the SR and therefore alter Ca²⁺ spark size and frequency. This thesis will largely focus on the role FKBP has in altering these Ca²⁺ sparks parameters.

When attempting to measure Ca²⁺ sparks in permeabilised cells, as this thesis sets out to do, there are perhaps two further questions that must be considered.

1.18 Can Ca²⁺ sparks and waves be measured in permeabilised ventricular cardiomyocytes, and if so, are they the same as those in intact cells?

Gyorke *et al* (1999) has established that spontaneous Ca²⁺ sparks and waves can be observed within permeabilised ventricular cardiomyocytes and have the same characteristics as those measured in intact cells [64]. Manipulations performed in intact cells can also be performed in permeabilised cells, e.g. applications of caffeine, intracellular buffers

(EGTA), as well as drug manipulations not able to be performed in intact cells due to being membrane impermeable, e.g. application of cytosolic adenosine diphosphate-ribose (cADPR) and calmodulin [64].

Perhaps the most important aspect when comparing and quantifying Ca^{2+} waves is ensuring that cellular conditions are kept the same between two populations of cells. The main advantage of the permeabilised cells is that this can be done with a high degree of accuracy not achieved by measurements in intact cells due to easier access to the intracellular environment. This is very important in regards to the following question:

1.19 What are the effects of intracellular $[\text{Ca}^{2+}]$ and SR $[\text{Ca}^{2+}]$ on Ca^{2+} sparks?

Under normal conditions these two parameters are probability interrelated in that increases in intracellular $[\text{Ca}^{2+}]$ lead to increases in SR $[\text{Ca}^{2+}]$. However both parameters can affect Ca^{2+} sparks and waves independently.

1.20 Regulation of Ca^{2+} sparks by $[\text{Ca}^{2+}]$ within the SR lumen

Satoh *et al* (1997) established much of the initial investigations. In rabbit ventricular cardiomyocytes a decrease in SR $[\text{Ca}^{2+}]$ content leads to a reduction in spark frequency, even when intracellular $[\text{Ca}^{2+}]$ remains unchanged, the converse is also true in that increases of SR $[\text{Ca}^{2+}]$ lead to increases of Ca^{2+} spark frequency, until macro-sparks are formed and eventually Ca^{2+} waves [31;65]. The relationship between intracellular $[\text{Ca}^{2+}]$ and spark frequency is the same as for SR $[\text{Ca}^{2+}]$ content. The amplitude of Ca^{2+} sparks has also been found to increase with greater SR $[\text{Ca}^{2+}]$ [65]. During post rest decay in rabbit ventricular cardiomyocytes a gradual decay

in SR [Ca^{2+}] content occurs and a concurrent decrease in the frequency of Ca^{2+} sparks [65]. The same study also provided evidence for time-dependent recovery of Ca^{2+} spark events during rest after periods of stimulation when SR [Ca^{2+}] and intracellular [Ca^{2+}] were not changed in rat cardiomyocytes, and in rabbit cardiomyocytes, where Ca^{2+} extrusion from the cell was prevented by inhibiting $\text{Na}^+/\text{Ca}^{2+}$ exchange.

The effect of increased SR [Ca^{2+}] content on the frequency of Ca^{2+} sparks and eventually the production of Ca^{2+} waves could reflect an increase in sensitivity to Ca^{2+} of the RyR by cytosolic activation or a more direct activation by luminal SR [Ca^{2+}]. The use of the local anaesthetic, tetracaine has provided much information on luminal regulation of RyR [33]. Tetracaine has a biphasic effect on the RyR. Firstly, the drug inhibits RyR, decreasing the frequency and amplitude of Ca^{2+} sparks and the frequency of Ca^{2+} waves, but secondly, and rather paradoxically, then goes on to produce late potentiation of RyR mediated Ca^{2+} release increasing the frequency of these events. This only occurs at intermediate concentrations of the drug (0.25-0.75mM). At higher doses (>1.25mM) RyR mediated Ca^{2+} release is terminated. The late potentiating effect of tetracaine has been shown to occur because of a gradual increase in SR [Ca^{2+}], (while RyR Ca^{2+} release is inhibited); eventually overcoming RyR inhibition and perhaps activating the channel by direct luminal activation. There are a number of studies suggesting a role for luminal SR [Ca^{2+}] in regulating RyR Ca^{2+} flux. Work has been performed using isolated RyR channels [66], and molecular mechanisms altering the Ca^{2+} sensing sites on the luminal surface [67]. One study however has shown no significant effect of partial

depletion of SR Ca^{2+} content on Ca^{2+} sparks [68].

1.21 RyR activity and SR Ca^{2+} leak

The leak associated with Ca^{2+} sparks at rest on SR Ca^{2+} content in some studies is thought to be significant factor in Ca^{2+} homeostasis [33;46;69-71] and in others, however not [60;72].

Finally, Ca^{2+} transport mechanisms can have an effect on Ca^{2+} spark morphology. For instance, when the main Ca^{2+} removal mechanisms are inhibited (SERCA and $\text{Na}^+/\text{Ca}^{2+}$ exchange) Ca^{2+} spark decline is decreased by 26% together with increases in spatial spread. The converse is observed when SERCA uptake rate is increased. This indicates the importance of removal mechanisms perhaps in aiding spark termination [73].

It can be seen that there is much evidence for the regulation of Ca^{2+} spark frequency and morphology by cytosolic and SR $[\text{Ca}^{2+}]$. It is therefore essential that these are considered when performing Ca^{2+} spark and wave measurements and this concept underlies much of the thought behind the development of experimental protocols within this thesis.

1.22 Other sources of Ca^{2+} entry

Work previous to Stern's (1992) theoretical paper had also suggested the importance of cardiomyocyte ultra-structure in regulating EC-coupling [28]. In fact together with observations made by Cannell *et al* (1987) (that substantial Ca^{2+} transients could be triggered with minimal L-type Ca^{2+} currents) other routes of Ca^{2+} entry able to trigger Ca^{2+} transients were

investigated [26].

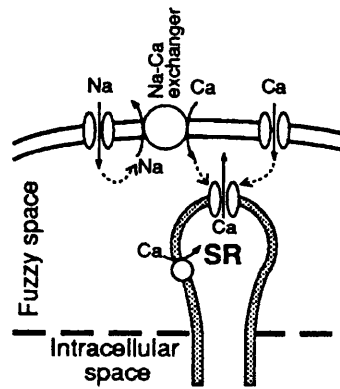


Figure 1.13 The 'fuzzy space'

A schematic illustrating the location of the restricted space envisaged to enable entry of Ca^{2+} via the $\text{Na}^+/\text{Ca}^{2+}$ exchange. The $\text{Na}^+/\text{Ca}^{2+}$ is located on the sarcolemma denoted by the doubled line. (Figure taken from Lederer (1990) *Science* 248, 283).

Leblanc and Hume (1990) showed that the $\text{Na}^+/\text{Ca}^{2+}$ exchanger could contribute to contraction during EC-coupling in the absence of an L-type Ca^{2+} current [74]. This contraction is TTX (tetrodotoxin) sensitive, i.e. it relies on influx of Na^+ to raise intracellular $[\text{Na}^+]$ levels such that the $\text{Na}^+/\text{Ca}^{2+}$ exchange works in reverse in order to bring Ca^{2+} into the cell and trigger SR Ca^{2+} release.

Lederer *et al* (1990) suggested though that the concentration of $[\text{Na}^+]$ could only be achieved if a micro-domain was present between the sarcolemma and the SR Ca^{2+} release channel [75]. This was termed the 'fuzzy space' (Figure 1.13). However, this result was contested by Sipido *et al* (1995) and others due to possible discrepancies in SR Ca^{2+} load or the actual cell voltage [76].

There is however another way in which influx of Ca^{2+} can arise on the

$\text{Na}^+/\text{Ca}^{2+}$ exchanger. E_m drive such that the membrane voltage increases above the reversal potential, e.g. during the rapid depolarisation of the action potential [77] can lead to Ca^{2+} influx [78]. At more positive potentials with higher intracellular $[\text{Na}^+]$ the bell shaped curve of voltage dependence on contraction becomes skewed such that there is a greater contraction at more positive potentials. This suggests that more Ca^{2+} enters the cell via the $\text{Na}^+/\text{Ca}^{2+}$ exchange as membrane potential increases. Sipido *et al* (1997) again contested this [79]. A normal bell shaped relationship was observed in this latter study using high intracellular $[\text{Na}^+]$ (20mM) in the first 20ms of the change of intracellular $[\text{Ca}^{2+}]$ but the skewed relationship described by Litwin *et al* (1998) was seen at longer times (250ms) [78]. Sipido *et al* (1997) concluded that the $\text{Na}^+/\text{Ca}^{2+}$ exchange was four times less efficient at triggering SR Ca^{2+} release due to the relatively long delay associated with Ca^{2+} influx using the exchanger compared to LCCs [79].

Other possibilities of Ca^{2+} entry include, T-Type/TTX sensitive I_{Ca} , and entry of Ca^{2+} through Na^+ channels 'slip mode conductance'. Other authors have suggested that CICR is not required in cardiomyocytes and the source of the Ca^{2+} transient is driven by voltage dependence or aided by inositol 1.4.5-triphosphate (IP3) -induced SR Ca^{2+} release. These mechanisms are reviewed elsewhere [9], and evidence for and against these mechanisms is out with the scope of this thesis since this study mainly concerns itself with permeabilised cells in which the function of sarcolemmal Ca^{2+} entry is bypassed.

CICR triggered by LCCs is the most favoured mechanism thought to

activate the myofilaments, with the possibility that the process is aided by Ca^{2+} entry via the $\text{Na}^+/\text{Ca}^{2+}$ exchanger [6].

1.23 Cardiomyocyte relaxation

Ca^{2+} dependent activation of the myofilaments results ultimately in cellular shortening and/or tension development. Ca^{2+} binds to troponin C that in turn increases its association with troponin I, thereby removing the molecule from the actin filament. Troponin T and tropomyosin as a complex are shifted to enable exposure of the actin filament to the myosin filament resulting in cellular shortening. To allow the heart to refill with blood and efficiently maintain cardiac output, filament relaxation must occur such that the filaments return to their original length. There are four main routes (presented below) by which Ca^{2+} can return to diastolic levels in order for this to occur.

1.23.1 SR mediated Ca^{2+} uptake

In most mammalian species, this is the main route whereby Ca^{2+} is removed from the myoplasm during a transient although the relative contribution differs from species to species. In rabbit, the fraction of Ca^{2+} transported by the SR during relaxation is 70% whereas, in the rat is 92% emphasising the dominance of the SR in ventricular contraction and relaxation in this species [80]. Uptake of Ca^{2+} is mediated via a SR Ca^{2+} -ATPase pump also referred to as the sarco(endo)plasmic reticulum Ca^{2+} -ATPase (SERCA). Two Ca^{2+} are transported in exchange for one ATP molecule [81]. Phospholamban is an endogenous inhibitor of the SR Ca^{2+} -ATPase pump but its inhibition can be relieved by phosphorylation by cAMP-dependent protein kinase (PKA). Uptake of Ca^{2+} into the SR can

also be prevented by the application of thapsigargin which binds to SERCA and prevents further cycling of this enzyme [82;83], or cyclopiazonic acid [84].

1.23.2 $\text{Na}^+/\text{Ca}^{2+}$ exchange

This route contributes to 28% in the rabbit and 7 % in the rat [85]. This route is reversible with a stoichiometry of 3 Na^+ to 1 Ca^{2+} . During diastole, this mechanism works in the forward mode to extrude Ca^{2+} . However, this exchanger may work in the reverse mode to bring Ca^{2+} into the cell and is therefore a potential source of Ca^{2+} entry during CICR [75].

1.23.3 Sarcolemmal mediated Ca^{2+} extrusion

Ca^{2+} extrusion is mediated via a Ca^{2+} ATPase pump and contributes less than 2% and 1% in the rabbit and rat respectively [80]. Ca^{2+} extrusion can be further enhanced via this route by Ca^{2+} -calmodulin and PKA dependent phosphorylation. One Ca^{2+} is transported per molecule of ATP hydrolysed and maybe linked to proton influx [86]. This pathway for Ca^{2+} extrusion together with mitochondria can be regarded slow since it would take approximately 60s for relaxation to occur after a Ca^{2+} transient had been triggered if all other pathways were blocked [87].

1.24 Mitochondria

Even though this organelle occupies 35% of the cell volume, the role of the mitochondria in Ca^{2+} handling on a beat-to-beat basis is not thought to be significant. Its relative removal contribution is the same as Ca^{2+} extrusion via the sarcolemmal Ca^{2+} ATPase pump. However mitochondria have a considerable potential for Ca^{2+} uptake, which can be further enhanced in

the presence of inorganic phosphate and subsequent precipitation into insoluble Ca^{2+} phosphate (matrix loading). If mean cellular Ca^{2+} is raised sufficiently Ca^{2+} uptake by this route on a beat to beat basis does become significant and under these circumstances, the accumulation may act to preserve cell function [88].

1.24.1 Ca^{2+} uptake into mitochondria

Two pathways exist which allow Ca^{2+} uptake into the mitochondria. The first is the Ca^{2+} uniporter. The interior of the mitochondria has a largely negative potential such that Ca^{2+} is driven into the organelle by this electrochemical gradient [89]. Carbonyl Cyanide *m*-Chlorophenolhydrazone (CCCP) is a protonophore which inhibits the proton motive force and therefore inhibits the uniporter. The second route for Ca^{2+} uptake is the rapid uptake mode. This mode is again dependent upon the large electrochemical gradient and may be related to the Ca^{2+} uniporter [90].

1.24.2 Inhibiting mitochondrial Ca^{2+} uptake

When attempting to prevent uptake of Ca^{2+} into the mitochondria, ionophores such as CCCP can be used. However it is important that oligomycin is also included. Oligomycin is an antibiotic, which acts by inhibiting the F_0 component of the H^+ -ATP synthase [91]. It inhibits therefore oxidative phosphorylation and minimises the mitochondrial ATP consumption during exposure to CCCP [87].

1.24.3 Ca^{2+} efflux from mitochondria

Efflux of Ca^{2+} from the mitochondria is thought to exist via two main routes.

The first is the Na^+ independent pathway. Ca^{2+} is exchanged for H^+ against an electrochemical gradient. The second is the Na^+ dependent pathway. This relies on a $\text{Na}^+/\text{Ca}^{2+}$ exchanger. The stoichiometry is thought to be 3Na^+ for each Ca^{2+} [92].

A final route in which the mitochondria may use to exchange substances to and from the cytosol is the Permeability Transition Pore (mPTP). This may allow the free permeation of low molecular weight solutes under certain conditions [90].

CHAPTER TWO

General methods

2.1 Rabbit ventricular cardiomyocyte isolation

Cell isolation was performed by one of two experienced technicians (Ann Ward and Aileen Rankin) with additional assistance provided by myself.

2.1.1 Isolation procedure

The procedure is based on the principle that cells within the intact heart can be isolated by gradual removal from their associated connective tissue and cellular syncytium. Before isolation can begin thorough cleaning of perfusion equipment was carried out. 2-3l of double distilled water was perfused through the system followed by 1-2l of sterile water. New Zealand White rabbits (2-2.5kg) were given an intravenous injection of 500U heparin together with an overdose of sodium pentobarbitone (100mg/kg). The hearts were rapidly excised, weighed and cannulated onto a Langendorff perfusion column via the aorta. The hearts were perfused in a retrograde fashion at a rate of 25ml.min⁻¹ (37°C), initially with 150ml of Krebs Henseleit solution with the following composition (mM): 120 NaCl, 20 HEPES, 5.4 KCl, 0.52 NaH₂PO₄, 3.5 MgCl₂.6H₂O, 20 Taurine, 10 Creatine, 11.1 Glucose; pH 7.4 with NaOH at 37°C. [Ca²⁺] within this solution is in the order of 6-7µM due to Ca²⁺ contamination. This solution aids in washing away blood and reduces the probability of clot formation. Taurine may aid in cardio-protection against Ca²⁺ paradox [93;94]. Thereafter, the hearts were perfused for 1min with Krebs Henseleit solution supplemented with 1.4 mg ml⁻¹ collagenase (type 1, Worthington Chemical Co.), 0.1 mg ml⁻¹ protease (type XIV, Sigma Chemical Co.) and a further addition of 50µM CaCl₂ to activate the enzymes. After a time, such that the enzyme

solution had fully perfused the heart and equipment the enzyme containing solution was re-circulated for a further 6min. The heart was then perfused with a 0.1% Bovine Serum Albumin (BSA) Krebs Henseleit solution with the addition of $62\mu\text{M}$ CaCl_2 . The BSA containing solution provides extra substrate for superfluous enzyme. The atria were removed and discarded whereas the right and left ventricle was kept for experiments.

2.1.2 Cells required for permeabilisation experiments

If cells were required for permeabilised cell work then the chosen ventricle was carefully cut into small pieces and placed into a culture flask containing 20ml of the Krebs Henseleit solution. The flask was gently shaken at room temperature for 30-60min. After the appropriate time the cell suspension was filtered using $250\mu\text{m}$ mesh and the filtrate centrifuged. The pellet was re-suspended in Krebs Henseleit solution. The cell concentration was approximately 10^4cells.ml^{-1} .

2.1.3 Cells required for intact cell experiments

If cells were required for intact cell work then the chosen ventricle was carefully cut into small pieces and placed into a culture flask containing 20ml of the 0.1% BSA containing Krebs Henseleit solution described above. This solution also contained 0.125mM CaCl_2 . The suspension was gently shaken for 30-60min. After the appropriate time the supernatant was removed and the cells re-suspended into 0.1% BSA containing Krebs Henseleit solution containing 0.25mM CaCl_2 . This process was repeated in the same solution containing increasing amounts of CaCl_2 (0.5mM and 1mM CaCl_2). This gradual increase in $[\text{Ca}^{2+}]$ is thought to prevent the Ca^{2+}

paradox and subsequent damage to cellular membranes [94;95]. The Langendorff perfusion system was then cleaned using 2l of boiling water, 1l of 100% ethanol and 10-12l of double distilled water.

2.1.4 Primary ventricular cardiomyocyte culture

Isolated rabbit ventricular cardiomyocytes were prepared as above under sterile conditions, with some subtle changes to the methods. All solutions had previously been filter sterilised and prepared with sterile water and autoclaved glassware. Perfused tissue was cut down and placed in a solution containing 0.1% BSA in sterile glassware and the tissue finely chopped using autoclaved instruments in a laminar flow hood. The chopped tissue was then placed in tissue culture grade sterile flasks and gently shaken at room temperature for 30-60min. The following steps were performed using aseptic technique in a laminar flow hood. The supernatant was removed and placed into sterile 15ml centrifuge tubes. The cells were allowed to sediment by gravity. The supernatant was removed and the pellet re-suspended in Krebs' solution containing 125 μ M CaCl₂. Again the cells were allowed to sediment by gravity, the supernatant removed and the pellet re-suspended in Krebs' solution containing 250 μ M CaCl₂. This step was repeated twice more and successively raised the extracellular Ca²⁺ to 500 μ M and then 1mM. The cells were counted using a haemocytometer, the cells subjected to gentle centrifugation and the pellet re-suspended in M199 medium (supplemented with 312.5mg Taurine, 500mg D,L Carnitine, 327.5mg creatine, 5ml penicillin/ streptomycin per 500ml) to a concentration of 1 \times 10⁵ cells.ml⁻¹.

2.2 The use of recombinant adenovirus to transfect adult cardiomyocytes

Recombinant adenovirus vectors are genetically modified forms of natural adenoviruses, which can be used to express a protein of choice within adult cardiomyocytes. If the DNA sequence codes for a naturally occurring protein, this protein is over-expressed. This technique can be used therapeutically in cases where the protein is absent due to a defective gene, i.e. gene therapy. The technique can also be used to study the function of a protein. A major part of this thesis concerns itself with the functional consequences of over-expressing FKBP12.6 within adult rabbit cardiomyocytes. This is achieved by the construction of an adenovirus, which acts as a vector for the FKBP12.6 DNA sequence. This sequence (under the control of incorporated promoters) leads to the enhanced production of the protein within the cardiomyocyte. Within this thesis, three such viruses have been used: Ad-FKBP12.6, Ad-FKBP12.6 mutant lacking a calcineurin binding site and a control virus that over-expresses β -galactosidase (Ad-LacZ). In this way the function of FKBP12.6 and the mutant can be investigated and compared to a control (Ad-LacZ) virus. The work involved in constructing and propagating the adenovirus vector was meticulously performed by Dr Tim Siedler and Dr. Jurgen Prestle from the University of Goettingen and Dr. Debbie Reynolds from the University of Glasgow. The amount of work and variety of molecular techniques used to create these viruses is out with the scope of this thesis which essentially only concentrates on the functional consequences of their subsequent transfection into cardiomyocytes. However a brief over view will be presented below:

2.2.1 Adenovirus

Adenoviruses are double stranded DNA viruses with an icosahedral capsid approximately 80nm in size (Figure 2.1). The virus is assembled in the cell nucleus and exists as several serotypes in most host species. To gain entry to the host cell the virus is adsorbed to the cell membrane and endocytosed. Once inside the cell the virus leaves the endosome and is released into the cytosol.

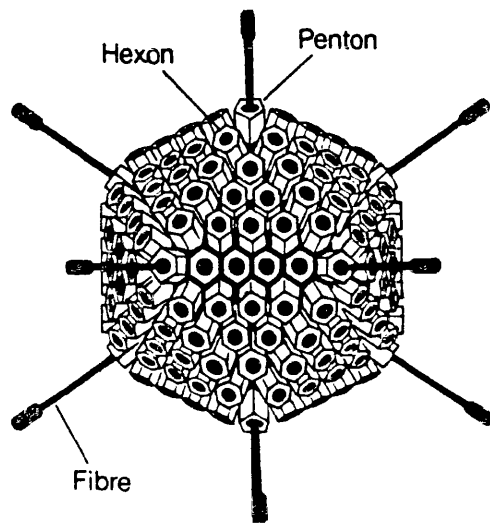


Figure 2.1 The capsid of a typical adenovirus

The capsid is icosahedral with 252 capsomeres. There are 12 points of five-fold symmetry. The polypeptides that form the hexon and penton are distinct. (Figure and text description adapted from University of Glasgow, Veterinary School, U.K. virology notes, Prof. Oswald Jarrett).

The virus particles make their way to the nuclear pores where their DNA genome is released and passed into the nucleus. The replication of the virus occurs in two stages: early and late events (Table 2.1).

2.2.2 Generation of the Ad-FKBP 12.6 virus

This following description follows the methods of Becker *et al* (1994) that have been adapted by the above co-workers for FKBP12.6 [96]. Essentially two plasmids are formed. The first plasmid (circular DNA) contains the cDNA of FKBP12.6. The second plasmid is called a shuttle vector, which contains a cytomegalovirus (CMV) early promoter to drive transcription of the cDNA of interest. The shuttle vector also contains fragments of the adenovirus (type 5) genome and an ampicillin resistance gene. The two plasmids are linearised by restriction enzymes (*EcoRI/HindIII*) and purified. The first plasmid can therefore be inserted into the shuttle vector within *E.coli* bacteria. Bacteria, which have this combined vector, can then be selected according to their resistance to ampicillin (Figure 2.2).

Transcription map area	Function
E1a	First gene to be transcribed and this activates other early genes.
E2	Encodes enzymes and proteins necessary for DNA replication.
E3	Encodes genes unnecessary for replication <i>in vitro</i> but aids virus growth <i>in vivo</i> by interfering with host immune response.
E4	Dispensable for growth <i>in vitro</i> but important for replication <i>in vivo</i> . encodes genes that shut down host cell protein synthesis and regulates late gene synthesis.
Late genes	Encode for structural proteins.

Table 2.1 The function of various regions of the transcriptional map of a typical adenovirus

The adenovirus genome consists of double stranded DNA approximately 36kb long. Viral replication is divided into early and late events. (Figure and text description adapted from University of Glasgow, Veterinary School, U.K. virology notes, Prof. Oswald Jarrett).

To allow amplification of this combined plasmid the circular DNA is co-transfected into HEK 293 cells with another plasmid (pJM17), which is

derived from the adenovirus (type 5) genome with the E1 region of the genome (which is essential for viral replication) deleted. The absence of this region makes it possible to allow site-specific recombination and subsequent insertion of cDNAs. The E1 function is complemented in HEK 293 cells thus allowing propagation. Co-transfection of pACCMV.pLpA and pJM17 is followed by homologous recombination to generate a functional adenovirus with the FKBP12.6 cDNA incorporated (Figure 2.2).

2.2.3 Infection with adenovirus

Adult rabbit cardiomyocytes were infected with Ad-FKBP12.6, Ad-FKBP12.6 calcineurin mutant, or Ad-LacZ. The infectivity of each virus had been assayed and expressed as a plaque forming unit.ml⁻¹ (pfu.ml⁻¹) by Dr Tim Siedler from the University of Goettingen and Dr. Debbie Reynolds from the University of Glasgow who had also constructed the viruses. The methods involved with this procedure are out-with the scope of this thesis [96]. Virus infection took place using a multiplicity of infection (MOI) of 100. This essentially means that 100 virus particles were used to infect each cell. After 48hrs of culture this resulted in at least 90% of the cells transfected (originally established by the workers above). Over-expression levels of these proteins were thought to be approximately 5 fold. In order to use permeabilisation techniques in these cultured cells the [Ca²⁺] in the M199 culture medium/cell suspension was diluted three-fold and 1mM EGTA added.

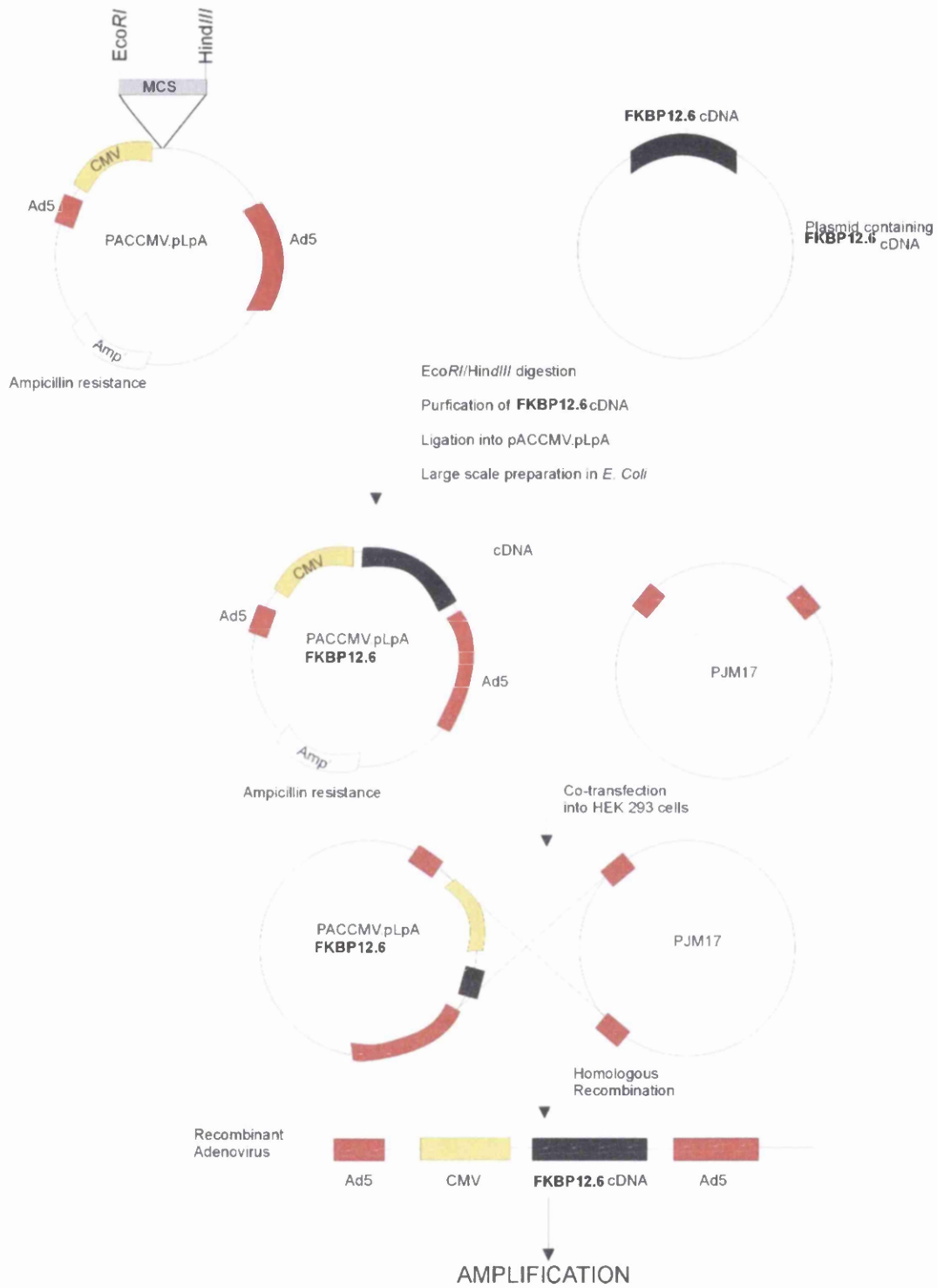


Figure 2.2 Construction of Ad-FKBP12.6

Refer to text for detailed description. (Figure taken from Debbie Reynolds' doctoral thesis 2003 with permission).

METHODS

Cell Permeabilisation and Laser Scanning Confocal Microscopy

2.3 Cell permeabilisation of cardiomyocytes

The ability to equilibrate an extracellular solution with the cell interior has been pivotal in elucidating cardiomyocyte function. Various techniques have been used to by-pass the sarcolemmal barrier. Mechanical removal ('skinning') of this membrane by meticulous micro-dissection was used to first identify the process of CICR within cardiomyocytes [14;95]. On cells as small as ventricular cardiomyocytes this is by no means an easy task and hence simpler techniques have been investigated. Winegrad (1971) attempted to use chemicals such as EDTA to skin strips of frog ventricle [97]. However, whether this was actually achieved has been debated [98]. Therefore, non-ionic detergents such as Brij58 and Triton x-100 were used to skin cardiomyocytes. However, while myofilaments remain unaffected by such treatments the SR may be damaged [99]. Since this thesis investigates spontaneous Ca^{2+} release from the SR, the above agents are not helpful. However, one agent, discussed below is currently used to successfully permeabilise cardiomyocytes.

2.3.1 β -escin

The source of β -escin is the Horse Chesnut tree (*Aesculus hippocastanum*). The tree seeds contain an active triterpene saponin mixture known as escin [100]. β -escin is therefore related to saponins, which are glycosides of triterpenoids or steroids (acetal form of glucose) [101]. The saponin molecule consists of a non-carbohydrate component (aglycone/sapogenin) and a carbohydrate component (sugar chain/s attached via glycoside/ester linkage). β -escin is based on the aglycone protoescigenin [102].

2.3.2 Mechanism of action

The mechanism of action involves formation of complexes with sterols/cholesterol located on the sarcolemma and subsequent lateral displacement with the formation of aqueous pores (8-15nm) [103]. The agents are not thought to disrupt the SR since the relative content of cholesterol on this organelle membrane is very low (<2% of SR lipid content). Within this thesis, this possibility is further prevented by a very careful acute exposure of the permeabilisation agent to cardiomyocytes. This results in a functional SR which produces not only Ca^{2+} waves but also produces Ca^{2+} sparks that required the coordinated release of Ca^{2+} from a cluster of RyRs. This would be hard to achieve if the SR had been damaged (in fact the production of Ca^{2+} sparks cannot occur if the permeabilisation agent is left on for too long).

2.3.3 Minimum effective concentration

The concentration of β -escin used within this thesis to permeabilise cardiomyocytes was $100\mu\text{g.ml}^{-1}$ for 0.5-1min. The use of this concentration was elucidated by two independent assays (Ca^{2+} contraction assay and trypan blue assay) within this laboratory. The above studies were carried out by Elspeth Elliott (BSc project). Some of the data produced in this report has been reproduced with permission in Figure 2.3. β -escin has a minimum effective concentration of $100\mu\text{g.ml}^{-1}$ that is, 95% of cells are permeabilised within 2min of exposure to the agent.

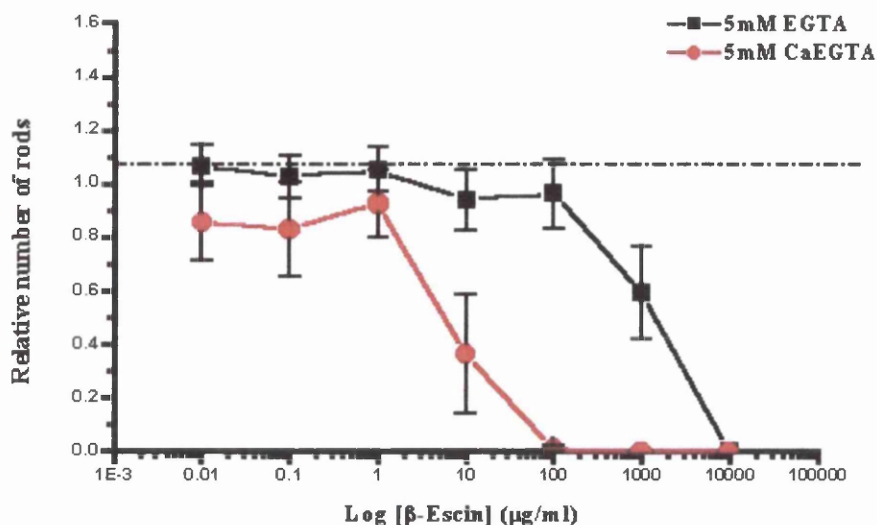


Figure 2.3 Minimum effective concentration of β -escin

A known number of cardiomyocytes were exposed to β -escin for 2min at concentrations as denoted. This was performed in both a $<1\text{nM}$ [Ca^{2+}] solution (5mM EGTA) and a $20\mu\text{M}$ [Ca^{2+}] solution (5mM EGTA) which resulted in Ca^{2+} contraction if cells were permeabilised. The minimum effective Ca^{2+} concentration is the concentration of agent required to permeabilise 95% of the population of cells. (Figure taken from Elspeth Elliott (BSc honours thesis) with permission).

However it is also clear from these studies that permeabilisation occurs over a concentration range of $1\mu\text{g.ml}^{-1}$ to $100\mu\text{g.ml}^{-1}$ with 50% cell permeabilisation occurring at $8.3\pm 1.1\mu\text{g.ml}^{-1}$. The danger is to leave the permeabilisation agent on for too long. With this information in mind, $100\mu\text{g.ml}^{-1}$ was the concentration of choice to permeabilise cardiomyocytes. The time of exposure to this chemical was variable but was approximately 0.5-1min. Cell permeabilisation was performed simultaneously with confocal microscopy and a mock intracellular solution (see section 3.2.4) containing $10\mu\text{M}$ Fluo-3/5F and 150nM [Ca^{2+}].

Permeabilisation of the cells was ascertained by a rise in intracellular fluorescence relative to the extracellular solution (see section 3.2.4) and the appearance of Ca^{2+} sparks. As soon as permeabilisation of the cell under study was achieved, the β -escin was immediately removed by subsequent perfusion with a solution of choice. Leaving the agent on for any longer may result in SR disruption. It is therefore not acceptable to perform 'blind' permeabilisation to measure Ca^{2+} sparks and waves, whereby cells are permeabilised as a batch and permeabilisation agent removed after a specific time period. This will result in some cells being rendered impermeable and (perhaps more detrimental) SR damage in others. It has been argued that saponin and not β -escin should be used for studying SR function, however these experiments were performed in skeletal muscle fibres with exposure times of 30min which would result in SR damage [104].

2.3.4 Other uses for permeabilisation agents

Permeabilisation agents are not only used to equilibrate external and internal solutions. They can also be used to introduce exogenous molecules into the cytoplasm, e.g. antibodies [105] and antisense deoxynucleotides [106]. Enzymatic systems, exocytosis, and direct measurements of intracellular $[\text{Ca}^{2+}]$ have also been investigated in permeabilised cell systems [105;107]. Finally, since intracellular $[\text{Ca}^{2+}]$ is known, the permeabilised cell system can be used to calibrate fluorophore characteristics (as described in section 3.2.4). This is harder to perform accurately within intact cells.

2.3.5 Other permeabilising agents

Recently bacterial toxins have been used to permeabilise cardiomyocytes. The main bacterial toxin used in cardiomyocytes is Streptolysin-O (SLO), a 57kDa oxygen-labile prototype of the cholesterol-binding 'thiol-activated' cytolysin family [108;109]. This is a pore-forming toxin produced by some gram-positive bacteria including *Streptococci*, *Clostridia*, and *Listeria* spp. The toxin targets cholesterol molecules within biological membranes. The binding is rapid (<1min). Pore formation involves the formation of an aqueous trans-membrane pore that displaces the lipid laterally. Pore formation is ATP independent and therefore the energy is derived from the conformational changes in the toxin molecules [110]. Essentially there is oligomerisation of toxin monomers to form partial or fully circularised protein complexes. Pores are very large (30nm) and theoretically large enough to permit SLO to enter the cytoplasm, but this is probably rare since toxin molecules rapidly bind to and are trapped in the plasma membrane. The main problem with SLO seems to be the large pore sizes. This could lead to loss of intracellular components. One way around this problem could be the use of tetanolysin which is very similar to SLO but has the ability for pore sizes to be determined depending on the concentration of toxin used. Staphylococcal alpha-toxin is another pore-forming toxin that is also a single chain polypeptide. It is the most researched pore-forming toxin and hence is used as a model to which other toxins are compared. Alpha-toxin binds to an unidentified receptor. Receptor binding only occurs at low concentrations (<50nM). At higher concentrations (>200nM), the binding is indiscriminate to lipid bi-layers. This factor may limit its use within rabbit cardiac cardiomyocytes since the receptor within the sarcolemma has yet to

be identified and the use of higher concentrations would lose the ability of the toxin to be sarcolemmal specific. In terms of pore formation the alpha-toxin is similar to SLO. The pore itself is selective for mono-valent ions and not a rapid flux of Ca^{2+} ions. This has obvious limitations in the measurement of intracellular $[\text{Ca}^{2+}]$.

2.4 Laser scanning confocal microscopy (LSCM)

Almost all the functional experiments presented in this thesis have been performed using Laser Scanning Confocal Microscopy (LSCM). The technique has been essential in enabling alterations in $[Ca^{2+}]$ within ventricular cardiomyocytes to be dynamically tracked through space and time. The following is a brief account of the principles behind LSCM and the experimental set-up used within this thesis.

2.4.1 Tracking the dynamics of $[Ca^{2+}]$ within ventricular cardiomyocytes

In order to track Ca^{2+} the use of a specific probe for this ion is needed. The conventional probes used to track Ca^{2+} are called fluorophores. The two main fluorophores used within this thesis are Fluo-3 and Fluo-5F, the particular characteristics of which are extensively covered in chapters 3 and 4 and will not be discussed further here. As the name suggests, fluorophores rely on the principle of fluorescence. Fluorescence is a type of luminescence in which light is emitted from a molecule for a very short period of time (10^{-8} to 10^{-6} s) following the absorption of light [111]. Fluorophores can absorb high-energy photons (e.g. from a LASER source) and achieve an excited state. Some energy is lost internally within the molecule but eventually fluorescence emission occurs with the release of a photon and a return of the molecule to the ground state. The photon emitted has less energy than the one absorbed. In practical terms this means that when using Fluo-3/5F the excitation wavelength may be blue (488nm) however the emitted wavelength that is collected is longer (>518nm) and appears green. The specific nature of the fluorophore for

Ca^{2+} ensures that the higher the $[\text{Ca}^{2+}]$ within the cell the greater the degree of binding to this molecule. This subsequently results in a greater amount of fluorescence produced. In this way the dynamic movement of Ca^{2+} and its concentration can be monitored over time. An accurate assessment of the $[\text{Ca}^{2+}]$ within ventricular cardiomyocytes can only be achieved through thorough calibration with solutions of known $[\text{Ca}^{2+}]$ and dye characteristics (Refer to chapters 3 and 4).

2.4.2 How do we measure cell fluorescence?

The technique used to both excite the fluorophore and collect the emitted photons is LSCM. A laser source is used to excite the cellular medium containing the fluorophore. The excitation light is passed by a series of dichromatic mirrors. The dichromatic mirrors reflect light shorter than a determined wavelength, and pass light longer than that same wavelength. The laser then hits scanning mirrors, which continually rotate back and forth in an arc in order to direct the laser across an area of the sample at a speed determined by the user. The laser then passes through the objective lens to the sample. The laser excites the dye and the emitted fluorescence is then collected by the same objective lens. This is referred to as epi-fluorescence. The emitted light is de-scanned by the same rotating mirrors and since it is of a longer wavelength, it is able to pass back through the same dichromatic mirrors to a detector called the photo multiplier tube (PMT).

2.4.3 How is the confocal principle achieved?

It is clear from the above description that that the excitation light excites an

area of the cell which is determined by the user. However fluorescence is being produced from that entire area at the same time. The highest degree of fluorescence will be produced at the focal plane, however other areas of the sample above and below that plane will also be excited and contributing to the fluorescence collected. This makes the tracking of Ca^{2+} ions within a ventricular cardiomyocyte very difficult. In order to eliminate out of focus light a pinhole is placed before the detector, positioned such that only light being emitted from the focal plane is able to pass through this hole to be detected. Out of focus light is therefore rejected. Since the focal point of the objective lens forms an image where the pinhole is located, the two points are conjugate. Thus the LSCM acquires its name from both the use of the confocal principle (since the pinhole is conjugate to the focal point of the objective lens), and the use of scanning mirrors to direct excitation and emission light, to and from the sample.

2.4.4 Image formation

Essentially the basis of LSCM is to reject out of focus fluorescence however a complete image of the whole of the sample is never achieved at any one time. The scanning mirrors direct the laser, point by point across the sample. The data is then acquired on a pixel-by-pixel basis (*Laser Sharp* software, *BioRad*). The conventional image collected is a 512 x 512 pixel array and since the usual scanning speed used is 500 lines per second, the time taken to cover the whole of the sample is approximately 1s. It follows from this that if the user scans a smaller area of the sample, faster acquisition times can be achieved. This can be further aided by the use of bi-directional scanning. Confocal systems can image up to 40 μm in depth.

This is ideal for cardiomyocytes, which are only approximately half this depth (~20 μ m).

2.4.5 What if events occur with frequencies greater than 1s?

Due to their high frequency Ca^{2+} sparks and waves can be missed if the LSCM scanning speed is 1 frame/s. Hence a particular method has been used throughout this thesis, which ensures enough temporal and spatial resolution of these events. This technique is referred to as line-scan imaging. Essentially, instead of using the LSCM to scan over the whole sample to create a 512 x 512 pixel image, the LSCM repeatedly scans across a single line across the sample, the position of which is determined by the user. This same line is repeatedly scanned at 500 lines per second. To image the data collected, each of these scanned lines (512x1 pixels) is placed on top of each other to create a 'waterfall' image whereby time is expressed on the vertical axis and distance across the sample is expressed on the horizontal.

2.4.6 Data recording and analysis

Confocal line-scan images were recorded using a BioRad Radiance 2000 confocal system. Fluo-3 (or Fluo-5F) in the perfusing solution (or when loaded within cardiomyocytes using and acetoxymethyl ester –AM form of the drug) was excited at 488nm and measured above 515nm using epifluorescence optics of a Nikon Eclipse inverted microscope with a Fluor 60X water objective lens (NA 1.2). The higher the numerical aperture of a lens the greater its light collection efficiency [112].

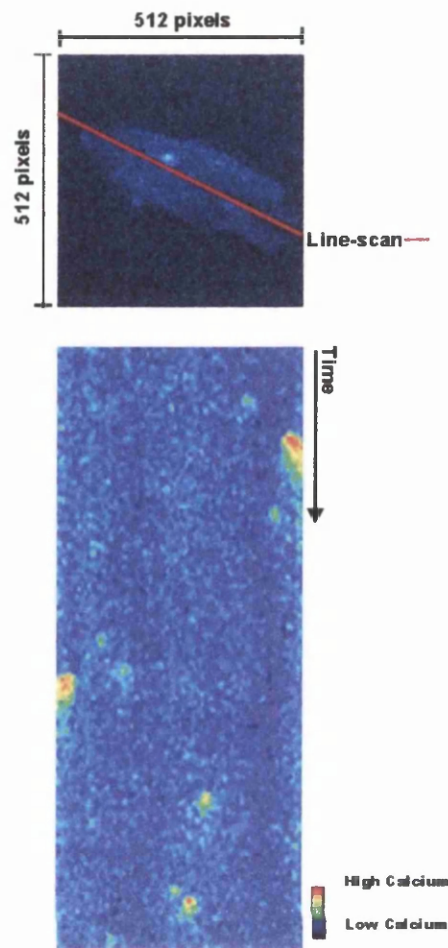


Figure 2.4 Line-scan confocal imaging

Top panel shows a 512 x 512 pixel image of a permeabilised cardiomyocyte and the positioning of the line-scan by the user. By repeatedly scanning this line an image is formed as in the lower panel where distance across the cell is expressed on the horizontal axis and time on the vertical. The extracellular signal has been cropped from the image.

Iris diameter was set at 1.9 providing an axial (z) resolution of about $0.9\mu\text{m}$ and X-Y resolution of about $0.5\mu\text{m}$ based on full width half maximal amplitude measurements of images of $0.175\mu\text{m}$ fluorescent beads (*Molecular Probes*). Prof. Godfrey Smith carried out these latter measurements in order to obtain the resolution of the confocal microscope. The principle behind these measurements is that due to diffraction, a point

source of light cannot be imaged as a single intense point. The point source is spread out in 3-dimensions. The spreading of which can be quantified using the point spread function (PSF). Hence fluorescent beads which are $0.175\mu\text{m}$ provide an almost point source of fluorescence. Due to diffraction, these beads will not appear $0.175\mu\text{m}$ in size but appear with the dimensions stated above. This is the actual resolution of the microscope and is a measure of the PSF. Another calibration method used, involved calculating the edge spread function in order to establish the resolution at the Ca^{2+} transient/ Ca^{2+} wave front. This involves taking a broken glass cover slip, which formed an almost perfect straight edge, and laying this on top of another cover slip, which formed the base of a $300\mu\text{l}$ bath. Within the section of the bath formed by the broken cover slip a glycerol solution containing the fluorophore Fluo-3 ($10\mu\text{M}$) was added. Using LSCM the edge of the broken cover slip was imaged with one half containing the fluorophore and one half with the absence of fluorophore due to the presence of the glass. A line scan image of this was then taken and analysed. A fluorescence line profile was obtained of this image and subsequently differentiated to obtain the width at half maximal fluorescence. This is another indication of the PSF and correlated well with the results above. Experimental data was acquired in line-scan mode at $2\text{ms}/\text{line}$; pixel width was $0.29\mu\text{m}$ ($512\text{ pixels}/\text{scan}$; $\text{zoom}=1.4$). In the majority of cases, unless stated, the scanning laser line was oriented parallel with the long axis of the cell and placed approximately equidistant between the outer edge of the cell and the nucleus/nuclei, to ensure the nuclear area was not included in the scan line.

2.4.7 Perfusion of cardiomyocytes

The perfusion system and rig that houses the LSCM was constructed with the assistance of Prof. Godfrey Smith. Perfusion of cardiomyocytes was achieved by a series of 50ml syringes, which allowed the various solutions to be applied. This was a gravity fed system with the incorporation of solenoid valves. The solutions entered a 300 μ l cell bath made from Perspex via a system of silicone rubber tubing. Isolated cardiomyocytes settled onto a glass cover slip (#1.5), which formed the base of this bath without the need for additional adhesives. The removal of solutions was achieved using a peristaltic pump and a microelectrode glass pipette. The perfusion rate for all experiments (unless otherwise stated) was 1.5ml.min⁻¹. Inflow was within 500 μ m of the cell to facilitate rapid solution change.

2.4.8 Disadvantages of confocal microscopy

There are some problems associated with LSCM that must be considered when calibrating [Ca²⁺] in live cells:

1. **Quenching** is the reduction of fluorescence intensity due to the physicochemical modification of a fluorophore in the excited state [111]. It can be caused by a variety of reasons including the presence of other fluorophores, oxidising agents and heavy metal salts. No major problems with fluorophore quenching were observed within this thesis. Any decrease in fluorescence due to quenching can be rectified by the application of calibrated compensation.
2. **Bleaching** is due to excessive illumination of the fluorophore. This

can result in changes in the emission spectrum of the dye. This is characterised by a gradual decrease in fluorescence obtained on a signal that should be constant. Decreasing the intensity of the laser source and reducing the time the cell is exposed to it can minimise this phenomenon.

3. The maximum **depth** the LSCM should be used for is 40 μm , above which spherical aberration can often degrade image contrast [112]. Since cardiomyocytes are only approximately 20 μm thick this technique is ideal. However for multi-cellular cardiac preparations a two-photon microscope is required.

4. **Photo-toxicity** can also be a problem due to the physicochemical changes within the cell due to the laser source. This can alter the binding characteristics of the dye. This is characterised by an increase in a fluorescence signal that should be constant. In our hands the laser power needs to be set at a laser power of 12% (3mW laser) for Ca^{2+} wave measurements and can be as high as 16% for Ca^{2+} sparks measurements since these protocols are shorter. The maximum time under which the cell should be exposed to these laser powers should be <5min.

5. **The non-ratiometric** properties of the fluorophores used, means the concentration of the dye within the cell alters the fluorescence signal produced. Movement artefact therefore can increase the concentration of the dye although the actual $[\text{Ca}^{2+}]$ might not have changed. These problems have been overcome and are discussed in the appropriate place (section 3.2.4).

2.4.9 Analysis programs used

Analysis was performed using a variety of different computer programs. The use of interactive data language (IDL) for Ca^{2+} spark analysis will be extensively reviewed later. The analysis of Ca^{2+} waves and stimulated Ca^{2+} transients relied on programs such as *Metamorph* (Universal imaging corporation) and *Laserpix* (BioRad) to bring in images created on line by LSCM. These convert images were then appended together using a program written by Dr. Francis Burton (*Nbands*). The data files from such amalgamations were then analysed on a graph analysis package called *Origin v6.1* (*OriginLab*). Macros written by Prof. Godfrey Smith enabled averaged waves and transients to be produced along with integration and differentiation programs to subsequently analyse these events in detail.

2.5 Automated Ca²⁺ spark detection method

Originally, the mean Ca²⁺ spark shape and frequency were measured by accumulating the data from a number of line-scan events. Ca²⁺ spark detection used to be performed 'by eye' [113;114]. A study by Cheng *et al* (1999) emphasised the subjective nature of this method and the bias of the results that arose as a consequence [115]. Cheng *et al* (1999) therefore created an automated detection algorithm that has been adopted as a standard. This algorithm is coded in the image-processing language - Interactive Data Language (IDL) - *Research Systems, Boulder, CO.* and provides an objective and more efficient way to detect Ca²⁺ release events from cardiomyocytes when dispersed in a noise signal. Although the subjective method of 'eye detection' has a sensitivity and reliability comparable to computer detection the distribution histogram produced from each method is different [115]. The reasons why they are different will be discussed below. Care must be therefore taken when interpreting Ca²⁺ spark characteristics from data ascertained by 'eye detection' [113;114].

2.5.1 Summarisation of Ca²⁺ spark detection programme

The IDL code used within this thesis was originally written by Cheng *et al* (1999) for use in intact cardiomyocytes and has therefore been adapted for use in permeabilised cardiomyocytes by Godfrey Smith (Appendix 2.1) [115]. The basis of this programme is the detection of conjoined areas of fluorescence that are above a signal noise level (via input of a certain threshold – a criterion).

The four main stages to enable Ca^{2+} spark detection are as follows:

Input – The raw 512 x 30000 pixel BioRad line-scan image (*.pic) is converted to a (*.tiff) image file. The image contains both the intracellular signal, which is required, and the extracellular signal, which is cropped.

Normalisation – Each of the 512 bands (30000 points) is averaged to provide a mean value. This produces a fluorescence baseline. At this time Ca^{2+} sparks are included. Using the mean value in each of the 512 lines the image is normalised to 1 and the mean (m) and standard deviation (σ) of this whole image is calculated. Using this normalised image, pixels that are greater than $m+2\sigma$ are excised and the whole process is repeated again. Pixels, which exceed the set deviation from the noise signal, are possible spark areas. This second estimate of background is used to provide the final normalisation of the data.

Detection – Two images are created. The first is the binary image at the level of $m+2\sigma$ and the second is a binary image at the level of $m+\text{Cri}\sigma$, where Cri (criterion) is a constant, which the user can input to determine the threshold for Ca^{2+} spark detection. Ca^{2+} sparks are identified as regions in the $m+2\sigma$ image that contain values above $m+\text{Cri}\sigma$. The $m+2\sigma$ image is then used to delineate the continuous area bounding the Ca^{2+} spark.

Measurement - The number of Ca^{2+} sparks is determined together with the peak, full width at half maximum (FWHM) and full duration at half maximum (FDHM) (Figure 2.5).

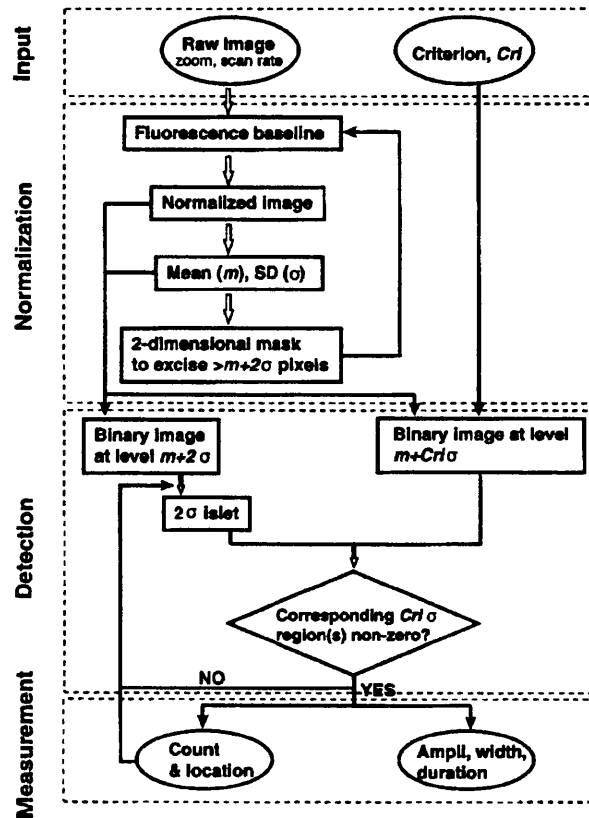


Figure 2.5 Computer automated Ca^{2+} spark detection

Flow diagram showing the various stages in Ca^{2+} spark detection using an algorithm from Cheng *et al* 1999. (Figure taken from Cheng *et al* (1999) *Biophys. J.* 76, 606-617).

2.5.2 Sensitivity and specificity

As the criterion is increased the sensitivity of detected events (percentage of sparks detected) decreases while the specificity (100% minus percentage of detections that are false) increases. Cheng *et al* (1999) suggests that a Cri of 3.5 is the most favourable compromise between these two parameters [115]. A Cri of 4.0 was used in the results presented in this thesis. This choice of Cri was based on the results of some simple measurements carried out in permeabilised cells described below:

(1) Ca^{2+} sparks were measured and detected at 150nM $[\text{Ca}^{2+}]$ as discussed

in section 6.3.5.

(2) The same cell was then perfused for 5min with 2.5 μ M thapsigargin and 10 μ M ryanodine to completely block Ca²⁺ release from the SR. Ca²⁺ spark calibration and detection was then performed on this image as above.

(3) Amplitude histograms of both images were performed. Since this latter image (Figure 2.6B) contains only noise and not Ca²⁺ sparks, the frequency of events in this histogram can be subtracted from the former image (Figure 2.6A), which contains Ca²⁺ sparks and noise (Figure 2.6C).

The cumulative amplitude histograms in Figure 2.6 are data from 4 freshly dissociated cells at 150nM [Ca²⁺]. As can be seen from the histograms data, where the SR has been blocked (Figure 2.6B) a number of events are detected which are attributable to noise. However at a Cri of 4.0 this number is minimal. This was therefore the Cri used in subsequent chapters.

2.5.3 Ca²⁺ spark detection from line-scan confocal images

It is clear that while spontaneous Ca²⁺ sparks are produced throughout the cell interior, the intrinsic nature of line-scan confocal imaging prevents the simultaneous imaging of all these events at any one time. It follows from this that Ca²⁺ sparks observed in a line-scan image originate at and a variable distance from the confocal plane (line-scan). Therefore even if Ca²⁺ sparks, are stereotypical in size, distribution amplitude histograms of these events will appear otherwise [115].

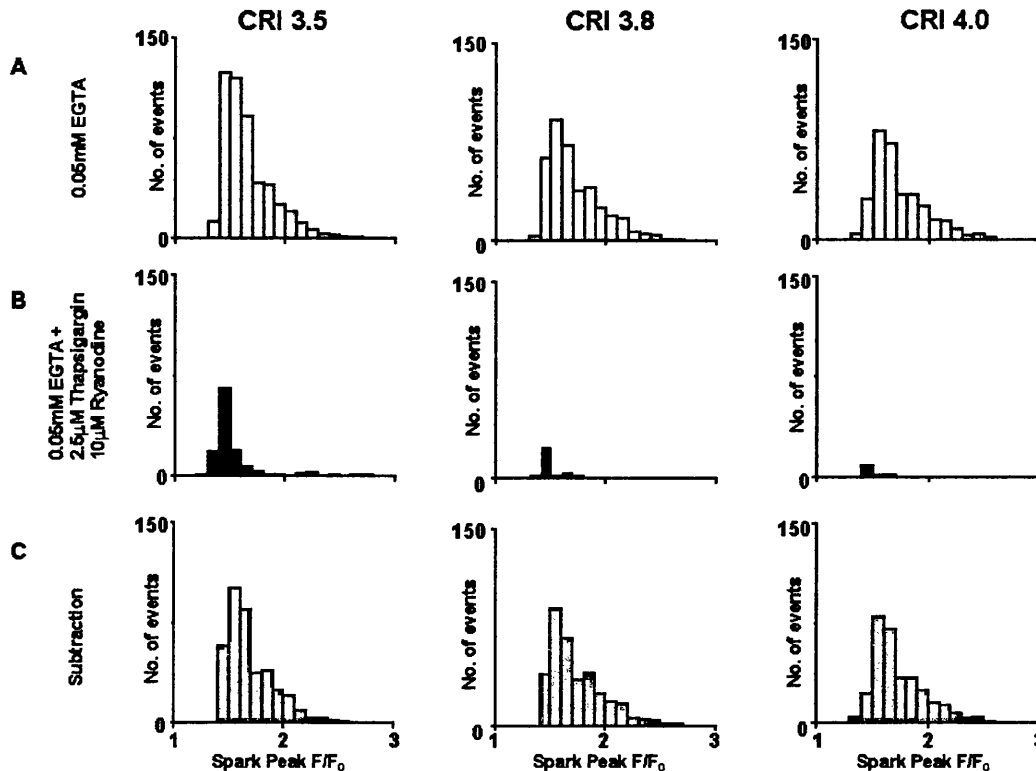


Figure 2.6 Amplitude histograms of Ca^{2+} sparks

Amplitude histograms are presented for four cardiomyocytes analysed with a criterion of 3.5 (left 3 panels), 3.8 (middle 3 panels), and 4.0 (right 3 panels), in the presence of 150nM $[\text{Ca}^{2+}]$ (panels in A) and in the presence of SR inhibitors (panels in B). Panels in C are the subtraction of data from panels B from A.

2.5.4 What should the amplitude distribution for Ca^{2+} sparks look like?

There are two considerations when establishing a theoretical distribution histogram for Ca^{2+} spark amplitudes. Firstly the Ca^{2+} spark is imaged as an increase in fluorescence signal that originates from a point source. Due to diffraction, the confocal cannot detect this signal as a point source and is optically blurred in three dimensions. This can be quantified in terms of the point-spread function (PSF). The second, which follows from this, is that, although the line-scan confocal images are at a particular focal plane, Ca^{2+} sparks originating out of that plane of focus due to their PSF, which will

encroach into the focal plane being measured. However the amplitude of these events will not be as high as those within the focal plane. Since these out of focus events are more numerous (due to a larger volume of the cell out of focus than in focus) it follows that there will be a larger quantity of small events compared to larger amplitude events. The amplitude distribution is therefore monotonic/non-modal [115]. This is in contrast to histograms produced as the result of 'eye detection', which show a Gaussian distribution. This is due to human bias against these small events. The theoretical non-modal distribution of Ca^{2+} spark amplitudes is confirmed by the use of the above automated detection algorithm [115] and is also seen in Figure 2.6. It can be seen from Figure 2.6 that as Cri is increased the monotonic relationship between Ca^{2+} spark amplitude and frequency of events begins to become modal but not to any great degree. There is therefore the possibility that an undercounting of low amplitude events occurs at Cri of 4. However the distribution is not dissimilar from the distribution produced at a Cri of the recommended 3.5 by Cheng *et al* (1999) [115] and is certainly not Gaussian ('eye detection' method). Therefore a Cri of 4.0 has been used within this thesis.

2.5.5 What should the width and duration distribution of Ca^{2+} sparks look like?

No detailed study has been produced on Ca^{2+} spark width and duration distributions, but these characteristics will be under the same considerations as for Ca^{2+} spark amplitude histograms with the addition that Ca^{2+} spark width would be expected to have a greater spatial dispersion when originating out of the plane of focus.

2.5.6 Calculation of Ca²⁺ spark width

The width distribution of Ca²⁺ sparks requires careful consideration. To determine the width of the detected Ca²⁺ spark, the algorithm determines a 2-dimensional relationship between the number of pixels and their corresponding intensity (Figure 2.7A). In this example, the width is measured at full width at half maximal peak. Therefore if the peak of the spark is 6 then any pixels above 3 are included in the width measurement. In Figure 2.7A, this corresponds to a Ca²⁺ spark width of 4 pixels (0.29µm per pixel). There is a criterion within the algorithm that enables the user to change the distance searched either side of the pixel with the highest intensity (width search distance (WSD)). Figure 2.7B demonstrates a possible problem when this parameter is set too large i.e. 5µm either side of the peak pixel. The same Ca²⁺ spark will be detected as in Figure 2.7A with a width of 4 pixels. However, since the WSD is now larger two additional sparks are now detected with this one. However the peaks of these sparks (intensity of 7) are larger than the original spark (intensity of 6) and since the algorithm uses the highest intensity pixel from which to look for sparks to measure the width from, it is the width of these sparks that are measured and not the central spark. Since they are only partially within the WSD the widths of these events are recorded to be much smaller than in reality they actually are. The width distribution therefore results in a sub-population of events at the left of the distribution because WSD is too large (Figure 2.8C). Figure 2.8A shows what happens to the width distribution if WSD is too narrow, i.e. 2.0µm. Any Ca²⁺ sparks larger than 4µm (i.e. 2 x WSD) are piled up to the right of the distribution since the programme recognises all sparks larger than this to be 4µm. As a compromise, this

thesis uses a WSD value of $2.5\mu\text{m}$, which prevents sub-population of events on either side of the width distribution (2.8B).

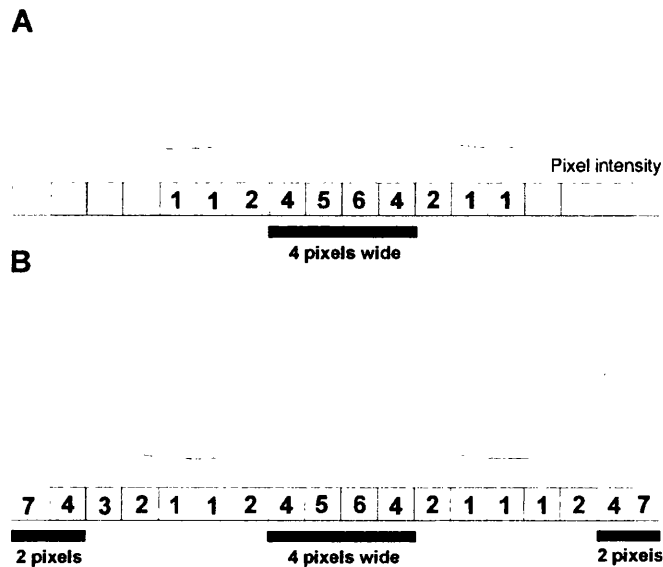


Figure 2.7 Adjustment of width parameters within the algorithm

Figure 2.7A shows a schematic to illustrate how the algorithm calculates the Ca^{2+} spark width. Panel A shows a schematic illustrating what happens when the width search distance is adjusted correctly and Panels B, when the search width distance is too large. Refer to text for discussion.

2.5.7 Is the Ca^{2+} spark a stereotyped event

Cheng *et al* (1999) demonstrated theoretically that a monotonic non-modal amplitude distribution would result if all Ca^{2+} sparks were the same size or were of different sizes [115]. To determine whether or not Ca^{2+} sparks are therefore stereotyped the amplitude distribution histograms cannot be used. However if the Ca^{2+} sparks are all the same size and are just at various distances from the in focal plane then Ca^{2+} spark amplitude will be negatively correlated with Ca^{2+} spark width.

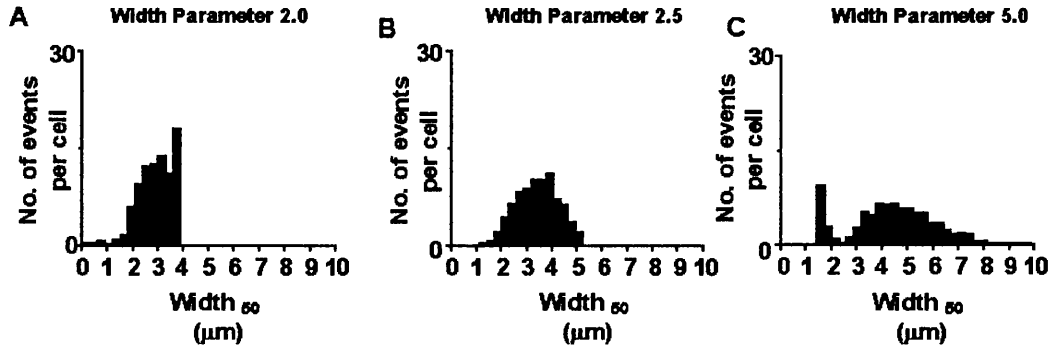


Figure 2.8 Effects of varying width search distance on width distribution

Panel A, B, and C shows the width frequency distribution when the width search distance is set to 2.0, 2.5, 5.0 μ M respectively. Refer to text for discussion.

This is thought to be because of an increased spatio-temporal spreading when sampled off centre. However a very weak positive correlation was found by Cheng *et al* (1999) suggesting that Ca²⁺ sparks may be different sizes. This is far from certain though and further work is needed on this fundamental concept [115].

CHAPTER THREE

The relationship between intracellular $[Ca^{2+}]$ and Ca^{2+} wave characteristics in permeabilised cardiomyocytes from the rabbit.

3.1 INTRODUCTION

3.1.1 The discovery of Ca²⁺ waves

In the early 1970's several authors described a phenomenon whereby isolated adult cardiomyocytes were seen to "beat" spontaneously [95;116;117]. Fabiato (1972), demonstrated that this was due to cyclical release and uptake of Ca²⁺ from the SR. This oscillation occurred in circumstances where the SR was overloaded with Ca²⁺ [95]. Originally, oscillations had been observed using light microscopy and tension measurements. However, the development of more sophisticated Ca²⁺ indicators and fluorescence microscopy confirmed the original hypothesis that these events were due to dynamic changes in [Ca²⁺] [118]. This latter study was one of the first to observe the 'wavelike' changes in fluorescence using Fura-2 [118]. The dynamic changes in [Ca²⁺] accompanied the propagating local contractions and were subsequently called Ca²⁺ waves. Intracellular Ca²⁺ waves arising from Ca²⁺ release from internal stores have been observed in a range of mammalian cell types [119]. In many cases, the Ca²⁺ waves constitute a physiological signal that triggers downstream cellular processes [120].

3.1.2 How do Ca²⁺ waves propagate?

In cardiomyocytes, Ca²⁺ waves arise from local spontaneous releases of SR Ca²⁺ (Ca²⁺ sparks/macrosparks) [121]. Ca²⁺ waves are also composed of the spatial and temporal summation of Ca²⁺ sparking events similar to Ca²⁺ transients. However, unlike Ca²⁺ transients the Ca²⁺ sparking events are not produced synchronously, but rather the rise in intracellular [Ca²⁺]

propagates from one area of the cell to the remainder, producing a global Ca²⁺ event [121-125]. The mechanism by which Ca²⁺ propagates from one region of the cell to another is still under debate.

3.1.3 Mathematical modelling

Cheng *et al* (1996) showed that the resolved image of a Ca²⁺ wave consists of Ca²⁺ sparks which are arranged at regular distances apart (~2µm) [121]. This correlation between Ca²⁺ sparks during a Ca²⁺ wave and the regular array of T-tubules, which are separated by a distance (~2µm), suggest that Ca²⁺ propagates from one site to another in a saltatory fashion. This was mathematically modelled by Keizer *et al* (1998) who showed that Ca²⁺ waves propagate with a speed that is proportional to the diffusion coefficient of Ca²⁺ [126]. The mathematical model incorporates Ca²⁺ release sites, which release Ca²⁺ (fire) when a threshold is reached. Once fired it cannot fire again. The model also incorporates a distance between release sites that mimics the regular array of T-tubules. Hence Ca²⁺ fires from one release site and diffuses continuously to the next release site in which it raises the Ca²⁺ threshold there to initiate firing of this second site. This is therefore termed a fire-diffuse-fire model [127]. Interestingly, it was suggested that since Ca²⁺ waves often occur under extreme conditions the arrangement of T-tubules may actually function to inhibit Ca²⁺ waves occurring, by making sure that propagation failure occurs under normal physiological conditions [127].

3.1.4 Factors involved in Ca²⁺ wave propagation

There are three main mechanisms, which may contribute to Ca²⁺ wave propagation.

(1) Ca²⁺ Induced Ca²⁺ Release (CICR)

It has been proposed that Ca²⁺ release is triggered by cytoplasmic Ca²⁺ acting at the cytoplasmic face of the SR [122]. This would suggest that there would always be an elevation in the Ca²⁺ concentration at a site before a Ca²⁺ wave. This is often observed, but not always [31]. That a mechanism such as CICR solely underlies Ca²⁺ wave propagation is hard to reconcile with the knowledge that Ca²⁺ sparks are local events, which do not propagate. If cytoplasmic [Ca²⁺] was the only stimulant for SR Ca²⁺ release then why do Ca²⁺ sparks not propagate? Clearly another factor is in play.

(2) SR Ca²⁺ overload

Since the Ca²⁺ spark frequency is proportional to the SR Ca²⁺ content, Ca²⁺ waves could be the result of Ca²⁺ overload within the SR [65;121;122;128]. It is possible that the Ca²⁺ within the SR initiates a Ca²⁺ wave via a luminal Ca²⁺ detector site, which senses when a certain [Ca²⁺] threshold is reached [66;67]. This mechanism would rely on release of Ca²⁺ from the SR and subsequent uptake into another overloaded SR terminal cisternae. There are two observations that may accompany such a theory. Firstly, since the SR Ca²⁺ content is higher when overloaded, it is likely that Ca²⁺ release is expected to be greater in amplitude than the Ca²⁺ stimulated Ca²⁺ transient (discussed further in section 4.4.6). This larger SR Ca²⁺ release would inevitably aid propagation of Ca²⁺ throughout the cell. Secondly, unlike the former theory, it is not necessary for the [Ca²⁺] prior to the Ca²⁺ wave to be increased.

(3) Combination of CICR and SR Ca²⁺ overload

This mechanism involves an overloaded SR, which sensitises the RyR2 to cytosolic [Ca²⁺] therefore allowing the Ca²⁺ wave to propagate via CICR. It is known that if SR [Ca²⁺] content is increased a smaller trigger can elicit the same response as a larger trigger [60;129]. Together with the finding that an increased SR [Ca²⁺] content leads to the production of Ca²⁺ waves [65;130] it is plausible that both these factors contribute to Ca²⁺ wave propagation.

3.1.5 Inactivation of SR Ca²⁺ release

A final point that must be considered is the intrinsic inactivation of SR Ca²⁺ release and the time taken for its subsequent recovery. This limitation on the positive feedback of CICR (as discussed in section 1.7) has obviously been superseded during the Ca²⁺ wave by the factors discussed above. However there is evidence that inactivation is not completely abolished during a Ca²⁺ wave. For example when ventricular cardiomyocytes are stimulated immediately after a Ca²⁺ wave has occurred, there is a time delay before RyRs recover from prior activation/inactivation during the Ca²⁺ wave and subsequent stimulation can lead to further Ca²⁺ release [121]. Furthermore when two Ca²⁺ waves approach each other, the two waves annihilated each other. This could be due to incomplete recovery from inactivation [131]. It could be that wave propagation relies not only on an increase in SR Ca²⁺ content and cytoplasmic activation, but also an increase in the sensitivity of RyR2 such that the channels refractoriness is shortened.

3.1.6 Are there different forms of Ca²⁺ waves?

Spontaneous Ca²⁺ waves occur during the diastolic period and have been linked to generation of arrhythmic electrical activity [132]. Previous studies have suggested that spontaneous Ca²⁺ waves are beneficial in: (i) minimising diastolic tone [133] and (ii) stimulating Ca²⁺ extrusion from the cell [69]. These studies have suggested that increasing cellular [Ca²⁺] leads to Ca²⁺ waves of uniform amplitude but increasing frequency. In contrast, a more recent study monitoring Ca²⁺ waves in intact rat myocardium using rapid confocal imaging identified three distinct types of Ca²⁺ waves differing in frequency, time course and amplitude depending on the cellular Ca²⁺ load [134]. Apart from these two studies [69;134] no other has addressed the specific issue of Ca²⁺ wave characteristics at varying cellular Ca²⁺ load. Furthermore, these previous studies arrive at quite different conclusions.

3.1.7 The aim of this chapter

The present study within this chapter is designed to address this dichotomy by examining the characteristics of spontaneous Ca²⁺ waves under standardised intracellular conditions using permeabilised cardiomyocytes.

3.2 METHODS

3.2.1 Cell isolation and permeabilisation

Cell isolation was performed as described within the general methods section (section 2.1.1). The cells were allowed to settle onto the cover-slip which formed the base of a small bath. β -escin (Sigma) was added from a freshly prepared stock solution to the cell suspension to give a final concentration of 0.1mg.ml⁻¹ for 0.5-1min. To assess permeabilisation, cells were examined using a confocal microscope. When intracellular fluorescence increased above extracellular fluorescence the cell was deemed permeabilised and the β -escin subsequently removed by perfusion with a mock intracellular solution (see below).

3.2.2 Solutions

Permeabilised cells were perfused with a mock intracellular solution with the following composition (mM): 100 KCl, 5 Na₂ATP, 10 Na₂Creatine Phosphate, 5.5 MgCl₂, 25 HEPES, 0.05 K₂EGTA, pH 7.0 (20-21°C). The [Ca²⁺] in the perfusing solution was varied by the addition of known amounts of 1M CaCl₂ stock solution (BDH). Fluorescent Ca²⁺ indicators Fluo-3 or Fluo-5F (Molecular Probes) were added to the solution to give a nominal final concentration of 10 μ M. All other chemicals were supplied by SIGMA (UK).

3.2.3 Data recording and analysis

Confocal line-scan images were recorded using a BioRad Radiance 2000 confocal system (the details of which are found in section 2.4.6). Data was

acquired in line-scan mode at 2ms/line; pixel width was 0.3µm (512 pixels/scan; zoom=1.4). The scanning laser line was oriented parallel with the long axis of the cell and placed approximately equidistant between the outer edge of the cell and the nucleus/nuclei, to ensure the nuclear area was not included in the scan line. As illustrated in Figure 3.4A, the LaserScan (BioRad) software saved the data as a series of image files each containing 30,000 line-scans (i.e. 1min of continuous recording). An experimental record was typically comprised of 4-5 line-scan image files; these were reviewed off-line and a single intracellular region (20 voxels wide) was selected on the basis of the earliest events in the majority of Ca²⁺ waves (as indicated in Figure 3.2A). This ensured that any movement artefact following the increase in [Ca²⁺] did not affect the estimation of peak [Ca²⁺]. Wave front was taken to be the mid-point of the upstroke. Using a 50-voxel region flanking the 20-voxel region, the gradient was used to calculate wave velocity. An average velocity (5-10 waves) was calculated for each cell.

3.2.4 Calibration of fluorescence indicators

The Ca²⁺ sensitivity of the fluorescence dyes was measured using a series of Ca²⁺ buffered solutions based on the mock intracellular solution containing 10mM EGTA. The equilibrium concentrations of metal ions in the calibration solutions were calculated using a computer program with known affinity constants for H⁺, Ca²⁺ & Mg²⁺ for EGTA [135] and for ATP and CrP [136]. Corrections for ionic strength, details of pH measurement, allowance for EGTA purity and the principles of the calculations are detailed elsewhere [137]. Under these conditions the apparent affinity constant of Fluo-3 for Ca²⁺ was 558±14nM (n=6); that of Fluo-5F was 1035±16nM

(n=4). To establish the behaviour of the dyes in the permeabilised cardiomyocytes, simultaneous fluorescence measurements were made from a 6µm (x) by 0.5µm (y) by 0.9µm (z) volume (20 voxels) within a cardiomyocyte and in the solution adjacent to the cardiomyocyte. In these calibration experiments, SR Ca²⁺ uptake was inhibited by prior treatment with thapsigargin (10µM, 20min). Figure 3.1A (i) and (ii) shows that a higher fluorescence was recorded from within the cell compared to an equivalent region in free solution suggesting either: (i) a higher Fluo-3 concentration within the cell or (ii) differing Ca²⁺ affinity of the dye within the cytosolic space. Rapidly increasing [Ca²⁺] perfusing the cell from 150nM (50µM EGTA, 10µM Fluo-3) to 1.12µM (10mM EGTA, 10µM Fluo-3) caused proportionate changes in fluorescence in both regions implied by the almost constant ratio of intracellular /extracellular fluorescence (F_{IC}/F_{EC} ; Figure 3.1A(ii)). Similarly, reducing [Ca²⁺] in the perfusing solution to <1nM (10mM EGTA) caused a proportionate decrease in fluorescence but no change in F_{IC}/F_{EC} . Using the fluorescence at 1.12µM and <1nM as calibration values, the [Ca²⁺] inside the cell and in the extracellular solution can be calculated assuming the Fluo-3 Ca²⁺ affinity is the same in both compartments. This yields a value that indicates an equivalent [Ca²⁺] (~150nM) in both compartments prior to the solution change (Fig 3.1A (iii)). In a number of calibration experiments F_{IC}/F_{EC} was measured in solutions containing ~150nM Ca²⁺ and on rapid application of solutions containing 375nM or 1.12µM Ca²⁺. The F_{IC}/F_{EC} value in 375nM Ca²⁺ was 0.99 ± 0.4 (n= 8) of that in ~150nM Ca²⁺ while the F_{IC}/F_{EC} value in 1.12µM Ca²⁺ was 1.01 ± 0.06 (n=4) of that in ~150nM Ca²⁺. This constancy of F_{IC}/F_{EC} values over a wide range of [Ca²⁺] indicates that Fluo-3 inside the cardiomyocyte has a Ca²⁺

affinity indistinguishable from that of free solution. While the F_{IC}/F_{EC} value was constant over a range of [Ca²⁺] in any one preparation, absolute value varied between cells, on average the fluorescence within a cardiomyocyte was $140 \pm 9\%$ (n=14) of that in free solution. Similar behaviour was observed for the lower affinity dye Fluo-5F. Figure 3.1B(i) shows the fluorescence signal from a cardiomyocyte (in the absence of thapsigargin) perfused with a [Ca²⁺], that was sub-threshold for Ca²⁺ waves. Calibration of both intracellular and extracellular signals was performed by perfusing with 375nM Ca²⁺ in the presence of 10mM EGTA to clamp the [Ca²⁺] in both compartments. Minimum fluorescence values were obtained by perfusion with a [Ca²⁺] of <1nM (10mM total EGTA). Thus the [Ca²⁺] could be calculated assuming an identical affinity of Ca²⁺ for the dye in both intracellular and extracellular compartments (Fig 3.1B(ii)). With 50 μ M EGTA present, the [Ca²⁺] was identical in both regions, additional noise in the intracellular signal is attributable to local release of Ca²⁺ from the SR (Ca²⁺ sparks).

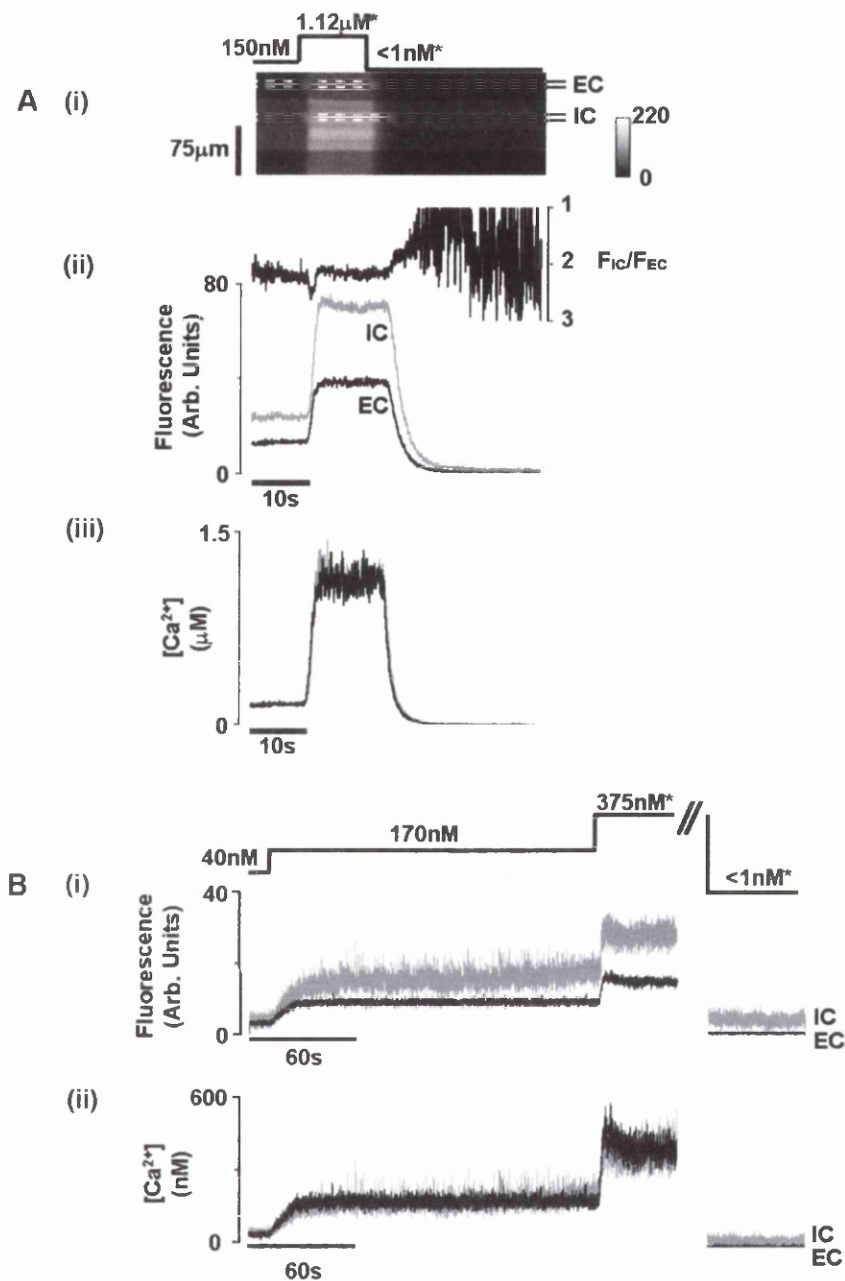


Figure 3.1 Line-scan epi-fluorescence imaging of cardiomyocytes

A (i), line-scan epi-fluorescence image of a single permeabilised cardiomyocyte after incubation with thapsigargin (10μM for 10min). The brighter central region is due to the presence of the fluorophore Fluo-3 in the cell; dimmer flanking signals are from the Fluo-3 in the perfusing solutions. The calculated [Ca²⁺] in the perfusion solution is shown above the trace; control solutions contained a total concentration of EGTA ([EGTA]) and Fluo-3 of 50μM and 10μM, respectively. [Ca²⁺] marked by * indicates solutions containing a total [EGTA] of 10mM. A (ii), mean fluorescence signal of a 20 voxel region from the intracellular (IC) and extracellular compartments (EC); these regions are indicated by

dashed lines in A (i). The ratio of IC fluorescence/EC fluorescence (F_{IC}/F_{EC}) is plotted above (see right-hand axis). A (iii), IC and EC signals converted to [Ca²⁺] on the basis of the signals in 1.12 μ M and <1nM Ca²⁺. B (i), mean fluorescence signals from within a cardiomyocyte (IC, grey trace) and a similar region outside the cell (EC, black trace) on raising the external [Ca²⁺] from 40nM to 170nM (in 50 μ M EGTA, 10 μ M Fluo-3). At the points indicated above the trace, the solution was switched to one containing 375nM Ca²⁺, then <1nM Ca²⁺ (10mM EGTA). B (ii), IC and EC signals converted to [Ca²⁺] on the basis of the signals in 375nM and <1nM Ca²⁺.

3.2.5 Statistics

The relationship between extracellular [Ca²⁺] and Ca²⁺ wave parameters was investigated using linear regression. The best-fit gradients are expressed with the asymptotic standard error (a measure of the uncertainty of parameter estimates). Where appropriate, curve fits were compared using an F-test, based on the sum-of-squares (SSQ) difference between the fitted curve and data values. Student's t-test or Anova and Tukey-Kramer Multiple comparisons test were used where appropriate.

3.3 RESULTS

3.3.1 Measurement of Ca²⁺ waves in permeabilised single myocytes

Figure 3.2A shows a section of a line-scan image recorded from a single permeabilised cardiomyocyte exposed to solution containing 260nM Ca²⁺. Due to the presence of Fluo-3 (10µM) in the perfusing solution, the fluorescence signal recorded from the complete line-scan contains signals from both intracellular and extracellular compartments. Intracellular and extracellular areas were distinguished by (i) the higher fluorescence from cardiomyocyte under quiescent conditions (see Figure 3.1) and the presence of Ca²⁺ waves. As described above, the complete series of line-scans recorded in the protocol (Figure 3.2B) were analysed by selecting a 20 voxel region from a site inside a permeabilised cardiomyocyte and an extracellular site ~6µm away from the cardiomyocyte (the fluorescence signals are shown in Figure 3.2C(i)). Increasing [Ca²⁺] in the perfusing solution from 40 to 260nM caused an increase in Fluo-3 fluorescence at both sites. The raised intracellular [Ca²⁺] initiated a series of Ca²⁺ waves recorded as transient increases fluorescence at regular intervals at the intracellular site. The delay between the increased cytosolic [Ca²⁺] and the first Ca²⁺ wave reflects a period of net SR Ca²⁺ uptake. The frequency of Ca²⁺ waves quickly (within 1-2 cycles) reaches a steady state suggesting a period of 10-15s before a new steady SR Ca²⁺ content is achieved. The average of the last 5 Ca²⁺ waves is shown in the adjacent panel (Fig 3.2C(ii)). At the point indicated, the perfusing solution was changed to one containing 375nM free [Ca²⁺] (buffered by 10mM EGTA). The high [EGTA] effectively clamped the [Ca²⁺], buffering Ca²⁺ release and uptake by the SR.

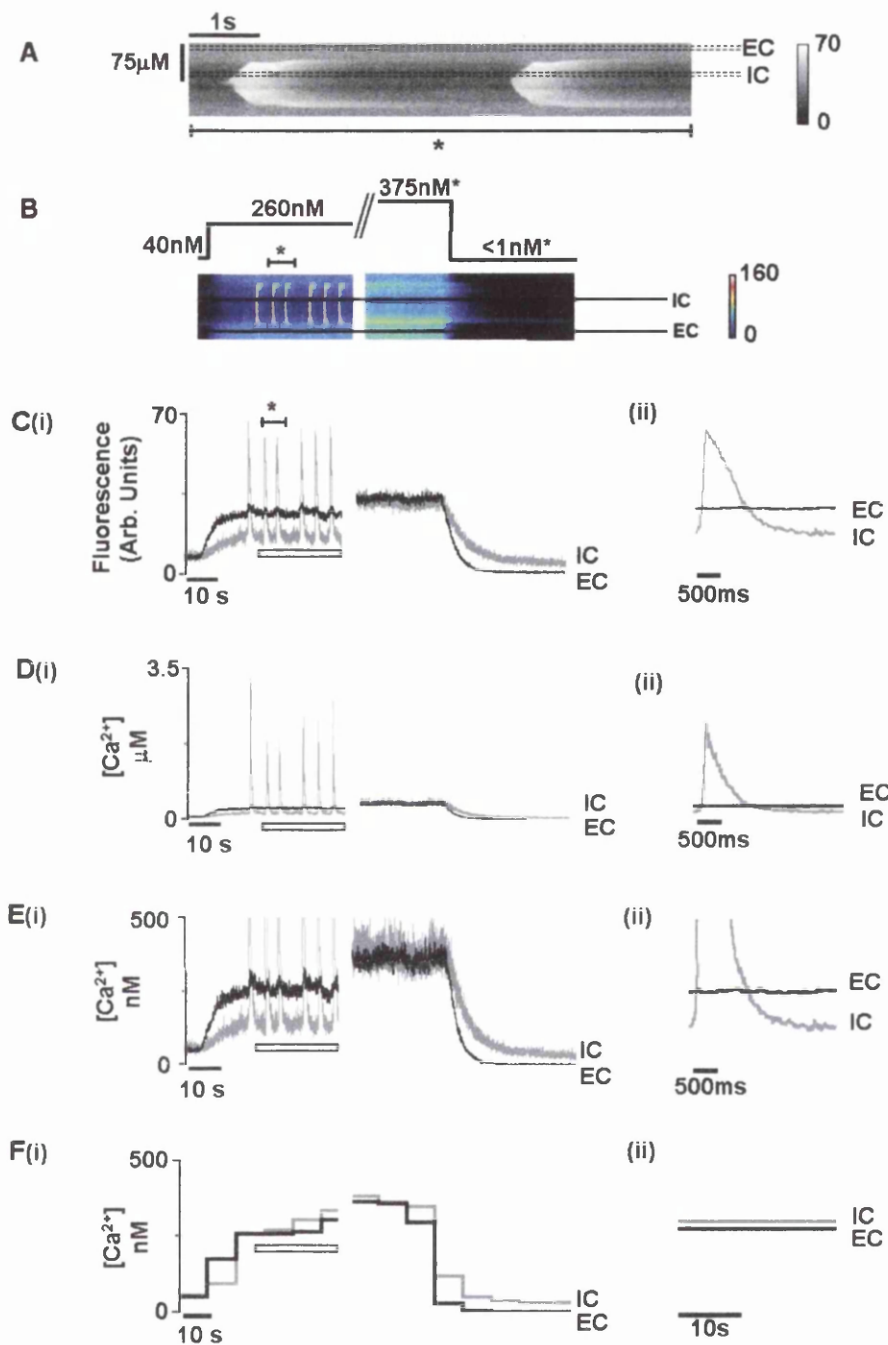


Figure 3.2 Analysis of confocal line-scan images of Ca²⁺ waves

A, line-scan image of Ca²⁺ waves measured on perfusion of a permeabilised cardiomyocyte with an extracellular [Ca²⁺] of ~260nM Ca²⁺. The sections marked with the dashed lines are 20 voxel wide regions within the cell (IC) and in the extracellular solution (EC). B, a longer record of line-scan images from the permeabilised cardiomyocyte while raising the [Ca²⁺] in the perfusate from 40nM to 260nM (50µM EGTA, 10µM Fluo-3). The section marked by an asterisk is the region corresponding to the expanded trace in A.

Subsequently; the cardiomyocyte was perfused with 375nM and <1nM Ca²⁺ (* indicates total [EGTA] = 10mM, 10µMFluo-3), as indicated above the trace. C (i), superimposed IC (grey trace) and EC fluorescence signals (black trace) from the line-scan shown in B. C (ii), average fluorescence signal of the last five Ca²⁺ waves (IC, grey trace) and the corresponding EC signal (black trace); the period averaged is indicated by the open box. D (i), IC and EC [Ca²⁺] signals calculated from the fluorescence signals obtained in 375nM and <1nM Ca²⁺. D (ii), the averaged IC (grey) and EC (black) [Ca²⁺] calculated from the averaged fluorescence signals during the period indicated by the open box. E (i), higher-resolution IC and EC [Ca²⁺] signals. E (ii), averaged IC (grey) and EC (black) [Ca²⁺] signals displayed at a higher resolution during the period indicated by the open box. F (i), averaged Ca²⁺ signals over 10s periods from IC (grey) and EC (black) signals. F (ii) mean IC and EC [Ca²⁺] signals during the period indicated by the open box.

The [Ca²⁺] was subsequently reduced to <1nM by perfusion with 10mM EGTA solution (no added Ca²⁺). Figure 3.2D shows the trace converted to [Ca²⁺]. There appeared to be a large variation in peak [Ca²⁺] of the Ca²⁺ wave. Some of this variation could be due to the noise associated with the photo-multiplier signal combined with the low Ca²⁺ sensitivity of Fluo-3 fluorescence signal at high [Ca²⁺]. A more reliable estimate of peak [Ca²⁺] can be obtained by converting the averaged fluorescence signal shown in Figure 3.2C(ii) to [Ca²⁺] (Figure 3.2D(ii)). In Figure 3.2E the minimum intracellular Ca²⁺ signal between Ca²⁺ waves and the extracellular signal have been plotted on a different scale to show the relationship more clearly. When [Ca²⁺] in the perfusing solution was increased the [Ca²⁺] inside the cell was consistently lower than the extracellular suggesting active Ca²⁺ uptake by the cell. Ca²⁺ waves began approximately 15s after an increase in extracellular [Ca²⁺] with a frequency about 0.2Hz. The minimum inter-wave [Ca²⁺] was maintained at approximately 140nM. To assess the mean [Ca²⁺] within the cell, average [Ca²⁺] over a series of 10s periods was

calculated for both intracellular and extracellular signals (Figure 3.2F(i)). Despite the presence of large amplitude waves, mean intracellular [Ca²⁺] over a 10s period was comparable to that in the extracellular space (Figure 3.2F(ii)). In several experiments, thapsigargin (10μM) was applied after a period of spontaneous Ca²⁺ waves. The resulting rapid inhibition of the SR Ca²⁺ pump abolished Ca²⁺ waves and caused both intracellular and extracellular signals to become superimposed (results not shown). Thus SR Ca²⁺ uptake and release results in a minimum inter-wave [Ca²⁺] that is considerably lower than the average value. This maintained concentration gradient is balanced by intermittent Ca²⁺ waves that reverse the concentration gradient and generate a net Ca²⁺ efflux from the cell.

3.3.2 Ca²⁺ wave characteristics measured at high cellular [Ca²⁺]

Elevating [Ca²⁺] in the extracellular solution led to Ca²⁺ waves arising more frequently (Figure 3.3A, B & C). These signals were recorded using Fluo-5F to ensure adequate sensitivity at higher [Ca²⁺]. Each panel shows sections of records of early and late periods (separated by ~60s) of a continuous 90s exposure to high [Ca²⁺]. In Figure 3.3A, stable Ca²⁺ wave activity was maintained with a mean extracellular and intracellular [Ca²⁺] of 1.3μM. In Figure 3.3B, in a separate cell, when the extracellular [Ca²⁺] was increased to >2μM, larger amplitude and more frequent Ca²⁺ waves occurred. It was consistently observed that the mean intracellular and extracellular [Ca²⁺] did not equalize over the 90s of the recording. In the presence of an extracellular [Ca²⁺] of 2.12±0.08μM, mean intracellular [Ca²⁺] was 1.46±0.06μM (n=4, P <0.01).

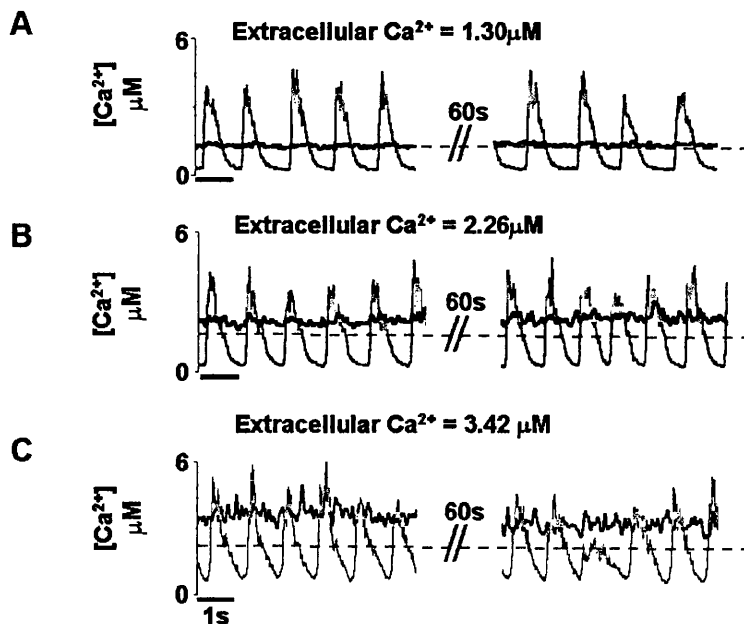


Figure 3.3 Records of Ca²⁺ waves at different values of extracellular [Ca²⁺]

Records of EC (black trace) and IC [Ca²⁺] (grey trace) derived from 20 voxel regions of line-scan images of cardiomyocytes perfused with solutions containing 50 μM EGTA, 10 μM Fluo-5F and the following [Ca²⁺]: A, 1.3 μM; B, 2.26 μM; C, 3.4 μM. The grey dashed line indicates the calculated mean intracellular [Ca²⁺].

In a separate set of measurements, cardiomyocytes were exposed to an extracellular [Ca²⁺] >3 μM, as shown in Figure 3.3C, mean intracellular [Ca²⁺] remained at ~2 μM over the 60-90s period of the recording. Furthermore, the characteristics of Ca²⁺ waves were not constant. Over the period of exposure (90s) the time course of the Ca²⁺ waves slowed, peak [Ca²⁺] decreased and the waves were of irregular amplitude (see Figure 3.3C). During short periods (90-120s) at these high cellular [Ca²⁺], the cardiomyocyte retained a normal relaxed cell length.

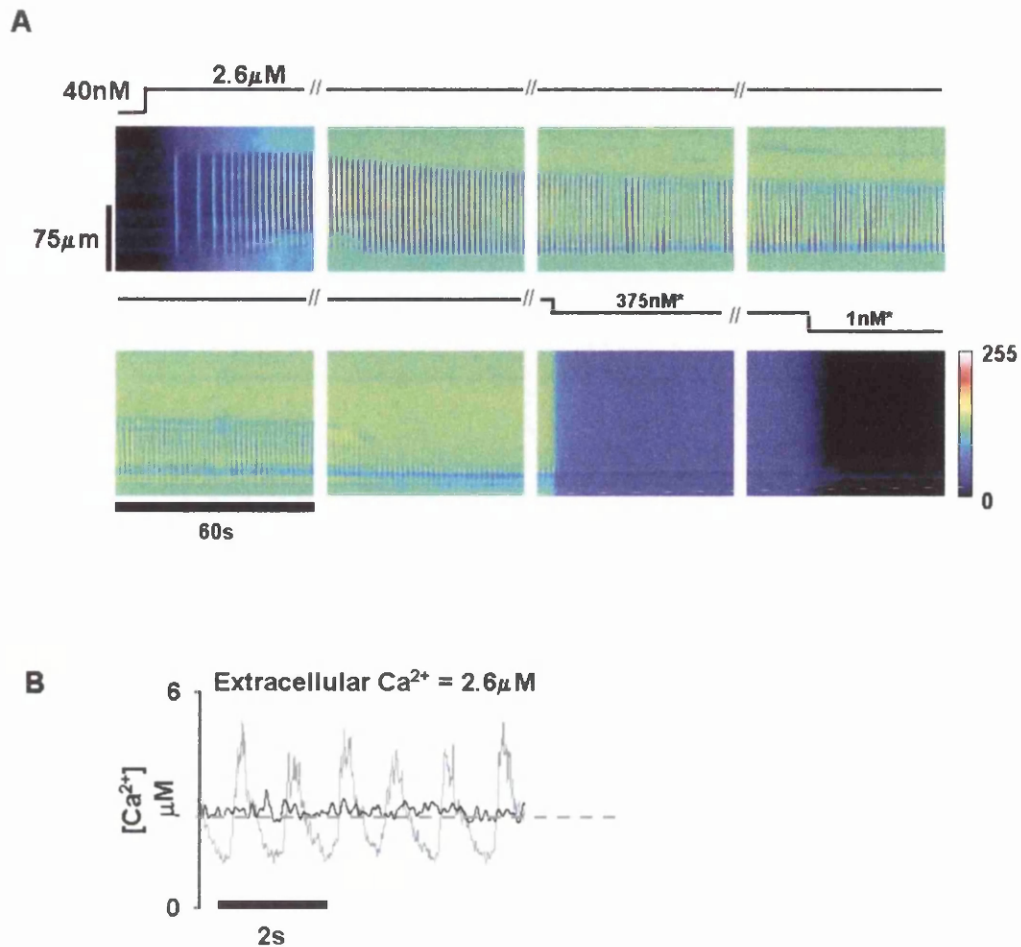


Figure 3.4 Effect of prolonged exposure to high extracellular [Ca²⁺] on Ca²⁺ waves in cardiomyocytes

A, series of eight sequential line-scan images recorded from a single cardiomyocyte perfused with 2.6 μM Ca²⁺ (50 μM EGTA and 10 μM Fluo-5F). The gaps between images represent ~ 5 s breaks between acquisition periods. Images during perfusion with 375 nM Ca²⁺ (10 mM EGTA*) and 1 nM Ca²⁺ (10 mM EGTA*) are indicated above the images. B, EC (black) and IC (grey) [Ca²⁺] signals derived from line-scan records of a hypercontracted cardiomyocyte during exposure to 2.6 μM Ca²⁺ (50 μM EGTA, 10 μM Fluo-5F). The grey dashed line indicates the calculated mean intracellular [Ca²⁺].

However, if the period was prolonged (>2 min) cardiomyocytes developed an irreversible hyper-contraction (i.e. did not relax when exposed to <1 nM [Ca²⁺]). This phenomenon is illustrated in Figure 3.4A. Marked cell shortening prevented the use of the calibration signals at 375 nM and <1 nM

to calculate the intracellular [Ca²⁺] inside the previously relaxed cell. However, the calibration protocol could be applied to regions of the shortened cell. As shown in Figure 3.4B, intracellular [Ca²⁺] in a cardiomyocyte after a sustained hyper-contraction, indicated that the SR within the cell was capable of generating low amplitude Ca²⁺ waves. Mean [Ca²⁺] measurements indicated equilibration between intracellular and extracellular [Ca²⁺] at these high cellular [Ca²⁺].

3.3.3 Mitochondrial Ca²⁺-uptake affects Ca²⁺ wave characteristics

Agents that dissipate the mitochondrial membrane potential such as CCCP (carbonyl cyanide m-chlorophenylhydrazone, 2 μ M), inhibit Ca²⁺-uptake by mitochondria. Under these conditions, the mitochondrial F₁, F₀ ATP synthase can work in reverse and breakdown ATP. This ATPase is inhibited by oligomycin (2 μ M). Figure 3.5A shows line-scan images recorded from two cardiomyocytes exposed to a short (90s) period of high (2.3 μ M) Ca²⁺. As Figure 3.3B, 3.4A and 3.5A showed, this [Ca²⁺] normally produced high frequency waves that were stable over short periods. However, in the presence of mitochondrial inhibitors (CCCP and oligomycin), the cardiomyocyte initially produces high frequency waves, but very quickly develops an irreversible hyper-contraction. Signals recorded from a cardiomyocyte exposed briefly (50-60s) to ~2.3 μ M Ca²⁺ and subsequent calibration solutions without developing a sustained hyper-contraction is shown in Figure 3.5B.

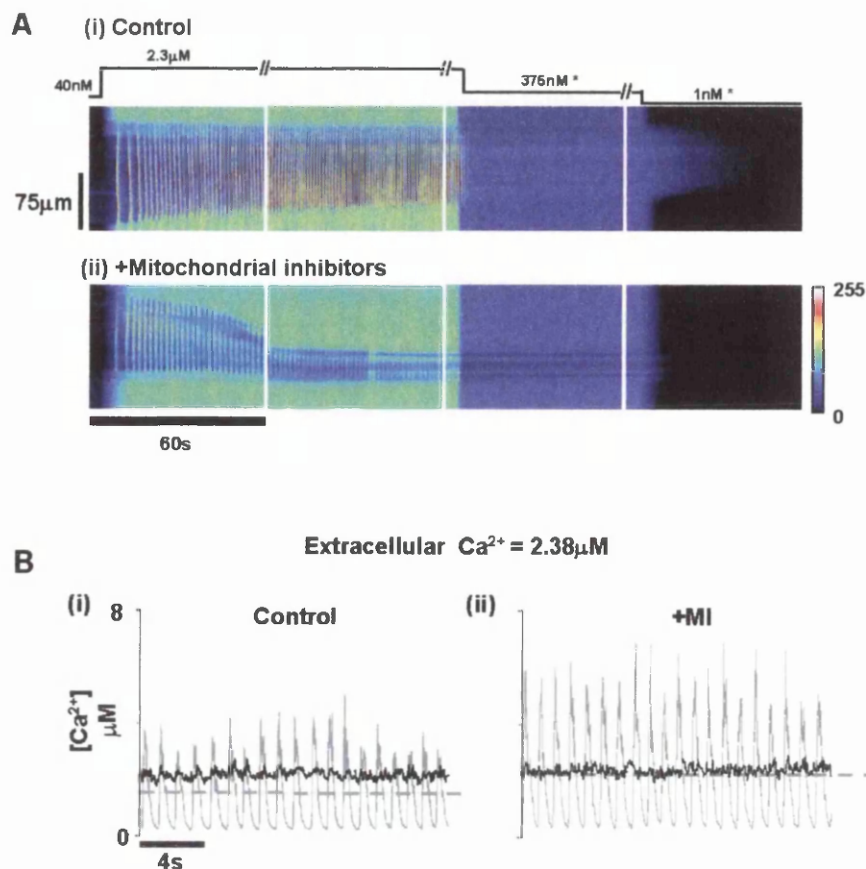


Figure 3.5 Effect of mitochondrial inhibitors on Ca²⁺ waves at high extracellular [Ca²⁺]

A (i) and (ii), sequential line-scan images recorded from permeabilised cardiomyocytes perfused with 2.3μM Ca²⁺ (50μM EGTA, 10μM Fluo-5F) followed by perfusion with 375nM* Ca²⁺ and 1nM* Ca²⁺ (*10mM [EGTA], 10μM Fluo-5F). The gaps between images represent ~5s breaks between acquisition periods. B, records of EC (black trace) and IC (grey trace) [Ca²⁺] signals derived from 20 voxel regions of line-scan images of a cardiomyocyte perfused with 2.3μM Ca²⁺ (50μM EGTA, 10μM Fluo-5F) under control conditions (i) and including mitochondrial inhibitors (+MI) carbonyl cyanide *m*-chlorophenylhydrazone (CCCP, 2μM) and oligomycin (2μM) (ii). The grey dashed lines represent the mean intracellular [Ca²⁺] over the period shown.

Ca²⁺ waves observed during mitochondrial inhibition reached higher peak values than that seen under control conditions (compare Figure 3.5B(i) and (ii)). Furthermore, the significant extracellular-intracellular [Ca²⁺] gradient

observed under control conditions was absent after mitochondrial inhibition. The effects of mitochondrial inhibitors on Ca²⁺ waves were studied in detail at two cellular [Ca²⁺]'s. At ~400nM, a level known to allow equilibration of [Ca²⁺] between intracellular and extracellular compartments, and ~2-2.2μM which, as shown in Figure 3.5B normally does not result in equilibration unless mitochondrial inhibitors are used. The mean values (\pm SEM) of maximum [Ca²⁺], minimum [Ca²⁺] during a Ca²⁺ wave, wave frequency along with mean extracellular and intracellular values are given in Figure 3.6A & B. At ~400nM, mitochondrial inhibition had no effect on any of the Ca²⁺ wave characteristics studied (Figure 3.6A). However the mean data shown in Figure 3.6B confirms that mitochondrial inhibition permits equilibration of Ca²⁺ between extracellular and intracellular compartments by increasing the maximum [Ca²⁺] reached during a Ca²⁺ wave. This suggests that mitochondria Ca²⁺ uptake normally buffers the peak of Ca²⁺ wave.

3.3.4 Relationship between extracellular and intracellular [Ca²⁺]

Figure 3.7 plots results from 15 cells using a range of extracellular [Ca²⁺]. No Ca²⁺ waves were recorded in cardiomyocytes exposed to <200nM over a 90s period, but raising mean [Ca²⁺] to approximately 240nM caused low frequency Ca²⁺ waves with the minimum [Ca²⁺] between the waves reaching ~140nM.

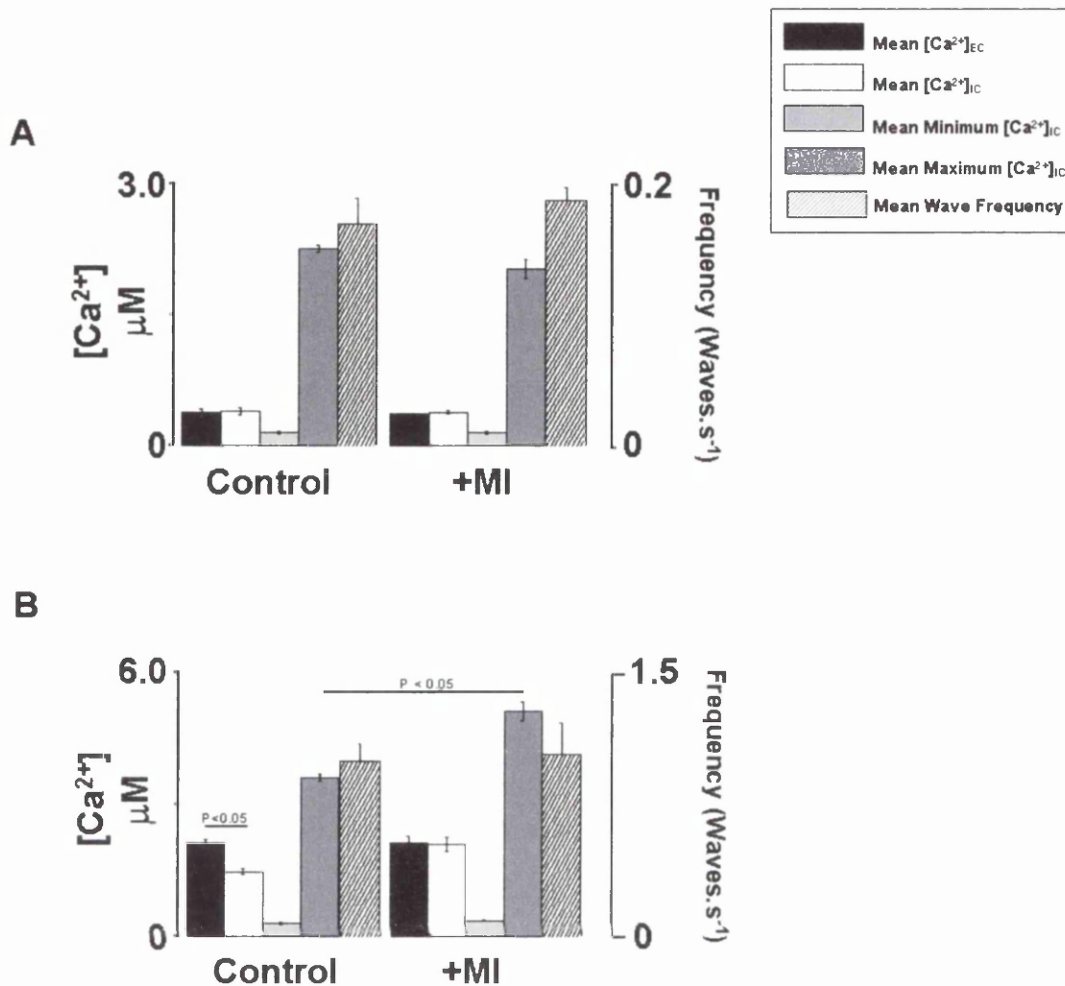


Figure 3.6 Effect of mitochondrial inhibitors on [Ca²⁺]_{EC} and Ca²⁺ wave parameters

Averages (\pm SEM) of Ca²⁺ signals recorded from line-scan images of cardiomyocytes after perfusion with $\sim 0.4 \mu\text{M}$ (A) and $\sim 2.1 \mu\text{M}$ Ca²⁺ (B) in the absence (Control) and presence (+MI) of $2 \mu\text{M}$ CCCP, $2 \mu\text{M}$ oligomycin ($n = 4$ in each group). For each parameter (i.e. mean extracellular [Ca²⁺]_{EC}, mean intracellular [Ca²⁺]_{IC}, minimum [Ca²⁺]_{IC}, maximum [Ca²⁺]_{IC} and wave frequency) significant differences between control and the +MI conditions are indicated (B). Significant differences existed between all of the individual Ca²⁺ wave characteristics measured at $\sim 0.4 \mu\text{M}$ and $\sim 2.3 \mu\text{M}$ [Ca²⁺]_{EC} ($P < 0.001$).

Using extracellular [Ca²⁺]_{EC} $> 200 \text{ nM}$ and $< 2 \mu\text{M}$, Ca²⁺ waves with nearly uniform amplitude and frequency occurred. At extracellular [Ca²⁺]_{EC} $> 3 \mu\text{M}$,

Ca²⁺ wave characteristics were not stable. A common feature in experiments using high (>2μM) [Ca²⁺] was the maintained [Ca²⁺] difference between intracellular and extracellular compartments over the 60-90s of recording. To examine the relationship between peak [Ca²⁺] or minimum [Ca²⁺] and the extracellular [Ca²⁺], the values obtained between 200-1000nM Ca²⁺ are plotted on a linear scale in panels (ii) and (iii). The straight lines represent the best-fit linear correlation. A similar format is used in Figure 3.7B to indicate the relationship between Ca²⁺ wave frequency and velocity at a range of extracellular [Ca²⁺]. Frequency was highly dependent on intracellular [Ca²⁺] but no clear relationship existed for wave velocity (Figure 3.7B(ii) & (iii)).

3.3.5 Time-course of the Ca²⁺ wave is influenced by the mean cellular [Ca²⁺]

Figure 3.7C (i) and (ii) indicates the relationship between the rate of rise and rate of decline of the averaged Ca²⁺ wave measured (rates measured at 1μM intracellular [Ca²⁺]). Both measurements show a weak but significant positive correlation indicating that the rate of release of Ca²⁺ and rate of uptake are increased at higher extracellular [Ca²⁺] (similar results were observed at 0.5 and 1.5μM). This indicates that the time-course of Ca²⁺ waves is sensitive to the mean cellular [Ca²⁺], as a consequence, the duration of the Ca²⁺ wave decreases as mean cellular [Ca²⁺] is increased.

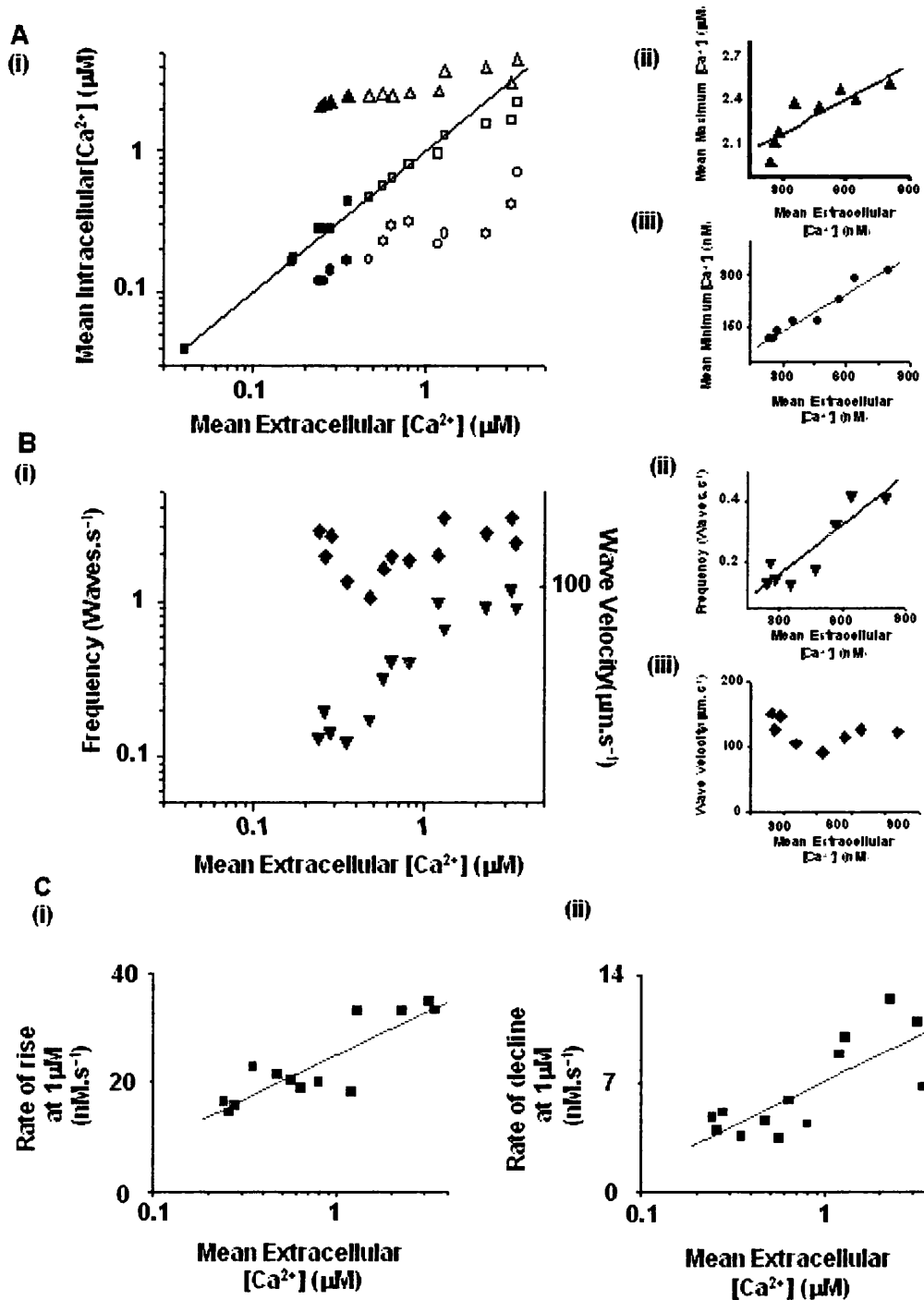


Figure 3.7 Relationship between various mean intracellular [Ca²⁺] and Ca²⁺ wave parameters and mean extracellular [Ca²⁺]

A (i), a log-log plot of extracellular [Ca²⁺] vs. mean intracellular [Ca²⁺] from 15 cardiomyocytes (Fluo-3: filled squares, Fluo-5F: closed squares), maximum [Ca²⁺] (wave peak), (Fluo-3: filled triangles; Fluo-5F: open triangles), minimum [Ca²⁺] (Fluo-3: filled

circles; Fluo-5F: open circles). The line indicates the unity relationship in panel A (i). A (ii), linear plot of extracellular [Ca²⁺] (300-900nM range) vs. maximum [Ca²⁺]. The continuous line is the best-fit linear correlation with gradient 0.77 ± 0.18 ($P < 0.01$). A (iii), linear plot of extracellular [Ca²⁺] (300-900nM range) vs. minimum [Ca²⁺] during a Ca²⁺ wave. The continuous line is the best-fit linear correlation, and has a gradient of 0.35 ± 0.03 ($P < 0.001$). B (i), a log-log plot of extracellular [Ca²⁺] vs. frequency of Ca²⁺ waves (filled inverted triangles) and wave velocity (filled diamonds). B (ii), linear plot of extracellular [Ca²⁺] (300-900nM range) vs. Ca²⁺ wave frequency. The continuous line is the best-fit linear correlation, with gradient $5.5 \times 10^5 \pm 1 \times 10^5$ (waves s⁻¹ M⁻¹; $P < 0.01$). B (iii), linear plot of extracellular [Ca²⁺] (300-900nM range) vs. wave velocity (no correlation). C (i), semilog plot of extracellular [Ca²⁺] vs. rate of rise of Ca²⁺ wave measured at 1 μM Ca²⁺. The line shows the best-fit linear correlation. C (ii), semilog plot of the rate of decline of the Ca²⁺ wave measured at various values of extracellular [Ca²⁺]. The line shows the best-fit linear correlation.

3.4 DISCUSSION

In this study, the permeabilised cardiomyocyte preparation is used as a simplified system to study the characteristics of propagated Ca²⁺ waves. A simple set of measurements revealed that the fluorescence from Ca²⁺ indicators Fluo-3 and Fluo-5F was higher within permeabilised cardiomyocytes than in an equivalent extracellular volume. This may be explained by either: (i) indicator binding to structures within the permeabilised cell or (ii) an interaction between the cytosol and indicator resulting in increased fluorescence. Regardless of the cause, measurements in this study indicated that affinity of Ca²⁺ for the dye in the cytosol is not significantly different to that measured in free solution.

3.4.1 Changes in Ca²⁺ wave characteristics at a mean cellular [Ca²⁺] <1.2μM.

This is the first study to report the relationship between Ca²⁺ wave characteristics and mean cellular [Ca²⁺] in single cardiac muscle cells. Spontaneous Ca²⁺ waves were recorded at a mean intracellular [Ca²⁺] of >200nM. Below this value no spontaneous release was evident, although individual Ca²⁺ sparks could be detected. Since the test period was only 90-120s, it is conceivable that at 150-180nM, propagated Ca²⁺ waves occurred at frequencies less than 1-2min⁻¹ (~0.01s⁻¹). However, this frequency is much lower than the value of 0.1s⁻¹ expected at 150nM Ca²⁺ based on a linear extrapolation of the relationship shown in Figure 3.7B(ii). In a recent study of intact rat myocardium at room temperature [134], "sporadic" Ca²⁺ waves occurred at very low frequencies (0.02-0.2Hz) with a distinctly lower velocity and amplitude from those observed at higher

cellular [Ca²⁺]. Waves with these characteristics were not observed in the present study. At moderate intracellular [Ca²⁺] (250-300nM), peak [Ca²⁺] of waves observed in this study was 2.1-2.2μM. These values are higher than that reported by some studies [138;139] but similar to others [122]. The peak of Ca²⁺ waves increased by approximately 0.4μM (i.e. from ~2.1 to ~2.5μM (120% increase) when cellular [Ca²⁺] was raised from 0.3μM to 0.9μM (300% increase). Minimum [Ca²⁺] increased by 200% over the same range of cellular [Ca²⁺] (from ~150nM to ~300nM), while Ca²⁺ wave frequency increased from ~0.15 to ~0.45Hz (300%). Interestingly, Ca²⁺ wave velocity was constant over the entire range of cellular [Ca²⁺] despite marked increases in the peak [Ca²⁺] during a wave. The mean value of 122±6μm.s⁻¹ (n=8) is similar to the values reported by other studies [122;130;134;139;140] and faster than others [64;121;138]. A positive correlation between peak [Ca²⁺] during a wave and velocity has been noted previously [124;138], but these measurements were made at a constant cellular [Ca²⁺] (and therefore constant minimum [Ca²⁺]). As shown in Figure 3.8, a positive correlation between velocity and Ca²⁺ wave amplitude (peak – minimum) was observed at each cellular [Ca²⁺], (mean gradient of 33.4±0.4μm.s⁻¹.μM⁻¹, n=8). Approximately parallel increases in minimum and peak [Ca²⁺] occur as mean intracellular [Ca²⁺] is increased. This results in a relatively constant wave amplitude (2.1±0.04μM, n=8) over the range of cellular [Ca²⁺] 0.2–1.2μM. This constant amplitude may explain the lack of marked changes in wave velocity despite increases in the peak [Ca²⁺] during a Ca²⁺ wave. The significant correlation between maximum [Ca²⁺], minimum Ca²⁺ and Ca²⁺ wave frequency and mean cellular [Ca²⁺]

was confirmed when the characteristics of the Ca²⁺ waves were studied in a number of cardiomyocytes at two specific extracellular [Ca²⁺]'s (~400nM and ~2.1μM, Figure 3.6).

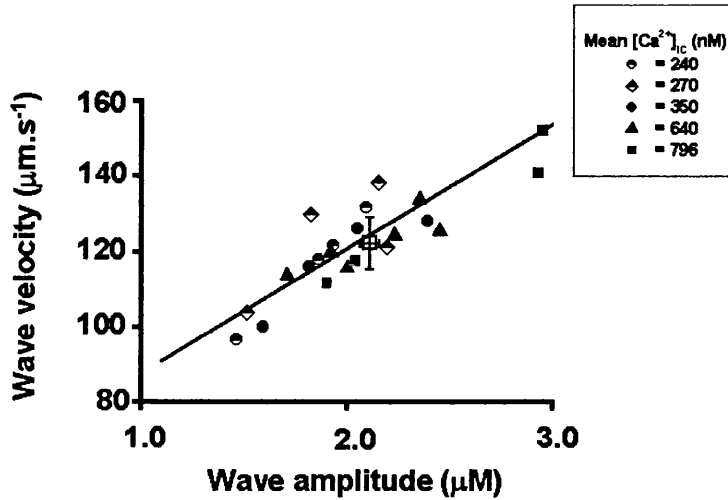


Figure 3.8 Relationship between wave velocity and wave amplitude at different values of intracellular [Ca²⁺]

Plot of Ca²⁺ wave amplitude (i.e. peak [Ca²⁺] - minimum [Ca²⁺]) vs. wave velocity for a range of mean intracellular [Ca²⁺] values (here denoted [Ca²⁺]_{ic}). Amplitude measurements were made from four to six Ca²⁺ waves from five cardiomyocytes. Each cardiomyocyte was exposed to an extracellular [Ca²⁺] ranging from 240nM to 796nM. The average (\pm SEM, $n=8$) Ca²⁺ wave amplitude and velocity for cardiomyocytes exposed to <1μM extracellular [Ca²⁺] is plotted on the same graph (open square). The line through the data is the best-fit linear correlation to the data, with a gradient of $33 \pm 5 \mu\text{m s}^{-1} \mu\text{M}^{-1}$ ($P < 0.03$).

Ca²⁺ wave frequency is the parameter most sensitive to mean [Ca²⁺]; an increase in the frequency and to a lesser extent the minima and maxima of Ca²⁺ waves accounts for the equilibration of intracellular and extracellular compartments up to a mean cellular [Ca²⁺] of 1.2μM. In this study, the highly permeable surface membrane allows equilibration of intracellular and extracellular [Ca²⁺]. In cardiomyocytes with intact membranes, similar mean cellular [Ca²⁺] is a consequence of influx and efflux of Ca²⁺ by trans-

membrane proteins. In both situations, Ca²⁺ waves serve to increase [Ca²⁺] transiently and stimulate net extrusion from the cell. The resultant 'buffering' of the minimum [Ca²⁺] will limit the development of resting contractile tone in the Ca²⁺ overloaded cardiomyocyte [69;133]. SR Ca²⁺ load was not assessed in this study, therefore it is unclear whether the changes in Ca²⁺ wave frequency were accompanied by increased intra-SR Ca²⁺. Diaz *et al* (1997) noted a higher frequency of spontaneous Ca²⁺ release in rat cardiomyocytes at higher extracellular [Ca²⁺], but no change in either spontaneous release amplitude or response to caffeine (a measure of SR Ca²⁺ content) [69]. This led the authors to conclude that spontaneous release occurred when intra-SR Ca²⁺ reached a set-point, increasing cytosolic Ca²⁺ increased the rate of uptake by the SR therefore shortening the time to reach the set-point.

3.4.2 Ca²⁺ wave time-course

As indicated in Figure 3.7C, the rate of rise and rate of decay of the Ca²⁺ wave increased as the mean cellular [Ca²⁺] increased. The cause of these changes in time course are unknown, an increased rate of rise of [Ca²⁺] could arise from a higher intra-SR [Ca²⁺] at higher cellular [Ca²⁺]. But an increased rate of Ca²⁺ uptake is more difficult to explain simply since a higher intra-SR [Ca²⁺] would be expected to reduce SR Ca²⁺ pump activity [141]. This would suggest the mechanism underlying the higher Ca²⁺ uptake rates may be based in the cytoplasm, for example via activation of a Ca-calmodulin kinase [142].

3.4.3 Ca²⁺ wave characteristics at high mean cellular [Ca²⁺] levels (>2μM).

When the permeabilised cell was exposed to an extracellular [Ca²⁺] close to the maximum [Ca²⁺] during a Ca²⁺ wave (>2μM), the cell produced high frequency waves of larger amplitude, but the mean intracellular [Ca²⁺] within the cell failed to equilibrate with the extracellular space. All cardiomyocytes studied were able to maintain stable Ca²⁺ wave characteristics over a 2-3min period when perfused with 2-2.5μM [Ca²⁺]. When 3.2-3.4μM extracellular [Ca²⁺] was used, uniform Ca²⁺ waves were not maintained over the 2-minute period, due to slowing in time course, a fall in maximum and a rise in minimum [Ca²⁺]. Cardiomyocytes that developed an irreversible hyper-contraction after prolonged periods of high [Ca²⁺] exhibited low amplitude oscillations of intracellular [Ca²⁺] and equilibration of extracellular and intracellular [Ca²⁺] (Figure 3.4B). The frequency of Ca²⁺ waves under these circumstances was variable, but not significantly different from that observed in cardiomyocytes prior to a sustained hyper-contraction. For this reason, these low amplitude Ca²⁺ waves are not consistent with the 'agonal waves' reported recently in intact rat myocardium at very high cellular Ca²⁺ loads which achieved frequencies of >2s⁻¹ [134]. Possible reasons for this disparity include: (i) the high cellular Ca²⁺ loads in intact cells would almost certainly be accompanied by changes in other intracellular factors (e.g. ATP and pH) which may affect Ca²⁺ wave characteristics; (ii) individual cardiomyocytes within the syncytium would not develop the same degree of hyper-contraction as an isolated cell.

3.4.4 Mitochondrial inhibitors modify Ca²⁺ wave characteristics in high [Ca²⁺].

The absence of any significant effect of mitochondrial inhibitors on the characteristics of Ca²⁺ waves at low (~0.4μM) extracellular Ca²⁺ suggests that mitochondrial Ca²⁺ uptake/release does not contribute to the characteristics of the Ca²⁺ wave at this level of Ca²⁺ overload. However, in the continued presence of mitochondrial inhibitors, perfusion with a higher extracellular [Ca²⁺] (~2μM) resulted in Ca²⁺ waves that reached significantly higher peak values (5.1±0.2μM, n=4) to those observed without inhibitors (3.6±0.08μM, n=4). Calculation of mean intracellular [Ca²⁺] in the presence of mitochondrial inhibitors generated a value close to the extracellular [Ca²⁺], which indicates there was no sustained gradient of [Ca²⁺]. These results strongly suggest that mitochondrial Ca²⁺ uptake attenuates the peak of a Ca²⁺ wave generated at an intracellular [Ca²⁺] >2μM. It is unlikely that this effect is due to a direct effect of CCCP and oligomycin on the SR since perfusion with these mitochondrial inhibitors had no effect on Ca²⁺ wave characteristics at lower cellular [Ca²⁺]. Although this is the first report of an effect in cardiac muscle, previous studies of Ca²⁺ waves in acinar cells [143] and pituitary cells [144] have shown increases in amplitude of Ca²⁺ waves after disruption of the mitochondrial membrane potential. Isolated rat heart mitochondria injected into oocytes were able to blunt and slow the intracellular Ca²⁺ transient in response to thapsigargin application [145]. In the present study, it is unlikely that these effects result from altered intracellular metabolite levels or pH as a result of mitochondrial inhibition since the permeabilised cardiomyocytes were continuously perfused with a

buffered mock intracellular solution. Previous studies have suggested that mitochondrial Ca²⁺ uptake and release occurs during Ca²⁺ sparks and waves/transients in cardiac muscle via the calcium uniporter [146;147]. These measurements were made at low cellular [Ca²⁺] and the kinetics of mitochondrial Ca²⁺ efflux were rapid and unlikely to generate the net Ca²⁺ uptake. The apparent threshold for mitochondrial Ca²⁺ uptake observed in this study (extracellular [Ca²⁺] =1.5-2μM) is in agreement with previous studies of the passive buffering by mitochondria in permeabilised cardiomyocytes [148;149]. An estimate of total Ca²⁺ released into the cytosol during a Ca²⁺ wave can be made using previously published values for passive Ca²⁺ buffering capacity of digitonin-treated rabbit cardiomyocytes [149]. These calculations would suggest that at an extracellular [Ca²⁺] of ~0.4μM, the increase of [Ca²⁺] during a wave (see Figure 3.6) would result from the release of 178μmol.l⁻¹ Ca²⁺ per litre non-mitochondrial cell volume. At the higher cellular [Ca²⁺] of ~2μM, the Ca²⁺ wave characteristics described in Figure 6 would predict a release of only 165μmol.l⁻¹ Ca²⁺ from the SR (see Table 3.1). However, the larger Ca²⁺ waves measured in presence of mitochondrial inhibitors suggest the amount of Ca²⁺ released by the SR is actually 176μmol per litre (similar to that at 0.4μM), of which ~10μmol per litre is taken up by the mitochondria at every Ca²⁺ wave.

	Free [Ca ²⁺]	[Ca ²⁺] Total	Buffers 1+2	Ca ²⁺ EGTA	Ca ²⁺ Fluo	ΔTotal [Ca ²⁺]
High [Ca²⁺] (2.3μM)						
Minimum [Ca ²⁺]	0.29	115.14	90.39	21.01	3.45	
Maximum [Ca ²⁺]	3.60	280.41	223.14	45.00	8.67	165.27
High [Ca²⁺] (2.3μM) + MI						
Minimum [Ca ²⁺]	0.35	128.40	100.83	23.33	3.89	
Maximum [Ca ²⁺]	5.12	301.95	241.43	46.38	9.03	173.56

Table 3.1 Calculation to determine the total amount of Ca²⁺ (μM) produced during a Ca²⁺ wave

Using the mean data shown in Figure 3.6 the free [Ca²⁺] was converted to total [Ca²⁺] by summing the [Ca²⁺] associated with each of the main buffers within a permeabilised cell (Hove-Madsen & Bers, 1993 *Am. J. Physiol* 264, C677-C686) without (upper panel) and with mitochondrial inhibitors present (lower panel). It can be seen that the change in total [Ca²⁺] is approximately 10μM less when mitochondrial inhibitors are present. Calculations are based on a two buffer system and the following equation and constants:

$$CaB = \frac{([Ca^{2+}]/K) \cdot B_T}{(1 + [Ca^{2+}]/K)}$$

CaB Ca²⁺ buffer complex
K Association constant
[Ca²⁺] Free [Ca²⁺]
B_T [Buffer]

Where (μM):	Buffer1	K = 0.42	B _T = 215
	Buffer2	K = 79	B _T = 702
	EGTA	K = 0.4	B _T = 50
	Fluo-3	K = 0.55	B _T = 10

Net mitochondrial Ca²⁺ accumulation via the Ca²⁺ uniporter has been reported in stimulated (intact) cardiomyocytes [150;151]. In the latter study,

net mitochondrial Ca²⁺ uptake was observed during depolarisation only when diastolic cytoplasmic [Ca²⁺] exceeded 300-500nM. This value agrees well with the value of minimum intracellular [Ca²⁺] measured in this study at which mitochondrial Ca²⁺ uptake was first evident (mean extracellular [Ca²⁺] >2μM). The results in this study suggest that mitochondrial Ca²⁺ uptake is not maintained, since cardiomyocytes that develop a hyper-contraction show no extracellular-intracellular [Ca²⁺] gradient (at >2μM). The use of the single wavelength dyes (Fluo-3/Fluo-5F) allowed accurate measurement of intracellular [Ca²⁺] signal before and after but not *during* hyper-contraction. On this basis it would appear that an event associated with the exhaustion of a mitochondrial Ca²⁺ uptake mechanism caused a rise in mean intracellular [Ca²⁺] and irreversible cardiomyocyte shortening. In a series of cell types, cell death has been linked to the collapse of the mitochondrial membrane potential and the inhibition of mitochondrial Ca²⁺ uptake [152]. Two possible causes of this event are (i) the opening of the mitochondrial permeability transition pore [153] or (ii) damage to the respiratory chain [152].

3.4.5 SUMMARY

In summary, this study suggests at cellular [Ca²⁺] between 0.2-1.2μM, spontaneous Ca²⁺ release and the generation of spontaneous Ca²⁺ waves can effectively buffer the minimum [Ca²⁺] between Ca²⁺ waves in cardiac cells. Higher cellular Ca²⁺ levels result in more frequent Ca²⁺ waves with only minor changes in time course. Attempts to increase intracellular [Ca²⁺] >2μM is resisted by mitochondrial Ca²⁺ accumulation occurring predominately at the peak of the Ca²⁺ wave. Working in this way, mitochondrial Ca²⁺ uptake will extend the period of time cardiomyocytes can maintain a low diastolic [Ca²⁺] and resist the development of a sustained and irreversible hyper-contraction when exposed to high intracellular Ca²⁺ loads.

CHAPTER FOUR

**Measurement of the dissociation constant of Fluo-3 for Ca^{2+} in
isolated rabbit cardiomyocytes using Ca^{2+} wave characteristics**

4.1 INTRODUCTION

Changes in intracellular Ca^{2+} concentration ($[\text{Ca}^{2+}]_{\text{IC}}$) play an integral part in the process of excitation-contraction coupling within mammalian cardiomyocytes. Recent developments in Ca^{2+} imaging using laser scanning confocal microscopy (LSCM) and fluorescent Ca^{2+} indicators enables the changes of $[\text{Ca}^{2+}]_{\text{IC}}$ to be followed within sub-compartments of the cell. Fluorescent signals obtained from these techniques can only be converted into changes in $[\text{Ca}^{2+}]_{\text{IC}}$ with accurate information concerning the behaviour of the dye within the cytoplasm. Aspects of the intracellular environment such as pH, viscosity, temperature, cell type, and the binding of the dye to intracellular proteins are all known to affect the affinity of the dye [154-161]. Fluo-3 is commonly used as a Ca^{2+} indicator in fluorescence and confocal studies of cardiomyocytes, yet information concerning the behaviour of Fluo-3 in the cytoplasm of cardiomyocytes is not available. Fluo-3 Ca^{2+} dissociation constants ranging from 0.4-1.09 μM have been used in published work on excitable cells [109;123;138;162-166]. These values are based mainly on the measurements of Fluo-3 fluorescence in free solution. Only in one paper, was the K_d measured under conditions approximating the intracellular space [163]. This uncertainty leads to large differences in estimates of $[\text{Ca}^{2+}]_{\text{IC}}$ and the corresponding Ca^{2+} fluxes and buffering within the cell. This study aims to measure the Ca^{2+} dissociation constant (K_d) of Fluo-3 in two different situations: (i) within the cytosol of a permeabilised cardiomyocyte and (ii) in an intact cardiomyocyte after incubation with Fluo-3 AM. These K_d values are then used to measure dynamic changes in $[\text{Ca}^{2+}]_{\text{IC}}$ that occur within

intact and permeabilised cardiomyocytes.

4.2 METHODS

4.2.1 Cell isolation and permeabilisation

Cell isolation was performed as described within the Chapter 2: section 2.1. The cells were allowed to settle onto the cover-slip at the base of a small bath. β -escin (Sigma) was added from a freshly prepared stock solution to the cell suspension to give a final concentration of $0.1\text{mg}\cdot\text{ml}^{-1}$ for 0.5-1 min. To assess permeabilisation, cells were examined using a confocal microscope. When intracellular fluorescence increased above extracellular fluorescence the cell was deemed permeabilised and the β -escin subsequently removed by perfusion with a mock intracellular solution (see below).

4.2.2 Solutions for the production of spontaneous Ca^{2+} waves within permeabilised cells

Permeabilised cells were perfused with a mock intracellular solution with the following composition (mM): 100 KCl, 5 Na_2ATP , 10 Na_2CrP , 5.5 MgCl_2 , 25 HEPES, 0.05 K_2EGTA , pH 7.0 (20-21°C). The $[\text{Ca}^{2+}]$ in the perfusing solution was varied by the addition of known amounts of 1M CaCl_2 stock solution (BDH). An estimate of the $[\text{Ca}^{2+}]$ in these solutions was calculated using a computer program (React, Smith, G.L.). For example, in the absence of added Ca^{2+} , and assuming $\sim 5\mu\text{M}$ contamination, free Ca^{2+} in 50 μM EGTA is $\sim 40\text{nM}$. Addition of Ca^{2+} to achieve a total $[\text{Ca}^{2+}]$ of 15 μM generates a free $[\text{Ca}^{2+}]$ of $\sim 150\text{nM}$. Further addition of Ca^{2+} to achieve a total of 25 μM generates a free $[\text{Ca}^{2+}]$ of $\sim 300\text{nM}$. Fluorescent Ca^{2+} indicators Fluo-3 or Fluo-5F (Molecular Probes) were added to the solution

to give a nominal final concentration of $10\mu\text{M}$. All other chemicals were supplied by SIGMA (UK).

4.2.3 Solutions for the production of spontaneous Ca^{2+} waves within intact cells

Intact cells were perfused with a modified Krebs solution [167] [168] with the following composition (mM): 140 NaCl, 4 KCl, 1 MgCl_2 , 5 HEPES, 11.1 Glucose, 0.3 $\text{NaH}_2\text{PO}_4 \cdot 2\text{H}_2\text{O}$, 0.01 Strophanthidin, pH 7.4 (20-21°C). The $[\text{Ca}^{2+}]$ in the perfusing solution was varied (0.1-1mM) by the addition of known amounts of 1M CaCl_2 stock solution (BDH). The solution used to obtain a maximal fluorescence reading where the indicator dye was saturated with Ca^{2+} (F_{max}) contained the above solution with the addition 0.02mM ionomycin (Calbiochem) and an increased $[\text{Ca}^{2+}]$ of 20mM. To load cells with Fluo-3AM (acetoxymethyl ester form, Molecular Probes), the cells were incubated in $20\mu\text{M}$ Fluo-3AM (Molecular probes) for 10min at 37°C. The cells were centrifuged (5 x g, 15s); re-suspended in modified Krebs solution and left for 20min before use. The perfusing solution used during electrical stimulation experiments was the modified Krebs described above with the addition of 1.8mM CaCl_2 (without strophanthidin).

4.2.4 Laser-scanning confocal Fluo-3 fluorescence measurements in free solution and permeabilised cardiomyocytes

The Ca^{2+} sensitivity of Fluo-3 and Fluo-5 in free solution was measured using a series of Ca^{2+} buffered solutions (10mM EGTA) based on the mock intracellular solution described above. The equilibrium concentrations of metal ions in the calibration solutions were calculated using a computer program with known affinity constants for H^+ , Ca^{2+} & Mg^{2+} for EGTA [135]

and for ATP and CrP [136]. Corrections for ionic strength, details of pH measurement, allowance for EGTA purity and the principles of the calculations are detailed elsewhere [137]. The behaviour of Fluo-3 in permeabilised cardiomyocytes was established by making simultaneous fluorescence measurements from a $6\mu\text{m}$ (x) by $0.5\mu\text{m}$ (y) by $0.9\mu\text{m}$ (z) volume (20 voxels) within a cardiomyocyte and in the perfusing solution adjacent to the cardiomyocyte. In these calibration experiments, SR Ca^{2+} uptake was inhibited by prior treatment with thapsigargin (Calbiochem, $10\mu\text{M}$, 20min). These simultaneous measurements were also used to examine Ca^{2+} waves inside the cells in relation to the extracellular $[\text{Ca}^{2+}]$, but no thapsigargin was added to these cells. Confocal line-scan images were recorded using a BioRad Radiance 2000 confocal system. Fluo-3 (or Fluo-5F) in the perfusing solution was excited at 488nm and measured above 500nm (HQ500LP emission filter) using epi-fluorescence optics of a Nikon Eclipse inverted microscope with a Fluor 60X water objective lens (Plan Apochromat NA 1.2). The 3mW Kr laser was set to 12% power, and the gain on the photomultiplier tube (PMT) set to 25%. Iris diameter was set at 1.9 providing an axial (z) resolution of about $0.9\mu\text{m}$ and X-Y resolution of about $0.5\mu\text{m}$ based on full width half maximal amplitude measurements of images of $0.175\mu\text{m}$ fluorescent beads (Molecular probes). Data was acquired in line-scan mode at 2ms/line; pixel width was $0.3\mu\text{m}$ (512 pixels/scan; zoom=1.4). The scanning laser line was oriented parallel with the long axis of the cell and placed approximately equidistant between the outer edge of the cell and the nucleus/nuclei, to ensure the nuclear area was not included in the scan line. The LaserScan (BioRad) software saved the data as a series of image files each containing 30,000 line-scans (i.e. 1 min

of continuous recording). An experimental record typically comprised 4-5 line-scan image files; these were reviewed off-line and a single intracellular region (20 voxels wide) was selected on the basis of the earliest events in the majority of Ca^{2+} waves. This ensured that any movement artefact following the increase in $[\text{Ca}^{2+}]$ did not affect the estimation of peak $[\text{Ca}^{2+}]$. The same methods were used to record and analyse the data from Ca^{2+} waves and stimulated transients within intact cells. Cellular autofluorescence values (F_{ca}) were obtained by measuring intrinsic fluorescence from cardiomyocytes not loaded with Fluo-3 or bathed in fluorescent solution. Cardiomyocytes (either intact or permeabilised) were bathed in a low (<50nM) Ca^{2+} solution and imaged using the same laser power and PMT gain setting used to make the experimental measurements. Average autofluorescence values were subtracted from the fluorescence measurements to obtain accurate values of Fluo-3/Fluo-5F associated fluorescence (intact cells $F_{\text{ca}} = 9.8 \pm 0.49$ (n=4), permeabilised cells $F_{\text{ca}} = 5.29 \pm 0.43$ (n=6), extracellular $F_{\text{ca}} = 3.56 \pm 0.21$ (n=6).

4.2.5 Field stimulation of intact cardiomyocytes

Cells were field stimulated with 2ms voltage pulses delivered through parallel platinum wires, and the stimulation voltage was set to 1.5 times the threshold. The exact timing of electrical stimulation was marked in the confocal image by activating a light-emitting diode mounted above the cell bath for 2ms (i.e. the duration of one line-scan) 8ms before electrical stimulation.

4.3 RESULTS

4.3.1 The Ca^{2+} sensitivity of Fluo-3 in free solution and in permeabilised cardiomyocytes

A mock intracellular solution containing 10mM EGTA to buffer Ca^{2+} at a range of concentrations was used to ascertain the K_d of Fluo-3 and Fluo-5F in free solution. Figure 4.1A shows examples of calibration measurements for Fluo-3 (10 μM) and Fluo-5F (10 μM). The average K_d from a series of individual curves was $558 \pm 15 \text{ nM}$ ($n=6$) for Fluo-3 and $1035 \pm 16 \text{ nM}$ ($n=4$) for Fluo-5F respectively. To establish the K_d of Fluo-3 within permeabilised cardiomyocytes, thapsigargin pre-treated cells were perfused with a mock intracellular solution (0.05mM EGTA, 150nM [Ca^{2+}]) which was rapidly changed to a high [Ca^{2+}] solution (10mM EGTA, 1.12 μM [Ca^{2+}]) as shown in Figure 4.1B(i)(iii). This manoeuvre resulted in a rapid increase in intracellular fluorescence (F_{IC}) and extracellular fluorescence (F_{EC}). A subsequent decrease in [Ca^{2+}] as indicated by Figure 4.1B(ii) resulted in a rapid decrease in F_{EC} and F_{IC} as shown in Figure 1B(iv). These changes in fluorescence were proportionally equivalent, i.e. had the same F_{IC}/F_{EC} ratio, and if converted to [Ca^{2+}] using the two standard solutions (1.12 μM and <1nM [Ca^{2+}]) the [Ca^{2+}] inside and outside the cell emerged as $\sim 150 \text{ nM}$. In a number of calibration experiments the ratio F_{IC}/F_{EC} was measured in solutions containing $\sim 150 \text{ nM}$ Ca^{2+} and on rapid application of solutions containing 375nM or 1.12 μM Ca^{2+} . The F_{IC}/F_{EC} value in 375nM Ca^{2+} was 0.99 ± 0.4 ($n=8$) of that in $\sim 150 \text{ nM}$ [Ca^{2+}] while the F_{IC}/F_{EC} value in 1.12 μM

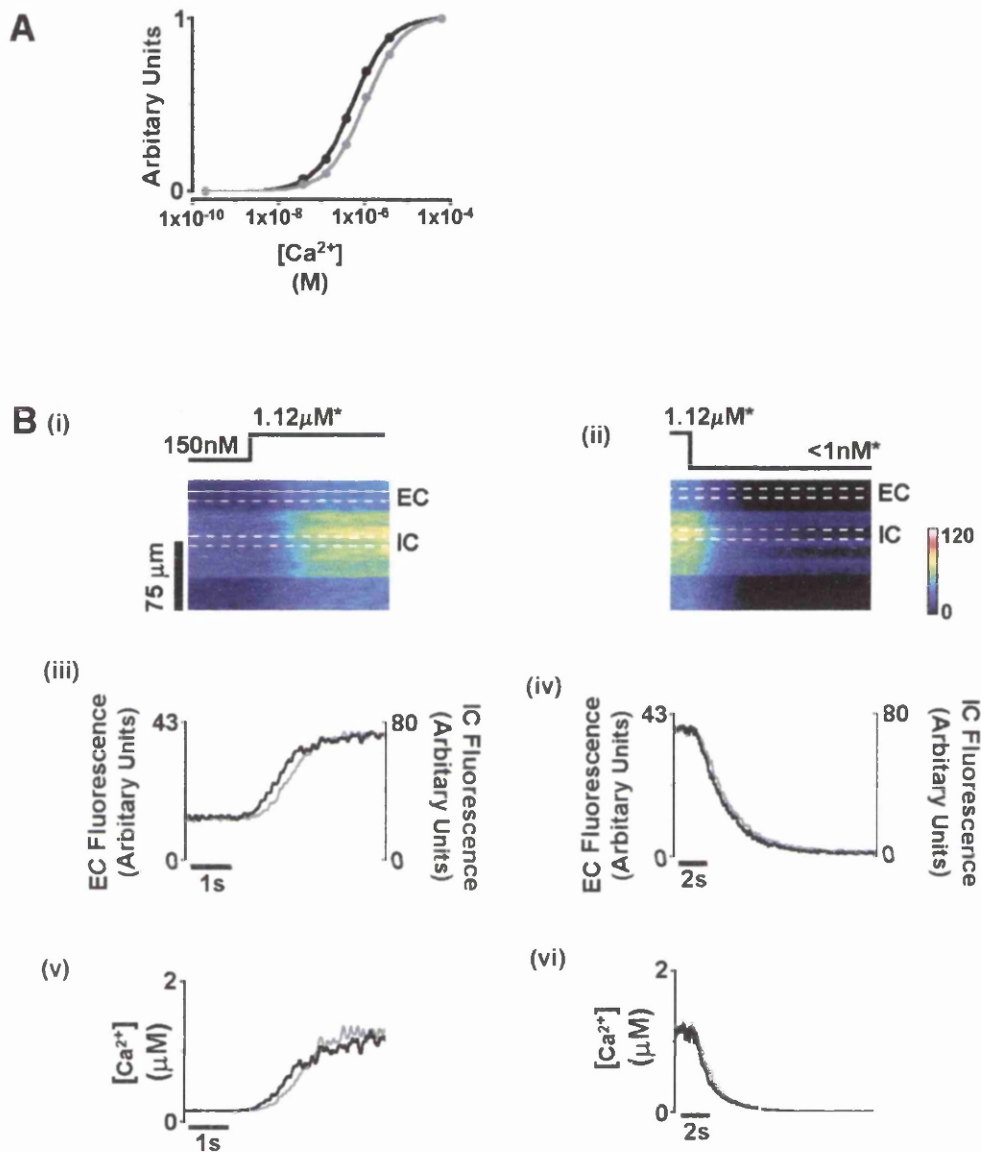


Figure 4.1 Establishing the K_d value for Fluo-3 in free solution and within a permeabilised cardiomyocyte

Panel A, examples of individual Fluo-3 (black), and Fluo-5F (grey) Ca^{2+} calibration curves measured in free solution using confocal fluorescence microscopy. Calibration solutions with $[\text{Ca}^{2+}]$ ranging from 0.2nM to 60 μM (10mM EGTA with 10 μM Fluo-3/5F). The mean dissociation constant (K_d) for Ca^{2+} -Fluo-3 and Ca^{2+} -Fluo-5F was $558 \pm 15 \text{nM}$ ($n=6$) and $1035 \pm 16 \text{nM}$ ($n=4$) respectively. Panel B (i-ii), confocal line-scan image of a permeabilised cell treated with thapsigargin, with the inclusion of 10 μM Fluo-3. The calculated free $[\text{Ca}^{2+}]$

in the mock intracellular solution is shown above the trace and was increased from 150nM to 1.12 μM and back to <1nM. The EGTA concentration was 0.05mM unless marked by (*) in which case it was 10mM. Panel B (iii-iv), mean fluorescence signal of a 20 voxel region was taken from the intracellular (IC) and the extracellular (EC) compartments the position of which is shown by the dotted lines in B (i-ii). Panel B (v-vi) shows fluorescence traces shown in panel B (iii-iv) converted to $[\text{Ca}^{2+}]$.

Ca^{2+} was 1.01 ± 0.06 ($n=4$) of that in $\sim 150\text{nM}$ Ca^{2+} . This constancy of $F_{\text{IC}}/F_{\text{EC}}$ values over a wide range of $[\text{Ca}^{2+}]$ indicates that Fluo-3 inside the cardiomyocyte has a Ca^{2+} affinity indistinguishable from that of free solution. While the $F_{\text{IC}}/F_{\text{EC}}$ value was constant over a range of $[\text{Ca}^{2+}]$ in any one preparation the absolute value varied between cells, however, on average the fluorescence within a cardiomyocyte was $140 \pm 9\%$ ($n=14$) of that in free solution. Similar behaviour was observed for the lower affinity dye Fluo-5F. A slower rate of rise in F_{IC} (Figure 4.1B (v)) when $[\text{Ca}^{2+}]$ is increased is attributed to diffusion of $\text{Ca}^{2+}/\text{Ca}^{2+}\text{EGTA}$ into the permeabilised cell. This is confirmed by the lag in F_{IC} due to a decrease in $[\text{Ca}^{2+}]$ to <1nM (Figure 4.1B(vi)).

4.3.2 A Protocol to produce Ca^{2+} waves in permeabilised cardiomyocytes

Figure 4.2A (i) shows the routine protocol to produce and calibrate Ca^{2+} waves. Simultaneous fluorescence measurements were taken both inside and outside the cell using confocal line-scan imaging with Fluo-3.

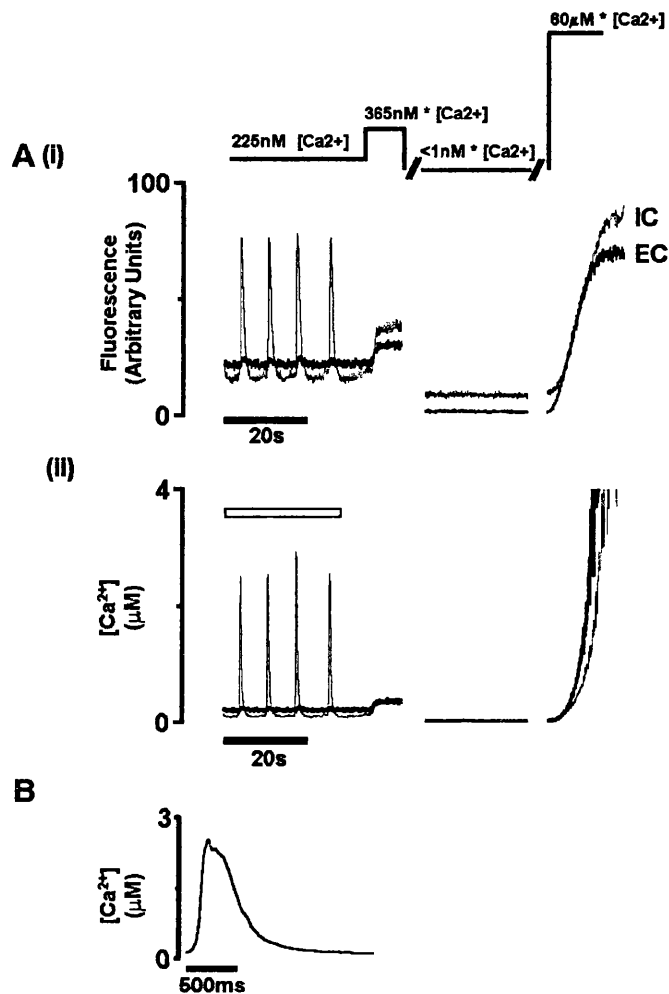


Figure 4.2 Protocol to produce Ca^{2+} waves within permeabilised cardiomyocytes

Panel A (i) Mean 20 voxel fluorescence signals taken from a line-scan confocal image from the intracellular compartment (IC, grey) and extracellular compartment (EC, black) of a permeabilised cardiomyocyte (no thapsigargin added). The calculated free $[\text{Ca}^{2+}]$ in the mock intracellular solution is shown above the trace. The permeabilised cell was perfused with 225nM $[\text{Ca}^{2+}]$ (0.05mM EGTA), which initiated a series of Ca^{2+} waves. The cell was subsequently per-fused with a series of calibration solutions containing 10mM EGTA denoted by the (*) and a free $[\text{Ca}^{2+}]$ of 365nM, <1nM, 60 μM . Using the calibration solutions (*) the fluorescence trace can be converted to $[\text{Ca}^{2+}]$ as shown in A (ii). The open box indicates the section of trace used to produce the average Ca^{2+} wave as shown in panel B.

The permeabilised cell was perfused with a 225nM $[\text{Ca}^{2+}]$ solution, which

triggered the production of Ca^{2+} waves. Ca^{2+} waves were seen as regular transient increases in fluorescence within the intracellular compartment. Intracellular and extracellular compartments were distinguished by both, higher fluorescence signal in the intracellular compartment and the production of these propagating waves. To enable this trace to be converted to $[\text{Ca}^{2+}]$ a series of calibration solutions were used. At the point indicated, the perfusing solution was changed to one containing 365nM free $[\text{Ca}^{2+}]$ (10mM EGTA). This [EGTA] effectively buffered Ca^{2+} uptake and release by the SR and was used as a reference $[\text{Ca}^{2+}]$. The solution was then changed to one containing <1nM $[\text{Ca}^{2+}]$ to enable a reading of minimal fluorescence (F_{min}) to be made (10mM EGTA) (no added Ca^{2+}). The last calibration solution was one containing a saturating 60 μM $[\text{Ca}^{2+}]$ (10mM CaEGTA) to ascertain a maximum fluorescence reading (F_{max}). Although the reference $[\text{Ca}^{2+}]$ solution of 365nM did not cause any noticeable change in cell shortening the F_{max} solution caused the cell to develop a gradual irreversible hypercontracture. Due to the non-ratiometric characteristics of Fluo-3, consequent movement of the cell has an impact on fluorescence readings and subsequent conversions to $[\text{Ca}^{2+}]$. This does not affect the F_{max} reading taken in the extracellular space. Great care was taken in the selection of a site for recording of the intracellular compartment to ensure F_{max} readings were taken from regions of the cell that remained approximately constant throughout changes in cell length. The F_{max} reading was taken as the initial steady state fluorescence reading obtained after perfusing the cell with 60 μM $[\text{Ca}^{2+}]$ solution (Figure 4.2A(i)).

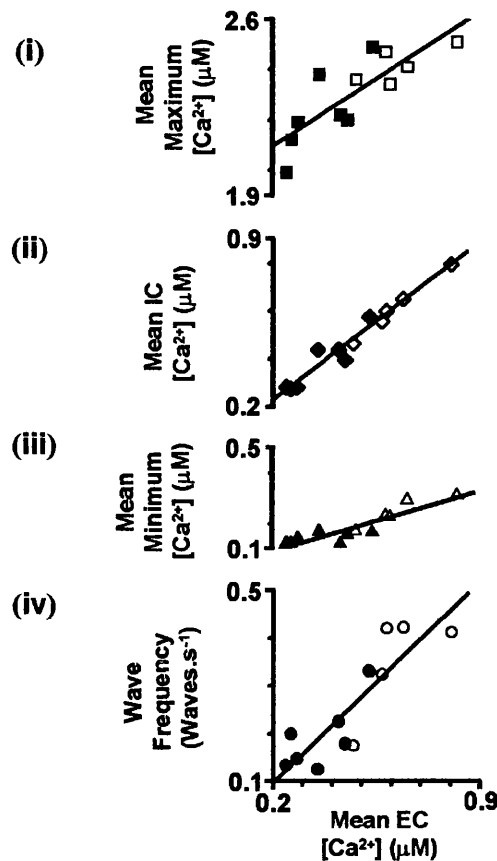


Figure 4.3 Ca^{2+} wave characteristics taken from permeabilised cardiomyocytes over a range of $[\text{Ca}^{2+}]$

Mean extracellular (EC) $[\text{Ca}^{2+}]$ from 200-900nM plotted against the wave, (i) mean maximum $[\text{Ca}^{2+}]$ (Fluo-3: filled squares, Fluo-5F: open squares), (ii) mean intracellular (IC) $[\text{Ca}^{2+}]$ (Fluo-3: filled diamonds, Fluo-5F: open diamonds), (iii) mean minimum $[\text{Ca}^{2+}]$ (Fluo-3: filled triangles, Fluo-5F: open triangles), (iv) frequency (Fluo-3: filled circles, Fluo-5F: open circles). The continuous lines through these graphs (i-iv) are the best-fit linear correlations with gradients, (i) 0.79 ± 0.17 ; $p < 0.001$, (ii) 0.94 ± 0.1 ; $p < 0.0001$, (iii) 0.35 ± 0.05 ; $p < 0.0001$, (iv) $6.03 \times 10^5 \pm 1.07 \times 10^5$ waves. $\text{s}^{-1} \cdot \text{M}^{-1}$; $p < 0.001$.

Figure 4.2A (ii) shows the trace converted to $[\text{Ca}^{2+}]$ using F_{\min} and the reference $[\text{Ca}^{2+}]$. A reliable estimate of the peak of the Ca^{2+} wave can be obtained by converting an averaged fluorescence trace (of four or more waves) to $[\text{Ca}^{2+}]$ (Figure 4.2B). The $[\text{Ca}^{2+}]$ inside the cell was consistently lower than the extracellular $[\text{Ca}^{2+}]$ during the inter-wave diastolic period

suggesting active SR uptake, this was transiently reversed by the production of Ca^{2+} waves. Although these dynamic changes in $[\text{Ca}^{2+}]$ were present the mean $[\text{Ca}^{2+}]_{\text{IC}}$ and mean $[\text{Ca}^{2+}]_{\text{EC}}$ were equal when averaged over 10s periods. The inter-wave diastolic $[\text{Ca}^{2+}]$ refers to the minimum $[\text{Ca}^{2+}]$ reached between waves. The peak of the Ca^{2+} wave is synonymous with the maximum $[\text{Ca}^{2+}]$. The maximum and minimum $[\text{Ca}^{2+}]$ of the waves was taken from the averaged spontaneous wave record as shown in Figure 4.2B.

4.3.3 Ca^{2+} wave characteristics in permeabilised cardiomyocytes

The three main characteristics of Ca^{2+} waves that enable a calculation of K_d for Fluo-3 are: (i) the Ca^{2+} wave frequency, (ii) maximum $[\text{Ca}^{2+}]$ and (iii) minimum $[\text{Ca}^{2+}]$. These values can be correlated with the mean extracellular Ca^{2+} concentration ($[\text{Ca}^{2+}]_{\text{EC}}$) and mean intracellular ($[\text{Ca}^{2+}]_{\text{IC}}$) as shown in Figure 4.3(i-iv). This figure shows results from a series of permeabilised cells perfused with differing $[\text{Ca}^{2+}]$ ranging from 0.2 to 0.9 μM . The maximum $[\text{Ca}^{2+}]_{\text{IC}}$, minimum, $[\text{Ca}^{2+}]_{\text{IC}}$ and wave frequency have been plotted on linear scales in relation to $[\text{Ca}^{2+}]_{\text{EC}}$. There is a positive linear correlation between these parameters measured and $[\text{Ca}^{2+}]_{\text{EC}}$. The straight lines represent the best-fit linear correlation. On an approximate basis it was found that as $[\text{Ca}^{2+}]_{\text{IC}}$ (and therefore $[\text{Ca}^{2+}]_{\text{EC}}$ as shown by Figure 4.3A(ii)) was increased from 300-900nM (i.e. 300%), the maximum $[\text{Ca}^{2+}]$, minimum $[\text{Ca}^{2+}]$, and wave frequency increased by 120%, 200%, and 300% respectively.

4.3.4 The use of Ca^{2+} waves characteristics in permeabilised cells to calibrate the K_d of Fluo-3 in intact cardiomyocytes.

The change in minimum $[\text{Ca}^{2+}]$ over a large range of mean cellular $[\text{Ca}^{2+}]$ is small (150nM – 300nM) in permeabilised cardiomyocytes. This reflects the ability of cardiac muscle SR to buffer cytosolic $[\text{Ca}^{2+}]$. Assuming the minimum $[\text{Ca}^{2+}]$ follows the same relationship in intact cardiomyocytes, this phenomenon can be used to provide a calibration point to allow the estimate of the K_d of Fluo-3 in intact cardiomyocytes. Measuring F_{max} in intact cardiomyocytes after recording a period of spontaneous Ca^{2+} waves allow the K_d of Fluo-3 to be calculated by the following equation (assuming that $F_{\text{min}} = 0$):

$$K_d = ((F_{\text{max}} - F_{\text{dia}}) \cdot [\text{Ca}^{2+}]_{\text{dia}}) / F_{\text{dia}}$$

Where: F_{max} = Fluorescence at saturating $[\text{Ca}^{2+}]$

F_{dia} = Fluorescence at the minimum $[\text{Ca}^{2+}]$

$[\text{Ca}^{2+}]_{\text{dia}}$ = $[\text{Ca}^{2+}]$ at minimum fluorescence

Figure 4.4A shows a section of a line scan recording from an intact cardiomyocyte exposed to strophanthidin after Fluo-3AM incubation. The Ca^{2+} waves produced transient increases in fluorescence similar to those seen in the permeabilised cell protocol (Figure 4.2A). After a period of 120s the perfusing solution was changed to one containing ionomycin and 20mM $[\text{Ca}^{2+}]$. This resulted in a rapid increase in intracellular Fluo-3 fluorescence and an irreversible hyper-contraction of the cell. The initial steady state fluorescence obtained in this situation was used as F_{max} . Using the frequency of spontaneous Ca^{2+} waves as an indicator of cellular Ca^{2+} load (in this case 0.4Hz); the relationships described in Figure 4.3

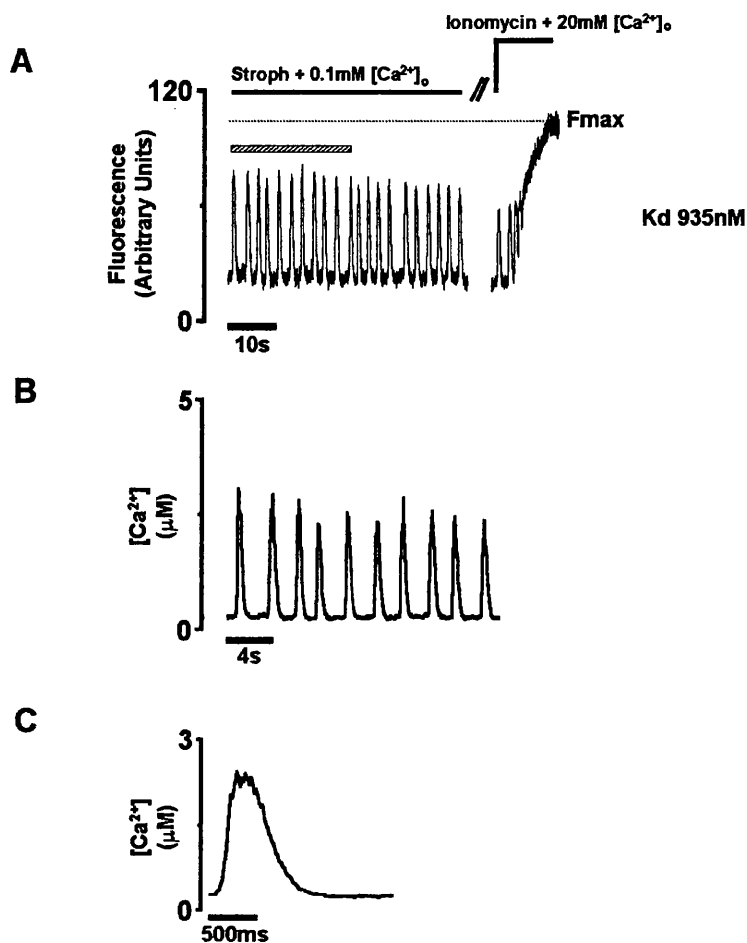


Figure 4.4 Protocol to produce Ca^{2+} waves within intact cardiomyocytes

Panel A, Mean 20 voxel fluorescence signal from a line-scan confocal image within the intracellular compartment of an intact cell treated with strophanthidin ($10\mu\text{M}$) and perfused with a free $[\text{Ca}^{2+}]_o$ indicated above the trace. Ionomycin (0.02mM) was then added to the perfusate together with a higher $[\text{Ca}^{2+}]_o$ as indicated above the trace. Panel B, section of trace from A (shown by hatched box) converted to $[\text{Ca}^{2+}]$. Panel C, the averaged Ca^{2+} wave from the waves shown in B.

were used to estimate the average minimum $[\text{Ca}^{2+}]$ during the Ca^{2+} waves (267nM). Using the equation shown above, this predicts a K_d of 935nM . The protocol described in Figure 4.4A was performed on intact cardiomyocytes over a range of $[\text{Ca}^{2+}]_{EC}$ from $0.1\text{-}1\text{mM}$ to enable different Ca^{2+} wave frequencies to be obtained. On average, the K_d of Fluo-3 in intact cardiomyocytes was found to be $898\pm 64\text{nM}$ ($n=6$) in comparison to

$558 \pm 15 \text{ nM}$ ($n=6$) for Fluo-3 in free solution (Figure 4.5A).

4.3.5 Comparison of Ca^{2+} wave characteristics in permeabilised and intact cardiomyocytes.

Figure 4.4B shows the result of applying the higher Fluo-3 K_d to the fluorescence record shown in Figure 4.4A.

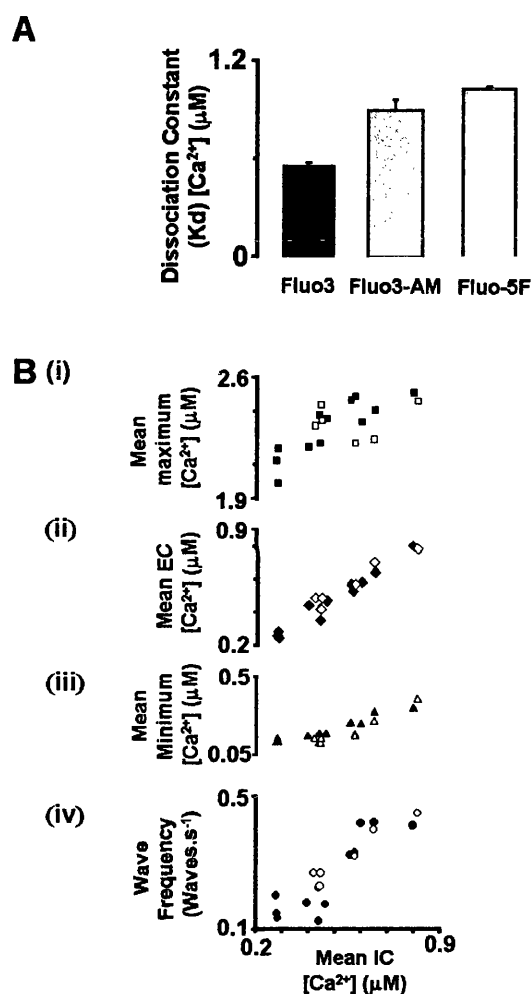


Figure 4.5 Using the K_d for Fluo-3AM to compare Ca^{2+} waves within permeabilised and intact cardiomyocytes

Panel A, Comparison of the intracellular dissociation constants (K_d) for Fluo-3 in permeabilised ($558 \pm 15 \text{ nM}$), Fluo3-AM in intact ($898 \pm 64 \text{ nM}$), and Fluo-5F in permeabilised cardiomyocytes ($1035 \pm 16 \text{ nM}$). Panel B(i-iv), Mean intracellular (IC) $[\text{Ca}^{2+}]$ from 200-900nM plotted against wave characteristics in order to compare the wave, (i) mean

maximum $[\text{Ca}^{2+}]$ in permeabilised (filled squares) and intact (open squares) cardiomyocytes, (ii) mean extracellular (EC) $[\text{Ca}^{2+}]$ in permeabilised (filled diamonds) and intact (open diamonds) cardiomyocytes, (iii) mean minimum $[\text{Ca}^{2+}]$ in permeabilised (closed triangles) and intact (open triangles) cardiomyocytes, (iv) frequency in permeabilised (filled circles) and intact (open circles) cardiomyocytes.

This example predicted a mean maximum $[\text{Ca}^{2+}]$ attained during a Ca^{2+} wave of $2.24\mu\text{M}$, similar to values seen in permeabilised cells. A section of Ca^{2+} record of $\sim 20\text{s}$ can be used to calculate the mean $[\text{Ca}^{2+}]_{\text{IC}}$, in the case of Figure 4.4B this value was $0.65\mu\text{M}$. The mean Ca^{2+} wave for this section (Figure 4.4B) is shown in Figure 4.4C. The amplitude and time-course of the Ca^{2+} wave is similar to that measured in permeabilised cells (Figure 4.2B). Figure 4.5B(i-iv) shows, in a similar format to Figure 4.3A, the relationship between Ca^{2+} wave characteristics (mean, maximum, minimum $[\text{Ca}^{2+}]_{\text{IC}}$ and wave frequency) this time plotted against the calculated mean $[\text{Ca}^{2+}]_{\text{IC}}$. The diagram indicates that the maximum $[\text{Ca}^{2+}]_{\text{IC}}$ predicted by this technique is similar to the measured values from permeabilised cells. A further indication that Ca^{2+} waves in intact and permeabilised cardiomyocytes are comparable is the calculation of the mean extracellular $[\text{Ca}^{2+}]$ that would be necessary in a permeabilised cell to produce Ca^{2+} waves of the range of frequencies observed in intact cardiomyocytes. As shown in Figure 4.5B (ii), the intact-cardiomyocyte data points lay on a relationship that is indistinguishable from the permeabilised cell data.

4.3.6 Stimulated Ca^{2+} transient characteristics.

Figure 4.6A shows a section of a line-scan record taken from an intact cardiomyocyte loaded with Fluo-3 by incubation with the -AM form. The cell was stimulated at 0.5Hz and transient increases in fluorescence can be

seen at these time intervals. At the point indicated the solution was changed to one containing ionomycin and a high $[\text{Ca}^{2+}]$ as in Figure 4.4A to enable the estimation of F_{max} . The hatched box above the transients represents the section of trace shown in Figure 4.6B converted to $[\text{Ca}^{2+}]$ using the mean value of K_d estimated from previous experiments.

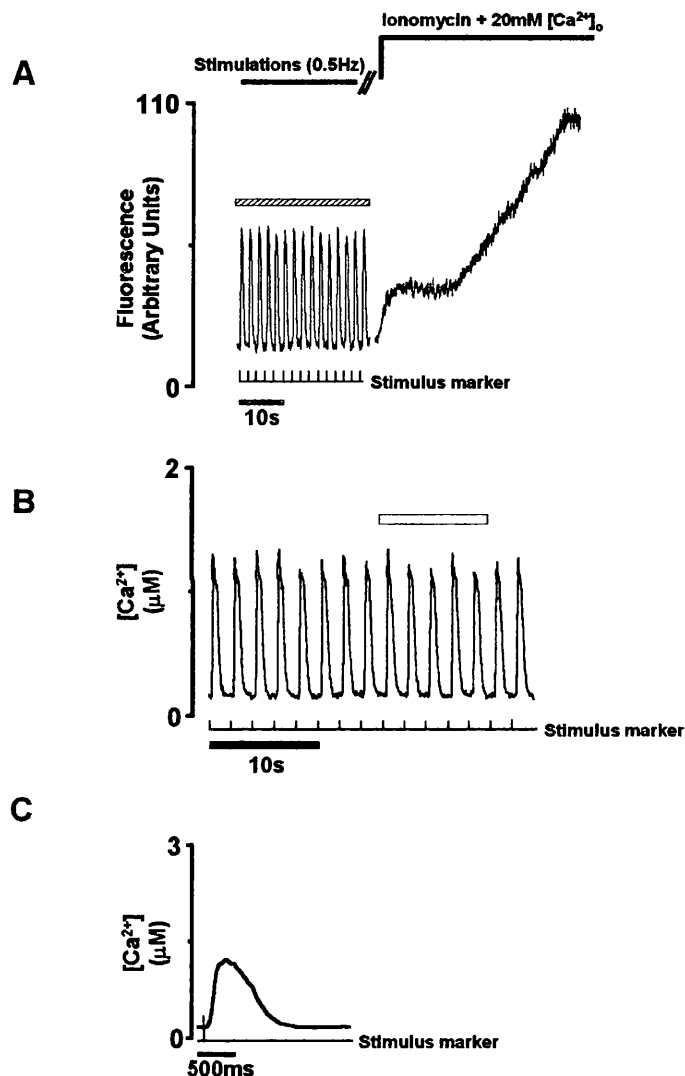


Figure 4.6 Stimulated $[\text{Ca}^{2+}]$ transient characteristics using the K_d of Fluo-3AM in intact cardiomyocytes

Panel A, Mean 20 voxel fluorescence signal taken from a line-scan confocal image within the intracellular compartment of an intact cardiomyocyte stimulated at 0.5Hz as shown below the trace. The period of stimulation is shown above the trace together with the subsequent perfusion of 0.02mM ionomycin and a high $[\text{Ca}^{2+}]$ as indicated. Panel B,

Conversion of the trace underneath the hatched box in panel A, converted to $[\text{Ca}^{2+}]$ with the stimulus marker provided below the trace. Panel C, the averaged Ca^{2+} transient from the region marked by the open box in panel B.

On average this predicts the maximum and minimum $[\text{Ca}^{2+}]$ of the transient to be $1.19 \pm 0.2 \mu\text{M}$ $n=11$ and $158 \pm 30 \text{nM}$, $n=11$ respectively. As shown in Figure 4.6C, the peak $[\text{Ca}^{2+}]$ of the average Ca^{2+} transient is lower than the values observed during a Ca^{2+} wave in both intact and permeabilised cells.

4.4 DISCUSSION

The purpose of this study was to establish the intracellular K_d of the commonly used Ca^{2+} indicator Fluo-3 in cardiomyocytes and compare the Ca^{2+} wave characteristics in permeabilised and intact cells. This chapter shows that the permeabilised cardiomyocyte can be used as a simplified system allowing accurate indicator calibration and therefore measurement of cytosolic $[\text{Ca}^{2+}]$ during Ca^{2+} wave activity and stimulated Ca^{2+} transients.

4.41 The K_d value for Fluo-3 in free solution

The K_d of $0.56\mu\text{M}$ for Fluo-3 in free solution is within 60nM of some previously published values [138;163-165], within 160nM of others [109] [162] [123] and 220nM lower than one other report [166]. These dissociation constants (measured in free solution) are commonly applied to fluorescence measurements measured in intact cardiomyocytes to determine the $[\text{Ca}^{2+}]_{\text{IC}}$, e.g. [33;169]

4.4.2 The K_d value for Fluo-3 in permeabilised cardiomyocytes

A simple set of measurements indicate that Fluo3 (and Fluo-5) fluorescence is higher within the cytosol compared to free solution, yet the affinity of Ca^{2+} for the dye is not significantly altered. These results are at odds with a previous study by Harkins *et al* (1993) that characterised the K_d of Fluo-3 in a salt solution in the presence of 55mg/ml aldolase to simulate intracellular conditions [163]. The presence of the soluble protein caused a shift in K_d from $0.51\mu\text{M}$ (salt solution only) to $1.09\mu\text{M}$ (salt solution plus soluble protein). However, Baylor (2000) stressed that in intact cells, both structural, and soluble proteins are important in any shift in K_d and

concluded that *in vitro* salt solution calibrations, even with added soluble protein, may be unreliable indicators of fluorophore behaviour within the intracellular environment [155]. The present study is the first to expand upon the work of Harkins *et al* (1993) by characterising the intracellular K_d of Fluo-3 by using isolated permeabilised cardiomyocytes [163]. The permeabilised cell (with the exception of a proportion of the sarcolemma) has the advantage of retaining its structural and functional intracellular organelle membrane composition. It has been shown by earlier workers [170] that permeabilisation procedures using 50 $\mu\text{g/ml}$ saponin for 30min caused the loss of soluble protein from *xenopus laevis* muscle fibres. Conceivably, a loss of soluble protein could explain the lack of change in K_d within the intracellular environment seen in this study. However, this is unlikely for the following reasons: (1) exposure to the permeabilising agent by Endo (1980) was x30 longer than in this study [170]. It would be anticipated that the extent of soluble protein loss by using an acute permeabilising technique will be less; (2) the compound β -escin is thought to be less disruptive to the sarcolemma than saponin [104] and may therefore limit loss of soluble protein; (3) measurements reported in this study suggest significant Fluo-3 binding/interaction to intracellular constituents and yet no apparent change in the K_d of Fluo-3.

4.4.3 The K_d value for Fluo-3 in intact cardiomyocytes

This study is the first to report a K_d for Fluo-3 using -AM loading within cardiomyocytes. The K_d for Fluo-3 in intact cardiomyocytes was found to be 1.61x higher than in permeabilised cardiomyocytes or free solution. One option to explain the difference between the K_d in AM loaded and

permeabilised cells is the difference in intracellular environment. One aspect that may vary is the intracellular pH. The pH in the intracellular mock solutions is pH 7.0 but can be as high as 7.2 within the intact cell. The literature concerning fluo-3 suggests that changes in pH are proportional to the affinity of the indicator for Ca^{2+} . It has been shown by Lattanzio (1990) that an increase in pH from 7.0 to 7.4 would cause a decrease in K_d of 33nM [157]. This change in K_d is neither in the correct direction or sensitive enough to account for the differences in Fluo-3 dissociation constant seen between permeabilised and intact cardiomyocytes using acetoxymethyl ester loading. Another possibility is that Fluo-3AM enters organelles and sub-compartments of the cardiomyocyte. The subsequent signal would be a mixture of cytosolic and organelle Ca^{2+} signals. In this study, as with others, short loading periods were used to minimise organelle-loading [171]. This was supported by the absence of discrete areas of high fluorescence in images of -AM loaded cells (results not shown). One final possibility could be due to incomplete cleavage of the acid by esterases within the cardiomyocyte [154]. If this does occur, then the presence of partially hydrolysed forms of Fluo-3 could alter the apparent affinity of the indicator.

4.4.4 The use of Ca^{2+} wave characteristics to assess Fluo-3 K_d

The basis of these calculations is the assumption that the minimum $[\text{Ca}^{2+}]$ that occurs between Ca^{2+} waves in permeabilised cardiac cells is within approximately 20% of that in Ca^{2+} waves of comparable frequency in intact cardiomyocytes. This assumption is thought to be reasonable since the minimum $[\text{Ca}^{2+}]$ is determined by balance between the release via the

ryanodine receptors and uptake via SERCA pump, both of which are retained after sarcolemma permeabilisation. The studies on permeabilised preparations indicated that over wide range of mean cellular $[\text{Ca}^{2+}]$ (a factor of 3), the frequency of Ca^{2+} waves changed by a factor of 3 but the minimum $[\text{Ca}^{2+}]$ between waves ranged from only 150 to 300nM. This frequency - $[\text{Ca}^{2+}]$ relationship was used to provide an accurate estimate of minimum $[\text{Ca}^{2+}]$ in intact cardiomyocytes at a set Ca^{2+} wave frequency.

4.4.5 Characteristics of Ca^{2+} waves within intact cells

As shown in Figure 4.5B, the characteristics of Ca^{2+} waves measured in intact and permeabilised cells are very similar. In this study no major differences in Ca^{2+} wave characteristics were evident between the two preparations. In particular, the calculated peak of the Ca^{2+} wave during spontaneous release in intact cells appears to be very similar to that observed in permeabilised cells. This may be an unexpected result since the absence of a sarcolemma and the consequent change in the associated Ca^{2+} extrusion processes may alter the peak Ca^{2+} values. But, as described by others [172;173] the net Ca^{2+} efflux at the time of the peak of the wave is relatively small. The bulk of the efflux from the cell occurs during the longer declining phase of the Ca^{2+} wave. Since this latter phase is dominated by SERCA-mediated Ca^{2+} uptake, changes in the rate of Ca^{2+} extrusion will have only small effects of the rate of decline.

4.4.6 Characteristics of electrically stimulated Ca^{2+} transients

Application of the K_d values for intracellular Fluo-3 to signals derived from stimulated cells (0.5Hz) predicted a lower maximum $[\text{Ca}^{2+}]$ (~1200nM) and minimum $[\text{Ca}^{2+}]$ (~160nM) than observed in Ca^{2+} waves. Ca^{2+} waves at a

frequency of ~ 0.5 Hz have a maximum $[\text{Ca}^{2+}]$ of ~ 2600 nM and minimum of ~ 325 nM. The values for stimulated cardiomyocytes are similar to published values measured at room temperature using an indicator calibrated within the cell [174]. Obviously using the K_d from extracellular calibration curves would have predicted a diastolic and systolic $[\text{Ca}^{2+}]$ of approximately half this value.

The relationship between frequency of Ca^{2+} waves and extracellular $[\text{Ca}^{2+}]$ also raises an interesting phenomenon in relation to Ca^{2+} wave production in stimulated intact ventricular cardiomyocytes. This point is illustrated in Figure 4.7. Data from two intact cells are presented, the first showing spontaneous Ca^{2+} waves, (panel A(i)), and the second showing stimulated Ca^{2+} transients (panel B(i)). The mean intracellular $[\text{Ca}^{2+}]$ within the spontaneously active cells is 713 nM, and the stimulated cell is 464 nM. The frequency of events however is very similar (0.4 vs. 0.5 waves or transients. s^{-1} respectively). Using the data presented in Figure 4.4B the mean $[\text{Ca}^{2+}]$ in both these cells would predict a spontaneous Ca^{2+} wave frequency of $0.4 \cdot \text{s}^{-1}$ in the spontaneously active cell (which it is), & $0.26 \cdot \text{s}^{-1}$ in the stimulated cell (as denoted by *). However since the latter cell is being stimulated at a faster rate ($0.5 \cdot \text{s}^{-1}$) the production of Ca^{2+} waves is prevented because the stimulated transient in-between the predicted spontaneous events empties the SR. This may illustrate a general rule, that mean cellular $[\text{Ca}^{2+}]$ determines the frequency of spontaneous events. These will not occur as long as stimulated Ca^{2+} transient frequency is greater than Ca^{2+} wave frequency.

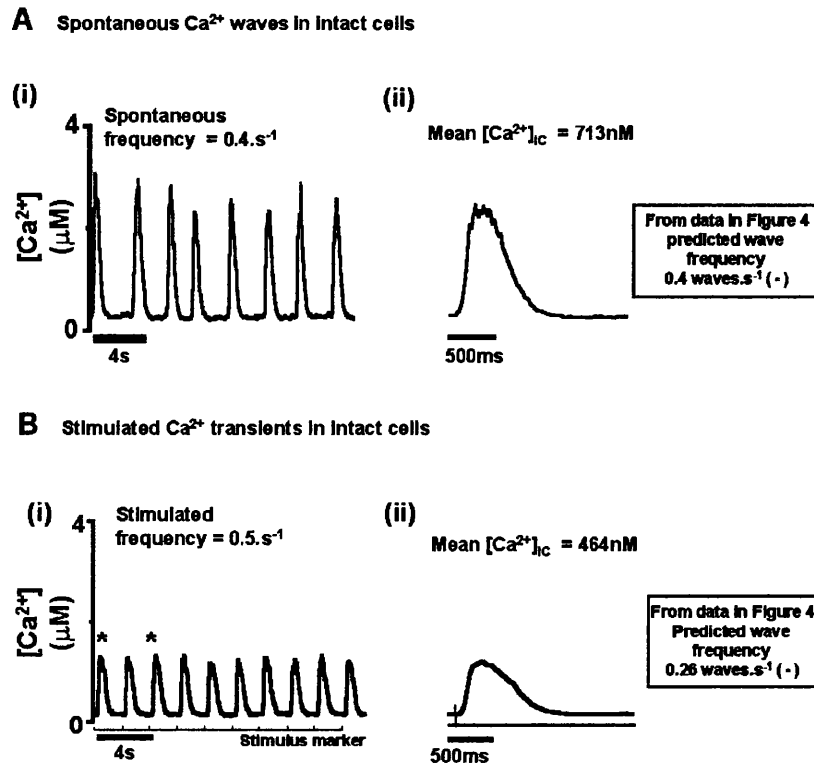


Figure 4.7 Prevention of Ca^{2+} waves within stimulated cells

Data from intact cells with spontaneous Ca^{2+} waves (Panel A(i)), and stimulated transients (Panel B(i)). The averaged Ca^{2+} wave or transient is shown in Panel A(ii) and Panel B(ii) respectively. Refer to text for discussion.

This study emphasises the need to establish the behaviour of the indicator within the cytosol of the cell under study, before attributing values to the $[\text{Ca}^{2+}]$ from Fluo-3 fluorescence. Based on the measurements in this study, the K_d for Fluo-3 in free solution is appropriate for measurements on permeabilised cells and perhaps for Fluo-3 acid loaded into cardiomyocytes via a patch pipette. However, this K_d is not necessarily appropriate for cardiomyocytes loaded with Fluo-3 by incubation in the $-\text{AM}$ form.

CHAPTER FIVE

The role of FK506-binding protein in ventricular cardiomyocytes

5.1 INTRODUCTION

In order to understand how the heart works, cardiac physiologists have continually reduced its complexity into smaller, more elementary components. Unfortunately, while this approach has successfully revealed many answers it has often provided many more questions. This evolving complexity has prompted extensive research on a subject that is continually expanding. Cardiac research in a form that is familiar today began on the gross anatomical level with pioneers such as Andreas Vesalius (1514-1564) and William Harvey (1578-1657) making monumental discoveries. Further progress required a reduction in the scale of research to that made possible by microscopy (Marcello Malpighi 1628-1694). In the last sixty years the scale has been reduced even further - to the level of the molecule. The subject of molecular cardiology within the post genomic era focuses not only on how the normal heart works, but also on finding genetic targets for the treatment of heart failure. One such potential molecular target, associated with the cardiac ryanodine receptor (RyR2), is FK506-binding protein. With the recent discovery of its role in stabilising the coordinated gating behaviour of RyR2 in human heart failure (in which RyR2 had become 'unstable') it was hoped that the search for a cure was near completion. This chapter focuses on the role of FKBP in the heart and why it may not be the much-anticipated molecular panacea for heart failure.

5.2 FK506 Binding Protein 12.0

FK506-binding protein (FKBP) is a prototypic member of the immunophilin family. It is a protein with peptidyl-prolyl isomerase (PPIase/rotamase) activity and is a receptor for the binding of the immunosuppressant drugs - FK506 (*Prograf - tacrolimus*) and rapamycin (*sirolimus*). Immunophilins are a highly conserved family of proteins, widely expressed and present in high levels within some tissue [175]. The following discussion focuses on the role of FKBP within ventricular cardiomyocytes. However, the wide interest in this immunophilin did not stem from its presence within the heart but rather its presence within T-lymphocytes [176]. As mentioned above, FK506 (a macrocyclic lactam-lactone) was found to bind to FKBP and the resulting complex was found to prevent T-cell proliferation. The clinical application of FK506 (or the related but structurally different drug cyclosporine) therefore helps to prevent immunological graft rejection of patients undergoing organ transplantation. The immunosuppressant action of the FKBP-FK506 complex is discussed further in section 6.1.1.

5.2.1 Discovery of the association between FKBP12.0 and RyR1

FK-binding proteins are present within various cell types [175] and named according to their molecular weight in kDa. Two such FK-binding proteins have been associated with mammalian cardiac and skeletal tissue. The first is FKBP12.0 - a ubiquitous protein and the second is FKBP12.6, which will be focussed on later. FKBP12.0 is associated with RyR1. Who this finding was initially attributed to is ambiguous. Marks *et al* (1989) performed extensive proteolytic mapping and micro sequencing of a highly purified RyR1 from rabbit skeletal muscle [177]. Two of the peptides could

not be placed within the sequence of the intact protein. These were denoted KC7 and KC5. Collins (1991) performed a homology search of these proteins using computer-assisted sequence analysis [178]. This search found that KC7 was almost identical to FKBP. Collins suggested in the same study that RyR1 had an *in vivo* interaction with FKBP and more importantly, that the protein may modulate Ca^{2+} release. Later, in 1992 the association of a 12KDa FKBP (FKBP12.0) and RyR1 was shown to exist by the Marks group [179]. This study was based on co-purification, co-immuno-precipitation, and sub-cellular localisation of both RyR1 and FKBP12.0 to the SR terminal cisternae (TC) and not SR longitudinal tubules. The Marks group proposed that since they were the first to show the existence of the unknown protein KC7 back in 1989 they had provided the first initial indication that FKBP12.0 was tightly associated with the RYR1. It is often omitted that the Collins study had identified KC7 as FKBP [178].

5.2.2 The role of the association between FKBP12.0 and RyR1

Timerman *et al* (1993) performed functional studies on skeletal RyR1 present in TC vesicles [180]. There were three major findings within this study: (1) the stoichiometry of FKBP-RyR1 was found to be four using [^3H] FK-816. Thus RyR1 consists of four ryanodine receptor protomers and four molecules of FKBP. Its chemical formula is therefore often represented as $(\text{FKBP12.0})_4/(\text{RyR1 protomer})_4$. This was later confirmed by the use of another radioactive isotope [^{35}S] FKBP [181], (2) when the drug FK506 was applied to the preparation, it formed a complex with FKBP12.0 and was dissociated from the RyR1, (3) FKBP12.0 was found to stabilise the closed

conformation of RyR1 in skeletal TC. The finding that FKBP12.0 modulated RyR1 activity in this way was fundamental and has important implications for excitation-contraction (EC) coupling. Various studies were subsequently published in an attempt to further investigate the role of FKBP12.0 on RyR1. Single channel recordings of RyR1 located within TC in the presence and absence of FKBP12.0 provided the basis for much of this work [182]. FKBP deficient RyR1 (formed by the incubation of the TC with FK506) were shown to have: (i) enhanced channel activation due to an increased sensitivity to Ca^{2+} , (ii) enhanced sensitivity to caffeine, (iii) decreased sensitivity to Mg^{2+} [181], (iv) greater mean open times in 70nM to 1.2 μM [Ca^{2+}]. Importantly the rebinding of recombinant FKBP12.0 reversed this enhanced channel activation. In a separate study FK506 was found to activate RyR1 in TC vesicles between 100nM and 1mM [Ca^{2+}] [183]. The increase in RyR1 mean open time was not due to the increase in openings to full conductance but mainly due to the appearance of long periods of sub-conductance states (28%-38% of full conductance), which were distinct from the sub-conductance state seen when ryanodine is applied (45%). Whereas both studies [182;183] showed an increase in the open probability of RyR1 only the later [183] showed sub-conductance states. If taken together the studies above all suggest that the role of FKBP12.0 is to keep RyR1 in a state of control such that 'leak' of Ca^{2+} through RyR1 is reduced.

5.2.3 Further studies on the role of FKBP on RyR

There are two studies in the literature that encompass the above findings and go on to define the two classic roles of FKBP12.0 on RyR1. The first

role is that of stabilisation. Brillantes *et al* (1994) expressed recombinant RyR1 in *Spodoptera frugiperda* (Sf9) cells [184]. These insect cells were chosen because they do not express FKBP12.0, FKBP12.6, RyR-mRNA and RyR-protein [175]. RyR1 was fully functional as a Ca^{2+} release channel and had a molecular mass of 2.3×10^6 daltons. The purified recombinant RyR1s were reconstituted into planar lipid membranes and their properties were found to be very similar to that of native SR RyR1 channels. The channels typically exhibited sub-conductance states to distinct levels with full conductance only being reached very occasional. No RyR1 channels were stable in the full conductance state. If FKBP12.0 was co-expressed with RyR1 in Sf9 cells or added to the purified expressed RyR1 in the bi-layer, stable channels with openings to the full conductance were formed. RyR1 channels associated with FKBP12.0 had a longer mean open time and decreased open probability after activation by caffeine (5mM) and a decreased sensitivity to caffeine. To verify the properties shown above, FK506 or rapamycin was applied to native channels that exhibited full conductance. Both of these drugs induced the reappearance of sub-conductance states. Since channels without FKBP12.0 are capable of occasionally opening to full conductance (albeit not in a stable state) it can be concluded that FKBP12.0 is not required for the achievement of full conductance. Therefore, FKBP12.0 reduces the open probability of RyR but stabilises the open state once it is open. It is thought that FKBP12.0 allows the four sub-units of the RyR1 channel to gate co-ordinately allowing the channel to function to full conductance and therefore eliminating the appearance of sub-conductance states [185]. This phenomenon has obvious implications in reducing non-activated Ca^{2+} release from the SR if

this is indeed the role of FKBP12.0 in the whole cell.

5.2.4 How does FKBP stabilise RyR?

A model has been produced showing how stabilisation of the RyR1 is possible [186]. The model is based on the binding site of RyR1 for FKBP12.0. The binding site is composed of a tetra-peptide (Ser-Leu-Pro-leu). The Leucyl-Prolyl bond is constrained in a twisted amide conformation. Since FKBP is a cis-trans peptidyl-prolyl isomerase this bond is a high affinity substrate for the enzyme FKBP. However if the isomerisation reaction took place from cis to trans this would lower the affinity for FKBP to RyR1 [187] and they would dissociate from each other. Since FKBP12.0 has been shown to be tightly associated with the RyR1 [179] this reaction is thought not to occur. However the twisted amide is a high-energy structure that is unstable. Therefore the tight binding of four FKBP12.0 to the four RyR1 protomer binding sites stabilises the channel [188;189]. Why the isomerase reaction does not occur is unknown but could be due to the spatial constraints imposed by RyR1. FK506 and rapamycin dissociate FKBP12.0 from RyR1 since they have a substructure that mimics the twisted amide conformation of the peptidyl-prolyl bond and have a high affinity for FKBP12.0.

5.2.5 Coupling of RyRs by FKBP

The second role of FKBP12.0 is its induction of couple gating. Although touched on in the previous paper [184] a study by Marx *et al* (1998) investigated this phenomenon more fully [185]. Coupled gating refers to the phenomenon whereby RyR1s in planar bi-layers exhibit simultaneous openings and closings. The results taken from both recombinant Sf9 RyR1

co-expressed with FKBP12.0 and native skeletal muscle RyR1 from SR vesicles were used to investigate coupling. Three scenarios were presented whereby channels exhibited:

- (1) Stable openings to 4pA in planar lipid bi-layers with current amplitude histograms with two discrete peaks corresponding to closed channels (0pA) and openings to the full amplitude of single channels (4pA).
- (2) Two channels opening and closing independently in the same bi-layer one to 4pA, the other opening independently of the first. Current amplitude histograms corresponded to closed channels (0pA), opening to full amplitude for one channel (4pA), or for two (8pA) (9 out of 44 experiments).
- (3) Openings to 8pA twice the normal current. Current amplitude histograms revealed two discrete peaks corresponding to closed channels (0pA) and openings to 8pA (10% experiments).

The distributions indicated that the 8pA currents did not result from openings of two independent RyR1 channels and that the gating of the two channels was likely to be coupled. That this scenario occurred in 10% of experiments is of some importance since ultra-structural studies show that 10% of purified RyR1 homo-tetramers are physically connected to form contacting pairs. Specific [³H] ryanodine binding detected fractions of the preparation with sedimentation coefficients suggesting more than two RyR1 homo-tetramers can remain physically connected during purification. The

physical association of RyR1s was not affected by the removal of FKBP12.0 and is therefore not needed to keep RyR1s conjoined. Openings to 12, 16 and 20 pA indicative of coupled gating between 3, 4 and 5 channels respectively were also observed. The theory of coupled gating was further reinforced when rapamycin (2 μ M) induced two coupled RyR1 channels to uncouple. The potential for coupling to allow synchronous Ca²⁺ release by a number of RyR1 by activating only one RyR1 has important implications for EC-coupling [190]. Skeletal dihydropyridine receptor (DHPR) voltage sensors activate only half the RyR1 channels, which are thought to be due to a direct protein-to-protein interaction [191]. The remaining half must be activated by some other means. Coupling would be an energy efficient way to achieve this. The cardiomyocyte is even more reliant on an efficient mechanism since Ca²⁺ induced Ca²⁺ release (CICR) is thought to rely on influx of Ca²⁺ from even less (DHPR) channels per RyR2 than skeletal muscle with no direct protein to protein interaction between the two.

5.2.6 Is there a role for the PPlase activity of FKBP?

Although FKBP12.0 is tightly bound to RyR1, it is a soluble receptor, which is in constant equilibrium with the myoplasmic pool of FKBP (~3 μ M). This was emphasised using a novel technique involving an exchange reaction between soluble ³⁵S-labeled FKBP12.0 and the FKBP12.0-RyR1 complex [181]. This process is temperature and concentration dependent and therefore at 37°C and myoplasmic concentrations, the technique showed that there should be rapid exchange of myoplasmic FKBP12.0 with that bound to RyR1 in skeletal muscle. Using this technique the need for prolyl

isomerase activity of FKBP12 was investigated. Since PPlase activity is inhibited by both rapamycin and FK506 it is not unreasonable to suspect that it is involved in the process of RyR1 modulation by FKBP12.0. The exchange of the FKBP12.0-RyR1 complex with wild type or PPlase deficient FKBP mutants (W59H, F36Y, F99Y - 0.3%, 5%, 0.1% activity respectively) had the same effects on RyR1 modulation as seen previously [180;182]. Therefore this study [181] concludes that the PPlase activity of FKBP is not critical for modulating the channel behaviour of RyR1. However a review by Marks (1986) provides some unpublished data suggesting that a mutant form of FKBP12.0 (F36Y - which lacks most of the prolyl isomerase activity but still binds to RyR1) does not modulate channel gating [175]. Approximately 15% of the myoplasmic pool of FKBP12.0 is thought to be associated with the SR in skeletal fibres [181]. The information obtained from the exchange technique [181] has important implications for the use of permeabilised cells to study the function of FKBP (see section 5.13) and will be discussed later.

If FKBP12.0 is associated with RyR1 in skeletal muscle and has such important implications for Ca^{2+} homeostasis then the most understandable tissue to investigate next had to be cardiac muscle.

5.3 FK506 Binding Protein 12.6

5.3.1 The discovery of the association between FKBP12.6 and RyR2

Although FKBP12.0 was found within myoplasm of canine heart tissue, a novel FKBP was found to have a specific tight association with RyR2 [192]. This protein called FKBP-C, was readily distinguished from human recombinant FKBP12.0 by its slower mobility in Sodium Dodecyl Sulfate -

Polyacrylimide Gel Electrophoresis (SDS-PAGE). Its molecular weight was thought to be approximately (but not) 13kDa [192] and later confirmed to be 12.6kDa [193]. The interaction between cardiac RyR2 and FKBP12.6 was found to be tissue specific rather than species specific (a point that will be discussed later). FKBP12.6 is not detected in canine skeletal muscle TC of SR or canine heart myoplasm [192]. A further study isolated and cloned human FKBP12.6 and showed that FKBP12.6 is pharmacologically almost indistinguishable from FKBP12.0 such that both isoforms when present as a complex with FK506 inhibit calcineurin and are equipotent inhibitors of calcineurin dependent signalling pathways in Jurkat cells [193]. FKBP12.0 and FKBP12.6 show 85% amino acid sequence homology [194] and PPIase activity that is inhibited by either FK506 or rapamycin [193]. The stoichiometry of FKBP12.6 is approximately four as determined by [³H] dihydro-FK506 [193] and exchange with soluble ³⁵S-labeled FKBP12.6 [195], hence the same macromolecular formula can be applied as for FKBP12.0 (RyR2)₄/(FKBP12.6)₄.

5.3.2 Are all potential RyR sites filled with FKBP?

Although there is a tight association between FKBP and the RyR receptor, the protein is in constant equilibrium with the myoplasm and there are a proportion of sites that are unoccupied. The idea of FKBP equilibrium was addressed by the novel exchange technique using soluble ³⁵S-labeled FKBP12.6/FKBP12.0 mentioned above [193;195]. The proportion of unoccupied sites using this technique can be calculated. Whereas only 6% receptor unoccupancy was calculated for rabbit skeletal muscle TC [193] 17% was calculated for FKBP12.6 binding sites in the dog cardiac TC. The

reason why this proportion of sites remain unoccupied is unclear but if such sites could be physiologically regulated such that they are filled when enhanced coupled gating is required (e.g. in heart failure) then this provides a useful resource enabling an enhancement of EC-coupling.

5.3.3 Specificity of binding

Timerman *et al* (1996) defined the selectivity for FKBP12.0 and FKBP12.6 for canine RyR by the use of exchange methodology together with co-immuno-precipitation and competitive binding studies [195]. The binding of FKBP to SR vesicles is specific to the RyR isoform such that RyR2 has specificity for FKBP12.6 but RyR1 binds both FKBP12.0 and FKBP12.6. The mRNA of both isoforms is present in skeletal and cardiac muscle, the mRNA for FKBP12.0 being higher than FKBP12.6. The information provided in this study was important in regards to Western blot analysis that had previously only shown FKBP12.0 in the cytosol of tissues. As mentioned above, the cytosolic concentration of FKBP12.0 in skeletal muscle is thought to be 3 μ M [193]. It is thought to be the same within cardiac tissue [195]. The FKBP12.6 concentration in cardiac tissue is unknown since it is too small to be detected by current assay methods. This is the reason why RyR2 is isolated as a complex with FKBP12.6 and FKBP12.0 is only detectable within the cytosol.

5.3.4 Does FKBP12.6 affect RyR2?

The physiological function of FKBP12.6 on RyR2 is somewhat controversial and will be discussed in detail in the next section, suffice to say that the above study [193] showed no modulation of RyR2 by FKBP12.6. This was an unexpected finding since studies had showed such similarity (both

physically and pharmacologically) between FKBP12.0 and FKBP12.6. Three well-established techniques were used: (a) single channel recordings, (b) ryanodine binding studies, and (c) Ca^{2+} uptake measurements. There is no doubt that the authors would have desperately tried to find some similarity between alterations in RyR2 channel modulation by FKBP12.6 as had been shown in skeletal muscle [195]. However, they did not, and their excellent biochemical findings were not supported by any fundamental physiological role for FKBP12.6 within myocardial tissue. This was supported by a direct comparison between the role of FKBP12.6 and FKBP12.0 on rabbit skeletal RyR1 and canine cardiac RyR2 [196]. Again using bi-layer studies, ryanodine binding and SR uptake experiments Barg *et al* (1997) established that rabbit skeletal muscle responded to removal of FKBP from RyR1 (using FK506) by enhanced channel activation whereas repletion with FKBP12.0 or importantly FKBP12.6 resulted in channel quiescence similar to control [196]. This was evidence that RyR1 was physically and functionally modulated by FKBP12.0 and FKBP12.6 equivalently. No such effects with cardiac RyR2s were observed. However, much research that followed these two studies did find a very important role for FKBP12.6 within cardiomyocytes and this work will be discussed in the next section.

5.3.5 The role of FKBP12.6 in ventricular cardiomyocytes

As with FKBP12.0 the role of FKBP12.6 and its association with RyR2 was investigated initially using single channel experiments and ryanodine binding studies [197]. Kaftan *et al* (1996) showed that as with FKBP12.0, the addition of rapamycin to cardiac SR channels comprised of RyR2 and

FKBP12.6 induced activation whereby there was an increase in the open probability and the appearance of sub-conductance states. These results were very similar to the application of FK506 to the FKBP12.0-RyR1 complex [183]. There were two interesting points made in this study that shed light on the mechanistic behaviour of RyR2 gating. Firstly, the effect of rapamycin on the FKBP12.6-RyR2 complex was bi-phasic. Channel activation occurs for the first 2-10min and is maintained even after removal of rapamycin from the bath. After 10min channels are activated with smaller current amplitudes (i.e. sub-conductance states). There are two possible hypotheses as to why there is a temporal effect separating channel activation and channel amplitude. The first suggests that there is a mechanical difference between channel activation and channel amplitude. That you can separate these individual processes comes from studies using natural products called bastadins on RyR (discussed in section 5.10). The more favourable hypothesis (that resembles more clearly the known structure and function of the FKBP12.6-RyR2 complex) involves the proposal that progression from increased channel activation to sub-conductance states is a multi-step process. Since the stoichiometry of FKBP12.6 to RyR2 is four the gradual dissociation of each FKBP12.6 from the RyR2 homo-tetramer induces different states in RyR2 gating, i.e. the initial loss of one FKBP12.6 enhances channel activation and the subsequent loss of the second, third, and fourth induces sub-conductance states, reduced channel conductance and restructuring of the channel finally leading to altered permeation [197]. One counterintuitive result in this study was the finding that dissociation of FKBP12.6 from RyR2 resulted in decreased ryanodine binding to RyR2. Since ryanodine binds to the

open channel and the channel is more activated then in theory ryanodine binding should have increased. This could be explained possibly by the increase in sub-conductance states and the induction of conformational changes in RyR2 leading to a decreased affinity for ryanodine.

5.3.6 Does FKBP12.6 play a role in coupling of RyR2s?

Three years after showing FKBP12.0 is needed for functional coupling between skeletal RyR1 channels (although physical coupling does not [185], the same phenomenon was found to occur between cardiac RyR2 channels via FKBP12.6 [63]. All the observations made in the previous study [185] were valid for FKBP12.6 with three additional findings:

(1) The removal of FKBP12.6 from RyR2 with rapamycin first uncoupled channels and then each individual channel exhibited sub-conductance states. This is similar to the bi-phasic action of rapamycin discussed above [197], and the multi-step removal of FKBP12.6 from RyR2.

(2) In some experiments the open state but not baseline/closed states of the coupled channels showed more signal noise than those of single channels. This was especially so during the uncoupling transition. It was suggested that this was consistent with the stabilisation theory of FKBP12.6 on RyR2.

(3) Two coupled RyR2 channels exhibit an increased open probability compared with a single channel. It was thought this might be due to the doubling up of Ca^{2+} activating sites present, i.e. the two coupled RyR2s

essentially function as one channel but retain two Ca^{2+} binding sites. The finding that coupled channels exhibited increased sensitivity to caffeine reinforced this theory.

Influx of Ca^{2+} from the exterior to the interior of skeletal myocytes and the subsequent release of Ca^{2+} from intracellular stores is well co-ordinated via protein-to-protein interactions, which are voltage dependent. In cardiac muscle however there are no such protein-to-protein interactions and Ca^{2+} is thought to be the link between the influx of trigger Ca^{2+} and release of amplified SR Ca^{2+} (CICR). Since this is a positive feedback system and naturally unstable, more emphasis must be put on how this actually terminates than compared to skeletal muscle. Coupled gating is a possible way in which release of SR Ca^{2+} can be synchronously released and terminated when required to do so. Interestingly when barium or potassium is used as the charge carrier coupled gating is still observed and rules out the possibility of local CICR between isolated channels in lipid bi-layers. Although the role of FKBP12.6 seems to be very similar to FKBP12.0 (stabilisation of the co-ordinated gating behaviour of RyR), this is not always a consistent finding. Further studies such as those presented below have tried to resolve this inconsistency.

5.4 On the scale of things

5.4.1 The progression from molecule to bedside

John Gribbin once summarised why he chose to become a writer about science rather than a scientific researcher [198]:

The fate of specialists in any one area of science is to focus more narrowly on their special topic, learning more and more about less and less, until eventually they end up knowing everything about nothing.

I stated at the beginning of this chapter that cardiac physiologists have often reduced the complexities of the heart into smaller more elementary components. The description of FKBP12.0 and 12.6 in previous sections has been the epitome of that reduction all the way to the level of the molecule and specialists in this area have gradually learned more and more about less and less. Although they have not reached the stage whereby they know everything about nothing it is necessary to bring the scale of things back up to the level of the whole heart. Only when this is achieved will the full importance of the role of FKBP12.6 within the heart be known. A logical progression would involve proceeding from the above studies on single (or coupled) RyR2 channels in lipid bi-layers to the level of the RyR channel cluster located on the SR. The Ca^{2+} spark is the functional consequence of Ca^{2+} release from the RyR2 cluster and its morphology and frequency is a function of its gating behaviour. The next possible scale of expansion would then involve the whole cell. This can of course be done in conjunction with the investigation of Ca^{2+} sparks but should also include an appreciation of the numerous other Ca^{2+} homeostatic mechanisms and biochemical pathways present within cardiomyocytes. The penultimate stage would involve whole heart studies, which would allow the function of FKBP12.6 to be investigated with the heart functioning as a syncytium together with its extracellular matrix. Perfusion of whole hearts with drugs such as FK506 with concurrent measurements of changes in Ca^{2+} and

voltage would provide invaluable insights into the role of FKBP12.6. Lastly and perhaps most importantly it must be remembered that the heart does not stand in isolation and integrative physiology using whole body studies are vital in ascertaining whether or not any of the previous studies are biomedically significant. This section will look at work attempting to investigate some of these logical progressive steps and evidence that FKBP12.6 is indeed clinically relevant.

5.4.2 A step in the right direction

Investigating RyR2 within lipid bi-layers is very specific i.e. it can be made sure that RyR2 is the only channel within the preparation the functional effects of which can be examined. Returning RyR2 back into the whole cell where it should be, while only investigating the specific role of FKBP12.6 requires new technical approaches. While there are drugs that can be easily applied to whole cells that effect FKBP12.6 bound to RyR2 the specificity of these drugs is poor. This point is exemplified in studies investigating the effect of FK506 on cellular Ca^{2+} regulation in intact ventricular cardiomyocytes during EC-coupling and rest [113;114].

5.4.3 The role of FKBP12.6 on EC-coupling in intact cardiomyocytes

FK506 (5 μ M) was found to increase the amplitude of steady state twitches and Ca^{2+} transients during EC-coupling in rat ventricular cardiomyocytes [114]. This occurred when SR Ca^{2+} content was either moderately enhanced (with FK506) or the same as control (which was without FK506). FK506 was not found to alter influx of Ca^{2+} via the DHPR or uptake of Ca^{2+} into the SR via SERCA2a. The larger Ca^{2+} transient was thought to be due to a higher fraction of SR Ca^{2+} release when FK506 was applied due to

enhanced sensitivity of RyR2 for Ca^{2+} . The authors suggested that these findings were consistent with a previous investigation showing FK506 increased channel open probability by enhancing the sensitivity of skeletal RyR1 to caffeine [182]. However, these observations had been seen in rat cardiac tissue RyR2 [114] not skeletal muscle RyR1 as in the previous study [182]. There is actually only one paper previous to this study [114] which had showed similar effects on cardiac RyR2s. This was observed by applying rapamycin not FK506 [197]. There is also a study previous to this showing no such effect on FK506 on RyR2 [195]. Using information obtained from studies on RyR1 and extrapolating it to studies on RyR2 should be done with the greatest care. There are three main reasons why this is so:

(1) It is quoted in reviews that RyR1 and RyR2 share 66% genetic structural homology [199], they perhaps more importantly do not share 34% of the genetic sequence. This could have major functional consequences.

(2) The various accessory proteins and biochemical pathways that physically attach to and modulate RyR2 could be very different in skeletal tissue; this could have a profound effect on gating behaviour.

(3) The difference behind Ca^{2+} release from the SR in skeletal and cardiac muscle is mediated by the two different mechanisms - voltage sensitive sensors and CICR respectively and indeed RyR2 cannot replace RyR1 during skeletal EC-coupling in RyR1 knock-out mice [200].

The suggestion that enhanced sensitivity of RyR2 to Ca^{2+} leading to larger Ca^{2+} transients when SR Ca^{2+} content, L-type Ca^{2+} influx, and SERCA are

all unchanged seems at first counterintuitive. FK506 should act to uncouple the RyR2 channels in the clusters and presumably decrease the efficiency of EC-coupling leading to a possible reduction in transient size. This dichotomy will be the focus of much of the majority of the next section.

5.4.4 The effects of FK506 on ventricular cardiomyocytes

It is possible that FK506 is having indirect effects to enhance Ca^{2+} release rather than effects directly on FKBP12.6. FK506 for instance cannot discriminate between FKBP12.0 and FKBP12.6 and could be acting via FKBP12.0 to release more Ca^{2+} during the transient. It could also be the result of FK506 acting on other biochemical pathways. Evidence for the later is presented within the same study [114]. In the majority of cells during FK506 application, there was an increase in steady state Ca^{2+} load and a slowed decline of $[\text{Ca}^{2+}]_i$ during caffeine induced contractures. These effects were shown to be due to a decreased ability to extrude Ca^{2+} from the cytosol via $\text{Na}^+/\text{Ca}^{2+}$ exchange. FK506 does not affect $\text{Na}^+/\text{Ca}^{2+}$ exchange or Na^+K^+ -ATPase in rat ventricular sarcolemmal vesicles and enzyme activities in homogenates and microsomes respectively. Therefore the affect of FK506 was thought to be indirect within the rat ventricular cardiomyocyte. This is one important effect of FK506, which would not have been picked up in previous bi-layer experiments. Xiao *et al* (1997) also performed experiments on rat ventricular cardiomyocytes [113]. This study showed that FK506 (50 μM) rapidly and reversibly enhanced cell contraction, increased the $[\text{Ca}^{2+}]_i$ transient and the diastolic $[\text{Ca}^{2+}]_i$ level. The concentration of FK506 used in this study is 10 times larger than that used by McCall *et al* (1996). The reason McCall *et al* (1996) used only 5 μM

was due to the production of FK506 toxicity and the production of Ca^{2+} waves [114]. At higher concentrations of FK506 and higher $[\text{Ca}^{2+}]_i$ there was an increased incidence of Ca^{2+} waves. Xiao *et al* (1997) when using $50\mu\text{M}$ showed the production of Ca^{2+} oscillations in their contractile studies. The propagation of Ca^{2+} waves involves the spontaneous release of Ca^{2+} in a co-ordinated fashion from one RyR2 cluster to the next. The frequency of Ca^{2+} waves should increase at higher $[\text{Ca}^{2+}]_i$ and therefore higher SR Ca^{2+} loads, however that they occur at a greater frequency when RyR2 coupling has been reduced by FK506 seems again counterintuitive. A possible explanation to this phenomenon could be the inhibition of $\text{Na}^+/\text{Ca}^{2+}$ exchange by FK506, which could have led to Ca^{2+} overload within the SR, and hence an increase frequency of Ca^{2+} waves rather than a direct effect of FK506 on RyR2 to produce them. However, McCall *et al* (1996) showed that a positive inotropic effect could be achieved even when SR Ca^{2+} load was the same as control. The indirect effects of FK506 alluded to above are controversial but are further backed up by the effect of FK506 on the action potential [201]. DuBell *et al* (2000) showed that FK506 can inhibit repolarising K^+ currents and have suggested that the prolonged action potential duration results in an increased Ca^{2+} transient in rat cardiomyocytes [202]. The effects of FK506 whether they are direct or indirect on RyR2-FKBP12.6 seem to vary from one study to the next and from one species to another. It has recently been shown that FK506 does not have any effects on $\text{Na}^+/\text{Ca}^{2+}$ exchange in mouse or rabbit [203]. Su *et al* (2003) showed that transients in mouse were increased with no change in SR content, L-type Ca^{2+} current, or $\text{Na}^+/\text{Ca}^{2+}$ exchange [203]. However rabbit transients were decreased when exposed to FK506 ($10\mu\text{M}$). The

finding in rabbit is similar to a report by Prestle *et al* [204]. No substantial changes in action potential duration were noted and the suggested explanations were with reference to the species differences in intracellular $[Na^+]$. Since $[Na^+]$ is higher in rat and mouse (12-15mM) this would reduce the potential for Ca^{2+} extrusion from the cell via Na^+Ca^{2+} exchange and an increased leak of Ca^{2+} from SR induced by FK506 will not cause Ca^{2+} depletion. The diastolic $[Ca^{2+}]$ levels would subsequently rise and SERCA2a would pump Ca^{2+} back up into the SR. FK506 will then increase the sensitivity of RyR2 and this phenomenon will dominate resulting in an increased Ca^{2+} transient. Since in rabbit $[Na^+]$ is much lower (4-5mM) [205] Ca^{2+} leaks from the SR and is extruded from the cardiomyocytes via Na^+/Ca^{2+} , decreasing SR Ca^{2+} content and the amplitude of the Ca^{2+} transient. Although this hypothesis fits well with their observations it does not incorporate the role of coupling. Specifically, it does not address the issue of why an increased Ca^{2+} transient can occur despite a decrease in RyR2 coupling due to FK506 application.

5.4.5 The effects of FK506 at rest in ventricular cardiomyocytes

Two of the above studies [114] [113] went on to look at the effects of FK506 at rest. The first study [114] showed an accelerated loss of SR Ca^{2+} and increased resting Ca^{2+} spark frequency. This could have been due to an increased sensitivity of RyR2 to activating Ca^{2+} . The size of the Ca^{2+} spark however was not altered. The authors explanation as to why Ca^{2+} spark morphology did not change in this study was that the increase in SR Ca^{2+} load seen when FK506 was applied was very small or that the effects on SR Ca^{2+} load are separate from the effects on SR Ca^{2+} release. This later

explanation is unlikely since it has been shown that increases in SR load should increase the size of the spark along with the frequency [66;121]. One possible problem with this study on Ca^{2+} sparks [114] is the lack of automated computer algorithm to detect Ca^{2+} sparks; eye detection has been shown to distort the distributions of spark characteristics [115]. Treatment of cardiomyocytes with FK506 has also been shown to increase the duration of Ca^{2+} sparks but with no change in frequency [113]. This is consistent with the idea that uncoupling RyR2 channels by the addition of FK506 results in a defect in RyR2 closure (spark termination). From the above study [114] the resting SR Ca^{2+} content would be expected to gradually decrease albeit at a faster rate than control. However, no such change was evident at rest or in results obtained assessing the caffeine releasable SR Ca^{2+} content [113]. The time period over which FK506 was applied to rat cardiomyocytes was 10min (5 μM). However it has been shown that an exposure of rapamycin for times greater than 32min [63] are needed to effectively uncouple RyR2. Perhaps exposure times were not sufficient in both the above studies [113;114] to achieve this. Therefore drawing conclusions from the studies performed using FK506 to elucidate the function of FKBP12.6 within intact ventricular cardiomyocytes [113;114] is problematic since while there is a possibility that FK506 may directly alter Ca^{2+} release it is hard to distinguish this effect from the non-specific effects of FK506 on Ca^{2+} homeostasis.

5.5 The need for novel techniques

It can be seen from the above two studies, studying the role of RyR2-FK506 within the whole cell is relatively complex when compared to the

specificity bi-layers offer. However, one technique has been used successfully to specifically study the role of the RyR2-FKBP12.6 complex within cardiomyocytes. The technique involves using adenovirus mediated gene transfer to over-express FKBP12.6 within cardiomyocytes. Using these transfected cardiomyocytes, experimental techniques such as electrophysiology, Ca^{2+} uptake measurements, Ca^{2+} spark measurements, and cell shortening can all be performed relative to a control population of cardiomyocytes transfected with a control virus (either Ad-GFP or Ad-LacZ). The advantage being that the RyR2 complex remains within the SR and within the cardiomyocyte and the only parameter changed is the over expression of FKBP12.6. Prestle *et al* (2001) performed studies showing that rabbit adult cardiomyocytes over-expressing FKBP12.6 exhibited an increase in fractional shortening (21%) relative to control cardiomyocytes [204]. Cells were then permeabilised and subject to Ca^{2+} uptake measurements. Cells over-expressing FKBP12.6 showed a significantly increased SR Ca^{2+} uptake rate without the addition of ruthenium red (5 μM) and similar uptake rate with ruthenium red (5 μM) compared to control. These results together with the finding of an increased caffeine induced contracture when FKBP12.6 was over expressed suggests that FKBP12.6 functions to increase the closed probability of the RyR2 and by doing so reduce resting Ca^{2+} leak (by 53%) and increase SR Ca^{2+} content.

5.5.1 The use of permeabilised cells to study the role of FKBP12.6

The permeabilised cell provides a unique way of manipulating the intracellular environment while maintaining structural and functional integrity. Since FKBP12.6 is a soluble protein present within the myoplasm,

permeabilisation may be thought to be problematic when performing these experiments due to possible protein loss. In our hands [88] this is not thought to occur for the following reasons:

(1) FKBP is tightly bound to RyR and the 'off' rate of the exchange reaction of soluble ^{35}S - FKBP12.0 from RyR1 is thought to be negligible [181].

(2) Despite vigorous homogenisation and biochemical purification steps the binding sites of RyR1 and RyR2 in isolated and washed TC are still filled with FKBP12.0 and FKBP12.6 by 94% and 83% respectively.

(3) The time period over which these experiments are performed is within 3-4 min (Ca^{2+} spark measurements only over a 60s period). Soluble protein loss has only been measured when experiments are performed for 30min [170].

(4) Functional effects are considerably different between cells over-expressing FKBP12.6 and control cardiomyocytes (see section 5.15.3). Over expression of FKBP12.6 results in an increased SR Ca^{2+} content but reduced spark size suggesting a functional effect of decreased RyR2 mediated Ca^{2+} leak (see section 5.15.3). Normally increased SR Ca^{2+} content would result in an increased spark size and frequency.

(5) Substantial intracellular binding of fluorescent indicators occurs when cells are permeabilised denoted by a higher intracellular fluorescence. The fluorophore is presumably bound to proteins retained by the permeabilised cell [88] (see section 3.2.4).

(6) The permeabilisation agent used (β -escin) is less disruptive to the sarcolemma than other permeabilisation agents such as saponin [104].

5.6 The biomedical significance of FKBP12.6

5.6.1 Are these studies relevant to the whole heart?

A clue as to the biomedical importance of FKBP12.6 came from a study involving five paediatric patients receiving prophylactic treatment of FK506 (tacrolimus) for organ transplantation [206]. These patients developed either congestive heart failure (CHF) or hypertrophic obstructive cardiomyopathy, which resolved after changing to cyclosporin treatment or lower doses of FK506. The effects of FK506 in most of these patients seemed to be partially reversible. This is an important observation and has similarities to the described mode of action of FK506 and its interaction with the FKBP12.6-RyR2 complex in that FKBP12.6 can rebind to depleted RyR2. This is also important since high concentrations of FK506 can lead to Ca^{2+} overload and the production of Ca^{2+} waves which diminish when the dose is lowered [114]. This was the first report of a cardiac toxicity effect in humans. Marx *et al* (2000) investigated cardiac dysfunction on a molecular scale [207]. The macromolecular complex of RyR2 incorporates not only four 565,000 dalton homo-tetramers but also muscle A kinase anchoring protein (mAKAP), protein phosphatase 2A (PP2A), protein phosphatase (PP1), protein kinase A (PKA), PKA regulatory subunit (RII), and FKBP12.6. The stoichiometry of PKA phosphorylation is 3.8 moles of phosphate per mole of channel (RyR2). PKA phosphorylation of RyR2 is significantly elevated in failing hearts from humans and dogs with pacing-induced heart failure compared to non-failing hearts by approximately four-fold. This is not due to increased levels of PKA protein associated with RyR2 and in this study was adjusted for any change in number of RyR2

due to heart failure. Marx *et al* (2000) investigated PKA dependent phosphorylation of RyR2 in human patients using left ventricular assisting devices (LVAD) [207]. The devices allow for the improvement of hemodynamic and contractile properties of diseased hearts until cardiac transplantation donors become available. When an LVAD is placed within the heart a core of tissue is removed. This pre-LVAD sample is therefore representative of end stage heart failure tissue and post-LVAD sample comes from hearts with improved function. PKA phosphorylation of RyR2 was significantly increased in heart failure tissue samples compared to samples from non-failing hearts and returned to normal levels following LVAD treatment. It is known that circulating catecholamines levels are raised in heart failure. Many patients with end stage heart failure are treated with β -adrenergic agonists prior to cardiac transplantation, however some are not. PKA phosphorylation of RyR2 is significantly elevated in the hearts from patients treated with β -adrenergic agonists prior to cardiac transplantation. Therefore exogenous β -adrenergic administration can increase levels of RyR2 PKA dependant phosphorylation. Hyperphosphorylation could be explained by the significant decrease in PP2A and PP1 associated with RyR2. PP1 associated with the RyR2 returned back to normal level post-LVAD (PP2A did not). The PKA phosphorylation of RyR2 was found to inhibit FKBP12.6 binding to RyR2 and therefore provides a possible mechanism for the physiological and pathophysiological regulation of FKBP12.6 dissociation from RyR2. It must be noted that protein kinase C (PKC) did not induce the dissociation of FKBP12.6 from RyR2. Dissociation of FKBP12.6 from the RyR2 due to PKA phosphorylation increased the open probability and induced the

appearance of sub-conductance states in single channel recordings. One additional finding in 15% of heart failure RyR2 channels was a long lasting sub-conductance state. This level of RyR2 channel activity was never observed in normal hearts, which were almost always completely inactive (50nM $[Ca^{2+}]$). If high circulating levels of β -adrenergic agonists are present in heart failure patients then the level of PKA phosphorylation will be high and FKBP12.6 will dissociate from RyR2. If β -adrenergic agonists are then given to these patients the response seems blunted. This could be because no further PKA phosphorylation can take place. It was shown in this study that pre-LVAD patients had a blunted response to isoproterenol compared to normal hearts and post-LVAD restored the β -adrenergic agonist response (measurements using contractile experiments). The localisation of the RyR2 macromolecular complex and β -adrenergic system to the T-tubule is advantageous for it allows local regulation for the RyR2 at the site of EC coupling. Overall it is seen from this study that inappropriate SR Ca^{2+} release via RyR2 in heart failure patients due to higher levels of PKA phosphorylation compared to normal hearts could lead to significant decreases in SR Ca^{2+} content (not shown) and hence contractile dysfunction.

5.6.2 Should the Ca^{2+} transient be increased or decreased on removal of FKBP12.6?

This chapter has tried to emphasise the need to progress in a logical fashion from whole heart to the scale of the molecule or vice versa. While the above study [207] is pivotal in the degree of knowledge gained on the role of FKBP12.6 in heart failure, it has jumped from bedside patient to the

molecular level without the intervening steps. This was done for obvious reasons. Human tissue is always in very short supply and in this case was an extremely precious commodity since it came from patients using LVAD's prior to cardiac transplantation. The tissue would also have been difficult to work with in terms of obtaining intact cardiomyocytes from which to do intact cell measurements from. As pointed out in an editorial by Terraciano (2000) the results from this study would indicate that higher levels of PKA phosphorylation of RyR2 are present in heart failure, which would lead to an increased leak from RyR2 and presumably a decrease in SR Ca^{2+} content [208]. This ultimately would lead to a decreased Ca^{2+} transient. However also noted, was that in theory alterations in RyR2 gating should not have a steady state effect on SR Ca^{2+} release in the whole cell and hence no steady state change in the peak of the Ca^{2+} transient. This phenomenon was described using rat cardiomyocytes and is termed auto-regulation [209]. However auto-regulation only holds true if: (1) there is no significant non-RyR2 mediated leak from the SR during diastole and (2) that other important proteins involved in Ca^{2+} homeostasis are working normally, i.e. $\text{Na}^+/\text{Ca}^{2+}$ exchange, L-Type Ca^{2+} influx, SERCA2a and phospholamban.

The activities of other Ca^{2+} regulatory proteins were not measured in this study [207]. Therefore the question still remains: will dissociation of FKBP12.6 from RyR2 in heart failure patients cause a decrease in SR Ca^{2+} content. The theory of auto-regulation suggests this will not occur since Ca^{2+} regulatory proteins will compensate for decreases in SR Ca^{2+} content. Possible evidence for this was seen in a previous study [114] whereby the

application of FK506 increased the open probability of RyR2, increased the resting leak of SR Ca^{2+} but indirectly inhibited $\text{Na}^+/\text{Ca}^{2+}$ exchange mediated efflux of Ca^{2+} . This resulted in a maintained or moderately increased SR Ca^{2+} content. The literature concerning whether or not SR Ca^{2+} content is altered in heart failure is extremely varied with different models of heart failure producing various differences in regulatory protein functional expression and related changes in SR Ca^{2+} content. It is beyond the scope of this thesis to discuss all the heart failure studies. However from the above, it must be borne in mind that the cardiomyocyte does not just consist of RyR2. Although molecular and biochemical studies shed important light on the function of specific proteins, it is their interaction with the other Ca^{2+} homeostatic mechanisms which are perhaps more important and which require whole cell studies.

A series of recent papers has tried to provide a more comprehensive picture of a particular model of heart disease and RyR2 gating abnormalities leading to changes in SR Ca^{2+} content. The first study introduced a model of tachycardia-induced heart failure induced by pacing Beagle dogs for 21 days using an externally programmable miniature pacemaker [208;210]. The hemodynamic characteristics of the heart failure model were progressive left ventricular dilation, contractile dysfunction, and relaxation disturbances. Using SR vesicles the characteristics of polylysine induced SR Ca^{2+} release at two concentrations was investigated together with Ca^{2+} uptake experiments in both normal and heart failure SR vesicles. The time course of rapid Ca^{2+} release induced by polylysine was decreased in heart failure SR vesicles. The Ca^{2+} uptake rates were also significantly decreased compared with normal SR vesicles

but the releasable fraction of sequestered Ca^{2+} upon addition of polylysine was significantly larger in failing SR vesicles than in normal vesicles. Ryanodine binding studies were also performed. The number of binding sites in failing hearts was significantly lower than normal hearts but there was no difference in K_d for [^3H] RyR binding between the two groups. The polylysine concentration dependency in terms of the initial rate of Ca^{2+} release and RyR2 binding shifted towards the lower concentration of polylysine in failing SR vesicles. These results suggest that RyR2 has an increased sensitivity in the heart failure model. From the descriptions presented in this chapter it seems likely the FKBP12.6 has some role to play in these observations. Indeed in their second paper the stoichiometry of FKBP12.6 to RyR2 was markedly decreased from 3.6 to 1.6 in normal and heart failure SR vesicles respectively [211]. The physiological consequence of this ratio change was investigated by the application of FK506 to the vesicles. There was a dose dependent Ca^{2+} leak in normal SR but in heart failure vesicles a significant Ca^{2+} leak was observed even in the absence of FK506. Increased doses of this drug produced no further increase in leak. An interesting method to monitor conformational changes in RyR2 concurrent with measurements of Ca^{2+} leak was also presented in this study. The technique involved the use of methyl-courmarin-acetamido (MCA). This is a fluorescent probe, which was bound to RyR2. The probe was excited at a wavelength of 360nm and the subsequent emission signal collected at 440nm. The fluorescence produced was an indication of the protein conformational change of RyR2 and nicely followed the observations made on leak analysis. This confirmed that RyR2 conformational changes are responsible for the increased Ca^{2+} leak seen in

normal SR vesicles when FK506 is applied in a dose dependant fashion. The third study produced by the same group used the same tachycardic model to study polylysine-induced enhancement of ryanodine binding during FK506 application [212]. This binding was reduced after increasing concentrations of FK506 in normal SR vesicles but no significant change was seen in failing SR vesicles. The inhibition by FK506 of polylysine-induced ryanodine binding was not thought to be a direct effect of FK506 since the binding sites for ryanodine and FK506 are different. However a conformational change in the RyR2 was thought to have occurred when FK506 dissociated FKBP12.6 from RyR2 ultimately resulting in a decrease in ryanodine binding. [³H] dihydro-FK506 binding in SR vesicles was also lower in failing vesicles than in normal vesicles. The rate of Ca²⁺ release was decreased after application of FK506 in normal SR vesicles but unchanged in failing SR vesicles. The total amount of Ca²⁺ released in normal vesicles was enhanced by FK506 suggesting that the releasable fraction of sequestered Ca²⁺ for the total amount of Ca²⁺ uptake is increased similar to failing SR vesicles. The application of this drug to failure vesicles however showed no such increase in Ca²⁺ release, the FKBP12.6 presumably removed already. Importantly it was also shown that FK506 does not have an effect on the activity of the Ca²⁺-ATPase of the SR.

One last study by this group continued the work of Marx *et al* (2000) on the use of β -adrenergic drugs in heart failure [207]. While it seems sensible to apply β -adrenergic agonists to a weakly contracting heart it seems counterintuitive to give β -adrenergic blockers to heart failure patients yet

they have proven to be one of the most important treatments for heart failure. It is thought that the beneficial effects to patients include increased relaxation, restoration of β -receptor population, decreased sympathetic nervous activity, and reduced heart rate [213]. However the molecular mechanisms underlying the reason why β -blockers are beneficial in heart failure is unclear. Doi *et al* (2001) investigated this [214]. Using the same tachycardic model of heart failure (but this time 4 weeks of pacing) the authors tried to assess whether or not a chronic low dose of propranolol (a β -blocker) could reverse the effects of PKA dependent hyper-phosphorylation of RyR2. Using SR vesicles and techniques used in their previous papers the findings suggested that dogs given propranolol did not develop heart failure and showed no signs of left ventricular remodelling. There was no spontaneous leak of Ca^{2+} via RyR2 and FK506 increased Ca^{2+} leak unlike SR vesicles from dogs not given propranolol. MCA fluorescence confirmed the conformational changes in RyR2. Untreated vesicles showed PKA hyper-phosphorylation, which was reversed by propranolol treatment. The chronic pacing decreased the amount of RyR-associated with FKBP12.6, but the decrease was prevented by propranolol treatment. [^3H] dihydro-FK506 binding was significantly larger in propranolol treated than that obtained for the propranolol-untreated vesicles, although it was still less than the normal vesicles. (The stoichiometry: of normal SR vesicles (3.62 ± 0.62), propranolol untreated (1.14 ± 0.16), propranolol treated (2.38 ± 0.46)). SR Ca^{2+} uptake and the amount of SR Ca^{2+} ATPase were decreased in heart failure SR vesicles and were no different with or without propranolol. These results suggest that RyR2 mediated Ca^{2+} leak when FKBP12.6 is dissociated from RyR2 is

inhibited by propranolol and prevents LV remodelling improving cardiac function in the tachycardic heart failure model. The mechanism behind these observations involved reversal of the PKA dependant phosphorylation of RyR2 and the re-association of FKBP12.6 to RyR2. A very interesting feature not reported in this study is that the full complement of FKBP12.6 was not restored to normal levels yet the heart failure was improved significantly. Does this mean that the full stoichiometry of FKBP12.6 to RyR2 of 4 is not needed? Perhaps only possibly 2-3 (2.38 ± 0.46) are required to achieve full co-ordination of RyR2? This must be taken into account when dissociating FKBP12.6 off of RyR2 and looking at the functional effects of the ryanodine receptor, simply dissociating some of the FKBP12.6 may not be enough and may explain why there is a variation in range of effects of FK506. Either way a questions that still remains is: what is the function of the other possible 50% of sites if they are not all involved in stabilising RyR2?

5.6.3 Concerns

There are possible concerns over the molecular studies described above: even though they have progressed from the lipid bi-layer experiments discussed earlier to the use of SR vesicles, this preparation is a long way from whole cell studies incorporating the effects of other regulatory proteins determining SR $[Ca^{2+}]$. There is also doubt as to whether the tachycardic model represents a true form of heart failure since the process is reversible three weeks after the termination of pacing. Furthermore, no hypertrophic compensatory phase was apparent in this model.

5.6.4 Future work is needed

Many models of animal heart failure exist and have been fully characterised using electrophysiological studies and data regarding Ca^{2+} regulatory protein expression. Unfortunately, to date, no one has studied the molecular role of FKBP12.6 on RyR2 in whole intact cells from one of these well-characterised failure models. The challenge to establish a coherent understanding of the role of RyR2 in Ca^{2+} homeostasis within intact cardiomyocytes with the incorporation of all other regulatory proteins associated with RyR2 and the sarcolemma, will ultimately be more beneficial in comparison to trying to establish the role of FKBP12.6 on RyR2 in isolated systems such as lipid bi-layers or SR vesicles.

5.6.5 The importance of FKBP12.6 stoichiometry within cardiomyocytes

It becomes apparent when reading this chapter that the literature on SR Ca^{2+} release due to dissociation of FKBP12.6 from RyR2 presents a dichotomy. On one hand, dissociation increases CICR gain and contractility (as in the application of FK506) or alternatively dissociation induces so much SR Ca^{2+} leak that CICR gain and contractility decreases (as seen in heart failure). It is hard to reconcile a mechanism whereby these two scenarios can co-exist. The former case requires a sufficient SR Ca^{2+} content to allow a larger Ca^{2+} transient to be triggered for any given L-type Ca^{2+} influx. The latter case suggests that the SR Ca^{2+} content is reduced to such an extent by RyR2 mediated Ca^{2+} leak that any Ca^{2+} transient produced will be decreased to a level such that it is not sufficient to produce an efficient contractile response. In both cases it should be

noted that coupling between RyR2 is considered decreased due to the dissociation of FKBP12.6 from RyR2. One way to reconcile these two situations is to consider the phosphorylated status of RyR2. Hyperphosphorylation resulting from increased levels of β -adrenergic stimulation in heart failure results in dissociation of FKBP12.6 from RyR2 and a subsequent increase in Ca^{2+} leak from the SR. However this same sympathetically driven phosphorylation must also occur during a fight or flight response. An increase in CICR would be desirable during this sympathetic drive as oppose to a decrease in SR Ca^{2+} content. It is apparent that the exposure time to β -adrenergic agonists differs in the two cases: in heart failure β -adrenergic agonists are present chronically however during the 'fight or flight' response the exposure is acute. The temporal effects are related to altered FKBP12.6 stoichiometry and thus provide a possible mechanism whereby increases and decreases in CICR gain can be achieved by a similar mechanism [215].

'In normal hearts, as each of the PKA sites is transiently phosphorylated there is a progressive physiological increase in RyR2 channel activity and increase EC coupling gain resulting in increased contractility. However, in failing hearts where on average three or four of the PKA sites are chronically depleted of FKBP12.6 they become destabilised or 'leaky'. Under these conditions uncoupling of RyR2s would occur due to PKA phosphorylation of RyR2 and depletion of FKBP12.6 from the macromolecular complex.'

This would mean that when the stoichiometry of FKBP12.6 is one or two (such as in heart failure) there would be a decrease in CICR gain due to decreased coupled gating. Evidence for this comes from the measurements of Ca^{2+} sparks within cardiomyocytes from failing hearts,

which show a prolonged decay and an increased width [215]. The decrease in RyR2 coupling would result in a decreased SR Ca^{2+} content and a shift in the Ca^{2+} activation curve to the left. Unusually in this study the Ca^{2+} sparks were smaller in amplitude when RyR2 was hyper-phosphorylated. This was thought to be due to a decreased SR Ca^{2+} content. However it seems more logical that de-coupling would have produced an increase in spark amplitude along with other the morphological characteristics and further aid the increase in SR Ca^{2+} leak and subsequent decrease in SR Ca^{2+} content similar to the report that will be discussed in depth later [216]. It becomes clear from these previous studies that without a handle of SR Ca^{2+} content spark characteristics are hard to interpret since so much of the size of the Ca^{2+} spark is reliant on SR Ca^{2+} content. More work therefore needs to be carried out with measurements of Ca^{2+} flux through RyR2 and the resultant change in SR Ca^{2+} content.

5.7 The balance between phosphorylation and phosphatase activity

The importance of the *in vivo* balance between phosphorylation and phosphatase activity on RyR2 has been emphasised by Reiken *et al* (2003) and provides a stark warning for those authors studying the effects of FKBP12.6 on RyR2 using isolated cardiomyocytes [215]. If RyR2 were hyper-phosphorylated (such as in heart failure) one would expect the function of the macromolecular complex to be altered. Furthermore, additional phosphorylation by β -adrenergic agonists would result in a blunted response. However, Gomez *et al* (1997) found that RyR2 function was unaltered in animals with heart failure [217]. To investigate this disparity [215] cardiomyocytes were isolated by Langendorff perfusion and

isoproterenol added to the perfusate. No significant change in RyR2 phosphorylation status was observed as reported by Gomez *et al* [217]. If however sodium fluoride (NaF) a weak phosphatase inhibitor, was added to the perfusate along with the isoproterenol a significant increase in PKA mediated phosphorylation was observed. This data suggests that when experiments are performed on isolated cardiomyocytes the balance between the phosphatase effects and PKA mediated phosphorylation of the RyR2 must always be considered. It seems that phosphatase mediated by PP1 and PP2a located on RyR2 has a dominant effect during Langendorff perfusion without phosphatase inhibitors to the extent that the true hyper-phosphorylated status of RyR2 is lost. Phospholamban was phosphorylated by isoproterenol with or without NaF. This could be because no such phosphatase or kinase is attached to this protein. In heart failure a chronic hyper-adrenergic state predominates along with a decrease in phosphatase attached to RyR2. PKA hyper-phosphorylation therefore ensues and FKBP12.6 is subsequently dissociated from RyR2. This might not be seen in acutely dissociated cardiomyocytes when perfused with isoproterenol since phosphatase dominates the situation. Flash freezing of the heart as soon as it removed from the body needs to be performed if the *in vivo* phosphorylation status of RyR2 is to be captured. When hearts are flash frozen after isoproterenol infusion a significant PKA mediated phosphorylation of RyR2 occurs and FKBP12.6 is dissociated [217].

5.7.1 The testing of other heart failure models

With this in mind multiple animal heart failure models were investigated

[215]. The salt sensitive Dahl rats, which developed hypertension and subsequent hypertrophic cardiomyopathy, showed evidence of hyper-phosphorylation of RyR2 in the presence of NaF but not in absence or control. PLB was also phosphorylated. This is an example of severe cardiac hypertrophy where RyR2 and PLB were hyper-phosphorylated which differs from heart failure in which RyR2 is PKA phosphorylated and PLB is not. Furthermore unlike heart failure where phosphatase is decreased hypertrophic cardiomyopathy showed no such decrease. This is therefore similar to acute β -adrenergic stimulation. Performing the same study in a six-month post-myocardial infarction (PMI) rat model showed PKA hyper-phosphorylation of RyR2 and hypo-phosphorylation of PLB. There was a concurrent decrease in phosphatase levels. This is similar to that of heart failure [207]. Again with another model concerning the cardiac-specific over-expression of human matrix metalloproteinase type 1 (MMP-1), which shows progressive cardiac dysfunction the same experiments carried out at six, twelve, and twenty-four months of age showed progressive PKA hyper-phosphorylation of RyR2. Mice with cardiac specific over expression of β 2-adrenergic receptor showed significant PKA hyper-phosphorylation of RyR2 [215]. All of these models were associated with increased dissociation of FKBP12.6 to RyR2. This study provides good evidence for the link between PKA hyper-phosphorylation, dissociation of FKBP12.6, increased spark size, and heart failure. The cardiac tissue has obviously been handled with extreme care and expertise to provide solid evidence. However, the complexity of the PKA phosphorylation status of RyR2 and its functional consequences are not so straightforward.

5.7.2 Controversy in interpretation of results due to PKA phosphorylation of RyR2

Li *et al* (2002) showed that PKA phosphorylation of RyR2 did not affect Ca^{2+} sparks in mouse ventricular cardiomyocytes [109]. Spark frequency was used as a measure of SR Ca^{2+} leak in permeabilised cardiomyocytes from control cells (wild type), PLB knock out cardiomyocytes which had no inhibition of SERCA2a dependent Ca^{2+} uptake, and PLB double mutant which lacked a regulatory phosphorylation site and therefore SERCA2a continually inhibited SR Ca^{2+} uptake. When cAMP was added to wild type cardiomyocytes a significant increase in Ca^{2+} spark frequency occurred. No such increase was evident in PLB knock out or double mutant cardiomyocytes. The study also assessed SR Ca^{2+} content, which together with the data above suggested that PKA dependent RyR phosphorylation did not affect resting SR Ca^{2+} leak in these myocytes and that the increased Ca^{2+} spark frequency and size is dependent on PLB phosphorylation and consequent increases in SR Ca^{2+} content. This study had therefore tried to separate the effects of PKA phosphorylation on RyR2 and SERCA2a mediated Ca^{2+} uptake and analyse the consequent SR Ca^{2+} content. This study is in direct contention with the studies by the Marks, A.R. group. There are some worrying aspects to this skinned cell study [109]. The most obvious was the major disparity in Ca^{2+} spark frequency between intact and permeabilised cells. This was by no means a small difference. At 50nM in permeabilised cells the control cell had a frequency of approximately $350 \text{ sparks} \cdot \text{pl}^{-1} \cdot \text{s}^{-1}$ but the spark frequency in intact cells was approximately $40 \text{ sparks} \cdot \text{pl}^{-1} \cdot \text{s}^{-1}$. Even more problematic with these measurements is that the resting $[\text{Ca}^{2+}]$ in intact cells ($\sim 150\text{nM}$) is

thought to be two or three times higher than that used in the permeabilised cells (50nM). This would result in a higher SR Ca^{2+} content in the intact cells and increased Ca^{2+} spark frequency yet this was by no means seen, in fact the reverse was observed and no indication of SR Ca^{2+} content in intact cells was given. In rabbit cardiomyocytes Ca^{2+} spark measurements in β -escin permeabilised cells are difficult to evaluate in comparison to intact rabbit cardiomyocytes since cellular $[\text{Na}^+]$ favours extrusion of Ca^{2+} from the cell and depletion of SR Ca^{2+} content. However the frequency of Ca^{2+} sparks in cultured cardiomyocytes compared to freshly dissociated cells (see section 5.15.3) is very similar and is comparable to the frequency in permeabilised and more importantly intact rat cardiomyocytes [64]. The controversy above could therefore represent a problem with the permeabilisation technique used. Even though the permeabilisation agent used in this study [109] (Streptolysin-O) produces more consistently sized pores (30nm) these are still twice the size of those produced by saponin and β -escin (8-15nm). The permeabilisation technique was shown to take 10-25min depending on the cell density. This combined with the experiment that lasted for a further 16min is problematic. Endo (1980) showed considerable loss of soluble protein from muscle cell cytoplasm in 30min [170]. That this study took place over a possible 41min is of concern and in the worst possible scenario resulted in the loss of FKBP12.6 from the permeabilised preparation. This would have resulted in no further phosphorylation of the mutant cells in this study. Experiments in this thesis take place over an acute time of 3-4min including permeabilisation times (~0.5min). That FKBP remains bound to SR vesicles despite vigorous homogenisation and biochemical purification steps suggest that

dissociation of the FKBP by permeabilisation is an unreasonable consequence. However this defence might only be plausible if the experiment is performed acutely. Another consideration with this study is the use of extremely low $[Ca^{2+}]$ of 10 and 50nM. This was achieved by the use of 10mM EGTA. In rabbit cardiomyocytes 10mM EGTA does not allow visualisation of Ca^{2+} sparks let alone caffeine release which was shown to occur in the mouse in this study. Why this disparity exists is unknown. Reiken *et al* (2003) would suggest that this $[Ca^{2+}]$ is too low to activate RyR2 [215]. This may have been used to ensure that the addition of cAMP did not cause enhanced SR uptake and Ca^{2+} waves. The use of the mutants in this study presents extremity cases of PLB regulation, which may mask the effects of PKA phosphorylation on RyR2, mediated Ca^{2+} release. The idea that PKA can affect the phosphorylation status of the RyR2 and alter Ca^{2+} release from the SR is far from certain. Ca^{2+} calmodulin kinase II (CaMKII), which also phosphorylates the cardiac RyR2 at Ser-2809, does not seem to produce similar bi-layer results as PKA [218-220]. PKA phosphorylation modulation of RyR2 is also complex when there are dynamic changes in myoplasmic $[Ca^{2+}]$. This phenomenon can alter the open probability of RyR2 [58]. Clearly further work is needed on this important topic.

5.8 The use of transgenic whole animal models

Shou *et al* (1998) published a different technique, which probably hoped to achieve a more integrated approach [221]. The approach was to create transgenic mice deficient in FKBP12.0 using embryonic stem cell technology. Unfortunately the mammalian need for FKBP12.0 (from birth)

has never been highlighted so vividly. The majority of mice were said to have died between embryonic day 14.5 and birth (8 out of 557 mice survived). Caesarean section was used to examine some embryos within this period of time. Pathology revealed severe cardiac abnormalities including dilated cardiomyopathy, ventricular septal defects, enlarged hearts, oedema, anatomical defects suggestive of non-compaction of the left ventricle, hypertrophic trabeculae and deep inter-trabecular recesses. Other systemic abnormalities including severe haemorrhage and necrosis of the liver (liver centrilobular necrosis), exencephaly and neural tube closure defects. Of the 1% that survived (8 animals) only 1 mouse lived past a few weeks (14 months) the others dying of a cardiac wasting syndrome. This 'fortunate' mouse showed clinical signs and anatomic defects consistent with human cardiomyopathy and heart failure. Even though FKBP12.0 is associated with skeletal muscle RyR1 not one single skeletal muscle abnormality was seen at the gross anatomical level or via electron microscopy. However on the molecular level when RyR1 was incorporated into lipid bi-layers from FKBP12.0 deficient mice abnormalities were present. FKBP12.0 deficient mice showed RyR1 channel abnormalities associated with removal of FKBP12.0 from RyR1, i.e. an increased open probability and appearance of sub-conductance states. When RyR2 was incorporated into lipid bi-layers and similar experiments carried out the same observations were noted as for FKBP12.0 i.e. an increased open probability and appearance of sub-conductance states. These results challenge the idea of functional selectivity of FKBP12.0 to RyR1 modulation and FKBP12.6 to RyR2 modulation suggested by various studies described above. FKBP12.0 deficient mice had abnormal gating of

both RyR1 and RyR2 yet no skeletal abnormalities were present. The FKBP12.6 present within the tissues of the FKBP12.0 deficient mice could not restore the normal channel properties to RyR1. This raises the question of whether or not *in vivo* FKBP12.0 is needed for EC-coupling. Although this study raises important questions on the role of FKBP12.0 at the systemic level its benefit as an important model for the testing of pharmacological agents and other therapies that may retard or reverse human heart failure as stated at the end of the study is somewhat controversial. Certainly a survival rate of 0.2% does not fit in with the attempt to reduce, refine, and replace animal experimental procedures. Another important aspect to transgenic models such as this one is the possibility of changes not usually present in adult mice representing adaptive changes to compensate for the lack of FKBP12.0. Therefore the slim chance of any surviving animal is somewhat obscured by the possibility of an abnormal physiology corresponding to an adaptive model. This is where the relatively acute procedure of over- expressing a protein in adult cardiomyocytes provides a more beneficial model in which adaptive changes are extremely limited due to the short time in which to occur. One way this could be incorporated into a transgenic model would be to produce conditional knockouts. This would ensure that embryonic or neonatal adaptive changes will be prevented and changes in expression for the selected protein will only be seen in the adult model if and when so desired. Since a transgenic model had been produced without FKBP12.0 it seems prudent to produce a mouse without FKBP12.6 [216]. However whereas the FKBP12.0 mouse lacked FKBP12.0 exons 3 and 4 encoding for the functional domains involved in FK506 and rapamycin binding, cis-trans

prolyl isomerase activity and TGF- β type 1 receptor binding, the FKBP12.6 mouse [216] lacked exon 3 on the FKBP12.6 gene encoding for the binding sites for RyR2, FK506 and calcineurin. The survival rate in this model compared to the FKBP12.0 transgenic mouse is somewhat unknown since there is no indication of the total number of transgenic mice produced. Whole cell experiments were performed on 5-6 mice, which survived to 4-6 months of age. There is also no indication whether other developmental abnormalities were produced other than the hypertensive induced cardiac hypertrophy seen in male mice. This could be due to the specific binding of FKBP12.6 to RyR2 in the heart and hence no other systemic abnormalities detected or a lack of reporting. This is in stark contrast to the widespread systemic problems associated with the FKBP12.0 transgenic and probably represents the ubiquitous nature of the protein. By using whole cell experiments performed on voltage clamped cardiomyocytes loaded with Fura-2, Xin *et al* (2002) showed that both male and female mice had unaltered L-type Ca^{2+} channel alterations but both had an increase in CICR gain, i.e. an equivalent I_{Ca} produced a much larger increase in the peak $[\text{Ca}^{2+}]_i$ transient. When voltage clamped at 10mV the CICR gain was 83% and 67% in male and female mice respectively (but not significantly different). Shortening measurements followed this trend. Using LSCM sparking events were detected in voltage clamped cells using 100 μM Fluo-4. This is the first study to associate an increase in spark amplitude with RyR2 deplete of FKBP12.6 and in this study was observed in FKBP12.6 null male and female mice in comparison to wild type, this situation being analogous to the application of FK506 which previously had only been shown to increase frequency [114] and duration [113]. An increase in width

and duration of Ca^{2+} sparks was also observed in FKBP12.6 null mice seen in comparison to wild type mice although duration was not expressed in the conventional way at the half maximal level. Instead spark duration was expressed with a prolonged rise time taken from the point of rise to peak of the spark, and an increased decay time constant, which was an exponential fit of the rapid phase of F/F_0 decay. It was suggested in this study that the increase in spark size and therefore longer opening times augments SR Ca^{2+} release and directly gives rise to the increase in CICR gain. This comment would be at odds with the theory of stoichiometry as proposed above by Reiken *et al* (2003) since the RyR2 is supposedly fully depleted of FKBP12.6 [215]. This latter study would suggest that longer openings times and a larger leak of SR Ca^{2+} into the myoplasm would decrease SR Ca^{2+} content and ultimately reduce the CICR gain. A mechanism therefore must be maintaining SR Ca^{2+} content or enhancing it to allow for the increase in gain. A mechanism to maintain SR Ca^{2+} content would be critical since FKBP12.6 mice will also have a lack of co-ordination between RyR2 channels (this being needed for efficient EC-coupling). Another possibility is that FKBP12.0 is compensating for the lack of FKBP12.6 in some way. No experiments were performed to assess SR Ca^{2+} content or the regulation of other Ca^{2+} regulating proteins. Despite the increase in CICR gain and similar spark characteristics in both male and female FKBP12.6 null mice only male mice suffered from hypertension and hypertrophic cardiomyopathy. If tamoxifen (a oestrogen receptor antagonist) was given to the female mice they also developed cardiac hypertrophy. This suggests that the stimulation to allow a hypertrophic response was prevented by oestrogen, and therefore is protective against

cardiac hypertrophy. The stimulation for cardiac hypertrophy is thought to be an increase in cellular $[Ca^{2+}]$. Oestrogen receptor signalling determines how the heart adapts to increased levels of $[Ca^{2+}]$. There could have been other stimuli responsible for the inducement of cardiac hypertrophy such as changes in calcineurin activity, which is known to affect NFAT, and subsequent gene expression (since this binding site has been deleted). Since hypertrophy is related to hypertension, increases in peripheral resistance could have been a triggering factor [216].

5.9 Novel modulators of RyR involving FKBP

Many studies have used FK506 to reveal the association between FKBP12.6 and RyR2. However FK506 is an exogenous modulator of RyR2 function. Endogenous substances *in vivo* must regulate the association between the two. Phosphorylation has proved to be used as an *in vivo* modulator of RyR2-FKBP12.6 function. The sheer complexity and abundance of biochemical pathways existing within cardiomyocytes suggest that there may be other *in vivo* modulators of FKBP-RyR function. The next section summarises some novel products that modulate RyR2 via their interaction with FKBP.

5.10 Bastadins

The first group of products are obtained from the sponge *lanthella basta* located in the Great Barrier Reef. The products are macrocyclic natural products derived from bromotyrosine. They have been called bastadins, two of which have been studied in depth. Bastadin 5 has been shown to modulate the skeletal and more weakly the cardiac RyR via FKBP [222]. Using ryanodine binding and RyR1, bastadin 5 was shown to increase the

specific [^3H] ryanodine binding in a dose-dependent manner. The mechanism by which this was achieved, involved stabilising high affinity binding sites for [^3H] ryanodine while minimising binding sites with a lower affinity. It does not alter the apparent affinity of the Ca^{2+} activator site for Ca^{2+} unlike caffeine. The compound also attenuates the inhibition of the binding of [^3H] ryanodine by mM concentrations of Mg^{2+} and Ca^{2+} . Bastadin 5 does not interact with known RyR1 channel modulators and has a greater potency and intrinsic activity toward enhancing [^3H] ryanodine occupancy compared to caffeine. Another *lanthella basta* product competes with Bastadin 5 and is called Bastadin 19. Bastadin 19 inhibits the activity of Bastadin 5 while behaving like a partial agonist. The potency of Bastadin 5 was three times greater than Bastadin 7 another Bastadin from the same sponge. Using SR vesicle experiments the author showed that Bastadin 5 (i) decreases the net rate of SR Ca^{2+} accumulation in a dose dependent manner, (ii) markedly enhances CICR, (iii) but is unable to release Ca^{2+} when added to loaded SR vesicles at low (<100nM) extra-vesicular Ca^{2+} , unlike a mixture of Bastadins from the same sponge. Using lipid bi-layer experiments it was established that Bastadin 5 slowed the gating transitions of RyR1 increasing the open and closed time constants without effecting channel unitary conductance for Cs^+ . Importantly FK506 suppresses the dose dependent activation of [^3H] ryanodine binding sites by Bastadin 5 to a level seen with FK506 alone. Further more Ca^{2+} efflux induced by addition of Bastadin 5 mixture added to loaded SR vesicles was completely inhibited by μM FK506. The results suggest some sort of interaction between bastadin and FKBP. SR pre-treated with bastadin 5 does not induce release of the FKBP to the supernatant unlike FK506. These results are

consistent with the hypothesis that bastadins modulate RyR1 function by interaction with FKBP12.0 and that dissociation of the immunophilin by FK506 removes the bastadin effector site. The above results were performed skeletal muscle RyR1. The effects were also observed in cerebellar microsomes enriched in RyR1 but the effects were less efficacious. Bastadin 5 was also less effective than caffeine towards the cardiac isoform RyR2. The isoform selectivity would suggest that FKBP12.0 is the target of bastadin 5 not FKBP12.6. What the bastadins are binding to in cardiac SR vesicles to affect RyR2 function remains unknown. It could be FKBP12.0 bound to RyR2 albeit to a much lower extent. Bastadin 5 markedly slows channel gating without changing the steady state channel open probability and stabilises the high affinity full conductance state of the RyR without causing a physical dissociation of FKBP12.0. This product could be mimicking an in vivo process within muscle cells. Another bastadin of importance in relation to FKBP is bastadin 10 [223]. This structure also interacts with FKBP12.0 and without physical dissociation alters the gating of RyR1. However the modulation of gating of RyR1 is different to that of bastadin 5. This natural product stabilises the open conformation of the channel and sensitises the channel to activation by Ca^{2+} to such an extent that it essentially eliminates regulation of the channel in the physiological range of Ca^{2+} . Bastadin 5 in comparison stabilises both open and closed channel states but has no effect on the Ca^{2+} sensitivity of the channel to activation by Ca^{2+} . Both products however alleviate the inhibition Mg^{2+} . Whereas changes in RyR1 gating caused by bastadin 5 were thought to be due to a decrease in negative co-operativity, Bastadin 10 is thought to decrease the free energy

associated with the open conformation of the channel. Again bastadins rely on binding to FKBP12.0 since RyR modulation by bastadin 10 was selectively eliminated by pre-treatment of channels with FK506 or rapamycin and was reconstituted by human recombinant FKBP12.0. The effects of bastadin 10 were importantly noted as being reversible and prevented run down of RyR1 channels in lipid bi-layers allowing them to open for periods of 20-30min.

The isolation of these products raises important issues regarding the possibility that there are indeed endogenous molecules within the cell that have the potential to activate the mechanisms illustrated above. The structure of the different bastadins also emphasises the point that subtle changes of structure can have major effects on modification of RyR1 gating behaviour.

5.11 Ivermectin and Midecamycin

It has been suggested that FK506 can have a direct effect on RyR [224]. This was observed when exposing FK506 to RyR channels with the subsequent production of sub-conductance levels, which were unrelated to the release of FKBP. It has also been shown that rapamycin can directly activate RyR1 without the need for FKBP12.0 [225;226]. Since rapamycin has a macrocyclic lactone structure, studies have looked at compounds with a similar structure to see if the same channel altering effects exist. Ahern *et al* (1999) investigated two such drugs [227]. The first was ivermectin, which is in wide spread use in veterinary medicine as an anthelmintic. The drug is derived from *Streptomyces avermitilis* and is a

member of the avermectin class of macrocyclic lactones. The second drug looked at in the study was midecamycin, which is an antibiotic. Using bi-layer studies of single RyR1 from native TC vesicles, Ahern *et al* (1999) established that ivermectin reversibly activates RyR1 without affecting single channel conductance. The open probability, mean open time and frequency of openings all increased. (In comparison Bastadin 5 does increase channel open time but not the open probability and structurally lacks a lactone group). These observations were also apparent in FKBP12 stripped channels, which had originally showed long openings to a submaximal, level with brief openings to higher conductance. The sub-conductance states were converted to maximum conductance levels reversibly. The ability of ivermectin to convert sub-conductance to full conductance is in comparison to FK506 and rapamycin which increase channel opening to sub-conductance states. Midecamycin showed similar effects to ivermectin on RyR1 isolated channels however a higher concentration was required than that of ivermectin. The results also observed that that removal of FKBP12.0 was not needed for the action of the two drugs. It was confirmed by western blotting that neither compound could dissociate FKBP12.0 from RyR. In comparison with bastadin studies presented above it was noted (unpublished result) that ivermectin did not act synergistically with rapamycin in promoting removal of FKBP12.0 from RyR1 unlike bastadin 5 and FK506. Using Ca^{2+} uptake studies it was established that ivermectin caused a concentration dependent decrease in rate of Ca^{2+} uptake in both the absence and presence of ruthenium red suggesting an increase leak from RyR1 and reduced rate of uptake by SERCA2a. Interestingly it was found that ethanol alone reduced SERCA2a

mediated Ca^{2+} uptake and DSMO increased SERCA2a mediated Ca^{2+} uptake, however ivermectin in either of these vehicles substantially reduced Ca^{2+} uptake. Midecamycin had minimal effects on SR Ca^{2+} uptake. Using thapsigargin to negate the effects of SERCA2a and assess RyR1 mediated Ca^{2+} release ivermectin was shown to enhance Ca^{2+} release via RyR1. Midecamycin however had no effect. Ivermectin added after 5mM MgCl_2 (used to ensure enough retention of Ca^{2+} within SR vesicles) increased Ca^{2+} release overcoming the block of RyR1 by 0.9mM free Mg^+ . Furthermore caffeine-activated Ca^{2+} release was greater with ivermectin than in control. The sensitivity of RyR1 to caffeine was enhanced. No such effect was seen with Midecamycin. Using skinned rat extensor *digitorum longus* fibres ivermectin was shown to reduce Ca^{2+} loading and increase caffeine-induced contraction. Midecamycin had no such effect. Again the emphasis here is on subtle structural changes that have the ability to alter channel gating. It is proposed in this study that rapamycin, ivermectin and midecamycin all bind to RyR1 at the same site.

Hyperthermia is an interesting toxicity of ivermectin that has been reported in a dog [228]. This is reminiscent of a similar process that occurs in humans and pigs called malignant hyperthermia (MH). The syndrome is characterised by muscle rigidity, hyperthermia, dyspnoea, arrhythmias, and death. It is thought to be the result of a single Arg to Cys mutation on RyR1. An autosomal recessive gene determines susceptibility. The metabolic consequences are due to a reduced sensitivity to inactivation by Mg^+ and Ca^{2+} and have the following sequence of events: (1) leak of Ca^{2+} into the myoplasm from the SR, (2) muscle contraction and hyper-

metabolism due to uncontrolled and sustained increase in myoplasmic Ca^{2+} , (3) ATP depletion, (4) increased aerobic and anaerobic metabolism resulting in excessive carbon dioxide and lactic acid production, (5) thermogenesis and peripheral vasoconstriction, (myoplasmic enzymes and electrolytes are released from the cell and more Ca^{2+} enters the myoplasm, (6) rhabdomyolysis, (7) contraction proceeding independently of myoplasmic Ca^{2+} levels. (8), death due to an increased potassium concentration, arrhythmias, and sudden cardiac death. The triggering event can be volatile anaesthetics, depolarizing muscle relaxants, exertional/environmental stress hence the alternative name of porcine stress syndrome (PSS). It is possible that the above macrocyclic lactones discussed in this section act in a similar way on RyR1 with an end result similar to that seen in this syndrome.

Overall, as predicted by Kaftan *et al* (1996) it is highly probable that associations between FKBP and other trans-membrane signalling molecules will be discovered [197].

5.12 Unresolved issues

5.12.1 What is the function of FKBP12.0 in cardiomyocytes

Although this question is not experimentally investigated within this thesis, a brief summary of current work on this subject is presented below.

Cardiac RyR2 is associated with FKBP in human, rabbits, rats, mice, dogs, chickens, frogs and fish [229]. As discussed earlier, dog heart only binds FKBP12.6 other species bind both FKBP12.6 and FKBP12.0. The stoichiometry of FKBP to RyR2 is thought to be four for both FKBP12.0 and

12.6 (except the dog). FKBP12.0 has a seven fold weaker affinity for RyR2 in the above selection of species whereas in the dog it is more likely to be 500 fold and hence binding is virtually negligible. This relatively large myoplasmic pool of FKBP12.0, which is thought to be 3 μ M, suggests a function within cardiomyocytes. This of course could be completely unrelated to EC-coupling. Immunophilins may have multiple sub-cellular locations in addition to the cytosol and it could be these locations that are regulated by the cytoplasmic pool by FKBP12.0. FKBP12.0 could be affecting many different binding sites for instance transforming growth factor has been reported to be associated with FKBP and may have an important role [230].

One investigation involving FKBP12.0 knock out mice [221] may provide an important clue as to a possible role for FKBP12.0 in the heart. Even though FKBP12.0 was knocked out, it was cardiac changes that were most apparent and not changes in skeletal muscle morphology. Therefore is FKBP12.0 required for cardiac development?

A study has however found that RyR2 channels obtained from FKBP12.6 knockout mice have shown no abnormalities when incorporated into SR vesicles [231]. This result is similar to reports using canine cardiac SR where removal and restoration of FKBP12.6 did not modulate RyR2 channel activity [195]. Since FKBP12.0 is present in the mice and can bind to RyR2, it could be that FKBP12.0 substitutes for the lack of FKBP12.6. However this hypothesis would be harder to reconcile in the dog where the affinity for FKBP12.0 for RyR2 is negligible.

Two studies presented in this thesis aim to investigate previously unresolved issues associated with FKBP function.

5.12.2 What is the role of FKBP12.6 in EC-coupling?

The controversy involving the role of FKBP12.6 in CICR has been reviewed above. The study presented here (see section 5.13) utilises the technique of FKBP12.6 over-expression in cultured cardiomyocytes in order to study the role FKBP12.6 plays in the formation of the Ca^{2+} transients, Ca^{2+} sparks, and waves. The study suggests that FKBP12.6 has a major effect on the size and frequency of Ca^{2+} sparks which is in line with the implication that FKBP12.6 is essential for coupling of RyR2 channels within a cluster and therefore termination Ca^{2+} sparks. Enhanced coupled gating is also suggested as a possible mechanism allowing for the enhanced synchronous Ca^{2+} release seen in cells over-expressing FKBP12.6. This finding was independent of SR Ca^{2+} content. This study shows that over-expression of FKBP12.6 reduces SR Ca^{2+} leak by reducing the size of Ca^{2+} sparks and results in an increased SR Ca^{2+} load. Thus over-expression of FKBP12.6 could be a therapeutic option for the treatment of heart failure in cases where the SR Ca^{2+} content has diminished due to enhanced RyR2 mediated leak. This function is usually the role of positive inotropic agents such as digoxin. However, as with such drugs, toxicity can occur. The SR can become overfilled with Ca^{2+} and Ca^{2+} waves occur. The production of Ca^{2+} waves, which are potentially arrhythmic, could be a fatal disadvantage to this novel therapeutic approach.

5.12.3 Is calcineurin activity required for modulation of RyR by FKBP

This question is discussed in chapter 6.

5.13 Over-expression of FK506-binding protein FKBP12.6 increases the synchronicity of SR Ca²⁺ release in adult rabbit cardiomyocytes.

5.13.1 METHODS

5.13.2 Single ventricular cardiomyocyte isolation from the rabbit heart

Single cell isolation from the rabbit was performed as in section 2.1.

5.13.3 FK binding protein 12.6 over-expression within rabbit cardiomyocytes

Recombinant adenoviruses were generated by standard procedures using full-length cDNA of the human FKBP12.6 gene [204]. Adenoviral infection with a multiplicity of infection (MOI) of 100 was performed to produce two populations of adenovirus transfected cardiomyocytes (i) over-expressing FKBP12.6 (Ad -FKBP12.6) and (ii) expressing β -galactosidase as control (Ad-LacZ). Infected cardiomyocytes were washed and subsequently cultured in supplemented M199 medium (Sigma) for 48hrs. Verification of transgene expression and virus transfection efficiency has been detailed elsewhere [204]. Previous measurements suggest that the level of FKBP12.6 over-expression was approximately 6 times normal values.

5.13.4 Measurement of intracellular Ca²⁺ within intact cardiomyocytes

Aileen Rankin of the University of Glasgow performed these experiments. Cells were incubated with 1 μ M Fura2-AM for 10 min at 37°C, after which Fura-2AM was removed and the cells incubated for a further 15 min. Cardiomyocytes were allowed to settle on a coverslip, placed on a custom-made microscope stage and super-fused with a modified Krebs-Buffer with

the following composition (mM): 140 NaCl, 4 KCl, 1 MgCl₂, 5 HEPES, 11.1 Glucose, 0.3 NaH₂PO₄·2H₂O, and 1.8 CaCl₂ at 37°C. Cells were stimulated at 1Hz with 2ms duration voltage pulses delivered through parallel platinum wires (stimulation voltage was set to 1.5 times the threshold). The Fura-2 fluorescence was measured at 180Hz using a spinning wheel spectrophotometer (Cairn Research Ltd UK). After 60-90s stimulation at 1Hz, SR Ca²⁺ load was estimated by rapidly switching the super-fusing solution to one containing 20mM caffeine for 8s. After a 15s wash to remove caffeine, electrical stimulation was restarted. This protocol was repeated several times on an individual cell. Fura-2 fluorescence measurements were converted to [Ca²⁺] using a calibration protocol previously outlined [168].

5.13.5 Simultaneous field stimulation of intact cardiomyocytes with confocal imaging

Intact cardiomyocytes were perfused with a modified Krebs solution (20-21°C) and field stimulated at 0.5Hz. The exact timing of electrical stimulation was marked in the confocal image by activating a light-emitting diode mounted above the cell bath for 2ms (i.e. the duration of one line-scan) 8ms before electrical stimulation.

5.13.6 Ca²⁺ spark and wave measurements in permeabilised cardiomyocytes

Intact cardiomyocytes were allowed to settle onto the cover-slip at the base of a small bath and subsequently superfused with a mock intracellular solution with the following composition (mM): 100 KCl, 5 Na₂ATP, 10 Na₂Creatine Phosphate, 5.5 MgCl₂, 25 HEPES, 0.05 K₂EGTA, 0.01 Fluo-3

free acid (Molecular Probes), pH 7.0 (20-21°C). The $[Ca^{2+}]$ in the solution was varied by the addition of known amounts of 1M $CaCl_2$ stock solution (BDH). Perfusion was terminated and β -escin $0.1\text{mg}\cdot\text{ml}^{-1}$ (Sigma) added to the cell suspension. When cardiomyocytes were permeabilised (ascertained by confocal imaging, 0.5-1min) the β -escin was immediately removed by re-perfusion of the bath. Confocal line-scan images were then recorded using a BioRad Radiance 2000 confocal system [88]. The $[Ca^{2+}]$ in the solution used to generate Ca^{2+} sparks was measured by ensuring the line-scan covered a significant region of extracellular space as well as the entire cell length. Under these conditions the fluorescence signal recorded from the line-scan contains signals from both intracellular and extracellular compartments. To enable this trace to be converted to $[Ca^{2+}]$ a series of calibration solutions were used at the end of each period of spark measurement. The cardiomyocyte was superfused sequentially with the following solutions: (i) a solution containing nominally $\sim 400\text{nM}$ Ca^{2+} ; (ii) a solution containing $<1\text{nM}$ Ca^{2+} ; (iii) a solution containing $33\mu\text{M}$ Ca^{2+} (all calibration solutions contained 10mM total [EGTA]). Since in the steady state, extracellular $[Ca^{2+}]$ will equal intracellular $[Ca^{2+}]$ in the permeabilised cell, the $[Ca^{2+}]$ in the experimental solution can be calculated (using an apparent affinity constant of Fluo-3 for Ca^{2+} of 558nM [88]). In all experiments included in the analysis, the $[Ca^{2+}]$ in the test solution was $145\text{-}165\text{nM}$. Ca^{2+} sparks were quantified using an automatic detection and measurement algorithm adapted from a previously published method [115]. All Ca^{2+} spark measurements were made within 2min of cell permeabilisation; this time was standardised to minimise loss of soluble proteins. Previous work on isolated SR vesicles indicates that FKBP loss

after vigorous homogenization procedures is minimal [195].

5.13.7 Statistics

Data was expressed as means \pm SEM. Comparisons were performed by using the paired students' *t*-test, and differences were considered significant when $P < 0.05$.

5.14 RESULTS

5.14.1 Measurement of Ca^{2+} transients in intact ventricular cardiomyocytes using Fura-2

Figure 5.1A shows changes in intracellular $[\text{Ca}^{2+}]$ measured in field stimulated (1Hz) cardiomyocytes (36-37°C) after transfection with (i) the control virus Ad-LacZ or (ii) Ad-FKBP12.6. Peak systolic $[\text{Ca}^{2+}]$ was higher in cardiomyocytes over-expressing Ad-FKBP12.6 compared to the control (Ad-LacZ). After 60s of continuous stimulation, SR Ca^{2+} load was assessed by rapid application of 20mM caffeine for 8 seconds. As shown in Figure 5.1A the caffeine-induced Ca^{2+} transient was larger in cardiomyocytes over-expressing Ad-FKBP12.6 compared to the control virus Ad-LacZ. The averaged data (Figure 5.1B) confirms that both the amplitude of the Ca^{2+} -transient and caffeine-induced release are significantly higher in FKBP12.6 over-expressing cardiomyocytes. Diastolic $[\text{Ca}^{2+}]$ was not significantly different between the two groups (Ad-FKBP12.6: $220 \pm 55 \text{ nM}$, $n=25$ vs. Ad-LacZ: $250 \pm 61 \text{ nM}$, $n=25$). Mean Ca^{2+} transient amplitude and associated caffeine-induced Ca^{2+} release amplitude for each cell from both experimental groups, are plotted in Figure 5.1B to illustrate the approximately linear correlation between these two parameters in the both experimental groups. The least-squares best fit to the control group (Ad-LacZ) is shown to indicate the relative position of the Ad-FKBP12.6 data. Consequently, cardiomyocytes with comparable amplitudes of caffeine-induced Ca^{2+} release, if anything, may generate larger Ca^{2+} transients when transfected with Ad-FKBP12.6. Since caffeine-induced Ca^{2+} release is an indication of SR Ca^{2+} content, this result implies

more effective coupling of SR Ca^{2+} release in the Ad-FKBP12.6 group.

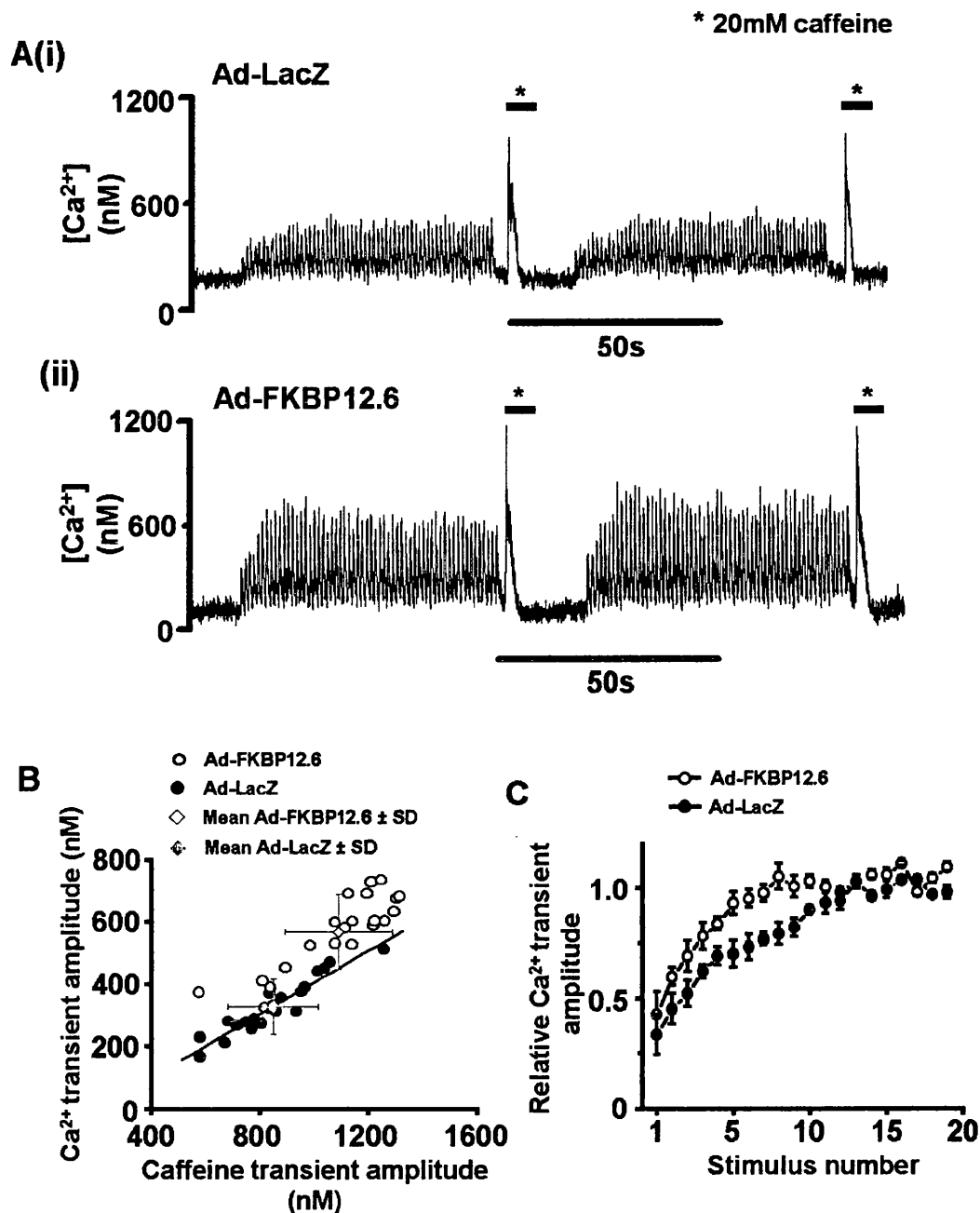


Figure 5.1 Ca^{2+} transients and caffeine-induced Ca^{2+} release

A, Intracellular $[\text{Ca}^{2+}]$ signals recorded 48hrs after transfection with (i) Ad-LacZ (ii) Ad-FKBP12.6 B, A plot of caffeine-transient amplitude vs. Ca^{2+} transient amplitude for individual cardiomyocytes from both Ad-LacZ (closed circles) and Ad-FKBP12.6 (open circles) groups. Mean values (\pm SD) for both groups are shown by grey diamond symbols. C, Time course of recovery of Ca^{2+} transient after a rest period, Ca^{2+} transients normalised to amplitude achieved in steady state values are expressed as mean \pm SEM, n=20 in each

group. (open circles, Ad-FKBP12.6; closed circles, Ad-LacZ).

After a 15s wash to remove caffeine, electrical stimulation was restarted and the time-course of the restoration of the Ca^{2+} transient noted. As shown in Figure 5.1C, a more rapid recovery of systolic $[\text{Ca}^{2+}]$ was observed in FKBP12.6 transfected cells compared to Ad-LacZ cells. The average time to reach 50% of the steady-state Ca^{2+} transient amplitude was $5.6 \pm 0.7\text{s}$ in Ad-LacZ compared with $3.14 \pm 0.5\text{s}$ with Ad-FKBP12.6 ($P < 0.05$, $n = 15$ cells in each group).

5.14.2 Line-scan imaging of Ca^{2+} transients in cardiomyocytes

Intact cardiomyocytes were loaded with Fluo-3 and subsequently field stimulated at 0.5Hz (20-21°C). Fluo-3 fluorescence was monitored with line-scan confocal imaging; the scan line was arranged parallel to the long axis of the cardiomyocyte. Figure 5.2A shows the average cellular fluorescence and the corresponding line-scan image from cardiomyocytes transfected with the control virus Ad-LacZ (Figure 5.2A(i)), and Ad-FKBP12.6 (Figure 5.2A(ii)). The average of 6 sequential Ca^{2+} transients from each cardiomyocyte was used to assess the kinetics of the transient. As shown in Figure 5.2B, the mean peak (F/F_0) of the averaged transient was significantly greater in the Ad-FKBP12.6 group by ~125%. The rate of rise ($\Delta F/F_0 \cdot \text{s}^{-1}$) of the Ca^{2+} transient at a standard Ca^{2+} ($F/F_0 = 1.4$, ~300nM) is greater by ~190% in the cardiomyocytes over-expressing FKBP12.6 than control cells (Figure 5.2C). In contrast, there is no significant difference in the rate of decline of $[\text{Ca}^{2+}]$ in the two groups.

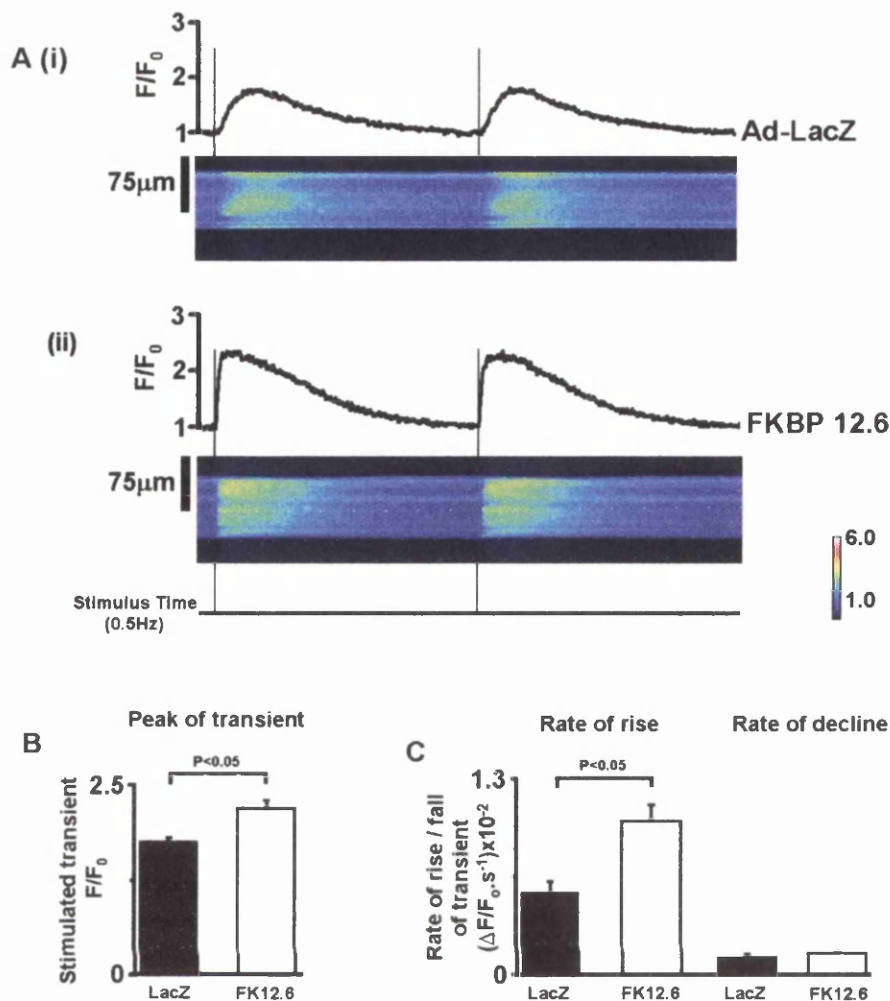


Figure 5.2 Imaging of Ca²⁺ transients

A, Confocal line-scan images of Ca²⁺-transients recorded from (i) Ad-LacZ infected and (ii) Ad-FKBP12.6 infected cardiomyocytes stimulated at 0.5Hz at 20-21°C. B, Mean (\pm SEM) Ca²⁺ transient peak (F/F₀ values) in the two experimental groups (n=9 cells in each group). C, Mean rate of rise and rate of decline of the Ca²⁺-transient at a set [Ca²⁺] (F/F₀=1.4).

5.14.3 Quantitative assessment of the degree of synchrony of Ca²⁺ release during stimulated Ca²⁺ transients using confocal line-scan imaging.

On examining the confocal images in Figure 5.2A, the cardiomyocytes over-expressing FKBP12.6 appeared to have a more uniform release

pattern compared to Ad-LacZ transfected cardiomyocytes. Some sites along the length of the Ad-LacZ cardiomyocyte did not respond to stimulation, others sites responded after a delay. This observation was quantified in the following manner: (1) the central intracellular area was divided into 12 x 20 voxel bands as illustrated in Figure 5.3A(ii); (2) the average fluorescence within each 20 voxel band was plotted as 12 individual Ca^{2+} transients (an example of 3 transients are shown in Figure 5.3B); (3) the time from stimulation to 50% of the peak of each transient (Time_{50}) was calculated for each of the 12 bands (see Figure 5.3B); (iv) this measurement was performed on 6 serial steady-state Ca^{2+} -transients from each cardiomyocyte. The range of Time_{50} values measured in a number of cardiomyocytes from the two experimental groups was displayed as histograms (Figure 5.3C) for: (i) Ad-LacZ cells; (ii) Ad-FKBP12.6; (iii) and freshly dissociated cardiomyocytes (FD), i.e. cells used within 3-4 hrs of animal sacrifice. Only the values for Time_{50} less than 0.5s are shown, values greater than 0.5s are considered 'missed-fires' and quantified separately. The distribution of Time_{50} values for the cells infected with FKBP12.6 had a much narrower profile than the control Ad-LacZ cells. As indicated in Figure 5.3D, the corresponding number of miss-fires was lower in FKBP12.6 infected cells (2.73%) than Ad-LacZ cells (7.5%). In comparison, cardiomyocytes that were freshly dissociated (FD), showed the lowest values of mean Time_{50} , range of Time_{50} and percentage of miss-fires (1.43%) of all 3 groups (Figure 5.3D).

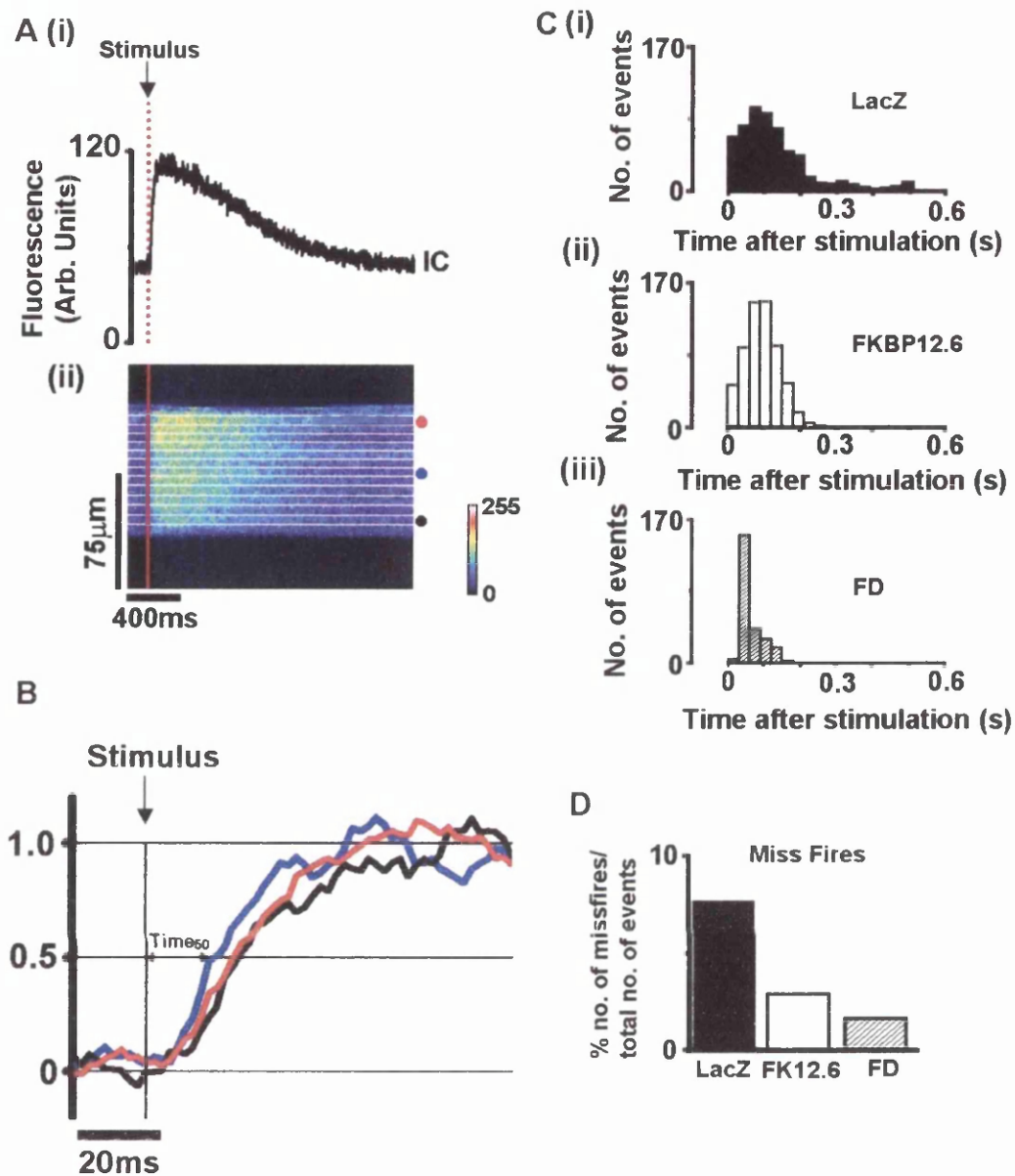


Figure 5.3 Measurement of Ca^{2+} transient synchrony

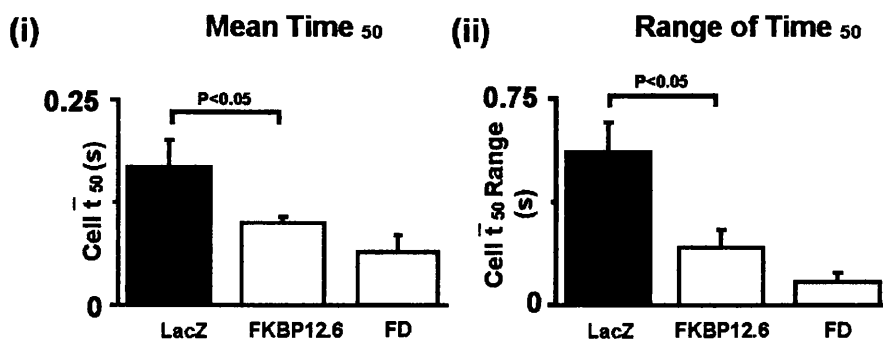
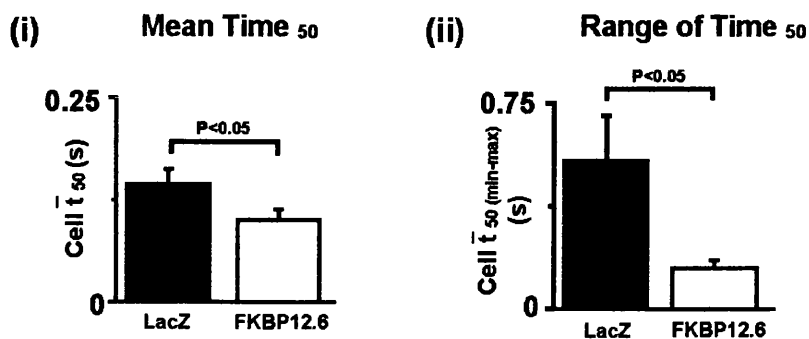
A(i) mean cellular fluorescence from a confocal line-scan image of a Ca^{2+} transient recorded from a cultured cardiomyocyte after transfection with Ad-FKBP12.6. A(ii) confocal line-scan image was split into 12x20 voxel sections as indicated in the pseudo-colour image. The mean fluorescence signal in each 20-voxel section was used to measure the time from stimulus to 50% of the transient amplitude (Time_{50}). An example of 3 selected regions indicated by blue, red and black circles in Panel A(ii) is shown as 3 separate transients (blue red and black lines correspond to sections shown in Fig. 5.3A(ii)). C, Distribution histograms of Time_{50} values measured from Ad-LacZ group ($n=9$ cells), Ad-FKBP12.6 group ($n=9$ cells) and freshly dissociated cells ($n=4$ cells). D, % of sites not

generating a Ca^{2+} transient ($\text{Time}_{50} > 0.5 \text{ s}$) in the three experimental groups.

Figure 5.4A summarises this data in terms of: (i) mean Time_{50} and (ii) mean range (of Time_{50}) values. FKBP12.6 over-expression significantly reduced both the mean (by 40%) and range of values (by 62%) towards the values measured in freshly dissociated (FD) cardiomyocytes (mean Time_{50} of the FD group is 61% lower than Ad-LacZ, the range of Time_{50} values is 84% lower than the Ad-LacZ group). Subsets of the data were constructed on the basis of Ca^{2+} -transient amplitude; the 4 largest Ca^{2+} transients in the Ad-LacZ group were compared with the 4 smallest Ca^{2+} transients in the Ad-FKBP12.6. The mean Ca^{2+} transient peak in these two sub-groups was not significantly different ($F/F_0 = 1.95 \pm 0.06$ vs. 1.93 ± 0.06 , Ad-LacZ vs. Ad-FKBP12.6), yet as shown in Figure 5.4B, the mean Time_{50} and range of Time_{50} values were still significantly lower in the Ad-FKBP12.6 group (mean Time_{50} is 31% lower than Ad-LacZ, the range of Time_{50} values is 73% lower than the Ad-LacZ group). This data suggests that in addition to increased Ca^{2+} transient amplitude, FKBP12.6 over-expression causes a more rapid and synchronous increase of intracellular Ca^{2+} .

5.14.4 Measurements in permeabilised cardiomyocytes

The above results suggest that FKBP12.6 modulates Ca^{2+} release from cardiac SR. The release of Ca^{2+} from the SR is via clusters of RyR2 units. The activity of individual RyR2 clusters generates localised Ca^{2+} release events termed Ca^{2+} sparks. The frequency, amplitude and time course of Ca^{2+} sparks determines the spontaneous Ca^{2+} leak from the SR.

A Complete Data Set (LacZ vs FKBP12.6 n=9)**B Overlapping Data Sub-set (n=4)****Figure 5.4 Mean and range of Time₅₀ values**

A, Mean Time₅₀ and mean range of Time₅₀ values for Ad-LacZ (n=9 cells), Ad-FKBP12.6 (n=9 cells) and freshly dissociated cardiomyocytes (FD, n=4 cells). B(i) Mean Time₅₀ and (ii) mean range of Time₅₀ values for a sub-set of the Ad-LacZ and FKBP12.6 groups with similar Ca²⁺-transient amplitudes.

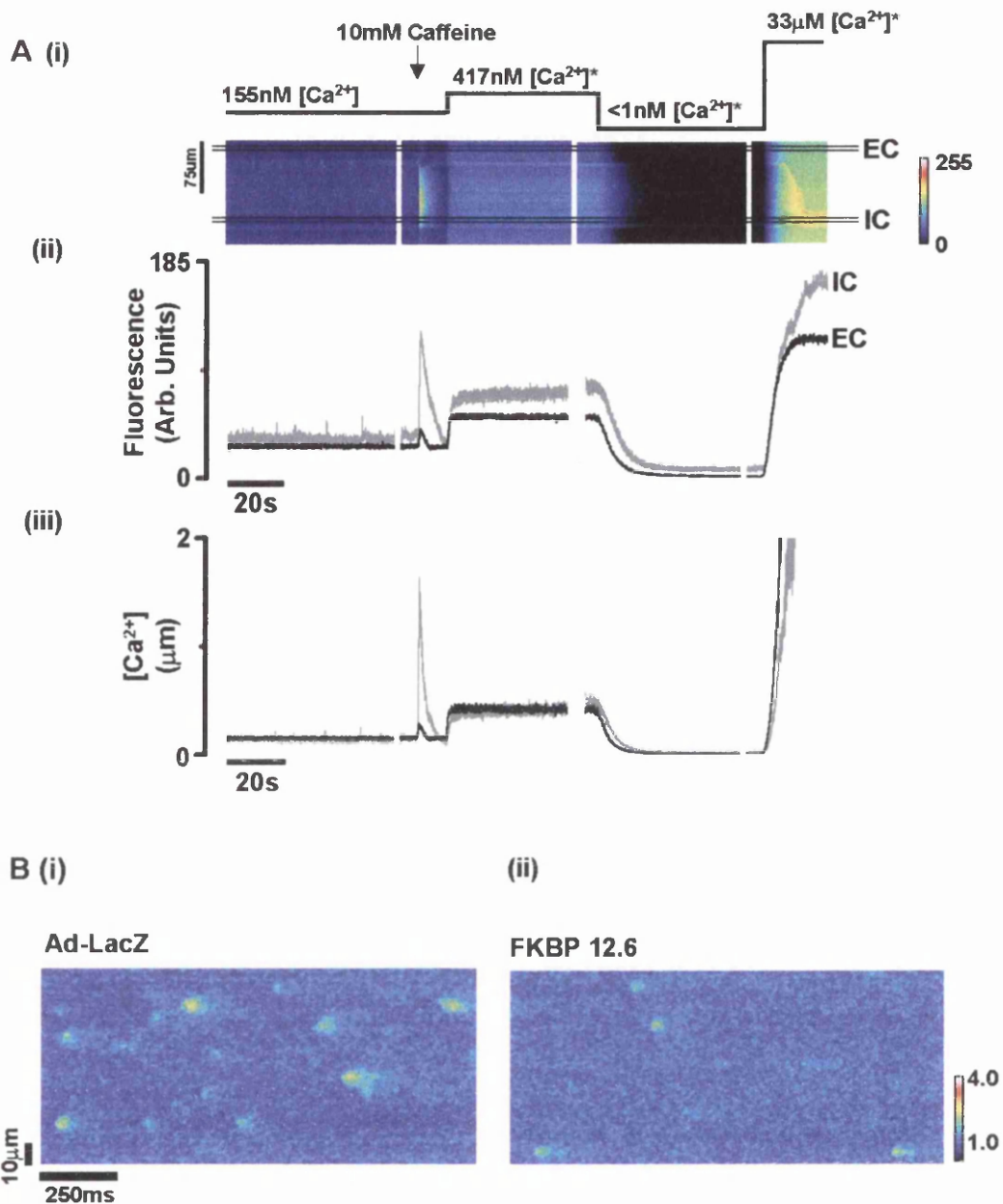


Figure 5.5 Ca^{2+} sparks and caffeine induced Ca^{2+} release in permeabilised cardiomyocytes

A(i) Sequential fluorescence confocal line-scan images (512x30000 pixels) from a single permeabilised cardiomyocyte exposed to experimental and calibration solutions. The cardiomyocytes brighter central region is due to a higher Fluo-3 fluorescence within the cell; dimmer flanking signals are from the Fluo-3 in the perfusing solutions. The calculated $[\text{Ca}^{2+}]$ in the perfusion solution is shown above the images, experimental solutions contained a total [EGTA] of 50 μM and 10 μM Fluo-3. $[\text{Ca}^{2+}]$ marked by * indicates solutions containing a total [EGTA] of 10mM. The arrow indicates addition of 10mM caffeine. As

indicated in A(i), two regions (20 voxels wide) of a series of line-scans were averaged and displayed as fluorescence signals (A(ii)) from the extracellular (EC - black line) and intracellular (IC - grey line). A(iii), $[Ca^{2+}]$ calculated from the mean fluorescence signal of a 20-voxel region from the intracellular (IC, grey trace, Fig. A(ii)) and extracellular compartments (EC, black trace, Fig. A(ii)). The $[Ca^{2+}]$ was calculated on the basis of the fluorescence signals in 417nM, <1nM Ca^{2+} and 30 μ M (buffered with 10mM total EGTA). B. pseudo-colour line-scan epi-fluorescence image of Ca^{2+} sparks within single permeabilised cardiomyocytes perfused with the experimental solution containing 155nM Ca^{2+} (i) Ad-LacZ infected cell and (ii) Ad-FKBP12.6 infected cell.

An investigation of the direct effects of FKBP12.6 over-expression on Ca^{2+} sparks in intact rabbit cardiomyocytes is complicated by the rapid sarcolemmal extrusion of intracellular Ca^{2+} and loss of SR Ca^{2+} during quiescent periods required for Ca^{2+} spark recording. For this reason, sarcolemmal fluxes were functionally by-passed by the permeabilisation of the sarcolemma with β -escin. Under these circumstances, single cardiomyocytes can be superfused with a standardised $[Ca^{2+}]$ and pH in the presence of ATP and CrP. Ca^{2+} spark activity was monitored by the inclusion of 10 μ M Fluo-3 in the perfusing solution. Figure 5.5A(i) shows the protocol used to measure Ca^{2+} sparks and assess SR Ca^{2+} content in permeabilised cells.

The cardiomyocyte was perfused with nominally 150nM $[Ca^{2+}]$ (0.05mM EGTA) for at least 1min prior to confocal measurements to ensure a steady state SR Ca^{2+} content. Ca^{2+} sparks were recorded for one minute and SR load was assessed by the rapid application of 10mM caffeine. To enable a more precise measurement of the $[Ca^{2+}]$ in the cytosol of the permeabilised cell, a series of calibration solutions were used, these consisted of: a reference $[Ca^{2+}]$ solution (~400nM free $[Ca^{2+}]$, 10mM EGTA); a low $[Ca^{2+}]$

solution ($<1\text{nM}$ $[\text{Ca}^{2+}]$, 10mM EGTA) to enable a recording of minimal fluorescence (F_{min}); a high $[\text{Ca}^{2+}]$ solution ($33\mu\text{M}$ $[\text{Ca}^{2+}]$, 10mM CaEGTA) to enable the recording of the maximum fluorescence (F_{max}). Although the reference $[\text{Ca}^{2+}]$ solution of $\sim 400\text{nM}$ did not cause any noticeable change in cell shortening, the F_{max} solution caused the cell to develop a gradual irreversible hyper-contraction. The recordings of fluorescence from the external solution (Figure 5.5A (ii)) allowed the calculation of the $[\text{Ca}^{2+}]$ in the reference solution (417nM). Subsequently, the intracellular fluorescence measured in the reference solution and in the low Ca^{2+} solution ($<1\text{nmol/L}$ Ca^{2+}) allowed the conversion of intracellular fluorescence in the experimental solutions to a $[\text{Ca}^{2+}]$ signal (Figure 5.5A (iii)). This established the $[\text{Ca}^{2+}]$ in the weakly buffered experimental solution (in Figure 5.5 this was 155nM). In these experiments, the integral of caffeine-induced Ca^{2+} release was used to assess the SR Ca^{2+} content.

5.14.5 Ca^{2+} sparks and caffeine-induced Ca^{2+} release in permeabilised cardiomyocytes overexpressing FKBP12.6

To quantify Ca^{2+} spark activity (Figure 5.5B (i) and (ii)) the first 15s of each line-scan image was analysed using an automated spark detection program adapted from a previously published method for use in permeabilised cardiomyocytes [115].

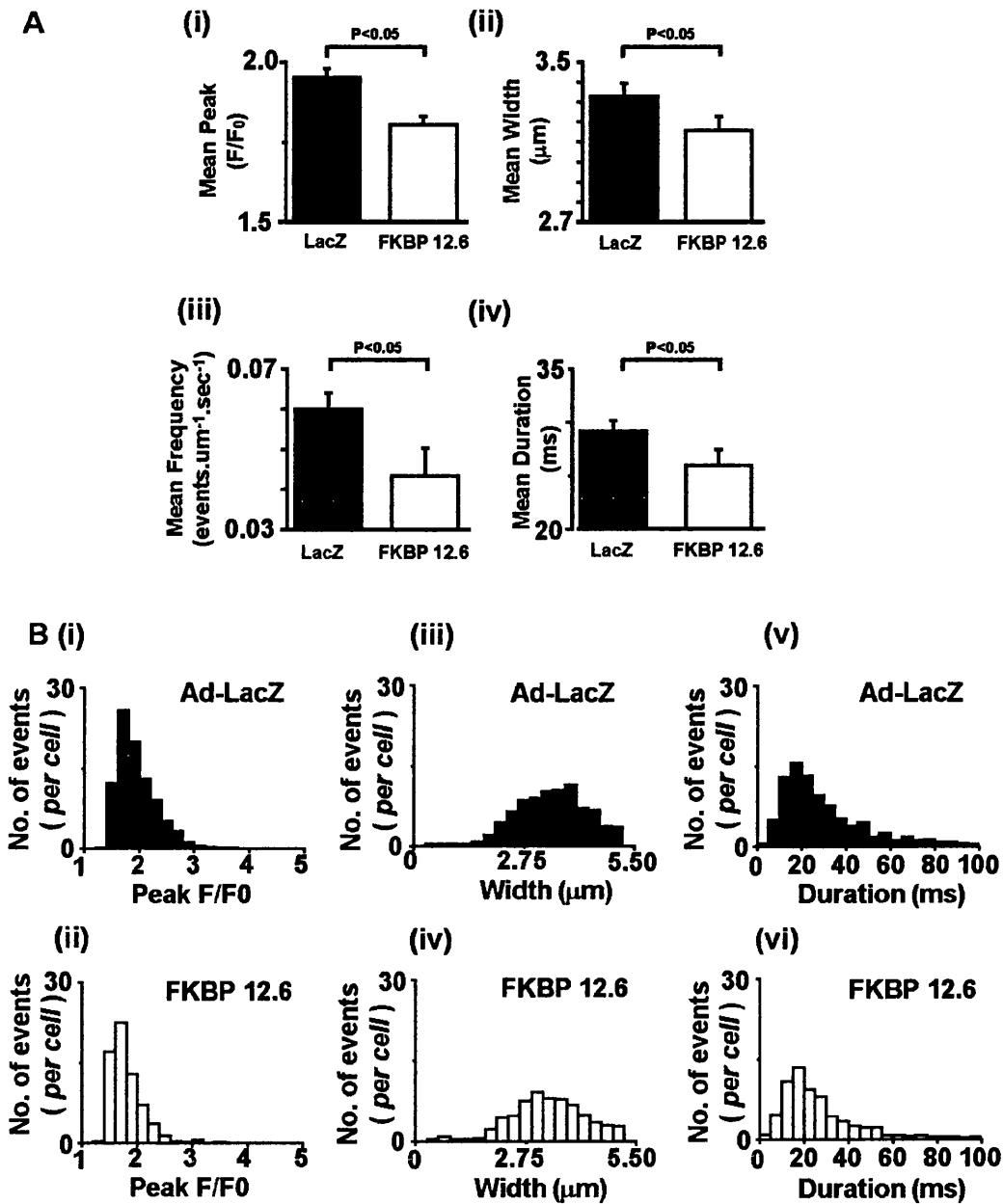


Figure 5.6 Mean Ca^{2+} spark characteristics

Mean \pm SEM values for: (i) peak F/F_0 ; (ii) spark width (full width half maximal) (iii) spark frequency; (iv) spark duration (full duration half maximal). 5B Distribution histograms for spark amplitude (i & ii), width (iii & iv) and duration (v & vi) measured in LacZ and FKBP12.6 transfected cardiomyocytes at 145-165nM $[\text{Ca}^{2+}]$. Distributions based on: 1631 sparks detected in 18 Ad-LacZ transfected cardiomyocytes and 587 sparks detected in 9 Ad-FKBP12.6 transfected cardiomyocytes.

The results collated from a number of cardiomyocytes are shown in Figure

5.6. It can be seen from this summary that the peak, width, duration and frequency of the Ca^{2+} sparks are all significantly less in cardiomyocytes over-expressing FKBP12.6 (n=9 cells) compared to Ad-LacZ (n=18 cells); Ca^{2+} spark peak F/Fo (1.80 ± 0.03 vs. 1.96 ± 0.02), width ($3.15 \pm 0.07 \mu\text{m}$ vs. $3.33 \pm 0.07 \mu\text{m}$); duration ($26.09 \pm 1.5\text{ms}$ vs. $29.21 \pm 1.0\text{ms}$) and frequency ($0.04 \pm 0.007 \text{events} \cdot \mu\text{m}^{-1} \cdot \text{s}^{-1}$ vs. $0.06 \pm 0.004 \text{events} \cdot \mu\text{m}^{-1} \cdot \text{s}^{-1}$). The spark peak, duration and width distribution histograms show no difference in the shape of the distribution between the two experimental groups (Figure 5.6B), indicating that a sub-population of Ca^{2+} sparking events could not be detected.

5.14.6 Effects of higher $[\text{Ca}^{2+}]$ on permeabilised cardiomyocytes overexpressing FKBP12.6

Perfusing with a weakly buffered solution containing $\sim 400\text{nM}$ Ca^{2+} has previously been shown to cause spontaneous Ca^{2+} release and propagated Ca^{2+} waves in freshly dissociated permeabilised cardiomyocytes [88]. Figure 5.7A and 5.7B shows mean signals from a 20-voxel intracellular (IC) and extracellular (EC) region of a permeabilised cardiomyocyte infected with Ad-LacZ. This protocol did not induce Ca^{2+} waves; instead, Ca^{2+} release consists of high frequency, smaller amplitude events that did not propagate significant distances (see Figure 5.7B(iii)).

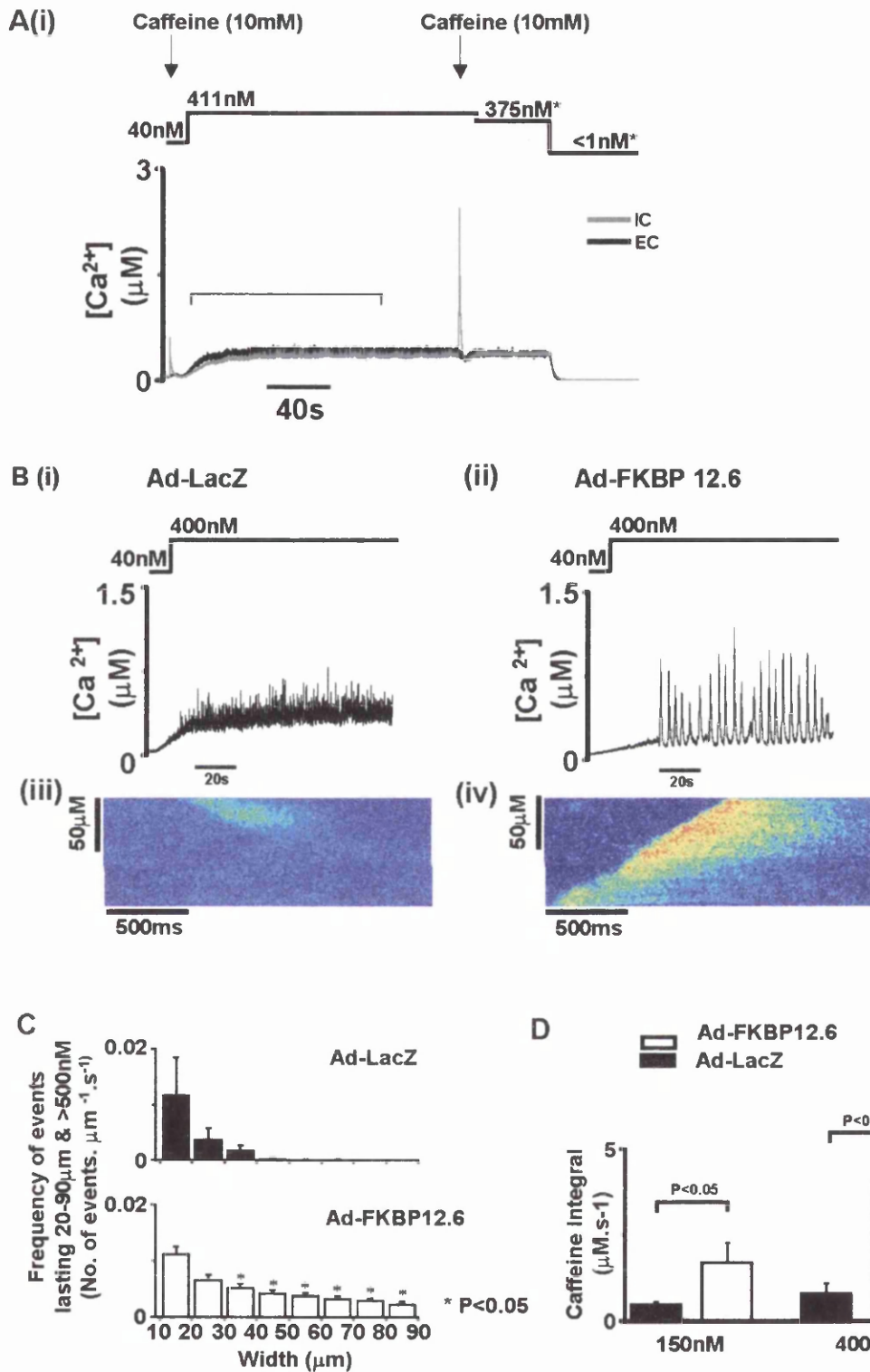


Figure 5.7 Ca^{2+} wave characteristics

A Protocol used to measure Ca^{2+} wave characteristics, signal based on a 20-voxel intracellular signal Ca^{2+} signal (IC, grey trace) and extracellular Ca^{2+} signal (EC, black trace). The solution changes are indicated above the record, addition of caffeine at points indicated. B(i) & (ii), examples of Ca^{2+} waves recorded in 20 voxel regions of

permeabilised cardiomyocytes perfused with solutions containing $\sim 400\text{nM}$ $[\text{Ca}^{2+}]$. B(iii) & B(iv) line-scan images of Ca^{2+} release events recorded in permeabilised cardiomyocytes from Ad-LacZ and Ad-FKBP12.6 groups. C, distribution histograms of the width of Ca^{2+} release events $>500\text{nM}$ $[\text{Ca}^{2+}]$ recorded from Ad-LacZ ($n = 4$ cells) and Ad-FKBP12.6 groups ($n = 6$ cells). D, Mean integrals of the caffeine induced Ca^{2+} release in permeabilised cardiomyocytes equilibrated in 150nM and 400nM $[\text{Ca}^{2+}]$.

However, as illustrated in Figure 5.7B(ii) & (iv), the same protocol in Ad-FKBP12.6 transfected cardiomyocytes causes the development of coherent Ca^{2+} waves that frequently propagate along the entire length of the cardiomyocyte. To quantify the distances propagated by Ca^{2+} release events, the line-scan images were thresholded to display Ca^{2+} release events over 500nM , and the width of release events were measured in each cell. This was performed using IDL as follows:

- (1) The experimental image file (A) (400nM $[\text{Ca}^{2+}]$, 0.05mM EGTA) containing the Ca^{2+} events is obtained, measured and median filtered (512×30000 pixels).
- (2) The experimental calibration file (B) (400nM $[\text{Ca}^{2+}]$ 10mM EGTA) is obtained measured and median filtered (9×9 box) (512×30000 pixels).
- (3) A third image file is created (C) by taking the first 30000 pixel strip in image (B) (of which there are 512) and averaging the fluorescence from these 30000 pixels. The mean fluorescence is then outputted as one averaged number for that pixel strip. This is then repeated for each of the remaining 512 pixel strips.
- (4) Image (A) is divided by image (C) to give image (D). This gives a fluorescence signal which is divided by the signal in the 400nM calibrating solution.
- (5) Image (D) is multiplied by a scaling factor of 50 .

(6) Assuming a K_d of 558nM a 'cut-off' fluorescence value, which represents 500nM, is calculated. This is used to threshold events $>500\text{nM}$.

(7) 32 pixel regions ($10\mu\text{m}$) are then averaged across each of the 30000 x 512 rows. If the mean value of this 32 pixel region is greater than the 'cut-off' then this is given a value of 1 in a new binary image (E). If the mean value of this 32 pixel region is $<$ than the 'cut-off' the value is given a value of 0. The data from this analysis is presented therefore as rows of 32 pixel regions that are either black (0) or white (1) in a binary image (E).

(8) Individual 32 pixel white bands are termed single events of $10\mu\text{m}$. If however if a single event touches another event either side of it or below it than this is counted as a single event, the width of which is denoted by how many individual $10\mu\text{m}$ bands are beside each other within one event.

The distribution histogram of the duration of release events is shown in Figure 5.7C. It is clear from this graph that there were very few release events that propagated further than $40\mu\text{m}$ in Ad-LacZ transfected cardiomyocytes, while a significant number of events propagated up to $100\mu\text{m}$ in the Ad-FKBP transfection group. Correspondingly fewer events of duration $<10\mu\text{m}$ occurred in the FKBP12.6 over-expressing cardiomyocytes compared to the control group (results not shown). Finally, the average of the integral of the Ca^{2+} signal induced by 10mM caffeine is shown in Figure 5.7D for the two bathing $[\text{Ca}^{2+}]$ used in this study, i.e. $\sim 150\text{nM}$ and $\sim 400\text{nM}$. Under both conditions (150nM and 400nM) the caffeine-induced Ca^{2+} release was 3-4 fold larger in the Ad-FKBP12.6 group.

5.15 DISCUSSION

This study examines the effects of over-expression of FKBP12.6 in cardiomyocytes cultured for 48 hours. Data from Fura-2 loaded cardiomyocytes indicated that FKBP12.6 over-expression increased the amplitude of the Ca^{2+} transient and SR Ca^{2+} content.

The term E-C coupling 'efficiency' is used within this study instead of the term 'gain' since the latter term requires an assessment of L-type Ca^{2+} current, SR Ca^{2+} release and SR Ca^{2+} content within the same cell. These types of electrophysiological experiments have not been performed here, however SR Ca^{2+} release and Ca^{2+} content have been assessed within this study while L-type Ca^{2+} current has been found to be similar between Ad-LacZ and Ad-FKBP12.6 cell types (results not shown) and so the looser term 'efficiency' compared to 'gain' is used below. Previous reports have indicated increased E-C coupling efficiency on *removal* of FKBP12.6 [114]. On the basis of these previous studies, over-expression of FKBP12.6 (as within this present study) should decrease E-C coupling efficiency. However the results in Figure 5.1 show that E-C coupling efficiency was, if anything increased. This discrepancy may reflect the complex relationship between different levels of FKBP12.6 occupancy and E-C coupling efficiency as indicated by a recent study [215]. This suggests that removal of a limited amount of FKBP12.6 will increase RyR2 activity and enhance E-C coupling gain. More complete removal of FKBP12.6 from the RyR2 cluster will cause uncoupling of RyR2 units within a cluster, and the development of sub-conductance states in individual RyR2 units. These

changes will have two consequences: (i) reduced effectiveness of L-type Ca^{2+} channel to initiate SR Ca^{2+} release and (ii) increased 'leak' of Ca^{2+} from the SR during diastole leading to a reduction in SR Ca^{2+} content consistent with previously published data [63;215]. The results of the present study suggest that cultured cardiomyocytes from the rabbit have a low FKBP12.6/RyR2 interaction since FKBP12.6 over-expression increased E-C coupling efficiency and decreased diastolic Ca^{2+} leak. In support of this, SR Ca^{2+} leak from rabbit cardiomyocytes cultured for 48hrs did not respond to FK506 sequestering agents, but sensitivity to rapamycin was restored by FKBP12.6 over-expression [204]. A more rapid recovery of Ca^{2+} transients after SR depletion by caffeine in FKBP12.6 over-expressing cardiomyocytes (Figure 5.1C) is consistent with reduced RyR2 mediated Ca^{2+} leak during diastole as suggested by earlier studies [204;211;232]. In summary, these results suggest that the enhanced Ca^{2+} transient after FKBP12.6 over-expression is a consequence two effects: (i) decreased SR Ca^{2+} leak from the SR allowing a higher SR content to be achieved during diastole and (ii) an additionally enhanced efficiency of the SR Ca^{2+} release mechanism, possibly as a result of increased coupled gating of RyR2 by FKBP12.6. This hypothesis may appear to be difficult to reconcile with a recent study in FKBP12.6 knockout mice [216]. In this case, absence of FKBP12.6 was associated with larger Ca^{2+} transients in mice cardiomyocytes. Previous work has shown that mouse RyR2 has significant affinity for FKBP12.0 [229]. Therefore, as suggested in the latter study, FKBP12.0 may substitute for FKBP12.6 with in mice heart cells, thus reducing the apparent effects due to the absence FKBP12.6.

5.15.1 Effects of FKBP12.6 over-expression on synchronicity of E-C coupling.

As shown in Figure 5.2, marked asynchrony of Ca^{2+} release was evident in cardiomyocytes transfected with the control virus Ad-LacZ. Similar asynchrony was observed in cardiomyocytes cultured for the same period of time (48hrs) without virus infection (results not shown). In cardiomyocytes over-expressing FKBP12.6, larger Ca^{2+} transients were accompanied by more synchronous Ca^{2+} release. The higher degree of synchrony is consistent with the more rapid rate of rise of the Ca^{2+} transient (Figure 5.2B). The similar rate of Ca^{2+} transient decay suggests that SR Ca^{2+} ATPase and $\text{Na}^+/\text{Ca}^{2+}$ exchanger activity are not dramatically different in the two experimental groups. This supports the direct measurements of SERCA2a activity measured previously [204]. Recent experiments measuring L-type Ca^{2+} channel amplitude found no effect of Ad-FKBP12.6 over-expression (Stewart Miller, University of Glasgow - results not published). These results show that E-C coupling efficiency is increased by FKBP12.6 over-expression. However, in determining the mechanism it is difficult to distinguish between two options: (i) an increased synchrony as a result of a higher SR Ca^{2+} content or (ii) a direct effect on the coupling L-type Ca^{2+} channel activity and SR Ca^{2+} release. Evidence for the latter comes from comparing Ca^{2+} transients of similar amplitudes in the different groups. In this sub-set, the Ad-FKBP12.6 group still retained lower mean Time_{50} and range of Time_{50} values. This latter result indicates that enhanced SR Ca^{2+} content alone cannot account for the increased synchrony of release and supports the hypothesis that E-C coupling efficiency is enhanced after FKBP12.6 over-expression.

5.15.2 Effects of FKBP12.6 over-expression of Ca²⁺ sparks in permeabilised cardiomyocytes.

Measurement of Ca²⁺ spark activity in the steady state is problematic in intact rabbit cardiomyocytes because intracellular [Ca²⁺] and SR Ca²⁺ content rapidly decreases on cessation of stimulation due to net sarcolemmal efflux. Furthermore, Ca²⁺ spark parameters are very sensitive to intracellular [Ca²⁺] [64;121], therefore interpretation of results is difficult without knowledge and/or control of the intracellular [Ca²⁺] in cells from different experimental groups. For these reasons, Ca²⁺ spark activity was monitored in permeabilised cardiomyocytes at a precisely measured bathing [Ca²⁺]. Previous work has established that Ca²⁺ spark characteristics (amplitude, time course and frequency) in permeabilised cells are indistinguishable from those observed in intact cells [64] and regulated by known modulators of RyR2 activity (Ca-calmodulin and cyclic-ADPribose) [64] but with the added advantage that cytoplasmic conditions can be standardised. As shown in Figure 5.3, Ca²⁺ sparks occurred less frequently and were smaller in amplitude, width and duration in FKBP12.6 over-expressing cardiomyocytes. These results are generally consistent with previous measurements of Ca²⁺ sparks on removal of FKBP12.6, since increases in Ca²⁺ spark frequency [114] amplitude [216], width and duration [113;216] were noted. These reports plus others on isolated RyR2 channels suggest that association of FKBP12.6 with RyR2 would shorten the averaged duration of a Ca²⁺ spark by decreasing the channel open-time [113] and enhancing the degree of coupled gating [63]. Mathematical modeling of the RyR2 cluster indicates that coupled gating is important in terminating Ca²⁺ release [48]. This work predicts that Ca²⁺ spark duration

would decrease on increasing the degree of coupling between RyR2 units in a cluster. Furthermore, the effect of FKBP12.6 on spark frequency is anticipated from studies on isolated RyR2 channels where FKBP12.6 decreased the open probability [63]. The overall effects of FKBP12.6 over-expression on Ca^{2+} spark activity is consistent with the reduction of diastolic SR Ca^{2+} leak indicated by the more rapid restoration of the steady state Ca^{2+} transient amplitude after a rest (Figure 5.1B). The direct effects of FKBP12.6 over-expression on RyR2 activity described above could not have been easily observed in intact rabbit cardiomyocytes since the SR Ca^{2+} content rapidly decreases on cessation of stimulation. Therefore the data on Ca^{2+} sparks from permeabilised cardiomyocytes should be regarded as verification that FKBP12.6 over-expression affects RyR2 activity analogous to studies of Ca^{2+} leak from the SR [204;212], or isolated RyR2 activity in a bi-layer [207].

Previous work has suggested that occupancy of RyR2 with FKBP12.6 is close to maximal (4FKBP12.6:1RyR2 tetramer) under basal conditions [207]. Thus, over-expression of FKBP12.6 would not be expected to boost FKBP12.6:RyR2 stoichiometry significantly. However, two lines of evidence suggest that FKBP12.6 binding to RyR2 is considerably lower than normal in 2-day culture cardiomyocytes: (i) previous work indicates that rapamycin has no effect on RyR2-mediated Ca^{2+} leak in 2 day cultured cardiomyocytes, but rapamycin sensitivity is regained after FKBP12.6 over-expression [204]; (ii) Ca^{2+} spark characteristics after 2 days in culture are significantly different from those observed in freshly dissociated cardiomyocytes. Ca^{2+} sparks measured in freshly dissociated

cardiomyocytes (n=20 cells) were smaller in amplitude ($F/F_0=1.72\pm 0.02$), narrower in width ($2.90\pm 0.03 \mu\text{m}$), shorter in duration ($24.1\pm 0.97 \text{ ms}$) compared to LacZ transfected cardiomyocytes. Therefore a possible explanation of the results is that 2-day cultured cardiomyocytes have a lower than normal FKBP12.6:RyR2 stoichiometry which dramatically increases diastolic Ca^{2+} leak. Over-expression of FKBP12.6 in these cells returns the FKBP12.6:RyR2 stoichiometry towards normal, reducing diastolic SR Ca^{2+} leak, increasing SR Ca^{2+} content and thereby increasing Ca^{2+} transient amplitude. The increased FKBP12.6 stoichiometry also increased the degree of coupled gating between RyR2 units in a cluster thereby increasing the efficiency of E-C coupling independent of SR Ca^{2+} content.

5.15.3 Effects of FKBP12.6 over-expression on spontaneous SR Ca^{2+} release.

Previous work has shown that increasing cytosolic $[\text{Ca}^{2+}]$ above 200nM in permeabilised cardiomyocytes initiates spontaneous SR Ca^{2+} release and propagated Ca^{2+} waves similar to that observed in Ca^{2+} -overloaded intact cardiomyocytes [64;88]. However, as shown in Figure 5.7, spontaneous Ca^{2+} release in permeabilised cardiomyocytes after 2 days of quiescent culture consisted of small amplitude events that propagated only limited distances within the cytosol. In contrast, when cardiomyocytes over-expressing FKBP12.6 were perfused with identical solutions, coherent Ca^{2+} waves that propagated along the majority of the length of the cardiomyocyte occurred in a similar fashion to those observed in freshly dissociated cells. Measurements of caffeine-induced Ca^{2+} release

suggested that SR Ca^{2+} content was ~4 times higher than the Ad-LacZ transfected cardiomyocytes when perfused with 400nM Ca^{2+} . The frequent low-amplitude Ca^{2+} release events observed in Ad-LacZ transfected cardiomyocytes would suggest a large diastolic Ca^{2+} leak and explain the reduced ability of the SR to retain Ca^{2+} . FKBP12.6 over-expression not only reduced the number of release events, allowing the SR Ca^{2+} content to increase to a higher steady state, but also permitted the generation of large amplitude propagating Ca^{2+} waves. The conditions necessary to generate Ca^{2+} waves in cardiomyocytes has been studied extensively and suggests that low amplitude Ca^{2+} release will not generate a sufficiently large cytosolic Ca^{2+} signal at the adjacent release site to allow propagation [121;138;233]. This appears to be the case in the 2-day cultured cardiomyocytes, while the higher SR Ca^{2+} content in FKBP12.6 over-expressing cells supports sufficiently large SR Ca^{2+} release to allow propagation.

5.15.4 SUMMARY

This is the first report to suggest that alterations in RyR2 activity associated with FKBP12.6 binding to RyR2 is necessary for the generation of propagating Ca^{2+} waves in cardiac muscle. This form of SR Ca^{2+} release is thought to be beneficial to the cell under conditions of Ca^{2+} overload since the transient increases of intracellular $[\text{Ca}^{2+}]$ are an efficient method of stimulating Ca^{2+} efflux from the cardiomyocyte while preventing the development of a sustained contraction [69;88;234]. However, spontaneous Ca^{2+} waves also generate potentially arrhythmic depolarising currents and are thought to be a common cause of triggered arrhythmias.

Recent work on myocardium from failing human hearts and animal models of heart failure has shown a reduction in FKBP12.6 binding to RyR2 [207]. This change in stoichiometry (as a result of PKA mediated hyperphosphorylation of RyR2) causes increased diastolic SR Ca^{2+} leak [211] and therefore would reduce twitch amplitude. The results presented in this study support the idea that returning FKBP12.6:RyR2 stoichiometry to normal will restore Ca^{2+} transient amplitude and may be a possible therapeutic approach in heart failure [235]. However, the data also indicates the possible detrimental consequences of this approach. If the mean cytosolic Ca^{2+} is above a crucial level as a result of other pathological changes, increasing FKBP12.6:RyR2 stoichiometry may increase SR Ca^{2+} content and alter RyR2 function in such a way as to increase the amplitude of spontaneous Ca^{2+} release from the SR and consequent arrhythmic depolarising currents.

CHAPTER SIX

**Over-expression of an FKBP12.6 mutant lacking a calcineurin binding
site in rabbit ventricular cardiomyocytes**

6.1 INTRODUCTION

6.1.1 The many roles of calcineurin

Calcineurin is a serine/threonine phosphatase, which is present within the cytoplasm of many cell types [236]. It has a wide range of cellular functions. These include migration of neutrophils [237], hippocampal long term depression [238], gene regulation and cell differentiation [239]. Calcineurin also mediates the effects of insulin like growth factor [240], cardiac hypertrophy [241] and T-cell immuno-suppression [176]. This latter mechanism is of particular relevance here since a link to the FK506 Binding Protein (FKBP) has been well documented. An intracellular rise in $[Ca^{2+}]$ upon stimulation of the T-cell receptor by antigen causes the phosphatase calcineurin to de-phosphorylate the cytoplasmic form of the transcription factor Nuclear Factor of Activated T-cells (NFAT). This causes the NFAT to translocate into the nucleus and initiate transcription of interleukin 2 (IL-2) and T-cell proliferation. However, exogenous application of the drug FK506, binds to FKBP. This complex binds to and inhibits calcineurin. Subsequent T-cell activation is prevented which results in immuno-suppression [175].

6.1.2 The molecular structure of immunophilin ligands

The molecular structures of the common immunophilin ligands are presented in Figure 6.1. FK506, rapamycin and cyclosporin are all immunosuppressive drugs, which bind to immunophilins (see Chapter 5 for discussion). FKBP's bind FK506 and rapamycin, while cyclophilins bind cyclosporin A. It can be seen from Figure 6.1 that while FK506 and

rapamycin share common structural characteristics, the structure of cyclosporin is markedly different. Cyclophilins and FKBP have rotamase activity and their corresponding exogenous ligands inhibit that enzymatic activity. The fourth structure in Figure 6.1 is 506BD. This drug is an unnatural ligand that shares similar structural characteristics to FK506 and rapamycin. However while 506BD inhibits the rotamase activity of FKBP12.0 it does so without preventing T-cell proliferation, suggesting that this enzymatic activity is not involved in immuno-suppression [175;242].

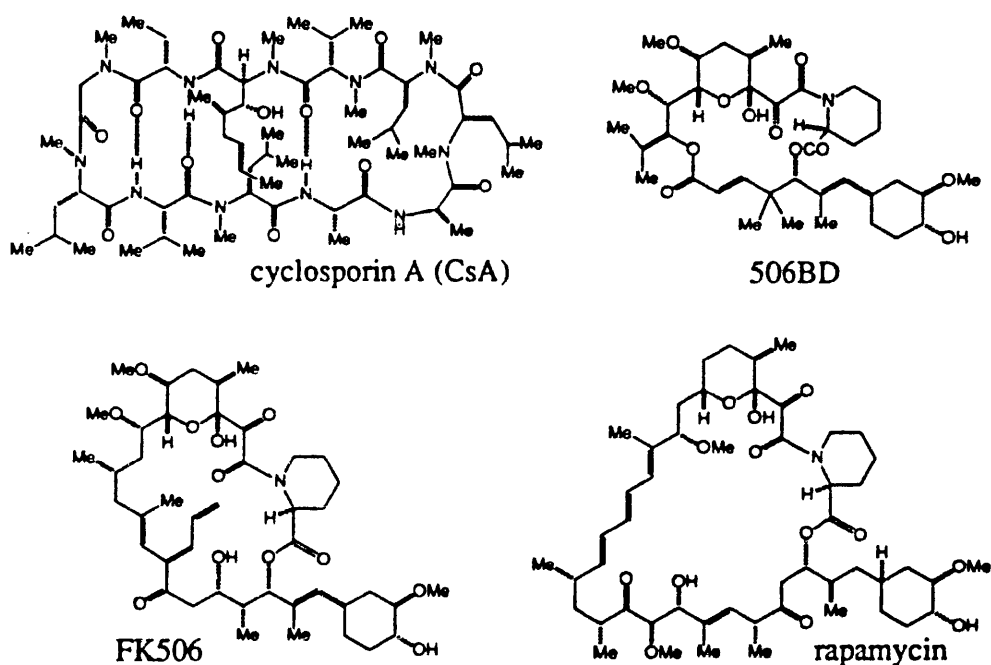


Figure 6.1 Molecular structure of exogenous immunophilin ligands

Refer to text for discussion. (Figure taken from Schreiber, S.L. (1992) *Immunology Today* 13, 136-142).

6.1.3 Complexes formed between FKBP, its ligands and calcineurin.

The molecular structure of the complex formed between FKBP, FK506 and calcineurin has been studied in detail [243]. It is thought that the FKBP12.0

molecule physically blocks the phosphatase active site of calcineurin to potential substrates (e.g. NFAT). Rapamycin is an immunosuppressive drug with similar actions to FK506 (see section 5.2.5). However, if rapamycin complexes with FKBP12.0 and attempts to bind to calcineurin, the larger effective domain of rapamycin (relative to FK506) penetrates into the calcineurin complex. FKBP12.0-Rapamycin cannot therefore inhibit the phosphatase activity of calcineurin.

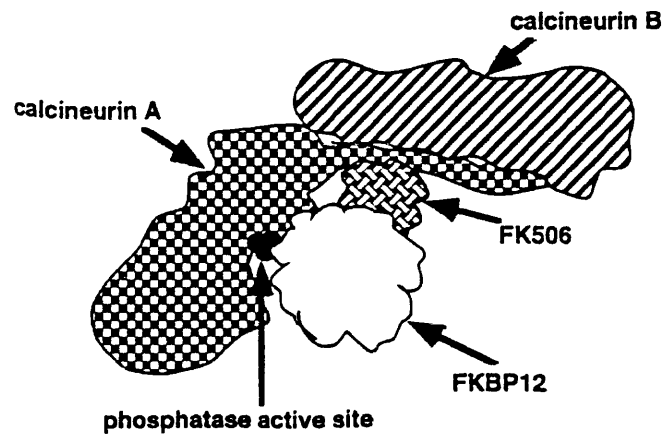


Figure 6.2 The effect of the FKBP-FK506 complex on calcineurin

FKBP12.0 is seen here to block the phosphatase active site when a complex is formed with FK506. Calcineurin is a heterodimeric protein consisting of a catalytic subunit - calcineurin A, and a Ca^{2+} binding subunit - calcineurin B. (Figure taken from Marks, A.R. (1996) *Physiological Reviews* 76, 631-649).

6.1.4 Is calcineurin important in RyR2 activity?

One method that has been used to investigate the function of FKBP on RyR2 involves the application of the drug FK506. This dissociates FKBP from RyR and results in an increase in open probability [180]. It is also known that phosphorylation of RyR2 can result in an increase in open probability [207]. This presents a dilemma, is the increased open probability induced by the FKBP-FK506 complex due to the removal of

FKBP from the RyR or the inhibition of calcineurin phosphatase activity within the cell and subsequent phosphorylation of RyR? To try to resolve this issue, authors have applied rapamycin to RyR2 [197]. Rapamycin dissociates FKBP from RyR2 and forms an FKBP-rapamycin complex. The result is also an increase in open probability of RyR2. However, in this case the increased open probability cannot be due to inhibition of cellular calcineurin phosphatase activity and subsequent phosphorylation of RyR2 since the FKBP-rapamycin complex cannot block the phosphatase active site on calcineurin. Rapamycin therefore can be used to investigate RyR2 open probability when FKBP has been removed without the possible side effects of cellular calcineurin inhibition. Therefore it is generally concluded the calcineurin plays no part in the modulation of RyR gating, and the observed change in RyR open probability can be explained simply by dissociation of FKBP from RyR2 [175].

6.1.5 The range of molecular species resulting from the use of drugs

Various drugs have been applied to the RyR2 complex in order to verify the role of FKBP and calcineurin on RyR2 function. Three such scenarios established by the use of drugs were presented above. The first scenario involves the application of FK506. This results in the dissociation of FKBP from RyR2 and inhibition of cellular calcineurin by the FKBP-FK506 complex within the cytosol. The status of calcineurin is assumed in this scenario to be **unbound** to the RyR2 macro-molecular complex and inhibited, i.e. **not working**. This status of calcineurin (unbound and not working) can also be achieved in a second scenario by the application of CsA and rapamycin since the latter drug dissociates FKBP from RyR2 and

cyclosporin A potently inhibits calcineurin [244] (Table 6.1). Both of these situations result in an increased open probability of RyR2.

Molecular Species	Calcineurin Status	Achieved by which drugs	Effect on RyR2
Scenario 1 + 2	UNBOUND NOT WORKING	FK506 or CsA + Rapamycin	Increased Activity
Scenario 3	UNBOUND WORKING	Rapamycin	Increased Activity
Scenario 4	BOUND WORKING	-	Decreased Activity
Scenario 5	BOUND NOT WORKING	CsA	Increased Activity
Scenario 6	UNBOUND WORKING	FKBP12.6 MUTANT	Decreased Activity

Table 6.1 The use of various drugs to produce different molecular species to investigate the role of calcineurin on RyR2

Refer to text for discussion.

The third scenario of **unbound and working** is achieved by the application of rapamycin alone since rapamycin only dissociates FKBP from RyR2 but cannot inhibit cellular calcineurin. This also results in an increased open probability (Table 6.1). As suggested above, this has been used by authors to suggest that calcineurin inhibition plays no role in RyR2 open probability and it is therefore the unbinding of FKBP that is responsible for the increase in RyR2 activity since when FKBP is bound to RyR2 there is a decrease in the open probability (scenario 4) [175].

6.1.6 What if calcineurin does not just exist within the cytosol but forms part of the RyR2 macromolecular complex?

The above conclusion is based on the principle that calcineurin does not form part of the macromolecular complex of RyR2 (i.e. is **unbound** as in scenario 1-3). But what if calcineurin is **bound** to the RyR2 macromolecular complex and **working**? This fourth scenario would result in

a decrease in the RyR2 open probability. This begs that questions of whether it is now the association of FKBP to RyR2 or the calcineurin phosphatase activity and subsequent decrease in phosphorylation status of RyR2, which leads to the decrease in the open probability?

6.1.7 Is calcineurin ever bound to the RyR2 macromolecular complex?

Whether or not calcineurin is bound to the RyR2 macromolecular complex is a controversial issue. A study performed on human solubilised cardiac protein [207] suggests that calcineurin is not part of the RyR2 complex and results associated with the change in open probability of RyR2 are solely due to FKBP. However recent evidence suggests that this may not be the case in all species. Bandyopadhyay *et al* (2000) has demonstrated that calcineurin is associated with RyR2 via FKBP12.6, which acts as an anchor [245]. These results were demonstrated in solubilised rat cardiac SR proteins. The association between RyR2 and calcineurin is Ca^{2+} dependent such that high concentrations of $[\text{Ca}^{2+}]$ (100 μM) lead to co-immuno-precipitation whereas low $[\text{Ca}^{2+}]$ (20mM EGTA) lead to an absence of calcineurin on RyR2. RyR2 is not the only Ca^{2+} channel that is associated with calcineurin. Cameron *et al* (1995) has demonstrated that calcineurin is anchored to IP_3R via FKBP [246].

6.1.8 So if calcineurin is indirectly bound to the RyR2 macromolecular complex does it play a role in RyR2 open probability?

Suggestions that calcineurin has a role in the heart originate from studies involving the treatment of rats with cyclosporine. This results in alterations to the contractile properties of rat hearts [247;248]. Cyclosporin (CsA) binds to the intracellular CsA binding protein cyclophilin (CyPA) and the

resulting complex inhibits phosphatase activity of calcineurin. It can therefore be used as an immunosuppressive agent. In the rat heart, CsA results in reduced peak systolic pressure, increased sensitivity to external Ca^{2+} and reduced maximal stress development [247]. The chronic application of CsA results in varying Ca^{2+} handling consequences some of which are hard to reconcile with a single function of CsA [249]. Ryanodine-binding studies indicate a reduced maximal RyR binding suggesting a reduced RyR density. This could explain the reduction of contractile properties. The affinity for ryanodine binding to RyR is also decreased in CsA treated rats (increased K_d). That these changes occurred at different times during the treatment period of three weeks indicated that the molecular mechanisms causing the changes in the ryanodine binding studies are different. If CsA inhibits calcineurin (and phosphatase activity) then an increase in RyR2 activity would be expected. This is consistent with the increased caffeine sensitivity and decreased ruthenium red sensitivity observed [249]. However, Ca^{2+} sensitivity in this same study was unaltered. This latter finding is hard to reconcile with the above observations [250]. Calcineurin was also up-regulated during the chronic treatment with cyclosporin which may explain the observations on ryanodine binding alterations but is again hard to reconcile with those regarding the caffeine and ruthenium red sensitivity of RyR2.

6.1.9 Can conclusions be made on the functional role of calcineurin on RyR2 from the above study on the chronic application of cyclosporin?

The above study is extremely hard to draw any definitive conclusions from,

since multiple physiological effects occurred during simultaneous changes in protein expression. However, another study involving 2-day-old neonatal rat hearts also demonstrated a role for calcineurin on RyR2 [245]. The authors demonstrated in non-beating neonatal cells that application of various calcineurin inhibitors 20 μ M deltamethrin, 10 μ M CsA, and 10 μ M FK506 all lead to Ca²⁺ oscillations. 10 μ M rapamycin does not result in Ca²⁺ oscillations as frequently (presumably because rapamycin cannot inhibit calcineurin) but 20 μ M for 30min resulted in oscillations (presumably because at this concentration and time exposure to rapamycin the drug results in dissociation of FKBP from RyR2 and hence calcineurin is no longer able to be anchored to RyR2). Importantly, further addition of CsA or deltamethrin to these pre-incubated cells results in no further action. Therefore this fifth scenario presented in this study suggests therefore that only the calcineurin when **bound and working** inhibits Ca²⁺ release in the neonatal cells but not when unbound or not working (Table 6.1).

6.1.10 Evidence for a role of calcineurin on RyR2 in skeletal muscle

Perhaps the most detailed study associating the function of calcineurin with RyR is data produced in a mouse skeletal muscle cell line (C2C12) [244]. As with the previous results [245] (with RyR2), a Ca²⁺ dependent interaction between RyR1, FKBP12.0 and calcineurin can be demonstrated in these cells. Pre-treatment with CsA caused an increased activity of RyR2 as assessed by the response to caffeine. Two mutant calcineurin isoforms were also used to investigate the functional role of calcineurin on RyR1. A constitutively active form of calcineurin (Δ CnA), results in a decrease in RyR1 activity, which can be partially reversed by CsA. While Δ CnA(H1-

101Q)), an inactive form of calcineurin, results in an increase in RyR1 activity. Using Cain, an endogenous calcineurin inhibitor, confirms this action.

6.1.11 The function of calcineurin on RyR2 within adult ventricular cardiomyocytes

The above studies would predict that when calcineurin is bound to RyR2 via FKBP12.6 it has an inhibitory effect on RyR2. However there is now a dichotomy. Is this decrease in RyR2 activity due to FKBP that is bound to the RyR2 macro-molecular complex or calcineurin, which is also bound, and possibly exerting its phosphatase activity on RyR2? (Figure 6.3). Since as discussed previously cyclosporin is a good method of inhibiting calcineurin, the above studies suggest the bound calcineurin can account for the decrease in RyR2 activity. However this is hard to reconcile with the data presented in the previous chapters on the role of FKBP12.6 on RyR2 in decreasing the open probability of RyR2. One conclusive scenario could help solve this inconsistency within the literature. The final scenario as presented in table 6.1 is to allow binding of FKBP12.6 to RyR2 but without FKBP anchoring calcineurin (Figure 6.3). This chapter describes preliminary results obtained from cultured adult ventricular cardiomyocytes over-expressing an FKBP12.6 mutant, which cannot bind to calcineurin. If FKBP12.6 is the predominant coordinator of RyR2 open probability then this virus should have the same effect as over-expressing FKBP12.6 alone.

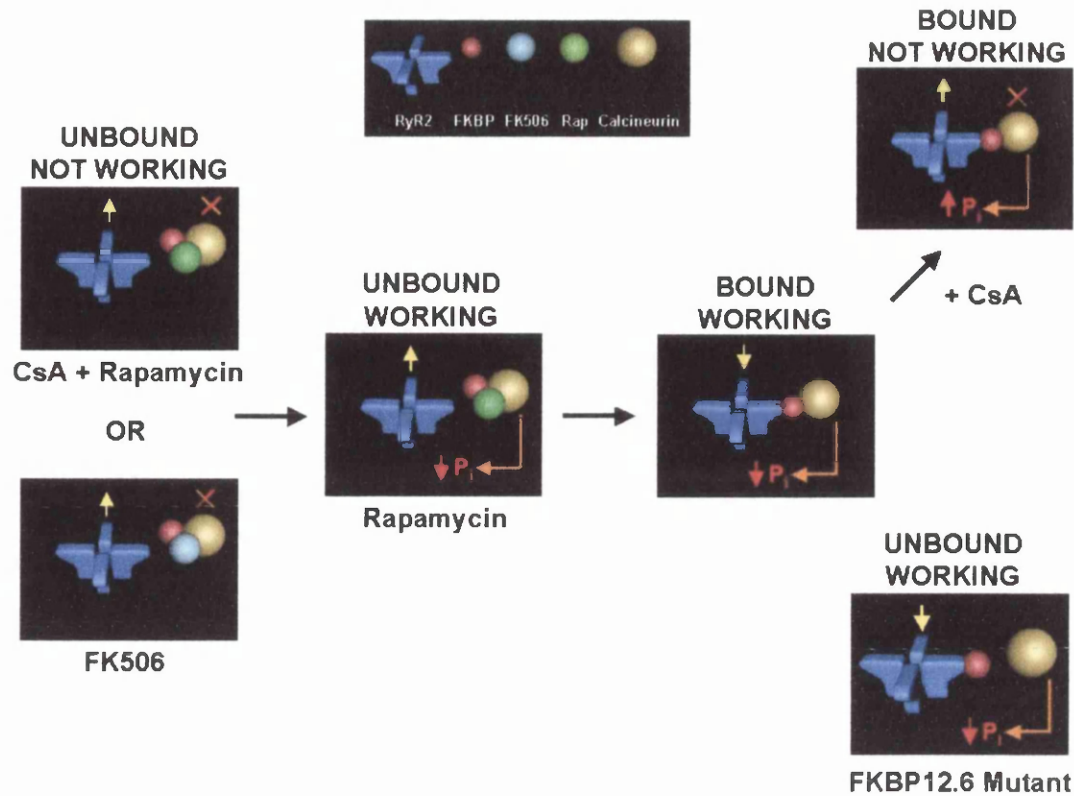


Figure 6.3 Various methods to elucidate the function of FKBP12.6 on RyR2

Refer to text for discussion. X defines that calcineurin is not working. NB. Rapamycin does not inhibit calcineurin and cannot form a complex consisting of FKBP12.6-FK506-rapamycin unlike FK506, which can.

However if calcineurin is important in regulating RyR2, the channel/RyR2 cluster should demonstrate increased activity compared to over-expressing FKBP12.6 alone.

6.1.12 Construction of the FKBP12.6 mutant virus

Although the experimental work on Ca^{2+} sparks was performed personally, the following is a brief account of work performed by Tim Siedler (University of Goettingen) who performed site directed mutagenesis of the calcineurin binding site on the FKBP12.6 DNA sequence. This alteration prevents FKBP12.6 from binding to calcineurin. The mutated sequence was then incorporated into an adenovirus vector and used to transfect rabbit

ventricular cardiomyocytes as in section 2.2.3. While the mutant virus produced - FKBP12.6^{G89P V90K} (Ad-FKBP12.6 mutant) does not bind to calcineurin, its FK-506 affinity and rotamase activity are preserved (results performed by Tim Seidler but not shown). The following is a summary of the methods used to generate the mutant virus. They are included only for reference purposes since the detail of the experiments are outwith the scope of this thesis. With the knowledge that the composite FKBP12.0-FK506 surface can contact calcineurin, mutation of amino acids G89P/V90K in FKBP12.0 has been demonstrated to increase the K_i for calcineurin to greater than 5000nM, while leaving the FK506 affinity similar to wild type levels (FK506 K_i =0.6nM) [251]. This mutation was introduced into FKBP12.6 at the analogous position (G89P V90K) by site directed mutagenesis. Site directed mutagenesis was performed using the human FKBP12.6 mRNA in the vector pACCMV.pLpA. The vector was mutated using the methods of Vandeyar *et al* (1988) using the following primers (included for reference only) [252]:

For: 5' ccacgggccacccccctaagatccctcccaatgcc 3'

Rev: 5' ggcattgggagggatcttaggggggtggcccgtgg 3'

(Where: *a* – adenine, *c* – cytosine, *g* – guanine, and *t* – thymine)

After DpnI digestion, positive clones were confirmed by automatic sequencing and the DNA amplified for co-transfection with pJM17 for virus production as described previously in section 2.2 [96]. Details of the sequence alignment for FKBP12.0, FKBP12.6 and FKBP12.6 mutant are presented in appendix 6.1.

6.2 METHODS

Single ventricular cardiomyocyte isolation from the rabbit heart was performed as described in section 2.1.1. Recombinant adenoviruses were generated by standard procedures using full-length cDNA of the human FKBP12.6 gene [204]. Adenoviral infection with a multiplicity of infection (MOI) of 100 was performed to produce three populations of adenovirus transfected cardiomyocytes (i) over-expressing FKBP12.6 (Ad -FKBP12.6), (ii) expressing β -galactosidase as control (Ad-LacZ) and over-expressing an FKBP12.6 Mutant which over-expresses FKBP12.6 protein which is unable to bind to calcineurin. Infected cardiomyocytes were washed and subsequently cultured in supplemented M199 medium (Sigma) for 48hrs.

6.2.1 Ca^{2+} spark measurements in permeabilised cardiomyocytes

Ca^{2+} spark measurements were then performed on these cells after permeabilisation and perfusion with a free $[\text{Ca}^{2+}]$ of 145-165nM. The $[\text{Ca}^{2+}]$ was calibrated using the same confocal protocol and automated spark detection programs as discussed section 5.14.4.

6.2.2 Statistics

Data was expressed as means \pm SEM. Comparisons were performed by using the paired students' t-test, and differences were considered significant when $P < 0.05$.

6.3 RESULTS

Figure 6.4 A(i-iii) shows confocal line-scan images recorded from permeabilised rabbit cardiomyocytes after transfection with (i) Ad-LacZ, (ii) Ad-FKBP12.6, (iii) Ad-FKBP12.6 Mutant respectively on the same day and conditions. Ca^{2+} sparks were evident as transient increases in fluorescence. Ca^{2+} sparks recorded in FKBP12.6 and FKBP12.6 Mutant transfected cardiomyocytes were smaller and less frequent than the Ad-LacZ control. The data taken from a number of cells is summarised in Figure 6.4 B(i-iv). The average Ca^{2+} spark peak, frequency, width and duration (Figure 6.4B i-iv) were all significantly reduced in cells over-expressing the Ad-FKBP12.6 mutant compared to Ad-LacZ (peak F/Fo, 1.72 ± 0.03 vs. 1.85 ± 0.06 , $P < 0.05$; frequency, $0.045 \pm 0.004 \mu\text{m}^{-1}\text{s}^{-1}$ vs. $0.067 \pm 0.005 \mu\text{m}^{-1}\text{s}^{-1}$, $P < 0.05$; width, $3.03 \pm 0.08 \mu\text{m}$ vs. $3.30 \pm 0.05 \mu\text{m}$, $P < 0.05$; duration, $24.62 \pm 0.9\text{ms}$ vs. $27.30 \pm 0.8\text{ms}$ vs, $P < 0.05$; Ad-FKBP12.6 Mutant (n=12 cells) vs. Ad-LacZ (n=11 cells)). Ca^{2+} spark characteristics from Ad-FKBP12.6 over-expressing cells are also presented: (peak F/Fo, 1.73 ± 0.03 ; frequency, $0.048 \pm 0.006 \mu\text{m}^{-1}\text{s}^{-1}$, width, $3.00 \pm 0.06 \mu\text{m}$, duration, $25.4 \pm 0.6\text{ms}$; Ad-FKBP12.6 n=10 cells). These were similar to spark characteristics within cells over-expressing Ad-FKBP12.6 Mutant.

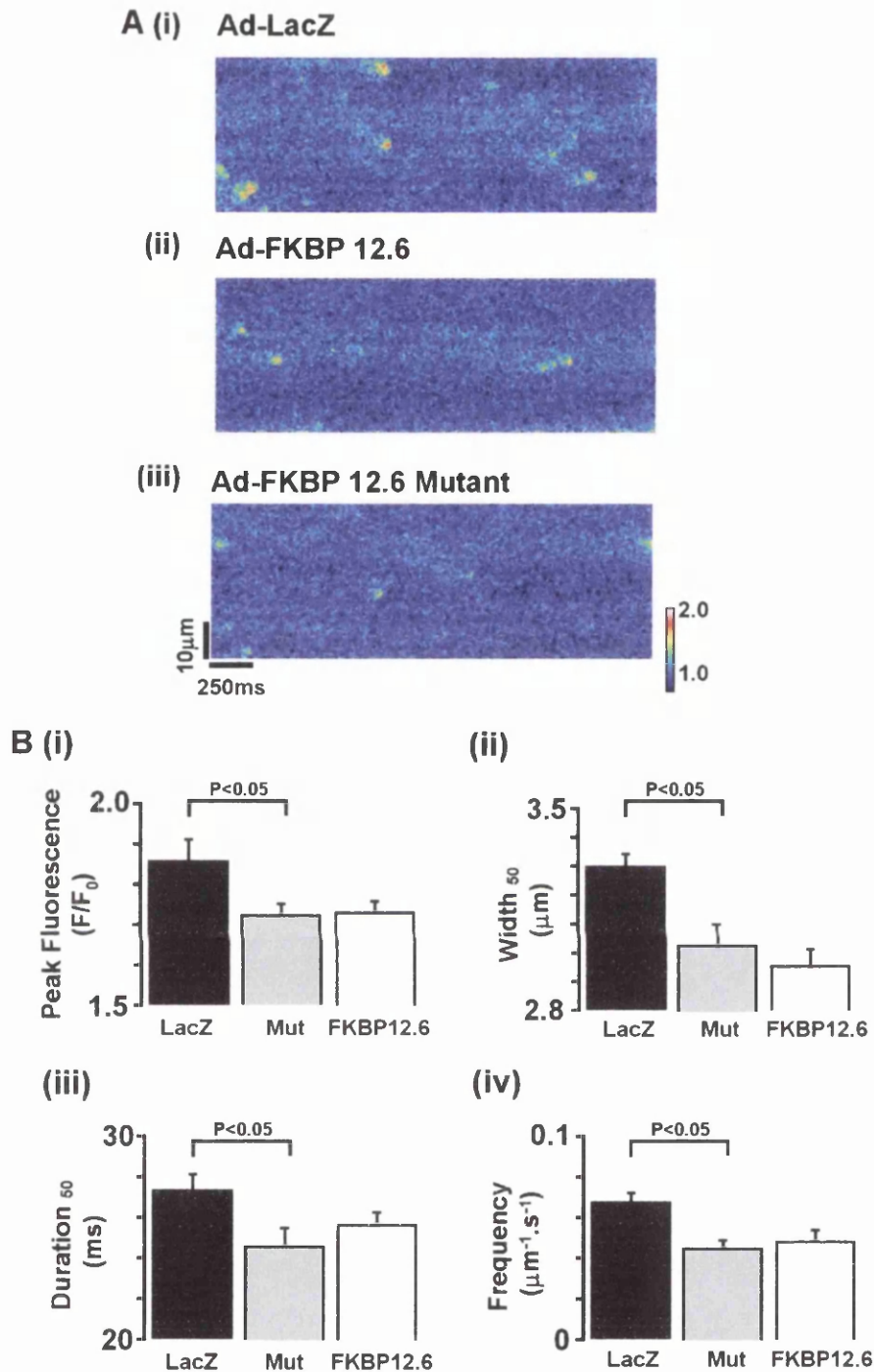


Figure 6.4 Effects of the FKBP12.6 mutant on Ca²⁺ sparks

A, Confocal images of Ca²⁺ sparks within ventricular cardiomyocytes transfected with; (i) Ad-LacZ (n=11), (ii) Ad-FKBP12.6 (n=10) and (iii) Ad-FKBP Mutant (n=12). Summary of mean Ca²⁺ spark data is presented in Panel B, Ca²⁺ spark (i) peak, (ii) width, (iii) duration and (iv) frequency.

6.4 DISCUSSION

Confocal imaging of Ca^{2+} sparks within adult rabbit ventricular cardiomyocytes over-expressing a FKBP12.6 Mutant unable to bind to calcineurin reveals Ca^{2+} sparks, which are similar to Ca^{2+} sparks from cells over-expressing unaltered FKBP12.6. This suggests that a reduction in Ca^{2+} spark size and frequency can be attributed to the over-expression of FKBP12.6 and not the phosphatase action of calcineurin on RyR2. This data verifies conclusions reached by Marks *et al* (1996) that suggest that bound calcineurin does not play a direct role in the reduction of RyR2 activity [175]. In fact the same group fails to find any biochemical evidence for the association between calcineurin and the RyR2 macromolecular complex in adult human cardiomyocytes [207]. This is in contrast to Bandyopadhyay *et al* (2000) who show a Ca^{2+} dependent association between the two proteins in neonatal rat cardiomyocytes [245]. It has been suggested that this inconsistency may be due to the low levels of $[\text{Ca}^{2+}]$ used to study this association by Marks *et al* (2003) in this latter study [245].

6.4.1 Dynamic changes in $[\text{Ca}^{2+}]$

It is understandable that the changes in $[\text{Ca}^{2+}]$ within the ventricular cardiomyocyte are dynamic and do not remain at a resting $[\text{Ca}^{2+}]$ as used in this study. However the $[\text{Ca}^{2+}]$ needed for calcineurin to bind to RyR2 has only been investigated at $100\mu\text{M}$ [245]. While $[\text{Ca}^{2+}]$ within the sarcolemmal cleft is unknown, it is possible that a $[\text{Ca}^{2+}]$ of $100\mu\text{M}$ may be reached however it would not be maintained for any length of time and certainly would not be the mean intracellular $[\text{Ca}^{2+}]$ which only rises to

approximately 1 μ M during a transient. Therefore further investigation is required to identify whether calcineurin can bind to RyR2 at more physiological dynamic ranges of $[Ca^{2+}]$.

6.4.2 Evidence on the effect of calcineurin on RyR2

While the effects of calcineurin on RyR2 in adult rabbit ventricular cardiomyocytes do not seem apparent, this is in marked contrast to the data presented in neonatal rat ventricular cells [245] and skeletal muscle cell lines [244]. It cannot be assumed that these cell types will have the same levels of protein expression and Ca^{2+} dynamics [253]. Bandyopadhyay *et al* (2000) demonstrated that a certain proportion of neonatal rat heart cells were spontaneously oscillating. This suggests that these cells are on the verge or have achieved SR Ca^{2+} overload. It could be that calcineurin within the cytosol or bound to RyR2 plays a predominant role in RyR2 inhibition over FKBP in these cell types. To date no study has demonstrated a direct role of calcineurin on RyR2 in adult ventricular cardiomyocytes. This study was the first to do so and has found no such mechanism.

6.4.3 Specificity of agents use to investigate the action of calcineurin

The use of calcineurin inhibitors to investigate the role of calcineurin on RyR2 has been the main focus of evidence for its possible role. However these drugs do not have 100% specificity for calcineurin. They are known to affect other Ca^{2+} regulatory pathways within cardiomyocytes such as the Na^+/K^+ pump [254]. These may in theory lead indirectly to a rise in SR Ca^{2+} content, which would increase RyR2 activity independent of calcineurin inhibition. The method of adenoviral over-expression used in this study

provides a novel way to investigate the possible role of calcineurin on RyR2 without the need for drug application.

6.4.4 Further work

This study is by no means a completed piece of work and further investigation is required. Firstly an assessment of SR Ca^{2+} content would be helpful to establish if the reduced diastolic SR Ca^{2+} leak leads to an increase in SR Ca^{2+} content as seen when Ad-FKBP12.6 is over-expressed. Secondly although calcineurin may not play a direct role in RyR2 Ca^{2+} release it may have a function on other Ca^{2+} regulatory processes that can only be assessed within the intact ventricular cardiomyocytes. Hence valuable investigation could be obtained by electrophysiological measurements on intact cells, especially regarding SR Ca^{2+} load and Ca^{2+} transients. It would also be important to clarify the levels of over-expression encountered within FKBP12.6 and FKBP12.6 mutant cells. Finally since the binding of calcineurin to FKBP12.6 may be Ca^{2+} dependent it will be important to establish the degree of binding in the physiological $[\text{Ca}^{2+}]$ found within ventricular cardiomyocytes. This could be extended to compare the effects of Ad-FKPB12.0/FKBP12.6 mutant virus on Ca^{2+} transients and waves.

CONCLUSIONS

The general aim was to study the role of FKBP12.6 in regulating sarcoplasmic reticulum (SR) Ca^{2+} release in permeabilised cardiomyocytes.

Initial work concerned the characteristics of spontaneous Ca^{2+} release from permeabilised cells. In particular, the aim was to discover the relationship between intracellular $[\text{Ca}^{2+}]$ and the ability of the SR to generate Ca^{2+} waves.

It was necessary to establish a permeabilisation technique that allowed spontaneous SR Ca^{2+} release in rabbit ventricular cardiomyocytes to be studied. This was achieved by acute exposure to the compound β -escin. Subsequent perfusion with solutions containing 0.05mM EGTA, 10 μ m Fluo-3 and set $[\text{Ca}^{2+}]$ allowed confocal visualisation of Ca^{2+} sparks and waves. It was deemed necessary to be able to accurately calibrate these events. The permeabilised cell provided the ideal preparation in which to achieve this. This is very difficult to achieve within intact cells since an assumption of the resting $[\text{Ca}^{2+}]$ is required. In permeabilised cells this parameter can be accurately assessed by subsequent perfusion of calibration solutions containing 10mM EGTA and therefore a known buffered $[\text{Ca}^{2+}]$. By varying the external and therefore the internal $[\text{Ca}^{2+}]$ within these permeabilised cardiomyocytes, Ca^{2+} waves were produced when $[\text{Ca}^{2+}]_{\text{IC}}$ was above 200nM. Increasing to 1000nM $[\text{Ca}^{2+}]_{\text{IC}}$ resulted in an increase in the frequency, peak, and minimum of the Ca^{2+} wave. At these $[\text{Ca}^{2+}]$ mean extracellular $[\text{Ca}^{2+}]$ and intracellular $[\text{Ca}^{2+}]$ were equal. However when cardiomyocytes were exposed to $[\text{Ca}^{2+}]$ above 2 μ M a significant gradient between extracellular and intracellular $[\text{Ca}^{2+}]$ existed. This was found to be due to mitochondria, which took up Ca^{2+} during the peak of the Ca^{2+} wave.

This was essential at these high $[Ca^{2+}]$ to prevent irreversible cell contracture and subsequent cell death.

The second aim was to compare the Ca^{2+} wave behaviour in permeabilised cardiomyocytes and Ca^{2+} wave behaviour within the intact cells

Since Ca^{2+} wave characteristics had been extensively calibrated within the permeabilised cell it was necessary to establish if these events were different from Ca^{2+} waves within intact ventricular cardiomyocytes. No such difference was encountered, concluding that sarcolemmal Ca^{2+} extrusions mechanisms were not prominent in removing Ca^{2+} during the peak of the Ca^{2+} wave.

...and to use the wave characteristics in intact cells to calibrate the commonly used fluorescent Ca^{2+} indicator – Fluo-3/AM.

The ability to equilibrate extracellular Ca^{2+} concentration very rapidly with the intracellular $[Ca^{2+}]$ in the permeabilised cell allowed accurate calibration of the affinity for Ca^{2+} by Fluo-3 both in the external solution and within the cell. The Ca^{2+} indicator dye Fluo-5F was also calibrated in the same fashion and was found to be of lower affinity than Fluo-3 and subsequently enabled more accurate assessment of the peak of the Ca^{2+} wave. The Ca^{2+} wave characteristics within the permeabilised cell were then used to calibrate the affinity of Fluo-3AM within intact cells. This was found to be of a lower affinity than Fluo-3 within the extracellular solution or within the permeabilised cardiomyocyte. This factor emphasised the need to accurately calibrate the fluorescent dye of choice within the intact cell and

not assume an affinity, which is assessed outside the cell to be the same as within the cell.

The main aim of this thesis was to study the effects of adenoviral mediated over-expression of FKBP12.6 on Ca²⁺ sparks and Ca²⁺ waves within adult rabbit ventricular cardiomyocytes.

Adenoviral over-expression of FKBP12.6 within rabbit cardiomyocytes was achieved successfully. Peak-systolic intracellular [Ca²⁺] (measured with Fura-2 in intact cells) was higher in the Ad-FKBP12.6 group compared to control, as was the rate of rise of the transient. Using confocal microscopy the transients were visualised to release Ca²⁺ more synchronously. This was quantitatively shown to be the case. Furthermore, this was achieved if anything, by an equivalent SR [Ca²⁺] between cells over-expressing FKBP12.6 and control group. Restoration of the Ca²⁺ transient to steady state amplitude after emptying the SR of Ca²⁺ was faster in cells over-expressing FKBP12.6 than control suggesting that diastolic leak of Ca²⁺ from the SR was reduced by FKBP12.6. This was further confirmed by Ca²⁺ spark measurements within permeabilised cells, which were reduced in size and led to an enhanced SR [Ca²⁺]. Finally Ca²⁺ waves were examined at 400nM [Ca²⁺] within permeabilised cells over-expressing FKBP12.6. Control cultured cells were only able to produce Ca²⁺ events which propagated approximately 40µm across the width of the cell. However, cells over-expressing FKBP12.6 were able to produce coherent global Ca²⁺ waves. The SR Ca²⁺ content was markedly higher at 400nM within these latter cells compared to control. Overall over-expression of

FKBP12.6 within rabbit ventricular cardiomyocytes led to both a reduced diastolic leak of Ca^{2+} from the SR and enhanced SR Ca^{2+} release, which was independent of SR Ca^{2+} content. This could be due to an enhanced E-C coupling efficiency. These characteristics may have obvious benefits within particular cases of heart failure where diastolic leak of Ca^{2+} has been increased to such an extent that SR Ca^{2+} content declines. However as with other positive inotropic agents the possible consequences of the production of Ca^{2+} waves when intracellular $[\text{Ca}^{2+}]$ is increased may be counterproductive.

The final aim was to study Ca^{2+} sparks within cardiomyocytes over-expressing a mutant form of FKBP12.6, which lacked the ability to bind to calcineurin.

Recent studies suggest that it is possible that calcineurin (a phosphatase) when (and if) bound to RyR2 is responsible for the decrease in open probability originally shown to be due to FKBP12.6. The construction of an adenovirus, which over-expresses FKBP12.6 which lacks a calcineurin binding site results in Ca^{2+} sparks that are indistinguishable from Ca^{2+} sparks when simply over-expressing FKBP12.6 alone. The mutant virus reduced the size of the Ca^{2+} spark relative to a control group. Therefore in adult rabbit cardiomyocytes it seems that calcineurin plays no direct role when (and if) bound to RyR2 in reducing the channels open probability

FINAL CONCLUSION

It can be seen therefore that the permeabilised cell together with confocal microscopy, represents an excellent model in which to study and accurately calibrate Ca^{2+} release events from the SR of ventricular cardiomyocytes. Furthermore accurate calibration of fluorescent indicators within the cellular environment can also be achieved. The ability to measure and manipulate Ca^{2+} dynamics such as Ca^{2+} sparks and waves within such a preparation can lead to furthering our knowledge of E-C coupling.

APPENDIX

Appendix 2.1

Automated spark detection algorithm originally composed by Cheng *et al* (1999) and adapted for the permeabilised cell by Godfrey Smith to enable the extracellular regions to be cropped from the image [115].

```

Pro proc_spark1, ima,tscan,zoom,psize,human,cri,run,outfile,left,right,time_up,time_down
;proc_spark picks out and quantifies sparks
;Procedure parameters:
;ima=image file
;tscan = ms per line
;zoom = zoom set
;psize = pixel size (um) when zoom=1
;human = user interface 1=active, other=inactive
;cri = criteria for spark region folds of SD above mean
;run = number of times procedure has been called in this program (optional)
;outfile = output filename (optional)

;setup LUT
device, decomposed=0
;Set up for 16 bit display
ired=220
loadct,0
;Load up grey scale
tvlct,r,g,b,/get
;Get r g & b values
r(ired)=255
;set red vales
g(ired)=0
b(ired)=0
r(ired-1)=255
g(ired-1)=255
b(ired-1)=255

tvlct,r,g,b
;Put values back into LUT

;measure up image file
a=size(ima)
nx=a(1)
ny=a(2)

;Iterative computation of variance or SD by Cheng (NIH)
;modified by Smith (Glasgow)

ima=float(median(ima,7))
;minimal median filter to remove data points at extremes (used to be 5)
imm=ima ;**imm is used later for spark
detection**

;window,0,xs=nx,ys=ny,title='Image after median filter',xpos=512,ypos=0
;tv, ima

;0.8-um and 10-ms spatiotemporal smoothing filter

```

```

ss=(0.8/psize)
;ss = no. of pixels in 0.8um
st=(10./tscan)
;st = no of pixels in 10ms
ct=0
;ct = time counter

imb=fltarr(nx,ny)
;set up image array
for ia=-fix(ss/2),fix(ss/2) do begin
;for groups of +/- 2um
imb=imb+shift(ima,ia,0)
;shift image +/- 2um
ct=ct+1
endfor
for ib=-fix(st/2),fix(st/2) do begin
;for groups of +/- 10ms
imb=imb+ shift(ima,0,ib)
;shift image +/- 10um
ct=ct+1
endfor
ima=imb/ct
imb=ima
ibmx=bytarr(nx,ny)

imbx=rebin(ima,nx,1)

imbx=rebin(imbx,nx,ny)

ima=ima/imbx
;initial normalization-divide image by mean at each x
sd=stdev(ima,mean)
;inital estimate SD within the cell edges
print,'1st cell area mean= ',mean, ' & SD= ',sd

;mask for potential spark regions >m+1.5SD
mask=bytarr(nx,ny)
;set up image mask array
mask(where(ima gt 1+1.5*sd))=1
;set everything above 2.5xSD in ima to 1 in

;the corresponding area of mask image
mask=median(mask,5)
;median filter to blur the edges
ima=imb*(1-mask)
;excise potential spark regions and put in ima

;calculate baseline spatial profile with potential spark regions excised
;** this is also used later for spark detection
base=smooth(rebin(ima,nx,1)/rebin(1.-float(mask),nx,1),3,edge=1)
imb=imb/rebin(base,nx,ny)
;normalize image imb with corrected baseline

;tem=imb(pl:pr,)*(1.-mask(pl:pr,*))
;final calculation of background SD
tem=imb*(1.-mask)
sd=stdev(tem(where(tem gt 0.)),mean)
print,'new cell area mean= ',mean, ' & SD= ',sd

;Spark detection bit:

```

```

;make a binary image of cri*SD i.e. spark sites
imx=(imb-(1.0+cri*sd)>0.0)*100000.<1.0
imi=fix(imx)
im=median(imi,5)

;take care the edge effect of the smoothing
im(0:ss/2,*)=0
im(nx-ss/2-1:*,*)=0
im(*,0:st/2)=0
im(*,ny-st/2-1:*)=0
;NB image im is a cri*sd mask

;make a 2*SD image for automated regional counting
imx=(imb-(1.0+2.0*sd)>0)*100000.<1.0
imi=fix(imx)
ime=median(imi,5)

;take care the edge effect of the smoothing
ime(0:ss/2,*)=0
ime(nx-ss/2-1:*,*)=0
ime(*,0:st/2)=0
ime(*,ny-st/2-1:*)=0
imf=ime
;NB images ime and imf is a 2*sd mask

;**Use the median filtered image imm (with sparks) and baseline image (spark areas
removed)
;NB, the rebin of imb will ensure that the areas of sparks will have a baseline
imb=imm/rebin(base,nx,ny)
;imb= new image (normalised with minimal filtering on sparks)

;Display two copies of this image
window,2,xs=nx,ys=ny,title='Normalised image (Win2)',xpos=512,ypos=0
window,0,xs=nx,ys=ny,title='Normalised image+2SD sparks(Win0)',xpos=1024,ypos=0
wset,0
tv,(imb-.5>0)*150<255
;display the normalized image with contrast enhanced
wset,2
tv,(imb-.5>0)*150<255

;window,3,xs=nx/2,ys=ny/2,title='3.8*SD image(Win3)',xpos=512,ypos=520
;window,1,xs=nx/2,ys=ny/2,title='2.0*SD image(Win1)',xpos=770,ypos=520
;wset,3
;imNew=congrid(im,nx/2,ny/2)
;tvsc1,imNew
;cri*SD image
;wset,1
;imeNew=congrid(ime,nx/2,ny/2)
;tvsc1,imeNew
;2-SD image

skc=0
;italize spark counter
s=fltarr(20,500)
;array to hold (up to 500) spark parameters (20 values)

jump1: ime=imf

While (total(im) ne 0) do begin
a=min(where(im eq 1))
;im is the cri*sd mask

```

```

Tline=a/nx
Xcord=a mod nx
    ;get coordinates of spark, Tline and Xcord

;Define search area
nnl=fix(min([left/psize, Xcord]))
;calculate length(nnl)
nnr=fix(min([right/psize, nx-Xcord-1]))
;calculate right hand coord (nnr)
mmb=fix(min([time_up/tscan, Tline]))
;calculate breadth (mmb)
mme=fix(min([time_down/tscan, ny-Tline-1]))
;calculate end coord (mme)
ym=bytarr(nnl+nnr+1,mmb+mme+1)
;array to hold growing points
ym(nnl,mmb)=1
    ;initial seeding for growth

sk=ym
    ;array to hold the spark as seen in the 2SD image

; extra window to observe spark detection
;window,4,title='Debug',xs=nnl+nnr+1,ys=mmb+mme+1

for iii=0,500 do begin
;surface growth generation count
yt=sk

;potential new surface points
;dilation of ym by 3*3 filter
;Odd integers='True'
yn=(ime(Xcord-nnl:Xcord+nnr,Tline-mmb:Tline+mme)) and
fix(smooth(float(ym),3,edge=1)*100.<1)

;no further growth, stop and calculate the parameters
if total(yn) eq 0 then goto, jump2

;update sk
sk=sk>yn

;excise the points that already included in the cluster
;ime = 2*SD mask im=3.8*SD mask
ime(Xcord-nnl:Xcord+nnr,Tline-mmb:Tline+mme)=ime(Xcord-nnl:Xcord+nnr,Tline-
mmb:Tline+mme)-fix(sk)>0
im(Xcord-nnl:Xcord+nnr,Tline-mmb:Tline+mme)=im(Xcord-nnl:Xcord+nnr,Tline-
mmb:Tline+mme)-fix(sk)>0

;true new surface point
ym=yn-fix(yt)>0

    ;wset,4
    ;tvscl,sk
    ;file=dialog_message('OK?')
    if iii eq 500 then print,'WARNING: SPARK SEARCH AREA MAY BE TOO SMALL'
endfor
jump2:skc=skc+1

;spark measurement
pixels=total(sk)
;total pixels

;time position
a=rebin(float(sk),1,mmb+mme+1)

```

```

a=where(a ne 0)
tpos=Tline-mmb+min(a)
;at, bt: initiation and end time
durmax=max(a)-min(a)+1
;max duration
at=max(a)
bt=min(a)

;x coordinate
a=rebin(float(sk), nnl+nnr+1, 1)
a=where(a ne 0)
xpos=Xcord-nnl+(max(a)+min(a))/2.
;ax, bx: left and right edges
ax=max(a)
bx=min(a)
; max width
breadthm=max(a)-min(a)+1

averdur=pixels/breadthm
;average duration
averwid=pixels/durmax
;average width

w=imb(Xcord-nnl:Xcord+nnr, Tline-mmb:Tline+mme)*sk
peak=max(w)
;peak pixel
p=where(w eq peak)
p=p(0)
xxx=p mod (nnl+nnr+1)
ttt=p/(nnl+nnr+1)
averp=total(imb((Xcord-nnl+xxx-1):(Xcord+xxx-nnl+1), Tline-mmb+ttt-1:Tline-
mmb+ttt+1))/9. ;3*3 average peak
amp=total(w)/pixels
; average amplitude

;amplitude, duration and width measured as usual
w=rebin(imb((fix(Xcord-nnl+xxx-2.5/psize)>0):(fix(Xcord-nnl+xxx+2.5/psize)<nx-1), $
Tline-mmb+ttt-1:Tline-mmb+ttt+1), (fix(Xcord-nnl+xxx+2.5/psize)<nx-1)-(fix(Xcord-
nl+xxx-2.5/psize)>0)+1, 1));used to be 2

pw=max(w)
w50=n_elements(where(w ge (pw+1.)/2.))

w=rebin(imb((fix(Xcord-nnl+xxx-.4/psize)>0):(fix(Xcord-nnl+xxx+.4/psize)<nx-1), $
((Tline-mmb)<(fix(Tline-mmb+ttt-30./tscan)>0)):(Tline+mme)>(fix(Tline-
mme+ttt+50./tscan)<ny-1)))$
, 1, ((Tline+mme)>(fix(Tline-mmb+ttt+50./tscan)<ny-1))-((Tline-mmb)<(fix(Tline-mmb+ttt-
30./tscan)>0))+1)

pk=max(w)
d50=n_elements(where(w ge (pw+1.)/2.))

ii=skc
s(0, ii)=1
;Image #
s(2, ii)=xpos
;X pixel
s(3, ii)=tpos
;Time pixel
s(4, ii)=peak

```

```

        ;Peak pixel
s(5,ii)=averp
        ;Peak amplitude (3*3)
s(6,ii)=amp
        ;Average amplitude in spark
s(7,ii)=durmax
;Max Duration
s(8,ii)=averdur
;Average duration
s(9,ii)=breadthm
        ;Max breadth
s(10,ii)=averwid
        ;Average width
s(11,ii)=pixels
;Sum of pixel values
s(12,ii)=Xcord-nnl+bx
;X co-ord of peak
s(13,ii)=Xcord-nnl+ax
;X co-ord
s(14,ii)=Tline-mmb+bt
;Time of peak?
s(15,ii)=Tline-mmb+at
;Time
s(16,ii)=pk
;
s(17,ii)=w50
        ;Width at 50% duration
s(18,ii)=d50
        ;Duration at 50% height
print,'ID#,P_max,P_33a,P_ave,D_max,D_ave, W_max,W_ave,pixels, P, W, D'
print,format='(115, 7f7.3,115,
3f7.3)',ii,peak,averp,amp,durmax,averdur,breadthm,averwid,pixels, pk,w50,d50
;
wset,0
z=tvrd(Xcord-nnl,Tline-mmb,nnl+nnr+1,mmb+mme+1)
z1=z*(1-(sk))
        ;make a block of image with spark area=0
z2=z1+sk*ired
        ;replicate the image block but spark image is coloured
tv,z2,Xcord-nnl,Tline-mmb
ytt=ym*0
ytt([bx,ax],bt:at)=1
ytt(bx:ax,[bt,at])=1

wset,0
z=tvrd(Xcord-nnl,Tline-mmb,nnl+nnr+1,mmb+mme+1)
tv,z*(1-(ytt))+(ytt)*(ired-1),Xcord-nnl,Tline-mmb
endwhile

;Optional user interface
old_font = !p.font
;p.font = 0
;Use hdw font

while human eq 1 do begin
wset,0
;image window
print,'click left button at a spark to be discarded'
print,'middle button to add a spark'
print,'right button to exit'
cursor,ix,iy,3,/dev
if (!Mouse.Button eq 4) then goto, jump4
if (!Mouse.Button eq 1) then begin

```

```

repeat cursor,ix,iy,0,/dev until !Mouse.Button eq 0
for i=1,skc do begin
  if ((ix le s(13,i)) and (ix ge s(12,i))) and ((iy le s(15,i)) and (iy ge s(14,i))) then begin

;update window by taking the image data from window 2.....
  wset,2
  xu=tvrd(s(12,i),s(14,i),s(13,i)-s(12,i)+1,s(15,i)-s(14,i)+1)

;... and use it in window 0
  wset,0
  tv,xu,s(12,i),s(14,i)

;delete spark data
  if i eq skc then s(*,i)=0
  if i le skc-1 then s(*,i:skc-1)=s(*,i+1:skc)
  skc=skc-1
  print, 'spark ',i,' deleted'
  endif
endfor
endif
if (!Mouse.Button eq 2)and(imf(ix,iy) eq 1) then begin
  im(ix,iy)=1
  print,'spark',skc+1,' will be added'
  goto,jump1
endif
endwhile

jump4: if skc ne 0 then s=s(*,1:skc)
if skc ne 0 then s(1,*)=findgen(skc)
print, 'total sparks ', skc

;data output to a file
if run eq 1 then begin
  outfile=dialog_pickfile(/write,filter="*.txt")
  if outfile eq "" then begin
    print,'No output filename?'
    goto, jump3
  endif else begin
    openw,2,outfile
    for j=0,skc-1 do printf,2,format='(4I5,3f7.3,5i5,1f7.3,2i5)' $
      ,run,s(1,j),s(2,j),s(3,j),s(4,j),s(5,j),s(6,j),s(7,j),s(8,j),s(9,j),s(10,j) $
      ,s(11,j),s(16,j),s(17,j),s(18,j)
    close,2
    jump3:
  endif else begin
    openu,2,outfile, /append
    for j=0,skc-1 do printf,2,format='(4I5,3f7.3,5i5,1f7.3,2i5)' $
      ,run,s(1,j),s(2,j),s(3,j),s(4,j),s(5,j),s(6,j),s(7,j),s(8,j),s(9,j),s(10,j) $
      ,s(11,j),s(16,j),s(17,j),s(18,j)
    close,2
  endif else
  wdelete, 0,1,2,3
  run=run+1
end

```

Appendix 6.1

Sequence alignment of base pairs (6.1.1) and amino acids (6.1.2) for FKBP12.6, FKBP12.0 and the FKBP12.6 mutant, which cannot bind calcineurin.

Appendix 6.1.1 Base pair sequence

FKBP12	1	ATGGGAGTGCAGCTGRLAACCATCTCCGAAAGGAGACGGCCACCTTCCCAAGCCGGCC
FKBP12.6	1	ATGGGAGTGGAGATTAAGCCATCTCCCTGGGAAAGGAAAGGACATTCCCAAGGAGGGCC
FKBP12.6G89PV90K	1	ATGGGAGTGGAGATDRAGACCATCTCCCTGGGAAAGGAAAGGACATTCCCAAGGAGGGCC
FKBP12	61	CAGACCTCCGTTGGTGCCTACACCCGGATGGCTGAAAGATGCCAAGAAATTTGATTCCCTCC
FKBP12.6	61	CAAAAGTGTGTCTGTACTACACAGAAATGCTCCAAAATGGGAAAGAAATTTGATTCCATCC
FKBP12.6G89PV90K	61	CAAAAGTGTGTCTGTACTACACAGAAATGCTCCAAAATGGGAAAGAAATTTGATTCCATCC
FKBP12	121	CTGGATAGRAATAGCTCTTAAAGTTTCTCTAGGCAAGCAGGAGCTGATCCAGGCTTGG
FKBP12.6	121	AGAGATAGAAAATAAACCTTTCAAGTTCAAGATTGGCAAAACAGGAAGTCAATCAAAAGGTTT
FKBP12.6G89PV90K	121	AGAGATAGAAAATAAACCTTTCAAGTTCAAGATTGGCAAAACAGGAAGTCAATCAAAAGGTTT
FKBP12	181	GAAAGATGAGCTTCCAGATGAGCTGGCTCAGAGAGCCAACTGACTATATCTCAGAT
FKBP12.6	181	GAAAGAGGATGGATCCAGATGAGCTGGGGCAGAGGGGGAGCTGATCTCAACCCCTGAT
FKBP12.6G89PV90K	181	GAAAGAGGATGGATCCAGATGAGCTGGGGCAGAGGGGGAGAGCTGACTCAACCCCTGAT
FKBP12	241	TATCCCTATGGCTCCCACTGGCCACCCAGGCCATCATCCGACCACATGCCACTCTCCTCTC
FKBP12.6	241	GTGGCATATGGAGGCCAGGGGCCACCCGGCTCATCCCTCCCATGGCCACCCCTCATCTTT
FKBP12.6G89PV90K	241	GTGGCATATGGAGGCCAGGGGCCACCCGGCTCATCCCTCCCATGGCCACCCCTCATCTTT
FKBP12	301	GATGTGGAGCTTATAAAGCTGAATGA
FKBP12.6	301	GACTGTGGAGCTTCTCAACTTAGAGTGA
FKBP12.6G89PV90K	301	GACTGTGGAGCTGCTCAACTTAGAGTGA

Where: a – adenine, c – cytosine, g – guanine, and t – thymine

Appendix 6.1.2 Amino acid sequence

FKBP12	1	MGVVETISPGDGRFFPKRGQTCVWHYTGMLDCKKFDSSRDENKFFKFMGRQEWIKGF
FKBP12.6	1	MGVEIETISPGDGRFFPKRGQTCVWHYTGMLQNGKFDSSRDENKFFKFRIGKQEVIRGF
FKBP12.6'	1	MQVEIETISPGDGRFFPKRGQTCVWHYTGMLQNGKFDSSRDENKFFKFRIGKQEVIRGF
FKBP12	61	EEGVAQMSVGRRAKLTISPLVAYGATGHPCLIPPHATLIFDVELLKLE
FKBP12.6	61	EEGAAQMSLGQRAKLTCTPRVAYGATGHPCTIPPNATLIFDVELLNLE
FKBP12.6'	61	EEGAAQMSLGQRAKLTCTPRVAYGATGHPCKIPPNATLIFDVELLNLE

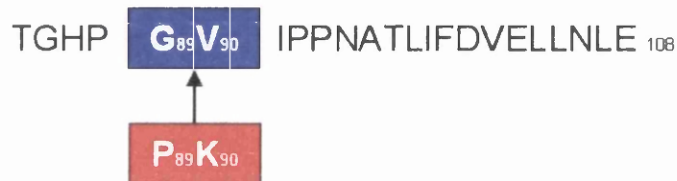
Appendix 6.1.3 Summary of construction of FKBP12.6 mutant

Below is a summary of the site directed mutagenesis, which enabled the production of the FKBP12.6 mutant virus (FKBP 12.6m). This virus cannot bind calcineurin (see section 6.1.12 for further details).

Amino Acid Sequence: **FKBP12.6/ FKBP12.6m**

MGVEIETISPGDGRTFPKKGQTCVVHYTGMLQNGKKFDSSRD

RNKPFKFRIGKQEVIKGFEEGAAQMSLGQRAKLTCTPDVAYGA



Calcineurin binding site

Amino acid (one-letter code abbreviation)

Aspartate (D), Glutamate (E), cysteine (C), methionine (M), lysine (K), arginine (R), serine (S), threonine (Y), asparagine (N), glutamine (Q), glycine (G), isoleucine (I), leucine (L), valine (V), alanine (A), tryptophan (W), histidine (H), proline (P).

REFERENCE

1. Ringer S. A further contribution regarding the influence of the different constituents of the blood on the contraction of the heart. *J Physiol* 1883; **4**: 29-42.
2. Page E. Quantitative ultrastructural analysis in cardiac membrane physiology. *Am J Physiol* 1978; **235**: c147-c158.
3. Page E, Surdyk-Droske M. Distribution, surface density and membrane area of diadic junctional contacts between plasma membrane and terminal cisterns in mammalian ventricle. *Circ Res* 1979; **45**: 260-267.
4. Page E, McCallister LP, Power B. Stereological measurements of cardiac ultrastructures implicated in excitation-contraction coupling. *Proc Natl Acad Sci USA* 1971; **68**: 1465-1466.
5. Soeller C, Cannell MB. Examination of the tranverse tubular system in living cardiac rat myocytes by 2-photon microscopy and digital image processing techniques. *Circ Res* 1999; **84**: 266-275.
6. Lederer WJ, Berlin JR, Cohen NM, Hadley RW, Bers DM, Cannell MB. Excitation-contraction coupling in heart cells. Roles of the sodium-calcium exchange, the calcium current, and the sarcoplasmic reticulum. *Ann N Y Acad Sci* 1990; **588**: 190-206.
7. Fabiato A. Calcium-induced release of calcium from the cardiac sarcoplasmic reticulum. *Am J Physiol* 1983; **245**: C1-14.
8. Harrison SM, Bers DM. The influence of temperature on the calcium sensitivity of the myofilaments of skinned ventricular muscle from the rabbit. *J Gen Physiol* 1989; **93**: 411-427.
9. Bers DM. *Excitation-contraction coupling and cardiac contractile force*. Kluwer Academic Publishers, 2001.
10. Puglisi JL, Yuan W, Bassani JWM, Bers DM. Calcium influx through calcium

- channels in rabbit ventricular myocytes during action potential clamp: Influence of temperature. *Circ Res* 1999; **85**: e7-e16.
11. Yuan W, Bers DM. Comparison of sarcolemmal calcium channel current in rabbit and rat ventricular myocytes. *Circ Res* 1996; **493**: 733-746.
 12. Delbridge LM, Bassani JWM, Bers DM. Steady-state twitch calcium fluxes and cytosolic calcium buffering in rabbit ventricular myocytes. *Am J Physiol* 1996; **270**: c192-c199.
 13. Fabiato A. Simulated calcium current can both cause calcium loading in and trigger calcium release from the sarcoplasmic reticulum of a skinned canine cardiac Purkinje cell. *J Gen Physiol* 1985; **85**: 291-320.
 14. Fabiato A. Time and calcium dependence of activation and inactivation of calcium-induced release of calcium from the sarcoplasmic reticulum of a skinned canine cardiac Purkinje cell. *J Gen Physiol* 1985; **85**: 247-289.
 15. Fabiato A. Rapid ionic modifications during the aequorin-detected calcium transient in a skinned canine cardiac Purkinje cell. *J Gen Physiol* 1985; **85**: 189-246.
 16. Fawcett DW. The ultrastructure of the cat myocardium. I. Ventricular papillary muscle. *J Cell Biol* 1969; **42**: 1-45.
 17. Beuckelmann DJ, Wier WG. Mechanism of release of calcium from sarcoplasmic reticulum of guinea-pig cardiac cells. *J Physiol* 1988; **405**: 233-255.
 18. London B, Krueger JW. Contraction in voltage-clamped, internally perfused single heart cells. *J Gen Physiol* 1986; **88**: 475-505.
 19. duBell WH, Houser SR. Voltage and beat dependence of the calcium transient in feline ventricular myocytes. *Am J Physiol* 1989; **257**: H746-H758.
 20. Callewaert G, Cleemann L, Morad M. Epinephrine enhances calcium current-regulated calcium release and calcium uptake in rat ventricular myocytes. *Proc Natl Acad Sci* 1988; **85**: 2009-2013.

21. Nabauer M, Callewart G, Cleemann L, Morad M. Regulation of calcium release is gated by calcium current not gating charge, in cardiac myocytes. *Science* 1989; **244**: 800-803.
22. Kentish JC, Barsotti RJ, Lea TJ, Mulligan IP, Patel JR, Ferenczi MA. Calcium release from cardiac sarcoplasmic reticulum induced by photorelease of calcium or Ins(1,4,5)P₃. *Am J Physiol* 1990; **258**: H610-H615.
23. Valdeolmillos M, O'Neill SC, Smith GL, Eisner DA. Calcium-induced calcium release activates contraction in intact cardiac cells. *Pflugers Arch* 1989; **413**: 676-678.
24. Nabauer M, Morad M. Calcium induced calcium release as examined by photolysis of caged calcium in single ventricular myocytes. *Am J Physiol* 1990; **258**: c189-c193.
25. Niggli E, Lederer WJ. Voltage-independent calcium release in heart muscle. *Science* 1990; **250**: 565-568.
26. Cannell MB, Berlin JR, Lederer WJ. Effect of membrane potential changes on the calcium transient in single rat cardiac muscle cells. *Science* 1987; **238**: 1419-1423.
27. Cleemann L, Morad M. Role of Ca²⁺ channel in cardiac excitation-contraction coupling in the rat: evidence from Ca²⁺ transients and contraction. *J Physiol* 1991; **432**: 283-312.
28. Stern MD. Theory of excitation-contraction coupling in cardiac muscle. *Biophys J* 1992; **63**: 497-517.
29. Stern MD, Song L-S, Cheng H et al. Local control models of cardiac excitation contraction coupling. *J Gen Physiol* 1999; **113**: 469-489.
30. Block BA, Imagawa T, Campbell KP, Franzini-Armstrong C. Structural evidence for direct interaction between the molecular components of the transverse tubule/sarcoplasmic reticulum junction in skeletal muscle. *J Cell Biol* 1988; **107**: 2587-2600.
31. Cheng H, Lederer WJ, Cannell MB. Calcium sparks: Elementary events underlying

- excitation contraction coupling in heart muscle. *Science* 1993; **262**: 740-262.
32. Fill M, Coronado R. Ryanodine receptor channel of sarcoplasmic reticulum. *Trends Neurosci* 1988; **11**: 453-457.
33. Gyorke S, Lukyanenko V, Gyorke I. Dual effects of tetracaine on spontaneous release in rat ventricular myocytes. *J Physiol* 1997; **500**: 297-309.
34. Cannell MB, Cheng H, Lederer WJ. The control of calcium release in heart muscle. *Science* 1995; **268**: 1045-1049.
35. Lopez-Lopez JR, Shacklock PS, Balke CW, Wier WG. Local calcium transients triggered by single L-type calcium channel currents in cardiac cells. *Science* 1995; **268**: 1042-1045.
36. Bridge JH, Ershler PR, Cannell MB. Properties of Ca^{2+} sparks evoked by action potentials in mouse ventricular myocytes. *J Physiol* 1999; **518 (Pt 2)**: 469-478.
37. Santana LF, Cheng H, Gomez AM, Cannell MB, Lederer WJ. Relationship between the sarcolemmal Ca^{2+} current and Ca^{2+} sparks and local control theories for cardiac excitation contraction coupling. *Circulation Research* 1996; **78**: 166-171.
38. Collier ML, Thomas AP, Berlin JR. Relationship between L-type Ca^{2+} current and unitary sarcoplasmic reticulum Ca^{2+} release events in rat ventricular myocytes. *J Physiol* 1999; **516 (Pt 1)**: 117-128.
39. Inoue M, Bridge JH. Ca^{2+} sparks in rabbit ventricular myocytes evoked by action potentials: involvement of clusters of L-type Ca^{2+} channels. *Circ Res* 2003; **92**: 532-538.
40. Takagishi Y, Yasui K, Severs NJ, Murata Y. Species-specific difference in distribution of voltage-gated L-type Ca^{2+} channels of cardiac myocytes. *Am J Physiol Cell Physiol* 2000; **279**: C1963-C1969.
41. Wang SQ, Song LS, Lakatta EG, Cheng H. Ca^{2+} signalling between single L-type Ca^{2+} channels and ryanodine receptors in heart cells. *Nature* 2001; **410**: 592-596.

42. Mejia-Alvarez R, Kettlun C, Rios E, Stern M, Fill M. Unitary Ca^{2+} current through cardiac ryanodine receptor channels under quasi-physiological ionic conditions. *J Gen Physiol* 1999; **113**: 177-186.
43. Gonzalez A, Kirsch WG, Shirokova N et al. Involvement of multiple intracellular release channels in calcium sparks of skeletal muscle. *Proc Natl Acad Sci U S A* 2000; **97**: 4380-4385.
44. Blatter LA, Huser J, Rios E. Sarcoplasmic reticulum Ca^{2+} release flux underlying Ca^{2+} sparks in cardiac muscle. *Proc Natl Acad Sci U S A* 1997; **94**: 4176-4181.
45. Lipp P, Niggli E. Submicroscopic calcium signals as fundamental events of excitation-contraction coupling in guinea-pig cardiac myocytes. *J Physiol* 1996; **492** : 31-38.
46. Lukyanenko V, Gyorke I, Subramanian S, Smirnov A, Wiesner TF, Gyorke S. Inhibition of calcium sparks by ruthenium red in permeabilised rat ventricular myocytes. *Biophysical Journal* 2000; **79**: 1273-1284.
47. Franzini-Armstrong C, Protasi F, Ramesh V. Shape, size, and distribution of calcium release units and couplons in skeletal and cardiac muscles. *Biophys J* 1999; **77**: 1528-1539.
48. Sobie EA, Dilly KW, Santos Cruz Jd, Lederer WJ, Jafri SM. Termination of cardiac calcium sparks: An investigative mathematical model of calcium induced calcium release. *Biophys J* 2002; **83**: 78-59.
49. Rousseau E, Meissner G. Single cardiac sarcoplasmic reticulum Ca^{2+} -release channel: activation by caffeine. *Am J Physiol Heart Circ Physiol* 1989; **256**: H328.
50. Rose WC, Balke CW, Wier WG, Marban E. Macroscopic and unitary properties of physiological ion flux through L- type Ca^{2+} channels in guinea-pig heart cells. *J Physiol* 1992; **456**: 267-284.
51. Cannell MB, Cheng H, Lederer WJ. Spatial non-uniformities in $[\text{Ca}^{2+}]_i$ during

- excitation-contraction coupling in cardiac myocytes. *Biophys J* 1994; **67**: 1942-1956.
52. Franzini-Armstrong C, Protasi F, Ramesh V. Shape, size, and distribution of Ca^{2+} release units and couplons in skeletal and cardiac muscles. *Biophys J* 1999; **77**: 1528-1539.
53. Sitsapesan R, Williams AJ. Do inactivation mechanisms rather than adaptation hold the key to understanding ryanodine receptor channel gating? *J Gen Physiol* 2000; **116**: 867-872.
54. Fabiato A. Spontaneous versus triggered contractions of "calcium-tolerant" cardiac cells from the adult rat ventricle. *Basic Res Cardiol* 1985; **80 Suppl 2**: 83-87.
55. Kawano S, Coronado R. Ca^{2+} dependence of Ca^{2+} release channel activity in the sarcoplasmic reticulum of cardiac and skeletal muscle. *Biophys.J.* [59]. 1991.
Ref Type: Abstract
56. Sham JSK, Song L-S, Chen Y et al. Termination of Ca^{2+} release by a local inactivation of ryanodine receptors in cardiac myocytes. *Proc Natl Acad Sci USA* 1998; **95**: 15096-15101.
57. Gyorke S, Fill M. Ryanodine receptor adaptation: control mechanism of Ca^{2+} -induced Ca^{2+} release in heart. *Science* 1993; **260**: 807-809.
58. Valdivia HH, Kaplan JH, Ellis-Davies GC, Lederer WJ. Rapid adaptation of cardiac ryanodine receptors: modulation by Mg^{2+} and phosphorylation. *Science* 1995; **267**: 1997-2000.
59. Negretti N, Varro A, Eisner DA. Estimate of net calcium fluxes and sarcoplasmic reticulum calcium content during systole in rat ventricular myocytes. *Journal of Physiology* 1995; **486.3**: 581-591.
60. Bassani JW, Yuan W, Bers DM. Fractional SR Ca^{2+} release is regulated by trigger Ca^{2+} and SR Ca^{2+} content in cardiac myocytes. *Am J Physiol* 1995; **268**: C1313-C1319.

61. Sharma MR, Penczek P, Grassucci R, Xin HB, Fleischer S, Wagenknecht T. Cryoelectron microscopy and image analysis of the cardiac ryanodine receptor. *J Biol Chem* 1998; **273**: 18429-18434.
62. Samsó M, Wagenknecht T. Contributions of electron microscopy and single-particle techniques to the determination of the ryanodine receptor three-dimensional structure. *J Struct Biol* 1998; **121**: 172-180.
63. Marx SO, Gaburjakova J, Gaburjakova M, Henrikson C, Ondrias K, Marks AR. Coupled gating between cardiac calcium release channels (Ryanodine receptors). *Circ Res* 2001; **88**: 1151-1158.
64. Lukyanenko V, Gyorke S. Ca^{2+} sparks and Ca^{2+} waves in saponin-permeabilized rat ventricular myocytes. *J Physiol* 1999; **521.3**: 575-585.
65. Satoh H, Blatter LA, Bers DM. Effects of $[\text{Ca}^{2+}]_i$, SR Ca^{2+} load, and rest on Ca^{2+} spark frequency in ventricular myocytes. *Am J Physiol* 1997; **272**: H657-H668.
66. Gyorke I, Gyorke S. Regulation of the cardiac ryanodine receptor channel by luminal Ca^{2+} involves luminal Ca^{2+} sensing sites. *Biophys J* 1998; **75**: 2801-2810.
67. Ching LL, Williams AJ, Sitsapesan R. Evidence for Ca^{2+} activation and inactivation on the luminal side of the cardiac ryanodine complex. *Circ Res* 2000; **87**: 201.
68. Song LS, Stern MD, Lakatta EG, Cheng H. Partial depletion of sarcoplasmic reticulum calcium does not prevent calcium sparks in rat ventricular myocytes. *J Physiol* 1997; **505 (Pt 3)**: 665-675.
69. Diaz ME, Trafford AW, O'Neill SC, Eisner DA. Measurement of sarcoplasmic reticulum Ca^{2+} content and sarcolemmal Ca^{2+} fluxes in isolated rat ventricular myocytes during spontaneous Ca^{2+} release. *J Physiol* 1997; **501.1**: 3-16.
70. Lukyanenko V, Viatchenko-Karpinski S, Smirnov A, Wiesner TF, Gyorke S. Dynamic regulation of sarcoplasmic reticulum calcium content and release by luminal calcium sensitive leak in rat ventricular myocytes. *Biophys J* 2001; **81**: 785-798.

71. Terentyev D, Viatchenko-Karpinski S, Valdivia HH, Escobar AL, Gyorke S. Luminal Ca^{2+} controls termination and refractory behavior of Ca^{2+} -induced Ca^{2+} release in cardiac myocytes. *Circ Res* 2002; **91**: 414-420.
72. Ginsburg KS, Weber CR, Bers DM. Control of maximum sarcoplasmic reticulum Ca^{2+} load in intact ferret ventricular myocytes. Effects of thapsigargin and isoproterenol. *J Gen Physiol* 1998; **111**: 491-504.
73. Gomez AM, Cheng H, Lederer WJ, Bers DM. Ca^{2+} diffusion and sarcoplasmic reticulum transport both contribute to $[\text{Ca}^{2+}]_i$ decline during Ca^{2+} sparks in rat ventricular myocytes. *J Physiol* 1996; **496 (Pt 2)**: 575-581.
74. Leblanc N, Hume JR. Sodium current-induced release of calcium from cardiac sarcoplasmic reticulum. *Science* 1990; **248**: 372-376.
75. Lederer WJ, Niggli E, Hadley RW. Sodium-calcium exchange in excitable cells: fuzzy space. *Science* 1990; **248**: 283.
76. Sipido KR, Carmeliet E, Pappano A. Na^+ current and Ca^{2+} release from the sarcoplasmic reticulum during action potentials in guinea-pig ventricular myocytes. *J Physiol* 1995; **489 (Pt 1)**: 1-17.
77. Levi AJ, Spitzer KW, Kohmoto O, Bridge JH. Depolarization-induced Ca^{2+} entry via $\text{Na}^+/\text{Ca}^{2+}$ exchange triggers SR release in guinea pig cardiac myocytes. *Am J Physiol* 1994; **266**: H1422-H1433.
78. Litwin SE, Li J, Bridge JH. $\text{Na}^+/\text{Ca}^{2+}$ exchange and the trigger for sarcoplasmic reticulum Ca^{2+} release: studies in adult rabbit ventricular myocytes. *Biophys J* 1998; **75**: 359-371.
79. Sipido KR, Maes M, Van de WF. Low efficiency of Ca^{2+} entry through the $\text{Na}^+/\text{Ca}^{2+}$ exchanger as trigger for Ca^{2+} release from the sarcoplasmic reticulum. A comparison between L-type Ca^{2+} current and reverse-mode $\text{Na}^+/\text{Ca}^{2+}$ exchange. *Circ Res* 1997; **81**: 1034-1044.

80. Bassani JWM, Bassani RA, Bers DM. Relaxation in rabbit and rat cardiac cells: species-dependent differences in cellular mechanisms. *J Physiol* 1994; **476.2**: 279-293.
81. Tada M, Katz AM. Phosphorylation of the sarcoplasmic reticulum and sarcolemma. *Annu Rev Physiol* 1982; **44**: 401-423.
82. Thastrup O, Cullen PJ, Drobak BK, Hanley MR, Dawson AP. Thapsigargin, a tumor promoter, discharges intracellular Ca^{2+} stores by specific inhibition of the endoplasmic reticulum Ca^{2+} -ATPase. *Proc Natl Acad Sci U S A* 1990; **87**: 2466-2470.
83. Young HS, Xu C, Zhang P, Stokes DL. Locating the thapsigargin-binding site on $\text{Ca}(2+)\text{-ATPase}$ by cryoelectron microscopy. *J Mol Biol* 2001; **308**: 231-240.
84. Goeger DE, Riley RT, Dorner JW, Cole RJ. Cyclopiazonic acid inhibition of the Ca^{2+} -transport ATPase in rat skeletal muscle sarcoplasmic reticulum vesicles. *Biochem Pharmacol* 1988; **37**: 978-981.
85. Bassani JW, Bassani RA, Bers DM. Relaxation in rabbit and rat cardiac cells: species-dependent differences in cellular mechanisms. *J Physiol* 1994; **476**: 279-293.
86. Kuwayama H. The membrane potential modulates the ATP-dependent Ca^{2+} pump of cardiac sarcolemma. *Biochim Biophys Acta* 1988; **940**: 295-299.
87. Bassani RA, Bassani JW, Bers DM. Mitochondrial and sarcolemmal Ca^{2+} transport reduce $[\text{Ca}^{2+}]_i$ during caffeine contractures in rabbit cardiac myocytes. *J Physiol* 1992; **453**: 591-608.
88. Loughrey CM, MacEachern KE, Smith GL. The relationship between intracellular $[\text{Ca}^{2+}]$ and Ca^{2+} wave characteristics in permeabilised cardiomyocytes from the rabbit. *J Physiol* 2002; **543.3**: 859-870.
89. Babcock DF, Hille B. Mitochondrial oversight of cellular Ca^{2+} signaling. *Curr Opin*

- Neurobiol* 1998; **8**: 398-404.
90. Buntinas L, Gunter KK, Sparagna GC, Gunter TE. The rapid mode of calcium uptake into heart mitochondria (RaM): comparison to RaM in liver mitochondria. *Biochim Biophys Acta* 2001; **1504**: 248-261.
 91. Shchepina LA, Pletjushkina OY, Avetisyan AV et al. Oligomycin, inhibitor of the F₀ part of H⁺-ATP-synthase, suppresses the TNF-induced apoptosis. *Oncogene* 2002; **21**: 8149-8157.
 92. Rizzuto R, Bernardi P, Pozzan T. Mitochondria as all-round players of the calcium game. *J Physiol* 2000; **529 Pt 1**: 37-47.
 93. Takahashi K, Schaffer SW, Azuma J. Taurine prevents intracellular calcium overload during calcium paradox of cultured cardiomyocytes. *Amino Acids* 1997; **13**: 1-11.
 94. Chapman RA, Rodrigo GC, Tunstall J, Yates RJ, Busselen P. Calcium paradox of the heart: a role for intracellular sodium ions. *Am J Physiol* 1984; **247**: H874-H879.
 95. Fabiato A, Fabiato F. Excitation-contraction coupling of isolated cardiac fibers with disrupted or closed sarcolemmas. Calcium-dependent cyclic and tonic contractions. *Circ Res* 1972; **31**: 293-307.
 96. Becker TC, Noel RJ, Coats WS et al. Use of recombinant adenovirus for metabolic engineering of mammalian cells. *Methods Cell Biol* 1994; **43 Pt A**: 161-189.
 97. Winegrad S. Studies of cardiac muscle with a high permeability to calcium produced by treatment with ethylenediaminetetraacetic acid. *J Gen Physiol* 1971; **58**: 71-93.
 98. Miller DJ. Are cardiac muscle cells 'skinned' by EGTA or EDTA? *Nature* 1979; **277**: 142-143.
 99. Orentlicher M, Reuben JP, Grundfest H, Brandt PW. Calcium binding and tension development in detergent-treated muscle fibers. *J Gen Physiol* 1974; **63**: 168-186.
 100. Yamahara J, Matsuda H. Bioactive saponins an glycosides. XIII Horse chesnut (3):

- Quantitative analysis of escins Ia, Ib, IIa and IIb by means of high performance liquid chromatography. *Journal of the pharmaceutical society of japan* 1999; **119**: 81-87.
101. Bruice. *Lipids In:organic chemistry*. New Jersey, 1998.
 102. Sirtori CR. Aescin: pharmacology, pharmacokinetics and therapeutic profile. *Pharmacol Res* 2001; **44**: 183-193.
 103. Bhakdi S, Weller U, Walev I, Martin E, Jonas D, Palmer M. A guide to the use of pore forming toxins for controlled permeabilization of cell membranes. *Med Microbiology Immunol* 1993; **182**: 167-175.
 104. Launikonis BS, Stephenson DG. Effects of beta escin and saponin on the tranverse - tubular system and sarcoplasmic reticulum membranes of rat and toad skeletal muscle. *Pflugers Arch - Eur J Physiol* 1999; **437**: 955-965.
 105. Ahnert-hilger G, Mach W, Fohr KJ, Gratzl M. Poration by alpha toxin and streptolysin O: An approach to analyse intracellular processes. *Methods in Cell Biology* 1989; **31**: 63-90.
 106. Lesh RE, Somlyo AP, Owens GK, Somlyo AV. Reversible Permeabilization. *Circ Res* 1995; **77**: 220-230.
 107. Kawai M, Konishi M. Measurement of sarcoplasmic reticulum calcium content in skinned mammalian cardiac muscle. *Cell Calcium* 1994; **16**: 123-136.
 108. Fawcett JM, Harrison SM, Orchard CH. A method for reversible permeabilization of isolated rat ventricular myocytes. *Experimental Physiology* 1998; **83.3**: 293-304.
 109. Li Y, Kranias EG, Mignery GA, Bers DM. Protein Kinase A phosphorylation of the ryanodine receptor does not affect calcium sparks in mouse ventricular myocytes. *Circ Res* 2002; **90**: 309-316.
 110. Bhakdi S, Tranumjensen J, Sziegoleit A. Streptolysin - O structure and mechanism of membrane damage. *Series A-Medical Microbiology Infectious Diseases Virology Parasitology* 1984; **256**: 420.

111. Mason WT. *Fluorescent and luminescent probes for biological activity*. Academic press limited, 1993.
112. Dempster J, Wokosin D. Fluorescence imaging systems: A quick overview of the technology. *Physiology News* 2002; **48**: 12-14.
113. Xiao R-P, Valdivia HH, Bogdanov K, Valdivia C, Lakatta EG, Cheng H. The immunophilin FK506-binding protein modulates Ca^{2+} release channel closure in rat heart. *J Physiol* 1997; **500.2**: 343-354.
114. McCall E, Li L, Satoh H, Shannon TR, Blatter LA, Bers DM. Effects of FK-506 on contraction and Ca^{2+} transients in rat cardiac muscle. *Circ Res* 1996; **79**: 1110-1121.
115. Cheng H, Song LS, Shirokova N et al. Amplitude distribution of calcium sparks in confocal images: theory and studies with an automatic detection method. *Biophys J* 1999; **76**: 606-617.
116. Berry MN, Friend DS, Scheuer J. Morphology and metabolism of intact muscle cells isolated from adult rat heart. *Circ Res* 1970; **26**: 679-687.
117. Bloom S. Spontaneous rhythmic contraction of separated heart muscle cells. *Science* 1970; **167**: 1727-1729.
118. Wier WG, Cannell MB, Berlin JR, Marban E, Lederer WJ. Cellular and subcellular heterogeneity of $[Ca^{2+}]_i$ in single heart cells revealed by fura-2. *Science* 1987; **235**: 325-328.
119. Jaffe L. On the conservation of fast calcium wave speeds. *Cell Calcium* 2002; **32**: 217-229.
120. Marchant JS, Parker I. Functional interactions in calcium signalling over different time and distance scales. *J Gen Physiol* 2000; **116**: 691-695.
121. Cheng H, Lederer MR, Lederer WJ, Cannell MB. Calcium sparks and $[Ca^{2+}]_i$ waves in cardiac myocytes. *Am J Physiol* 1996; **270**: C148-C159.

122. Takamatsu T, Wier WG. Calcium waves in mammalian heart: quantification of origin, magnitude, waveform, and velocity. *FASEB* 1990; **4**: 1519-1525.
123. Williams DA. Quantitative intracellular calcium imaging with laser-scanning confocal microscopy. *Cell Calcium* 1990; **11**: 589-597.
124. Trafford AW, Lipp P, O'Neill SC, Niggli E, Eisner DA. Propagating calcium waves initiated by local caffeine application in rat ventricular myocytes. *Journal of Physiology* 1995; **489.2**: 319-326.
125. Ishide N, Urayama T, Inoue K, Komaru T, Takishima T. Propagation and collision characteristics of calcium waves in rat myocytes. *American Journal of Physiology Heart Circulation Physiology* 1990; **259**: H940-H950.
126. Smith GD, Keizer JE, Stern MD, Lederer WJ, Cheng H. A simple numerical model of calcium spark formation and detection in cardiac myocytes. *Biophys J* 1998; **75**: 15-32.
127. Keizer J, Smith GD, Ponce-Dawson S, Pearson JE. Saltatory propagation of Ca^{2+} waves by Ca^{2+} sparks. *Biophys J* 1998; **75**: 595-600.
128. Lukyanenko V, Gyorke I, Gyorke S. Regulation of calcium release by calcium inside the sarcoplasmic reticulum in ventricular myocytes. *Pflugers Arch* 1996; **432**: 1047-1054.
129. Janczewski AM, Spurgeon HA, Stern MD, Lakatta EG. Effects of sarcoplasmic reticulum Ca^{2+} load on the gain function of Ca^{2+} release by Ca^{2+} current in cardiac cells. *Am J Physiol* 1995; **268**: H916-H920.
130. Kort AA, Capagrossi MC, Lakatta EG. Frequency, amplitude and propagation velocity of spontaneous Ca^{2+} dependent contractile waves in intact adult rat cardiac muscle and isolated myocytes. *Circ Res* 1985; **57**: 844-855.
131. Lipp P, Niggli E. Microscopic spiral waves reveal positive feedback in subcellular calcium signaling. *Biophys J* 1993; **65**: 2272-2276.

132. Miura M, Ishide N, Oda H, Sakurai M, Shinozaki T, Takishima T. Spatial features of calcium transients during early and delayed afterdepolarizations. *Am J Physiol* 1993; **265**: H439-H444.
133. Stern MD, Capagrossi MC, Lakatta EG. Spontaneous calcium release from the sarcoplasmic reticulum in myocardial cells: mechanisms and consequences. *Cell Calcium* 1988; **9**: 247-258.
134. Kaneko T, Tanaka H, Oyamada M, Kawata S, Takamatsu T. Three distinct types of Ca^{2+} waves in langendorff-perfused rat heart revealed by real time confocal microscopy. *Circ Res* 2000; **86**: 1093-1099.
135. Smith GL, Miller DJ. Potentiometric measurements of stoichiometric and apparent affinity constants of EGTA for protons and divalent ions including calcium. *Biochim Biophys Acta* 1985; **839**: 287-299.
136. Fabiato A, Fabiato F. Calculator programs for computing the composition of the solutions containing multiple metals and ligands used for experiments in skinned cells. *J Physiol (Paris)* 1979; **75**: 463-505.
137. Miller DJ, Smith GL. EGTA purity and the buffering of calcium ions in physiological solutions. *Am J Physiol* 1984; **246**: C160-C166.
138. Smith G, O'Neill SC. A comparison of the effects of ATP and tetracaine on spontaneous calcium release from rat permeabilised cardiac myocytes. *Journal of Physiology* 2001; **534.1**: 37-47.
139. Williams DA, Delbridge LM, Cody SH, Harris PJ, Morgan TO. Spontaneous and propagated calcium release in isolated cardiac myocytes viewed by confocal microscopy. *Am J Physiol Heart Circ Physiol* 1992; **262**: C731-C742.
140. Trafford AW, Diaz ME, O'Neill SC, Eisner DA. Comparison of subsarcolemmal and bulk calcium concentration during spontaneous calcium release in rat ventricular myocytes. *J Physiol* 1995; **488.3**: 577-586.

141. Mermier P, Hasselbach W. The effect of calcium and phosphate on the biphasic calcium uptake by the sarcoplasmic reticulum. *Z Naturforsch [C]* 1975; **30**: 777-780.
142. Jackson WA, Colyer J. Translation of Ser16 and Thr17 phosphorylation of phospholamban into Ca²⁺-pump stimulation. *Biochem J* 1996; **316 (Pt 1)**: 201-207.
143. Straub SV, Giovannucci DR, Yule DI. Calcium wave propagation in pancreatic acinar cells: functional interaction of inositol 1,4,5-trisphosphate receptors, ryanodine receptors, and mitochondria. *J Gen Physiol* 2000; **116**: 547-560.
144. Kaftan E, Xu T, Abercrombie F, Hille B. Mitochondria shape hormonally induced cytoplasmic calcium oscillations and modulate exocytosis. *J Biol Chem* 2000; **275**: 25465-25470.
145. Sheu SS, Sharma VK. Rapid report: a novel technique for quantitative measurement of free Ca²⁺ concentration in rat heart mitochondria. *J Physiol* 1999; **518 (Pt 2)**: 577-584.
146. Duchen MR, Leysens A, Crompton M. Transient mitochondrial depolarizations reflect focal sarcoplasmic reticular calcium release in single rat cardiomyocytes. *J Cell Biol* 1998; **142**: 975-988.
147. Sharma VK, Ramesh V, Franzini-Armstrong C, Sheu S-S. Transport of calcium from sarcoplasmic reticulum to mitochondria in rat ventricular myocytes. *Journal of bioenergetics and biomembranes* 2000; **32**: 97-103.
148. Fry CH, Powell T, Twist VW, Ward JP. Net calcium exchange in adult rat ventricular myocytes: an assessment of mitochondrial calcium accumulating capacity. *Proc R Soc Lond B Biol Sci* 1984; **223**: 223-238.
149. Hove-Madsen L, Bers DM. Passive Ca buffering and SR Ca uptake in permeabilized rabbit ventricular myocytes. *Am J Physiol* 1993; **264**: C677-C686.
150. Di Lisa F, Gambassi G, Spurgeon H, Hansford RG. Intramitochondrial free calcium in cardiac myocytes in relation to dehydrogenase activation. *Cardiovasc Res* 1993;

- 27:** 1840-1844.
151. Zhou Z, Mattlib MA, Bers DM. Cytosolic and mitochondrial Ca^{2+} signals in patch clamped mammalian ventricular myocytes. *J Physiol* 1998; **507**: 379-403.
152. Duchen MR. Mitochondria and calcium : from cell signalling to cell death. *J Physiol* 2000; **529.1**: 57-68.
153. Crompton M. Mitochondrial intermembrane junctional complexes and their role in cell death. *J Physiol* 2000; **529 Pt 1**: 11-21.
154. Takahashi A, Camacho P, Lechleitter JD, Herman B. Measurement of intracellular calcium. *Physiological Reviews* 1999; **79**: 1089-1125.
155. Baylor SM, Hollingworth S. Measurement and interpretation of cytoplasmic $[\text{Ca}^{2+}]$ signals from calcium indicator dyes. *News Physiol Sci* 2000; **15**: 19.
156. Eberhard M, Erne P. Calcium binding to fluorescent calcium indicators:calcium green, calcium orange, and calcium crimson. *Biochemical and Biophysical research communications* 1991; 209-215.
157. Lattanzio FAJ. The effects of pH and temperature on fluorescent calcium indicators as determined with chelex-100 and EDTA buffer systems. *Biochemical and Biophysical research communications* 1990; **171**: 102-108.
158. Konishi M, Olson A, Hollingworth S, Baylor SM. Myoplasmic binding of fura-2 investigated by steady-state fluorescence and absorbance measurements. *Biophys J* 1988; **54**: 1089-1104.
159. Ganz MB, Rasmussen J, Bollag WB, Rasmussen H. Effect of buffer systems and pHi on the measurement of $[\text{Ca}^{2+}]_i$ with fura 2. *FASEB* 1990; **4**: 1638-1644.
160. Ganitkevich VY. Use of Indo-1FF for measurements of rapid micromolar cytoplasmic free Ca^{2+} increments in a single smooth muscle cell. *Cell Calcium* 1998; **23**: 313-322.

161. Slavik J. Anilinonaphthalene sulfonate as a probe of membrane composition and function. *Biochim Biophys Acta* 1982; **694**: 1-25.
162. Minta A, Kao JPY, Tsien RY. Fluorescent indicators for cytosolic calcium based on rhodamine and fluorescein chromophores. *J Biol Chem* 1989; **14**: 8171-8178.
163. Harkins AB, Kurebayashi N, Baylor SM. Resting myoplasmic free calcium in frog skeletal muscle fibers estimated with fluo-3. *Biophys J* 1993; **65**: 865-881.
164. Xiang J-Z, Kentish JC. Effects of inorganic phosphate and ADP on calcium handling by the sarcoplasmic reticulum in rat skinned cardiac muscles. *Circ Res* 1995; **29**: 391-400.
165. Cleemann L, Wang W, Morad M. Two dimensional confocal images of organisation, density, and gating of focal Ca^{2+} release sites in cardiac myocytes. *Proc Natl Acad Sci USA* 1998; **95**: 10984-10989.
166. Lukyanenko V, Gyorke I, Subramanian S, Smirnov A, Wiesner TF, Gyorke S. Inhibition of Ca^{2+} sparks by ruthenium red in permeabilized rat ventricular myocytes. *Biophys J* 2000; **79**: 1273-1284.
167. Pogwizd SM, Qi M, Yuan W, Samarel AM, Bers DM. Upregulation of $\text{Na}^+/\text{Ca}^{2+}$ exchanger expression and function in an arrhythmogenic rabbit model of heart failure. *Circ Res* 1999; **85**: 1009-1019.
168. McIntosh MA, Cobbe SM, Smith GL. Heterogenous changes in action potential and intracellular Ca^{2+} in left ventricular myocyte sub-types from rabbits with heart failure. *Cardiovasc Res* 2000; **45**: 397-409.
169. Trafford AW, Diaz ME, Sibbring GC, Eisner DA. Modulation of CICR has no maintained effect on systolic Ca^{2+} simultaneous measurements of sarcoplasmic reticulum and sarcolemmal Ca^{2+} fluxes in rat ventricular myocytes. *J Physiol* 2000; **522.2**: 259-270.
170. Endo M, Iino M. Specific perforation of muscle cell membranes with preserved

- functions by saponin treatment. *Journal of Muscle Research and Cell Motility* 1980; **1**: 89-100.
171. Zhou Z, Matlib MA, Bers DM. Cytosolic and mitochondrial Ca^{2+} signals in patch clamped mammalian ventricular myocytes. *J Physiol* 1998; **507.2**: 379-403.
172. Bassani RA, Bassani JWM, Bers DM. Relaxation in ferret ventricular myocytes:unusual interplay among calcium transport systems. *J Physiol* 1994; **476**: 295-308.
173. Negretti N, O'Neill SC, Eisner DA. The relative contributions of different intracellular and sarcolemmal systems to relaxation in rat ventricular myocytes. *Cardiovascular Research* 1993; **27**: 1826-1830.
174. Bassani JWM, Bassani RA, Bers DM. Calibration of indo-1 and resting intracellular $[Ca^{2+}]$ in intact rabbit cardiac myocytes. *Biophys J* 1995; **68**: 1453-1460.
175. Marks AR. Cellular functions of immunophilins. *Physiological Reviews* 1996; **76**: 631-649.
176. Schreiber SL, Crabtree G. The mechanism of action of cyclosporin A and FK506. *Immunology Today* 1992; **13**: 136-142.
177. Marks AR, Tempst P, Hwang KS et al. Molecular cloning and characterization of the ryanodine receptor/junctional channel complex cDNA from skeletal muscle sarcoplasmic reticulum. *Proc Natl Acad Sci U S A* 1989; **86**: 8683-8687.
178. Collins JH. Sequence analysis of the ryanodine receptor:Possible association with a 12K, FK506-binding immunophilin/protein kinase C inhibitor. *Biochemical and Biophysical research communications* 1991; **178**: 1288-1290.
179. Jayaraman T, Brillantes A-MB, Timmerman AP et al. FK506 binding protein associated with the calcium release channel (Ryanodine Receptor). *J Biol Chem* 1992; **267**: 9474-9477.
180. Timmerman AP, Ogunbunmi EM, Freund EA, Wiederrecht G, Marks AR, Fleischer S.

- The calcium release channel of sarcoplasmic reticulum is modulated by FK-506 binding protein. *Journal of Biological Chemistry* 1993; **268**: 22992-22999.
181. Timerman AP, Weiderrecht G, Marcy A, Fleischer S. Characterisation of an exchange reaction between soluble FKBP-12 and the FKBP - Ryanodine receptor complex. *J Biol Chem* 1995; **270**: 2451-2459.
182. Mayrleitner M, Timerman AP, Wiederrecht G, Fleischer S. The calcium release channel of sarcoplasmic reticulum is modulated by FK-506 binding protein: Effect of FKBP-12 on single channel activity of the skeletal muscle ryanodine receptor. *Cell Calcium* 1994; **15**: 99-108.
183. Ahern GP, Junankar PR, Dulhunty AF. Single channel activity of the ryanodine receptor calcium release channel is modulated by FK-506. *FEBS* 1994; **352**: 369-374.
184. Brillantes A-MB, Ondrias K, Scott A et al. Stabilisation of calcium release channel (Ryanodine Receptor) function by FK506BP. *Cell* 1994; **77**: 513-523.
185. Marx SO, Ondrias K, Marks AR. Coupled gating between individual skeletal muscle Ca^{2+} release channels (Ryanodine Receptors). *Science* 1998; **281(5378)**: 818-821.
186. Ondrias K, Marx SO, Gaburjakova M, Marks AR. FKBP12 modulates gating of the ryanodine receptor/calcium release channel. *Ann N Y Acad Sci* 1998; **853**: 149-156.
187. Van Duyne GD, Standaert RF, Karplus PA, Schreiber SL, Clardy J. Atomic structures of the human immunophilin FKBP-12 complexes with FK506 and rapamycin. *J Mol Biol* 1993; **229**: 105-124.
188. Albers MW, Walsh CT, Schreiber SL. Substrate specificity of the human rotamase FKBP: A view of FK506 and rapamycin as leucine-(twisted amide)-proline mimics. *J Org Chem* 1990; **55**: 4984-4986.
189. Rosen MK, Standaert RF, Galat A, Nakatsuka M, Schreiber SL. Inhibition of FKBP rotamase activity by immunosuppressant FK506: twisted amide surrogate. *Science*

- 1990; **248**: 863-866.
190. Bers DM, Fill M. Coordinated Feet and the Dance of Ryanodine Receptors. *Science* 1998; **281(5378)**: 790-791.
191. Tanabe T, Beam KG, Adams BA, Niidome T, Numa S. Regions of the skeletal muscle dihydropyridine receptor critical for excitation-contraction coupling. *Nature* 1990; **346**: 567-569.
192. Timerman AP, Jayaraman T, Wiederrecht G, Onoue H, Marks AR, Fleischer S. The ryanodine receptor from canine heart sarcoplasmic reticulum is associated with a novel Fk-506 binding protein. *Biochemical and Biophysical research communications* 1994; **198**: 701-706.
193. Lam E, Martin MM, Timerman AP et al. A novel FK506 binding protein can mediate the immunosuppressive effects of FK506 and is associated with the cardiac ryanodine receptor. *J Biol Chem* 1995; **270**: 26511-26522.
194. Sewell TJ, Lam E, Martin MM et al. Inhibition of calcineurin by a novel FK-506-binding protein. *J Biol Chem* 1994; **269**: 21094-21102.
195. Timerman AP, Onoue H, Xin H-B, Copello J, Wiederrecht G, Fleischer S. Selective binding of FKBP12.6 by the cardiac ryanodine receptor. *J Biol Chem* 1996; **271**: 20385-20391.
196. Barg S, Copello J, Fleischer S. Different interactions of cardiac and skeletal muscle ryanodine receptors with FK-506 binding protein isoforms. *American Journal of Physiology* 1997; **272**: -C1726.
197. Kaftan E, Marks AR, Ehrlich BE. Effects of rapamycin on ryanodine receptor/ Ca^{2+} -release channels from cardiac muscle. *Circ Res* 1996; **78**: 990-997.
198. Gribbin J. *Almost everyone's guide to science*. Weidenfeld and Nicholson, 1998.
199. Marks AR. Cardiac Intracellular Calcium Release Channels. *Circulation Research* 2000; **87**: 8-11.

200. Yamazawa T, Takeshima H, Sakurai T, Endo M, Iino M. Subtype specificity of the ryanodine receptor for Ca^{2+} signal amplification in excitation-contraction coupling. *EMBO J* 1996; **15**: 6172-6177.
201. Dubell WH, GAA ST, Lederer WJ, Rogers TB. Independent inhibition of calcineurin and K^+ currents by the immunosuppressant FK506 in rat ventricle. *Am J Physiol Heart Circ Physiol* 1998; **275**: H2041-H2052.
202. Dubell WH, Lederer WJ, Rogers TB. K^+ currents responsible for repolarisation in mouse ventricle and their modulation by FK506 and rapamycin. *American Journal of Physiology Heart Circulation Physiology* 2000; **278**: H886-H897.
203. Su Z, Sugishita K, Ritter M, Barry William H. Effects of FK506 on $[\text{Ca}^{2+}]_i$ differ in mouse and rabbit ventricular myocytes. *The Journal of Pharmacology and Experimental Therapeutics* 2003; **304**: 334-341.
204. Prestle J, Janssen PML, Janseen AP et al. Overexpression of FK-506 binding protein FKBP12.6 in cardiomyocytes reduces ryanodine receptor-mediated Ca^{2+} leak from sarcoplasmic reticulum and increases contractility. *Circ Res* 2001; **88**: 188-194.
205. Yao A, Su Z, Nonaka A et al. Effects of overexpression of the $\text{Na}^+-\text{Ca}^{2+}$ exchanger on $[\text{Ca}^{2+}]_i$ transients in murine ventricular myocytes. *Circ Res* 1998; **82**: 657-665.
206. Atkison P, Joubert G, Barron A et al. Hypertrophic cardiomyopathy associated with tacrolimus in paediatric transplant patients. *Lancet* 1995; **345**: 894-896.
207. Marx SO, Reiken S, Hisamatsu Y et al. PKA phosphorylation dissociates FKBP12.6 from the calcium release channel (Ryanodine Receptor): Defective Regulation in Failing Hearts. *Cell* 2000; **101**: 365-376.
208. Terracciano CM. Sarcoplasmic reticulum calcium release function and FK binding proteins in heart failure: another piece of a complex jigsaw. *Cardiovasc Res* 2000; **48**: 191-193.
209. Eisner DA, Trafford AW, Diaz ME, Overend CL, O'Neill SC. The control of Ca^{2+}

- release from the cardiac sarcoplasmic reticulum regulation versus autoregulation. *Cardiovasc Res* 1998; **38**: 589-604.
210. Yamamoto T, Yano M, Kohno M et al. Abnormal Ca^{2+} release from cardiac sarcoplasmic reticulum in tachycardia-induced heart failure. *Cardiovasc Res* 1999; **44**: 146-155.
211. Yano M, Ono K, Ohkusa T, Kobayashi S, Matsuzaki M, Okamoto H. Altered stoichiometry of FKBP12.6 versus ryanodine receptor as a cause of abnormal Ca^{2+} leakage through ryanodine receptor in heart failure. *Circulation* 2000; 2131-2136.
212. Ono K, Yano M, Kohno M et al. Altered interaction of FKBP12.6 with ryanodine receptor as a cause of abnormal Ca^{2+} release in heart failure. *Cardiovasc Res* 2000; **48**: 323-331.
213. Eichhorn EJ. The paradox of beta-adrenergic blockade for the management of congestive heart failure. *Am J Med* 1992; **92**: 527-538.
214. Doi M, Yano M, Kobayashi S et al. Propranolol prevents the development of heart failure by restoring FKBP12.6-mediated stabilization of ryanodine receptor. *Circulation* 2001; **105**: 1374-1379.
215. Reiken S, Gaburjakova M, Guatimosim S et al. Protein kinase A phosphorylation of the cardiac calcium release channel (ryanodine receptor) in normal and failing hearts. Role of phosphatases and response to isoproterenol. *J Biol Chem* 2003; **278**: 444-453.
216. Xin H-B, Senbonmatsu T, Cheung D-S et al. Oestrogen protects FKBP12.6 null mice from cardiac hypertrophy. *Nature* 2002; **416**: 334-337.
217. Gomez AM, Valdivia HH, Cheng H et al. Defective excitation-contraction coupling in experimental cardiac hypertrophy and heart failure. *Science* 1997; **276**: 800-806.
218. Witcher DR, Kovacs RJ, Schulman H, Cefali DC, Jones LR. Unique phosphorylation site on the cardiac ryanodine receptor regulates calcium channel activity. *J Biol*

- Chem* 1991; **266**: 11144-11152.
219. Hain J, Onoue H, Mayrleitner M, Fleischer S, Schindler H. Phosphorylation modulates the function of the calcium release channel of sarcoplasmic reticulum from cardiac muscle. *J Biol Chem* 1995; **270**: 2074-2081.
220. Lokuta AJ, Rogers TB, Lederer WJ, Valdivia HH. Modulation of cardiac ryanodine receptors of swine and rabbit by a phosphorylation-dephosphorylation mechanism. *J Physiol* 1995; **487 (Pt 3)**: 609-622.
221. Shou W, Aghdasi B, Armstrong DL et al. Cardiac defects and altered ryanodine receptor function in mice lacking FKBP12. *Nature* 1998; **391**: 489-492.
222. Mack MM, Molinski TF, Buck ED, Pessah IN. Novel Modulators of Skeletal Muscle FKBP12/calcium channel complex from *Ianthella basta*. *J Biol Chem* 2002; **269**: 23236-23249.
223. Chen L, Molinski TF, Pessah IN. Bastadin 10 stabilizes the open conformation of the ryanodine-sensitive Ca^{2+} channel in an FKBP12-dependent manner. *J Biol Chem* 1999; **274**: 32603-32612.
224. Jamil G. Effects of FK506 analogs on ryanodine receptors. *Biophys.J.* 70. 1996.
Ref Type: Abstract
225. Ahern GP, Junankar PR, Dulhunty AF. Subconductance states in single-channel activity of skeletal muscle ryanodine receptors after removal of FKBP12. *Biophys J* 1997; **72**: 146-162.
226. Ahern GP, Junankar PR, Dulhunty AF. Ryanodine receptors from rabbit skeletal muscle are reversibly activated by rapamycin. *Neurosci Lett* 1997; **225**: 81-84.
227. Ahern GP, Junankar PR, Pace SM, Curtis S, Mould JA, Dulhunty AF. Effects of ivermectin and midecamycin on ryanodine receptors and the Ca^{2+} -ATPase in sarcoplasmic reticulum of rabbit and rat skeletal muscle. *J Physiol* 1999; **514.2**: 313-326.

228. Hopkins KD, Marcella KL, Strecker AE. Ivermectin toxicosis in a dog. *J Am Vet Med Assoc* 1990; **197**: 93-94.
229. Jeyakumar LH, Ballester L, Cheng DS et al. FKBP binding characteristics of cardiac microsomes from diverse vertebrates. *Biochemical and Biophysical research communications* 2001; **281**: 979-986.
230. Wang T, Donahoe PK, Zervos AS. Specific interaction of type I receptors of the TGF-beta family with the immunophilin FKBP-12. *Science* 1994; **265**: 674-676.
231. Copello JA, Xin HB, Fleischer S. Role of FKBP12.6 in cardiac ryanodine receptors (RyR2) as studied in FKBP12.6 gene knock-out mice. *Biophys.J.* 79. 2000.
Ref Type: Abstract
232. McCall E, Ginsburg KS, Bassani RA et al. Ca²⁺ flux, contractility, and excitation-contraction coupling in hypertrophic rat ventricular myocytes. *Am J Physiol* 1998; **274**: H1348-H1360.
233. Subramanian S, Viatchenko-Karpinski S, Lukyanenko V, Gyorke S, Wiesner TF. Underlying mechanisms of symmetric calcium wave propagation in rat ventricular myocytes. *Biophys J* 2001; **80**: 1-11.
234. Kort AA, Lakatta EG. Spontaneous sarcoplasmic reticulum calcium release in rat and rabbit cardiac muscle relation to transient and rest state twitch tension. *Circ Res* 1988; **63**: 969-979.
235. Yano M, Kobayashi S, Kohno M et al. FKBP12.6-mediated stabilization of calcium-release channel (ryanodine receptor) as a novel therapeutic strategy against heart failure. *Circulation* 2003; **107**: 477-484.
236. Rusnak F, Mertz P. Calcineurin: form and function. *Physiol Rev* 2000; **80**: 1483-1521.
237. Hendey B, Klee CB, Maxfield FR. Inhibition of neutrophil chemokinesis on vitronectin by inhibitors of calcineurin. *Science* 1992; **258**: 296-299.

238. Mulkey RM, Endo S, Shenolikar S, Malenka RC. Involvement of a calcineurin/inhibitor-1 phosphatase cascade in hippocampal long-term depression. *Nature* 1994; **369**: 486-488.
239. Chin ER, Olson EN, Richardson JA et al. A calcineurin-dependent transcriptional pathway controls skeletal muscle fiber type. *Genes Dev* 1998; **12**: 2499-2509.
240. Musaro A, McCullagh KJ, Naya FJ, Olson EN, Rosenthal N. IGF-1 induces skeletal myocyte hypertrophy through calcineurin in association with GATA-2 and NF-ATc1. *Nature* 1999; **400**: 581-585.
241. Molkentin JD. Calcineurin, mitochondrial membrane potential, and cardiomyocyte apoptosis. *Circ Res* 2001; **88**: 1220-1222.
242. Bierer BE, Mattila PS, Standaert RF et al. Two distinct signal transmission pathways in T lymphocytes are inhibited by complexes formed between an immunophilin and either FK 506 or rapamycin. *Proc Natl Acad Sci USA* 1990; **87**: 9231-9235.
243. Griffith JP, Kim JL, Kim EE et al. X-ray structure of calcineurin inhibited by the immunophilin- immunosuppressant FKBP12-FK506 complex. *Cell* 1995; **82**: 507-522.
244. Shin DW, Pan Z, Bandyopadhyay A, Bhat MB, Kim DH, Ma JM. Ca^{2+} dependent interaction between FKBP12 and calcineurin regulates activity of the Ca^{2+} release channel in skeletal muscle. *Biophys J* 2002; **83**: 2539-2549.
245. Bandyopadhyay A, Shin DW, Ahn JO, Kim DH. Calcineurin regulates ryanodine receptor/ Ca^{2+} -release channels in rat heart. *Biochem J* 2000; **352 Pt 1**: 61-70.
246. Cameron AM, Steiner JP, Roskams AJ, Ali SM, Ronnett GV, Snyder SH. Calcineurin associated with the inositol 1,4,5-trisphosphate receptor- FKBP12 complex modulates Ca^{2+} flux. *Cell* 1995; **83**: 463-472.
247. Kingma I, Harmsen E, ter Keurs HE, Benediktsson H, Paul LC. Cyclosporine-associated reduction in systolic myocardial function in the rat. *Int J Cardiol* 1991; **31**:

- 15-22.
248. Banijamali HS, Ter Keurs MH, Paul LC, Ter Keurs HEDJ. Excitation-contraction coupling in rat heart: influence of cyclosporin A. *Cardiovasc Res* 1993; **27**: 1845-1854.
249. Park KS, Kim TK, Kim DH. Cyclosporin A treatment alters characteristics of Ca^{2+} release channel in cardiac sarcoplasmic reticulum. *Am J Physiol* 1999; **276**: H865-H872.
250. Park KS, Kim TK, Kim DH. Cyclosporin A treatment alters characteristics of Ca^{2+} -release channel in cardiac sarcoplasmic reticulum. *Am J Physiol* 1999; **276**: H865-H872.
251. Yang D, Rosen MK, Schreiber SL. A composite FKBP12-FK506 surface that contacts calcineurin. *Journal of the American Chemical Society* 1993; **115**: 819-820.
252. Vandeyar MA, Weiner MP, Hutton CJ, Batt CA. A simple and rapid method for the selection of oligodeoxynucleotide- directed mutants. *Gene* 1988; **65**: 129-133.
253. Hohl CM, Livingston B, Hensley J, Altschuld RA. Calcium handling by sarcoplasmic reticulum of neonatal swine cardiac myocytes. *Am J Physiol* 1997; **273**: H192-H199.
254. Mardini M, Mihailidou AS, Wong A, Rasmussen HH. Cyclosporine and FK506 differentially regulate the sarcolemmal Na^+/K^+ pump. *The Journal of Pharmacology and Experimental Therapeutics* 2001; **297**: 804-810.